frontiers | Research Topics

Advances in malignant pleural mesothelioma: Diagnosis, treatment, and molecular mechanisms

Edited by
Glen Reid and Marco Lucchi

Published in
Frontiers in Oncology

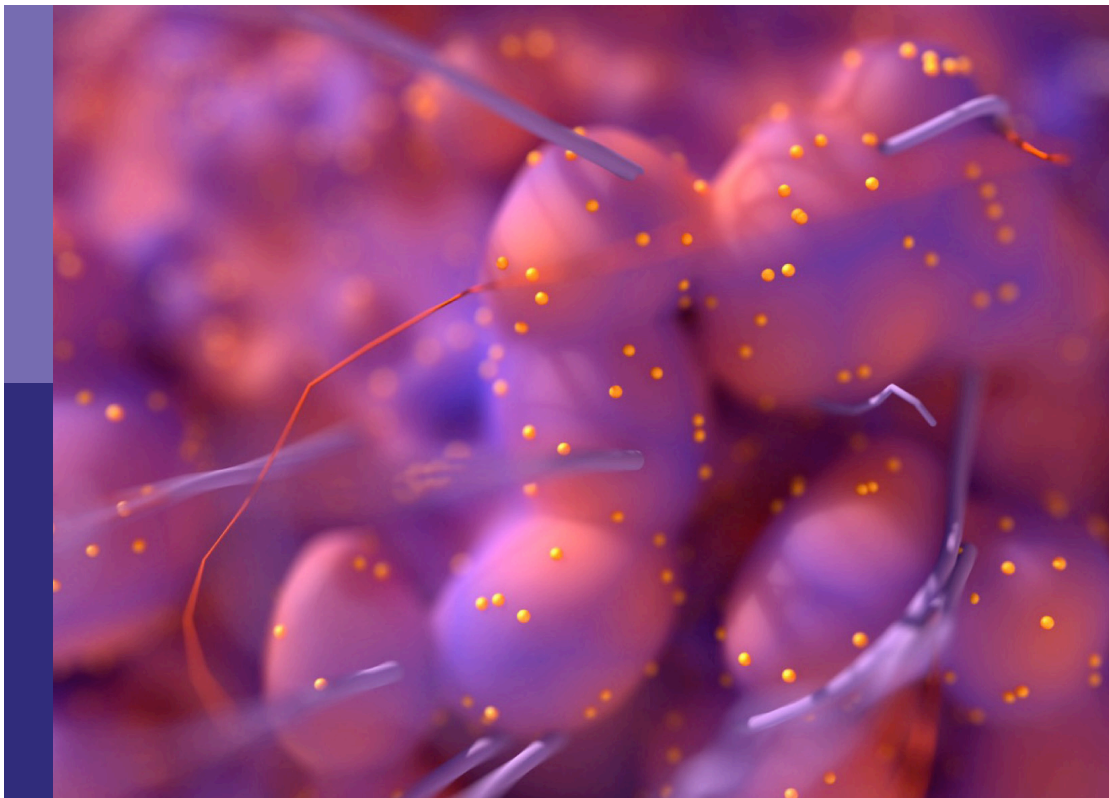

ISSN 1664-8714
ISBN 978-2-83251-806-9
DOI 10.3389/978-2-83251-806-9

About Frontiers

Frontiers is more than just an open access publisher of scholarly articles: it is a pioneering approach to the world of academia, radically improving the way scholarly research is managed. The grand vision of Frontiers is a world where all people have an equal opportunity to seek, share and generate knowledge. Frontiers provides immediate and permanent online open access to all its publications, but this alone is not enough to realize our grand goals.

Frontiers journal series

The Frontiers journal series is a multi-tier and interdisciplinary set of open-access, online journals, promising a paradigm shift from the current review, selection and dissemination processes in academic publishing. All Frontiers journals are driven by researchers for researchers; therefore, they constitute a service to the scholarly community. At the same time, the *Frontiers journal series* operates on a revolutionary invention, the tiered publishing system, initially addressing specific communities of scholars, and gradually climbing up to broader public understanding, thus serving the interests of the lay society, too.

Dedication to quality

Each Frontiers article is a landmark of the highest quality, thanks to genuinely collaborative interactions between authors and review editors, who include some of the world's best academicians. Research must be certified by peers before entering a stream of knowledge that may eventually reach the public - and shape society; therefore, Frontiers only applies the most rigorous and unbiased reviews. Frontiers revolutionizes research publishing by freely delivering the most outstanding research, evaluated with no bias from both the academic and social point of view. By applying the most advanced information technologies, Frontiers is catapulting scholarly publishing into a new generation.

What are Frontiers Research Topics?

Frontiers Research Topics are very popular trademarks of the *Frontiers journals series*: they are collections of at least ten articles, all centered on a particular subject. With their unique mix of varied contributions from Original Research to Review Articles, Frontiers Research Topics unify the most influential researchers, the latest key findings and historical advances in a hot research area.

Find out more on how to host your own Frontiers Research Topic or contribute to one as an author by contacting the Frontiers editorial office: frontiersin.org/about/contact

Advances in malignant pleural mesothelioma: Diagnosis, treatment, and molecular mechanisms

Topic editors

Glen Reid — University of Otago, New Zealand

Marco Lucchi — University of Pisa, Italy

Citation

Reid, G., Lucchi, M., eds. (2023). *Advances in malignant pleural mesothelioma: Diagnosis, treatment, and molecular mechanisms*. Lausanne: Frontiers Media SA. doi: 10.3389/978-2-83251-806-9

Table of contents

frontiers | Frontiers in Oncology

TYPE Editorial
PUBLISHED 16 February 2023
DOI 10.3389/fonc.2023.1158416

OPEN ACCESS

EDITED AND REVIEWED BY
Lizza E.L. Hendriks,
Maastricht University Medical Centre,
Netherlands

*CORRESPONDENCE
Vittorio Aprile
vittorio.aprile@unipi.it

SPECIALTY SECTION
This article was submitted to Thoracic Oncology, a section of the journal Frontiers in Oncology

RECEIVED 03 February 2023
ACCEPTED 09 February 2023
PUBLISHED 16 February 2023

CITATION
Mastromarino MG, Aprile V and Lucchi M (2023) Editorial: Advances in malignant pleural mesothelioma: Diagnosis, treatment, and molecular mechanisms. *Front. Oncol.* 13:1158416. doi: 10.3389/fonc.2023.1158416

Editorial: Advances in malignant pleural mesothelioma: Diagnosis, treatment, and molecular mechanisms

Maria Giovanna Mastromarino[1], Vittorio Aprile[1,2]* and Marco Lucchi[1,2]

[1]Division of Thoracic Surgery, Cardiac, Thoracic and Vascular Department; Pisa University Hospital, Pisa, Italy, [2]Department of Surgical, Medical and Molecular Pathology and Critical Care Medicine, University of Pisa, Pisa, Italy

KEYWORDS

malignant pleural mesothelioma, diagnosis, treatment, molecular mechanisms, multimodality strategy, precision oncology

Editorial on the Research Topic
Advances in malignant pleural mesothelioma: Diagnosis, treatment, and molecular mechanisms

Malignant pleural mesothelioma (MPM) represents a death sentence, with an estimated survival of less than one year after diagnosis in most cases (1). The new millennium has witnessed an MPM diagnosis outbreak due to the intensive past use of asbestos. A lack of knowledge of the pathogenesis and different prognostic aspects, together with its high socioeconomic cost, have forced research on this disease in the last decade. Nevertheless, the diagnostic modalities and treatment strategies of MPM are still far from being standardized, and the molecular mechanisms continue to be unclear.

Recently, considerable progress in molecular and histopathological analysis has led to a necessary update of the WHO Classification of Tumors of the Pleura (2). The substantial changes include the pathology revision of the latest classification system in order to incorporate architectural patterns and stromal and cytologic features as well as nuclear grading for epithelioid diffuse MPM and the molecular landscape of MPM. Particular attention has been reserved for the recognition of mesothelioma *in situ* as a precisely defined clinicopathologic entity, requiring a demonstration of loss of BAP1 and/or MTAP by immunohistochemistry and/or CDKN2A (p16) homozygous deletion by fluorescence *in situ* hybridization for differential diagnosis from reactive mesothelial proliferation (3). Despite all the advances achieved, a proper diagnosis of MPM still represents a challenge for the physician, hence the development of different biomarkers that could be useful to increase diagnosis accuracy and the efficiency of prognosis by assessing a more accurate patient risk stratification (4). In this scenario, new prognostic biomarkers as well as new potential molecular targets are strongly required to understand the molecular mechanisms of MPM and drive more efficient therapies.

To date, there is no universal standardization of therapeutic options since most patients have a late diagnosis, usually with advanced disease. In these cases, locoregional therapies gave way to systemic ones in which platinum-based combinations, with or without

pemetrexed, represent the most common doublet despite yielding poor long-term outcomes (5).

Recently, immune checkpoint inhibitors have demonstrated promising activity for the treatment of MPM and have been incorporated into some treatment regimens (6). Surgery represents an effective but seriously detrimental alternative that should be reserved for selected patients. In very selected cases, multimodality approaches, including surgical resection by either extra-pleural pneumonectomy or pleurectomy-decortication after neoadjuvant chemotherapy (CHT) or followed by adjuvant CHT and/or radiotherapy represent, to date, the best alternative that may be offered to these patients (7, 8). The main limitation of surgery for MPM, in fact, is the high locoregional relapse rate that reaches 75%, due to the impossibility of achieving a radical disease-free margins resection (R0) because of the laminar tumor growth (9). This critical success-limiting factor has encouraged further research into intracavitary therapies, such as hyperthermic intrathoracic chemotherapy, to improve locoregional control by shrinking microscopic residual foci (R1 margins) more effectively (10).

Finally, the role of the tumor microenvironment (TIME) and the identification of potential biomarkers of activity/resistance to novel treatment strategies is currently a field of active study to enhance anti-tumor immunity by investigating the interaction of the tumor cells with the stroma and the surrounding host niche (11).

Recently, we collaborated on a special series on advances in the fields of diagnosis, treatment, and molecular mechanisms of MPM.

Herein, Xu et al. review the current knowledge about vulnerabilities according to functional loss of major tumor suppressor genes and dependencies evolving out of cancer development and resistance to cisplatin-based chemotherapy, with the aim to elucidate the therapeutic landscape and promote precision oncology for MPM. Lauk et al. show preliminary results of the safety and oncologic efficacy of the addition of bevacizumab to standard induction chemotherapy prior to MPM surgery, demonstrating a significant improvement in response rates without increased intra- and postoperative bleeding complications. Tostes et al. describe the first case of complete pathological response obtained after neoadjuvant chemo-immunotherapy, with the sustained benefit for the patient of being disease and treatment free up to 14 months after surgery. In a multi-center national study, Dudnik et al. test the role of BAP-1 alterations in MPM patients regarding the outcomes of systemic treatments; they conclude that BAP1-altered MPM, as compared to non-selected MPM, is characterized by similar efficacy of standard platinum-based chemotherapy and immune checkpoint inhibitors, while no responses were observed with poly (ADP-ribose) polymerase inhibitors. Duan et al. perform a combined analysis of RNA-sequence and microarray data; authors were able to establish and validate the role of the competing endogenous RNA network as a novel prognostic and therapeutic biomarker of MPM. Another potential diagnostic and prognostic marker has been identified by Guo et al., who reveals a high sensitivity and specificity for Aurora Kinase A (AURKA gene encode, Aurora-A) searching from the Gene Expression Omnibus (GEO) database. The microarray dataset from the GEO database has also been used by Endo et al. to demonstrate the role of insulin-like growth factor 2 mRNA binding protein 3 (IGF2BP3) as one of the significantly upregulated genes in MPM, which might promote cell proliferation, a critical step in oncogenesis, by suppressing the expression of p27 in malignant mesothelioma cells. Ollila et al. study the effect of the tumor immune microenvironment in epithelioid MPM, revealing its prognostic value, while Janssens et al. describe headspace volatile organic compounds (VOCs) capable of distinguishing between MPM and lung cancer cells, as well as between the histological subtypes within MPM (epithelioid, sarcomatoid and biphasic), suggesting a useful role of VOCs in generating a clinically predictive breath model for MPM. Finally, Choi et al. summarize the current state of intraoperative intrapleural therapeutic agents, providing an updated review on pleural-directed adjuncts in the management of MPM as well as highlighting the most promising near-term technology breakthroughs.

Discovering ways and strategies to overcome diagnostic challenges and limited treatment options in MPM is a constantly evolving research field. The comprehension of the molecular mechanisms in tumor development and the biomolecular landscape of MPM might pave the way for new therapeutic strategies. The study of TIME is pivotal in identifying appropriate prognostic and predictive tissue biomarkers, attempting to detect the subgroups of patients who will benefit the most from multimodality approaches. The collective goal of this scientific endeavor will be to implement personalized treatment based on the specific MPM molecular features for each patient, thus promoting precision oncology.

In conclusion, the articles in the present Research Topic provide the reader with new and ongoing research in MPM, review current management strategies and updates, and encourage further contributions in this field to improve the life and prognosis of patients suffering from such a dismal cancer.

Author contributions

All authors listed have made a substantial, direct, and intellectual contribution to the work and approved it for publication.

Conflict of interest

The authors declare that the research was conducted in the absence of any commercial or financial relationships that could be construed as a potential conflict of interest.

Publisher's note

References

1. Tsao AS, Lindwasser OW, Adjei AA, Adusumilli PS, Beyers ML, Blumenthal GM, et al. Current and future management of malignant mesothelioma: A consensus report from the national cancer institute thoracic malignancy steering committee, international association for the study of lung cancer, and mesothelioma applied research foundation. *J Thorac Oncol* (2018) 13:1655–67. doi: 10.1016/j.jtho.2018.08.2036

2. WHO. *Classification of tumours editorial board. WHO classification of tumours: Thoracic tumours. 5th ed*. Lyon, France: International Agency for Research on Cancer (2021).

3. Nicholson AG, Sauter JL, Nowak AK, Kindler HL, Gill RR, Remy-Jardin M, et al. EURACAN/IASLC proposals for updating the histologic classification of pleural mesothelioma: Towards a more multidisciplinary approach. *J Thorac Oncol* (2020) 15:29–49. doi: 10.1016/j.jtho.2019.08.2506

4. Mastromarino MG, Lenzini A, Aprile V, Alì G, Bacchin D, Korasidis S, et al. New insights in pleural mesothelioma classification update: Diagnostic traps and prognostic implications. *Diagnostics* (2022) 12:2905. doi: 10.3390/diagnostics12122905

5. Network NCCN. *Malignant pleural mesothelioma* (2022). Available at: https://www.nccn.org/professionals/physician_gls/pdf/mpm.pdf.

6. Baas P, Scherpereel A, Nowak AK, Fujimoto N, Peters S, Tsao AS, et al. First-line nivolumab plus ipilimumab in unresectable malignant pleural mesothelioma (CheckMate 743): A multicentre, randomised, open-label, phase 3 trial. *Lancet* (2021) 397(10272):375–86. doi: 10.1016/S0140-6736(20)32714-8

7. Bueno R, Opitz I. IASLC mesothelioma taskforce. surgery in malignant pleural mesothelioma. *J Thorac Oncol* (2018) 13(11):1638–54. doi: 10.1016/j.jtho.2018.08.001

8. Krug LM, Pass HI, Rusch VW, Kindler HL, Sugarbaker DJ, Rosenzweig KE, et al. Multicenter phase II trial of neoadjuvant pemetrexed plus cisplatin followed by extrapleural pneumonectomy and radiation for malignant pleural mesothelioma. *J Clin Oncol* (2009) 27(18):3007–13. doi: 10.1200/JCO.2008.20.3943

9. Baldini EH, Richards WG, Gill RR, Goodman BM, Winfrey OK, Eisen HM, et al. Updated patterns of failure after multimodality therapy for malignant pleural mesothelioma. *J Thorac Cardiovasc Surg* (2015) 149(5):1374–81. doi: 10.1016/j.jtcvs.2014.10.128

10. Aprile V, Lenzini A, Lococo F, Bacchin D, Korasidis S, Mastromarino MG, et al. Hyperthermic intrathoracic chemotherapy for malignant pleural mesothelioma: The forefront of surgery-based multimodality treatment. *J Clin Med* (2021) 10:3801. doi: 10.3390/jcm10173801

11. Napoli F, Listì A, Zambelli V, Witel G, Bironzo P, Papotti M, et al. Pathological characterization of tumor immune microenvironment (TIME) in malignant pleural mesothelioma. *Cancers (Basel)* (2021) 13(11):2564. doi: 10.3390/cancers13112564

frontiers in Oncology

REVIEW
published: 23 September 2020
doi: 10.3389/fonc.2020.579464

Therapeutic Landscape of Malignant Pleural Mesothelioma: Collateral Vulnerabilities and Evolutionary Dependencies in the Spotlight

*Duo Xu[1,2], Haitang Yang[1,2], Ralph A. Schmid[1,2] and Ren-Wang Peng[1,2]**

[1] Division of General Thoracic Surgery, Inselspital, Bern University Hospital, University of Bern, Bern, Switzerland,
[2] Department for BioMedical Research (DBMR), Inselspital, Bern University Hospital, University of Bern, Bern, Switzerland

Malignant pleural mesothelioma (MPM) is the epitome of a recalcitrant cancer driven by pharmacologically intractable tumor suppressor proteins. A significant but largely unmet challenge in the field is the translation of genetic information on alterations in tumor suppressor genes (TSGs) into effective cancer-specific therapies. The notion that abnormal tumor genome subverts physiological cellular processes, which creates collateral vulnerabilities contextually related to specific genetic alterations, offers a promising strategy to target TSG-driven MPM. Moreover, emerging evidence has increasingly appreciated the therapeutic potential of genetic and pharmacological dependencies acquired en route to cancer development and drug resistance. Here, we review the most recent progress on vulnerabilities co-selected by functional loss of major TSGs and dependencies evolving out of cancer development and resistance to cisplatin based chemotherapy, the only first-line regimen approved by the US Food and Drug Administration (FDA). Finally, we highlight CRISPR-based functional genomics that has emerged as a powerful platform for cancer drug discovery in MPM. The repertoire of MPM-specific "Achilles heel" rises on the horizon, which holds the promise to elucidate therapeutic landscape and may promote precision oncology for MPM.

Keywords: malignant pleural mesothelioma, tumor suppressors, collateral and evolutionary vulnerabilities, targeted therapy, CRISPR/Cas9

OPEN ACCESS

Edited by:
Glen Reid,
University of Otago, New Zealand

Reviewed by:
Didier Jean,
Institut National de la Santé et de la Recherche Médicale (INSERM), France
Luciano Mutti,
Temple University, United States

***Correspondence:**
Ren-Wang Peng
Renwang.Peng@insel.ch

Specialty section:
This article was submitted to Thoracic Oncology, a section of the journal Frontiers in Oncology

Received: *02 July 2020*
Accepted: *02 September 2020*
Published: *23 September 2020*

Citation:
Xu D, Yang H, Schmid RA and Peng R-W (2020) Therapeutic Landscape of Malignant Pleural Mesothelioma: Collateral Vulnerabilities and Evolutionary Dependencies in the Spotlight. Front. Oncol. 10:579464. doi: 10.3389/fonc.2020.579464

Malignant pleural mesothelioma (MPM) is a rare but highly aggressive cancer etiologically associated with asbestos exposure and inherently resistant to treatment options (1). Although asbestos is banned in most industrialized countries, MPM incidence and mortality still increase globally owing to long latency of the disease (up to 50 years) and continued use of asbestos in developing countries (2).

For patients with advanced, unresectable MPM, a chemotherapy regimen that combines cisplatin and pemetrexed has for long been the only FDA (U.S. Food and Drug Administration) – approved first-line treatment, which, disappointingly, elicits only modest efficacy due to prevalence of drug resistance and no validated treatment beyond front-line therapy has emerged. However, a recent phase 3 trial has showed that overall survival of MPM patients can be further improved by cisplatin/pemetrexed plus bevacizumab, an antibody against vascular endothelial growth factor (VEGF) (3).

Comprehensive genomic studies have revealed frequent deletions or loss-of-function mutations of tumor suppressor genes (TSGs) in MPM, most often cyclin-dependent kinase inhibitor 2A (*CDKN2A*), BRCA1 associated protein-1 (*BAP1*) and neurofibromatosis type 2 (*NF2*) (4, 5) (**Figure 1A**), for which direct targeting has proven difficult, contrasted to oncogene-driven malignancies that benefit from a vast majority of molecular targeted anti-cancer drugs. However, aberrant cancer genome rewires biochemical networks, leading to synthetic lethal or collateral vulnerabilities that are contextually linked with specific genetic alterations, providing alternative approaches for targeting TSG-driven MPM (**Figure 2**). Moreover, cancer-specific dependencies that evolve out of tumor deveoplment and drug resistance offers additional dimensions to expand therapeutic arsenal for MPM. Here, we review the current knowledge about collateral vulnerabilities and evolutionary dependencies in MPM, with an emphasis on the clinical implications for better treatment of the disease (**Figure 3** and **Table 1**).

COLLATERAL VULNERABILITIES CAUSED BY INACTIVATION OF TUMOR SUPPRESSORS

CDKN2A

The 9p21 locus harboring *CDKN2A* is frequently inactivated in mesothelioma (6). *Cdkn2a* inactivation is a key driver of MPM in a conditional mouse model (7), and *CDKN2A* loss is associated with shorter survival in patients with MPM (8). *CDKN2A* encodes two important tumor suppressor proteins via alternative open reading frames, $p16^{Ink4a}$ and $p14^{Arf}$ that govern the activity of the retinoblastoma (pRb) and p53 pathways, respectively (9). While the absence of $p16^{Ink4a}$, an inhibitor of cyclin-dependent kinases 4/6 (CDK4/6)-mediated phosphorylation of pRb, abrogates the G1/S cell-cycle arrest and promotes aberrant proliferation, functional loss of $p14^{Arf}$, a central negative regulator of mouse double minute 2 homolog (MDM2), suppresses apoptosis by escape from p53-mediated anti-tumor surveillance (**Figure 1B**).

Recent studies showed that *CDKN2A* deficiency render MPM cells particularly vulnerable to CDK4/6-targeted therapies, and that targeting PI3K further enhances the efficacy by precluding resistance to CDK4/6 inhibition (10). CDK4/6 inhibitors, e.g., palbociclib, ribociclib, and abemaciclib, are FDA-approved drugs that provide readily translatable therapeutics for MPM. Clinical trial for efficacy of Ribociclib in CDK4/6 pathway activated hematologic malignancies and solid tumors including MPM has been completed (NCT02187783). Abemaciclib as monotherapy is being investigated in MPM bearing $p16^{Ink4a}$ deficiency (Clinicaltrials.gov no. NCT03654833).

Strikingly, in around 30% MPM cases *CDKN2A* alterations co-occur with biallelic deletion in type I interferon (IFN-I; mainly IFN-α and IFN-β) locus. The IFN-I pathway plays a key antiviral role, suggesting that *CDKN2A*-deficient MPM might particularly benefit from oncolytic viral therapy (11), a novel anti-cancer strategy that exploits oncolytic viruses, which preferentially replicate in cancer but not in normal cells (12).

BAP1

BAP1, originally identified as an associated protein of the breast cancer susceptibility gene product BRCA1, is a nuclear deubiquitinase with ubiquitin carboxy-terminal hydrolase activity and contributes to the inhibition of E3 ligase function of BRCA1/BRAD during DNA damage response (13) (**Figure 1B**). Germline mutations in *BAP1* causes a predisposition syndrome with increased risk to renal cell carcinoma, MPM and uveal melanoma (14). *BAP1* is also frequently inactivated by somatic mutations and loss of the 3p21.1 locus in MPM (15) (**Figure 1A**). Other mechanisms leading to inactivation of *BAP1* includes chromosomal rearrangements, gene fusion and splice alterations (4).

As a component of the polycomb repressive deubiquitinase (PR-DUB) complex, *BAP1* deletion causes defects in homologous recombination (HR), contributed by failure to deubiquitinate histone H2A on chromatin, which eventually leads to accumulation of DNA mutations and chromosomal aberrations (16). BAP1 has also been shown to regulate cell cycle through interactions with transcription regulators such as host cell factor-1 (HCF-1) and E2F transcription factor 1 (E2F1) (17). As *BAP1* loss causes deficient HR, *BAP1*-mutant tumors were reported to be particularly addicted to alternative DNA repair pathways, e.g., PARP1-mediated ones (16, 18). However, the sensitivity of mesothelioma cells to PARP inhibitors may be independent of the *BAP1* status (19, 20), warranting further studies to investigate the BAP1/PARP intersection. Interestingly, TNF-related apoptosis-inducing ligand (TRAIL) has been shown highly effective for *BAP1*-deficient MPM, likely via modulating the PR-DUB activity (21).

The heterozygous germline *BAP1* mutations were reported to increase aerobic glycolysis, also known as the "Warburg effect," due to impaired mitochondrial respiration (22), suggesting a role for BAP1 in metabolism. Indeed, recent evidence has indicated that loss of *BAP1* promotes cellular adaptability to metabolic stress by impairing ER stress gene regulatory network (e.g., *ATF3* and *CHOP*) and ferroptosis via modulating SLC7AL11 (23, 24). Informed by these findings, signaling pathways that regulate metabolic stress might be promising targetable vulnerabilities in *BAP1*-deficient MPM.

BAP1 has also been implicated in chromatin modulation by interacting with ASXL1 and polycomb repressive complex 1 (PRC1) (25), and further preclinical evidence revealed that *BAP1* loss renders MPM sensitivity to histone deacetylases (HDACs) inhibitors (26). However, a large phase 3 trial of MPM ($n > 600$) with Vorinostat, an FDA-approved HDAC inhibitor, showed disappointing results (27). Importantly, recent studies indicate that *BAP1* loss in MPM prioritizes the enhancer of zeste homolog 2 (EZH2)-targeted therapy (28), suggesting that aberrant expression of EZH2, known to lead to uncontrolled cell proliferation and tumorigenesis (29), might be an inherent feature enabled by the suppression of BAP1.

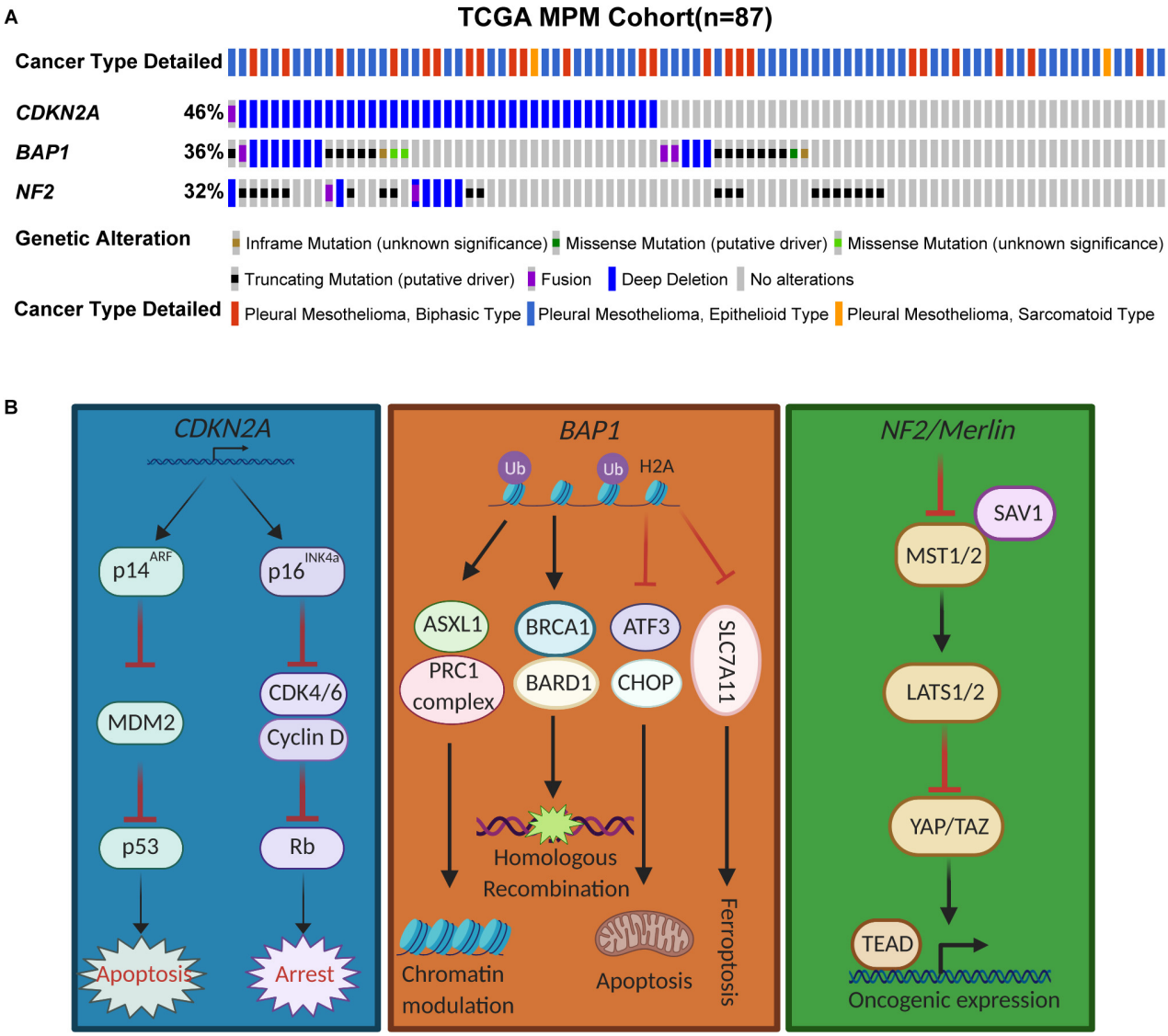

FIGURE 1 | Genomic landscape of *CDKN2A*, *BAP1*, and *NF2* in MPM. **(A)** Somatic mutations of *CDKN2A*, *BAP1*, and *NF2* in The Cancer Genome Atlas (TCGA) samples of MPM patients (*n* = 87). Data were downloaded from cBioPortal. **(B)** Schemtatic illustrating the pathways mediated by the tumor suppressor proteins.

Strikingly, a phase II study showed that tazemetostat, an oral EZH2 inhibitor, demonstrated promising clinical benefit in patients with malignant mesothelioma (30). Notably, it has been reported that sensitivity of uveal melanoma to EZH2 inhibitors is independent of *BAP1* mutational status (31), suggesting a lineage-specific effect of BAP1 on the activity of EZH2i (EZH2 inhibitors).

Surprisingly, several studies have revealed that *BAP1* mutaions in MPM are associated with favorable prognosis in patients (32, 33). One possible explanation is that BAP1 loss is accompanined with impaired DNA repair capacity, which enhances sensitivity to chemotherapy and thus may improve patients' outcome. In addition, *BAP1* deletion is linked with fewer chromosome arm gain and loss, as well as less somatic copy number alterations (SCNAs) (4, 5). Finally, *BAP1*-inactivated tumors might have a stronger activity of cytotoxic T cells due to increased interferon regulator factor 8 (IRF8) (5, 34).

NF2

NF2 encodes Merlin (moesin-ezrin-radixin-like protein) that mediates tumor suppression and contact-dependent inhibition through the Hippo pathway (35) (**Figure 1B**).

The Hippo pathway is evolutionally conserved that regulates organ size, tissue homeostasis and apoptosis, best characterized as a downstream transducer of Merlin/NF2 signaling (36). Merlin exerts tumor-suppressor function by translocating to the nucleus, where it promotes the degradation of two paralogous transcriptional co-activators, Yes-associated protein (YAP) and WWTR1 (WW domain containing transcription regulator 1)/transcriptional coactivator with PDZ-binding motif

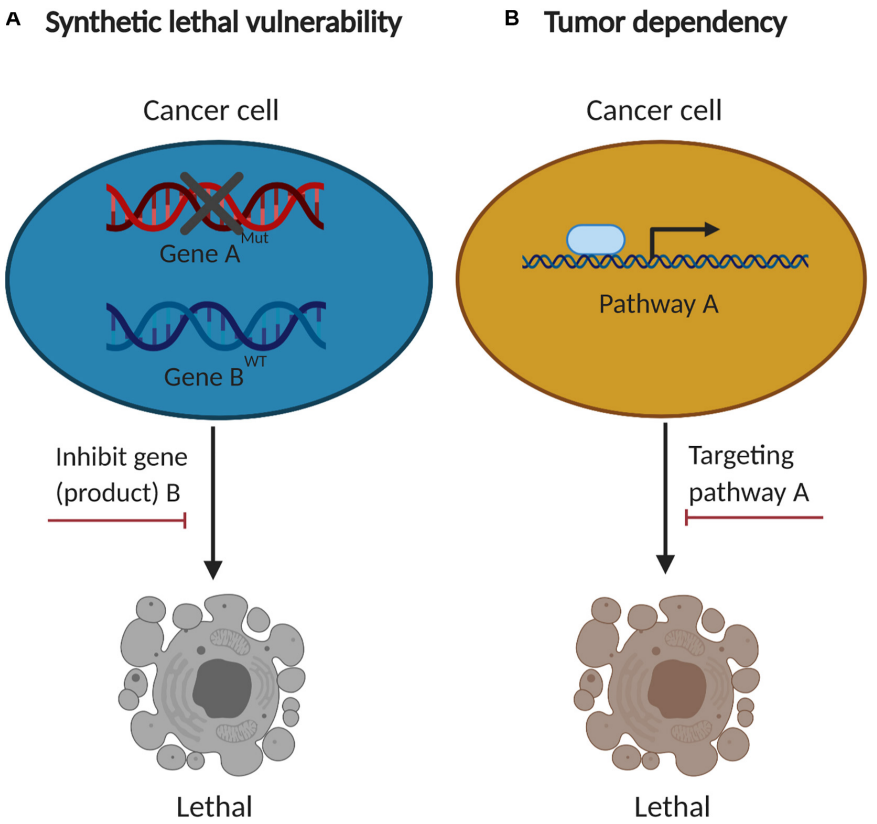

FIGURE 2 | The concept of synthetic lethal vulnerabilities and cancer-specific dependencies. **(A)** Cancer cells with functional loss of a tumor suppressor (gene "A") are contextually sensitive to inhibition of another gene product (gene "B"). **(B)** Cancer-specific dependencies co-opted by tumorigenesis are compelling therapeutic targets.

(TAZ) via the E3 ubiquitin ligase $CRL4^{DCAF1}$ (37). Merlin also activates serine/threonine kinase macrophage stimulating 1/2 (MST1/2), causing large tumor suppressor kinase 1/2 (LATS1/2)-dependent phosphorylation and degradation of YAP/TAZ (38). In addition to *NF2* mutations (**Figure 1A**), gene fusion and chromosomal rearrangements also result in nonfunctional NF2 and therefore inactivates Hippo pathway in MPM (4). In addition, other components of the Hippo pathway, such as *LATS2*, are also frequently inactivated in MPM (4), which inactivates the Hippo pathway as well. *LATS2* alterations (mutations, copy loss) occur in about 11% of MPM patients (5), and *LATS2*-deficient MPM might have similar vulnerabilities as those where the Hippo pathway is inactivated via other mechanisms. In particular, MPM with co-occuring mutations in *LATS2* and *NF2* has been reported to rely on an altered mTOR/PI3K/AKT signaling, and therefore highly sensitive to PF-04691502, a potent and selective oral inhibitor of PI3K and mTOR kinases (39). Finally, gene fusions involving *LIFR*, encoding a metastasis suppressor, was identified as an additional mechanism that inactivates Hippo pathway in MPM (4). The disrupted Hippo pathway constitutively activates oncogenic YAP/TAZ, which in turn transcriptionally activates cancer-promoting genes through interaction with TEA/ATTS domain (TEAD) transcription factors (40). Supporting this notion, verteporfin, an inhibitor against the YAP/TEAD interaction, exerts strong anti-MPM effects, suggesting that the YAP/TEAD axis might be a collateral vulnerability in *NF2*-deficient MPM (41). However, some other studies have shown that response to verteporfin can be independent on YAP activity (42, 43), indicating that the exact correlation between YAP activity and drug response remains to be determined. Further, inhibition of YAP/TAZ was reported to compensatorially activate the MAPK pathway and, as a consequence, co-targeting YAP/TAZ and MEK, a key constituent of the MAPK signaling cascade, synergizes in suppressing the growth of *NF2*-deficient tumors (44), providing a rational combination strategy for *NF2*-mutant MPM.

Finally, NF2/Merlin inactivation has been associated with upregulation of the focal adhesion kinase (FAK) activity in mesothelioma (45). FAK is a cytoplasmic tyrosine kinase that integrates signals from integrins and growth factor receptors to multiple cellular processes, ranging from cell proliferation and migration to renewal of cancer stem cells and resistance to chemotherapy (46). Merlin levels are predictive of sensitivity of MPM cells to the FAK inhibitor VS-4718 (47). Notably, the sensitivity to FAKi has also been shown independent of NF2/Merlin inactivation, and E-cadherin has been reported to be a predictive biomarker for FAK-targeted therapy (43, 48). Intriguingly, although a phase 1 study with FAK inhibitors

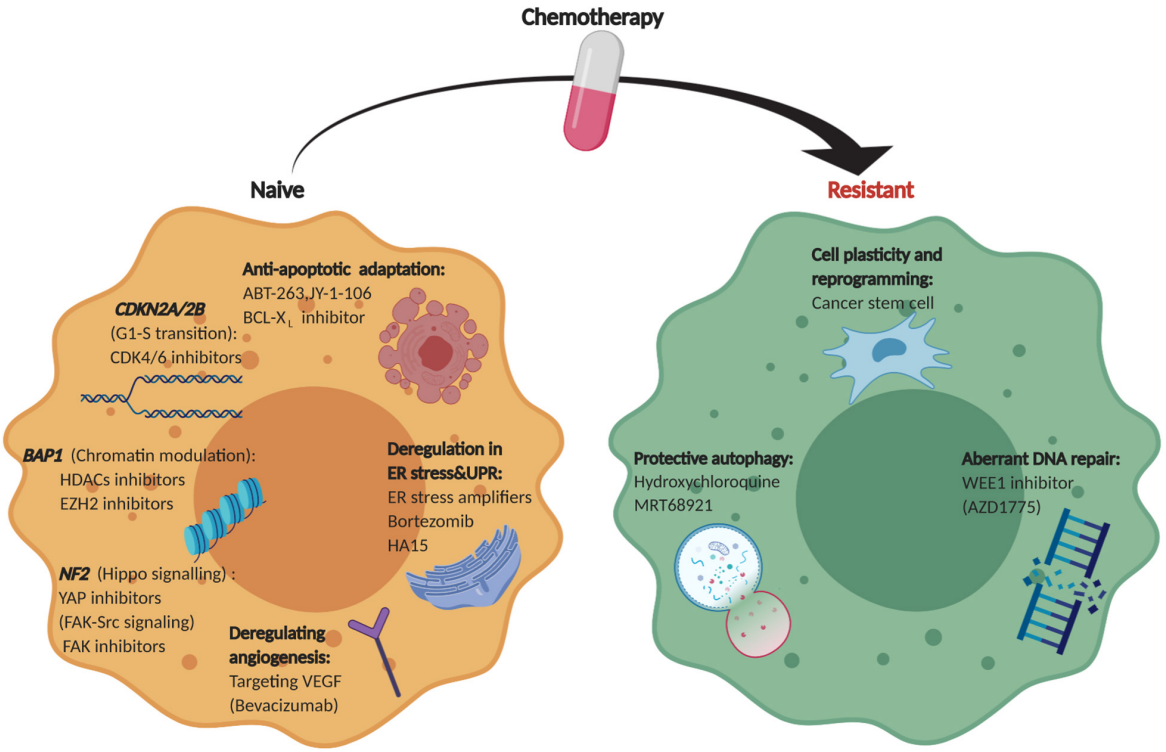

FIGURE 3 | Therapeutic landscape of MPM. An overview of collateral vulnerabilities and evolutionary dependencies identified in therapy-naïve and chemo-resistant MPM.

showed longer median progression-free survival (PFS) in patients with NF2-negative MPM than those with NF2-positive tumors (49), a large phase II COMMAND trial demonstrated that neither PFS nor OS (overall survival) was improved by FAK inhibitors in patients with NF2-low MPM and prior treatment with chemotherapy (50). Together, these results indicate that further investigations are required to establish the link between NF2 mutational status and response to FAK inhibition.

Other Genetic Alterations in MPM

In addition to the TSGs (*CDKN2A*, *BAP1*, and *NF2*) described above, several other genes, e.g., *TP53* (tumor protein p53), *LATS2*, *SETD2* (SET domain containing 2) and oncogenic changes in the *TERT* (telomerase reverse transcriptase) promoter are also altered by at non-negligible frequencies in MPM.

TP53 (encoding p53) is mutated in 6–16% MPM cases (51). Moreover, *CDKN2A* loss that depletes $p14^{Arf}$ and in turn releases MDM2 (mouse double minute 2 homolog), a negative regulator of p53, also inactivates p53, a key player in G1/S cell cycle regulation and apoptosis. We and others have shown that inactivation of *CDKN2A/2B* and *TP53* renders MPM cell particularly sensitive to G2 checkpoint inhibition, e.g., CBP501 (a peptide with G2 checkpoint-abrogating activity) and AZD1775 (selective inhibitor of the G2 checkpoint kinase WEE1) (52, 53).

Genetic alterations (mutation, gene fusion and splice alteration) in *SETD2*, an epigenetic tumor suppressor involved in histone methylation, are detected in more than 8% of MPM cases (4). *SETD2*-deficient MPM may respond favorably to inhibitors of histone methyltransferase EZH2 (54). In addition, synthetic lethality between *SETD2* deficiency and CDK7 inhibitor THZ1 has been recently reported in kidney cancer (55), although a similar efect on mesothelioma remains to be determined.

TERT promoter mutations, the first recurrent oncogenic muation identified in MPM, are frequent in MPM with sarcomatoid subtype and significantly associated with worse clinical outcome (56, 57). As expected, MPM cells carrying *TERT* promoter mutations show increased sensitivity to telomerase inhibition than those with wide-type *TERT*, indicating that targeting telomerase activity might be a promising treatment strategy for this MPM subset (57).

GENETIC AND PHARMACOLOGICAL DEPENDENCIES EVOLVE EN ROUTE TO CANCER DEVELOPMENT

In contrast with normal cells, tumor cells acquire unchecked cell growth en route to cancer development, a result of persistent activation of oncogenic pathways that concomitantly increases the level of cellular stresses (58). To deal with the stressful stimuli, cancer cells require the activity of a plethora of genes and cellular processes that become necessary to cancer cell survival.

TABLE 1 | Clinical trials investigating collateral vulnerabilities and evolutionary dependencies in MPM.

TSG/dependency	Target	Phase	No. patients	Results/trial status	Endpoint (experimental vs. control arms)	Biomarkers (Genetic or molecular)
CDKN2A/2B						
Ribociclib (NCT02187783)	CDK4/6	Phase 2	106	Completed (January, 2018)	ORR	CDK4/6, CCND1/3,CDKN2A
Abemaciclib (NCT03654833)	CDK4/6	Phase 2	120	Recruiting	DCR	p16INK4A
BAP1						
Vorinostat (27) (NCT00128102)	HDAC	Phase 3	661	Negative (November, 2011)	OS (30.7 vs. 27.1)	None
Tazemetostat (129) (NCT01897571)	EZH2	Phase 1	58	Positive (September, 2016)	Safety	None
Tazemetostat (NCT02860286)	EZH2	Phase 2	67	Completed (May, 2019)	Safety/DCR	BAP1
Niraparib (NCT03207347)	PARP1/2	Phase 2	57	Recruiting	ORR	BAP1/ DDR
NF2						
Defactinib (49) (NCT01870609)	FAK	Phase 2	372	Negative (January, 2016)	PFS (4.1 vs.4.0) OS (12.7 vs.13.6)	None
RTKs						
Erlotinib (NCT00039182)	EGFR	Phase 2	63	Negative (June, 2007)	OS	None
LY3023414 (NCT01655225)	PI3K/mTOR	Phase 1	156	Active Not Recruiting	Safety	None
Everolimus (NCT01655225)	mTOR	Phase 2	59	Negative (September, 2011)	4-month PFS	None
Tivantinib (NCT02049060)	Met	Phase1/2	31	Active Not Recruiting	Safety	None
Bemcentinib (NCT03654833)	AXL	Phase 2	120	Recruiting	DCR	None
Angiogenesis						
Thalidomide (76)	VEGF	Phase 3	222	Negative (December, 2009)	Progression (3.6 vs.3.5)	None
Bevacizumab (3) (NCT00651456)	VEGF	Phase 3	448	Positive (September, 2016)	OS (18.8 vs.16.1)	None
Deregulated UPR						
Bortezomib (130) (NCT00513877)	Proteasome	Phase 2	33	Negative (December, 2009)	CR/PR	None
Ganetespib (131) (NCT01590160)	HSP90	Phase1/2	27	Completed (November, 2019)	Safety PFS	None

Abbreviations: CR/PR, complete response/partial response; DCR, disease control rate; ORR, overall response rate; OS, overall survival; PFS, progression-free survival.

This phenomenon is referred to as non-oncogene addiction or cancer dependency (59), which represents the "Achilles' heel" of a specific type of cancers that can be therapeutically exploited without impairing normal cells. Recent studies have identified several genetic and pharmacological dependencies in MPM, covering various pathways involved in receptor kinase signaling, DNA damage repair and proteotoxic stress.

Receptor Tyrosine Kinases (RTKs)

Self-sufficiency in proliferative signaling, often through aberrant activation of receptor tyrosine kinases (RTKs), is a hallmark of cancer including MPM. Epidermal growth factor receptor (EGFR) is not mutated but overexpressed in MPM, leading to deregulation of EGFR signaling and aberrant activation of downstream pathways such as RAS/RAF/MAPK and PI3K/AKT/mTOR, which in turn promotes cell proliferation, tumor invasiveness and angiogenesis (60). Despite the high expression of EGFR, no clinical benefit was observed in MPM patients treated with erlotinib, an EGFR-specific inhibitor (61). Trametinib, a specific MEK inhibitor, exhibited anti-tumor effects in MPM, and displayed strong synergestic effects when combined with the FAK inhibitor GSK2256098 (62). Emerging evidence has also shown that multipoint targeting of PI3K/AKT/mTOR pathway is a promising strategy for therapeutic intervention of MPM (63). Although mTOR inhibition with specific inhibitors suppressed mesothelioma cell growth in pre-clinical models (64, 65), only limited clinical activity was observed in patients with advanced MPM (66). Additionally, preclinical studies identified MET and AXL as putative therapeutic targets in MPM (67, 68), and clinical trials testing Met-specific TKI (tivantinib; NCT02049060) and AXL-specific TKI (bemcentinib; NCT03654833) are ongoing.

Increasing evidence has indicated that other RTKs, including fibroblast growth factor receptor (FGFR) (69), insulin-like growth factor 1 receptor (IGF1R) (70), platelet-derived growth factor receptor (PDGFR) (71) and vascular endothelial growth factor receptor (VEGFR) are also aberrantly activated in MPM (72). In particular, preclinical studies have revealed that imatinib, a multi-target inhibitor of v-ABL, c-KIT and PDGFRβ, enhanced therapeutic effects of chemotherapeutic drugs (gemcitabine, pemetrexed) via AKT inactivation in malignant mesothelioma, which has encouraged the initiation of clinical trials (73, 74).

Given the crucial role of VEGF signaling in tumorigenesis, several anti-angiogenic drugs, including bevacizumab, thalidomide and nintedanib, have been investigated in MPM either alone or in combination with cisplatin plus pemetrexed over the past decade (75). To date, three randomized phase 3 studies that assess anti-angiogenic inhibitors in patients with MPM have been performed. In the 2013 study, no clinical benefit was observed for the addition of thalidomide to first-line chemotherapy (76), while the large randomized Mesothelioma Avastin Cisplatin Pemetrexed Study (MAPS) in 2016 showed that the triple combination of bevacizumab, cisplatin and pemetrexed significantly improved the median overall survival (OS) in MPM (3). More recently, another randomized phase 3 trial demonstrated no benefits of nintedanib addition compared to standard chemotherapy alone (77). The varied results highlight the need of further stratification for anti-angiogenic therapeutics in MPM.

Endoplasmic Reticulum (ER) Stress and Unfolded Protein Response (UPR)

The endoplasmic reticulum (ER) is the principal organelle monitoring proteostasis. Physiological and pathologic stimuli e.g., nutrient deprivation, aberrant glycosylation, oxidative stress and DNA damage, can disturb the ER environment, eliciting ER stress and unfolded protein response (UPR) (78). The UPR is mediated by three effector arms: double-stranded RNA-activated protein kinase (PKR)-like ER kinase (PERK), inositol-requiring enzyme 1α (IRE1α), and activating transcription factor 6 (ATF6) (79). At the steady state, the chaperone protein glucose-regulated protein 78 (GRP78, also known as BiP) binds and represses PERK, IRE1α and ATF6. When threatened by increased protein-folding demand (ER stress), BiP is released, which activates PERK, IRE1α, and ATF6, and in turn, their downstream effectors to alleviate proteotoxic stress placed on the ER and restore proteostasis in the ER (80).

Tumorigenesis entails aberrant proliferation, which is often confronted by limited oxygen supply and malfunctional vascularization, leading to increased demand for protein folding, assembly and transport (81). As such, the ER stress response or UPR is a cytoprotective mechanism that promotes survival and adaptation to adversary environment, which might render tumor cells particularly vulnerable to agents that further disturb ER stress. Indeed, therapeutic targeting of ER stress/UPR pathway has emerged as a promising strategy of cancer treatment (82). There is a positive correlation between expression of the ER stress-responsive phosphatase growth arrest and DNA damage 34 (GADD34) and differentiation status of mesothelial cells (83), suggesting that modulating ER stress might be effective for MPM. Consistently, we have recently showed that deregulated ER stress/UPR is a characteristic feature of MPM, and that therapeutic modulation of the signaling impairs the growth of MPM cells and overcomes resistance to standard chemotherapy (84, 85).

Anti-apoptotic Adaptation

Escape from apoptosis, a critical barrier of tumor development, is a prominent hallmark of cancer, including MPM. Apart from the loss of *TP53* tumor suppressor functions and increased expression of survival signals, overexpression of pro-survival B-cell lymphoma 2 (BCL-2) family proteins (BCL-2, BCL-X_L, MCL-1, BCL-W, BCL-B, BFL-1) that dampen apoptosis by sequestering pro-apoptotic activators (BAX, BIM, PUMA) is another pivotal strategy to circumvent apoptosis (86). In this scenario, cancer cells are thought to be "primed" for apoptosis, as they accumulate the pro-apoptotic activators (87). This trait can be exploited for cancer treatment by blocking specific or multiple pro-survival proteins with B-cell lymphoma

2 (Bcl-2) homology 3 (BH3)-mimetic therapy that overwhelms the anti-apoptotic defenses (88). In MPM, pro-survival or apoptosis suppression has been reported to be promoted by defects in core-apoptosis signaling (89), and the BH3 mimetic ABT-737 (targeting BCL-2/BCL-X_L/BCL-W) (90) and a pan-BCL-2 inhibitor (JY-1-106) are active against MPM cells (91, 92). More recently, BCL-X_L has been identified as a key anti-apoptotic mediator in MPM cells, further highlighting the promise of therapeutic strategies that modulate apoptotic threshold in MPM (93).

Tumor Microenvironment (TME)

A key feature of tumor microenvironment is hypoxia, which promotes acquisition of aggressive phenotypes. Emerging evidence has suggested that hypoxia-inducible factors (HIF-1α, -2α) play central roles in regulating hypoxic responses in MPM (94). HIF-1α/2α are transcription factors induced by hypoxic conditions, which in turn alter the expression of various target genes, such as those encoding the stem-like factor OCT4, anti-apoptotic BCL-2, glucose transporter 1 (GLUT1), VEGF, E-Cadherin and Vimentin, leading to the change of diverse biological functions, e.g., angiogenesis, anti-apoptosis, cell motility and metabolism (95, 96). Moreover, hypoxia is associated with increased genome instability by downregulating several DNA repair genes such as *MLH2*, *MSH2*, and *RAD51* (97). Thus, targeting tumor hypoxia might be a promising strategy for treating MPM.

A Roadmap to Cancer Dependencies

The Cancer Dependency Map Project (DepMap)[1] is dedicated to systematic identification of cancer-specific vulnerabilities for targeted therapy and further stratification based on genomic diversity and molecular characteristics for precision oncology (98). DepMap provides a range of information for the genetic landscape, expression profile, genetic essentiality and drug sensitivity across a broad spectrum of human cancers including MPM by incorporating The Cancer Cell Line Encyclopedia (CCLE), Project Achilles and PRISM, which may facilitate the prioritization of therapeutic targets for the development of precision cancer medicines.

EVOLUTIONARY VULNERABILITIES CO-OPTED BY CHEMOTHERAPY RESISTANCE

Despite decades of enormous efforts, cisplatin plus pemetrexed chemotherapy remains one of the few treatment options that achieve survival benefit in MPM. However, clinical evidence indicates that this combination therapy rarely achieves complete/durable clinical response in MPM patients due to drug resistance, intrinsic and/or acquired after initial treatment. Therefore, identification of therapeutic vulnerabilities to target chemoresistant MPM represents a significant yet unmet clinical challenge.

Cancer Cell Plasticity and Cancer Stem Cells

Cancer cells can shift at different cell states, most prominently the transition from epithelial to mesenchymal (EMT) or vice versa (MET). The epithelial state is a differentiated cell state while the mesenchymal more undifferentiated and reminiscent of cancer stem-like cells (CSCs), so coined as they recapitulate normal stem cells characterized by the capacity of self-renewal and differentiation. Cancer cell plasticity is an important process that generates CSCs and drives therapy resistance (99), partly due to relative dormancy of slowing cell-cycle kinetics, efficient DNA repair capacity and expression of multidrug-resistance transporters and resistance to apoptosis of the cells (100).

Putative CSCs identified in MPM express high levels of CD24, ABCG2, ABCB5 and OCT4 and confer drug resistance (101). We have showed that MPM cells populated as spheroids are highly resistant to standard chemotherapy (84). Mesothelioma stem cells (MSCs) might be responsible for tumor repopulation after chemoradiation in murine mesothelioma (102), and cisplatin-resistant, CSC-like subpopulations could be enriched by aldehyde dehydrogenase $(ALDH)^{high}$ and $CD44^{+}$ in mesothelioma cell lines (103). Despite the progress, the molecular mechanisms underlying cancer cell plasticity and the malignancy of CSCs remain incompletely understood.

Aberrant DNA Repair

The DNA damage response (DDR) synchronizes DNA repair and checkpoint signaling activation to arrest cell cycle progression (104). Compelling evidence suggests that DDR protects against genomic instability and affects responses to genotoxic agents (105), although loss of some elements involved in DNA repair pathways is predisposed to malignancy. Conversely, upregulated DDR signaling confers resistance to DNA-damaging chemotherapy and inhibitors targeting the altered pathways have the potential to revert resistance and augment the efficacy of conventional chemotherapy (106). MPM patients with germline mutations in *BAP1* or other DNA repair genes (*CHEK2*, *PALB2*, *BRCA2*, and *MLH1*) show increased sensitivity to cytotoxic chemotherapy due to impaired DDR (107). Moreover, the Fanconi anemia (FA)/BRCA2 pathway involved in the homologous recombination DNA repair has been shown to play a key role in MPM chemoresistance (108), and a potential link of deregulated G2/M checkpoint pathway with tumor progression and sensitivity to chemotherapeutic agent cisplatin has been proposed (109). Notably, p53 signaling is frequently inactivated in MPM (4, 51), a consequence of *TP53* mutaions (6–16% in MPM) and, more often, of inactivating alterations in *CDKN2A*, which depletes $p14^{Arf}$ and promotes proteasome-mediated degradation of p53. Consequently, p53 deficient MPM cells might have greater dependence on G2/M checkpoint to protect the toxicity of chemotherapy, and abrogation of the G2/M checkpoint activity,

[1]https://depmap.org/portal/depmap/

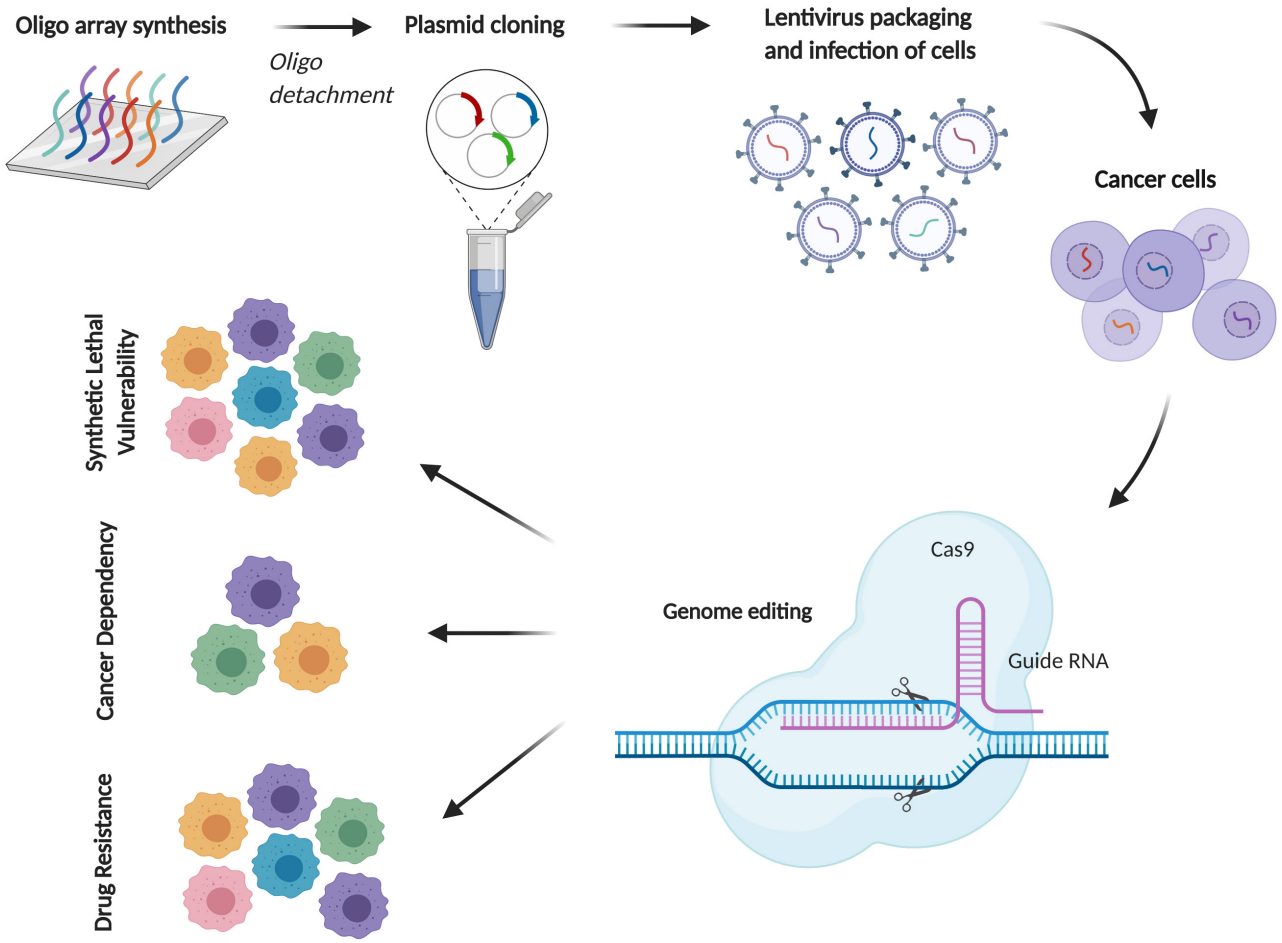

FIGURE 4 | CRISPR/Cas9 screening for cancer drug discovery in MPM. A schematic diagram of CRISPR/Cas9 screening using pooled sgRNA libraries. Depending on the experimental setting, comparison of sgRNA abundance with reference samples can identify essential genes for drug resistance, cell proliferation or context-dependent events (e.g., synthetic lethal vulnerability with specific mutations).

e.g., WEE1 inhibition, sensitizes MPM cells to chemotherapy (53, 110).

Autophagy

Macroautophagy (hereafter autophagy) is an evolutionally conserved catabolic process, whereby long-lived proteins and damaged organelles are sequestered in a double-membraned vesicle (autophagosome) and delivered to the lysosomes for degradation and recycled to fuel cellular growth (111). Autophagy is regulated by a variety of autophagy-associated genes (ATGs), with its contribution to cancer being controversial, as autophagy can be either pro-survival (oncogenic) or tumor suppressive at different stages of cancer progression (112). It has been reported that MPM cells display a generally high basal level of autophagy, which is critical for tumor growth (113). Albeit autophagic cell death (also known as type II programmed cell death) is potentially exploitable as an anticancer therapy, the vast majority of studies have demonstrated that autophagy is a protective mechanism linked with increased resistance to chemo and targeted therapy (114, 115). Supporting this notion, autophagy inhibition was shown to effectively improve chemosensitivity in mesothelioma (116).

SYSTEMATIC APPROACHES FOR CANCER DRUG DISCOVERY IN MPM

RNA Interference (RNAi) Screening

RNAi confers transient or stable gene silencing by small interfering RNAs (siRNA) or short hairpin RNAs (shRNA). Genome-wide screens with pooled shRNA libraries are widely pursued to identify cancer drivers and context-dependent events such as synthetic lethal interactions and collateral vulnerabilities (117). Experimentally, cancer cells infected with shRNA vectors that are specifically identified by molecular barcodes are monitored for growth and subsequently subjected to genomic DNA isolation, polymerase chain reaction (PCR) amplification and quantification of the molecular barcodes. Comparison of barcode abundance between experimental and reference samples, genes required for cancer cell proliferation can be identified.

Several groups have performed shRNA screes in MPM (118, 119), which however, surveyed relatively few cell lines and none represented the diversity of MPM. Although RNAi is ideal to evaluate the temporary gene disruption (e.g., to mimic the effect of cancer drugs), the utility of RNAi is limited by incomplete silencing, high off-target effects and stimulated immune response.

CRISPR/Cas9 Mediated Genome Editing

CRISPR/Cas9 (clustered regularly interspaced short palindromic repeats/CRISPR- associated 9) is a gene-editing technology allowing for rapid and accurate assessment of gene functions with fewer off-target effects compared to RNAi, which, due to its scalability, has emerged as an important tool for large-scale screens. Functional genomics using CRISPR have to date focused on identifying genes required by cancer cells for growth or response to a therapy, which provides a novel genetic tool to ascertain gene functions by customizing the single guide RNA (sgRNA) sequence. After transduced by pooled sgRNA library, the recipient cells become genetically heterogeneous, each one with a knockout of a different gene. Following culture and selection, e.g., drug treatment, cells expressing sgRNAs that target the genes essential for proliferation or drug resistance will die, thereby depleting them from residual tumor cells after culture or treatment (**Figure 4**).

CRISPR screens of genome and customized sgRNA libraries in numerous disease models have identified novel oncogenic drivers and cancer dependencies (120, 121), synthetic lethal interactions with mutant *RAS* and *BRAF* (122, 123) and mechanisms of resistance to anti-cancer drugs (124). Amenability to *in vivo* systems greatly enhances CRISPR applicability in clinically relevant settings (125). CRISPR-based functional genomics in MPM is still at its infancy, we recently screened MPM kinome and delineated that deregulated G2-M checkpoint activity dictates MPM response to chemotherapy (53).

Further Considerations in Systematic Approaches

MPM displays high heterogeneity, characterized by inter- and intratumor variability at cellular and molecular levels (4, 5, 126, 127). Heterogeneity represents a key mechanism underlying the poor response of MPM patients to current therapeutic interventions and is a challenge in systematic studies aimed at identifying effective treatment and curtailing drug resistance. Notably, cancer cell lines utilized predominantly in current RNAi- and CRISPR-based functional genomic studies poorly recapitulate the condition under which heterogeneous tumors arise and evolve. More instrumental *in vitro* models that more closely capture the heterogeneity of patient samples include cancer stem cells and patient-derived organoids (128). Moreover, *in vivo* models that recapitulate the cellular and genetic complexity of human cancer during tumor evolution and progression amid drug treatment, such as genetically engineered mouse models (GEMMs), syngeneic mouse models, and patient-derived xenografts (PDX), should be considered in systematic approaches (125). Despite in its infancy, future studies taken into account of tumor heterogeneity is likely the only way toward the development of precision medicine for MPM patients.

CONCLUDING REMARKS

Unlike many other solid tumors, MPM is characterized by overwhelming prevalence of loss of function alterations in tumor suppressor genes, for which direct pharmacological targeting proves difficult. However, collateral genotoxic, proteotoxic, and metabolic stresses caused by abnormal tumor genome or anti-cancer drugs can generate context-dependent vulnerabilities and dependencies, which has profound implications for alternate treatment of TSG-driven MPM. Recent studies have identified previously unappreciated vulnerabilities contextually linked with aberrant TSGs and dependencies acquired during cancer development and drug resistance, which provides unprecedented insights into MPM pathobiology and may bring about unprecedented hopes for the development of biomarker-guided precision medicine for the disease (**Figure 3**). Integrative molecular characterization enabled by large-scale RNA and proteomic profiling studies, partnered by functional genomics, holds importance to completely unfold the therapeutic landscape for MPM.

AUTHOR CONTRIBUTIONS

DX conducted literature search, drafted and revised the manuscript, and prepared the figures and table. HY and RS reviewed the manuscript. R-WP designed the study and revised and proofread the manuscript. All authors contributed to the article and approved the submitted version.

FUNDING

This work was funded by grants from the Swiss Cancer League/Swiss Cancer Research Foundation (#KFS-4851-08-2019 to R-WP) and Swiss National Science Foundation (310030_192648 to R-WP).

REFERENCES

1. Lin R-T, Takahashi K, Karjalainen A, Hoshuyama T, Wilson D, Kameda T, et al. Ecological association between asbestos-related diseases and historical asbestos consumption: an international analysis. *Lancet*. (2007) 369:844–9. doi: 10.1016/s0140-6736(07)60412-7
2. Stayner L, Welch LS, Lemen R. The worldwide pandemic of asbestos-related diseases. *Annu Rev Public Health*. (2013) 34:205–16. doi: 10.1146/annurev-publhealth-031811-124704
3. Zalcman G, Mazieres J, Margery J, Greillier L, Audigier-Valette C, Moro-Sibilot D, et al. Bevacizumab for newly diagnosed pleural mesothelioma in the Mesothelioma Avastin Cisplatin Pemetrexed Study (MAPS): a randomised, controlled, open-label, phase 3 trial. *Lancet*. (2016) 387:1405–14. doi: 10.1016/S0140-6736(15)01238-6

4. Bueno R, Stawiski EW, Goldstein LD, Durinck S, De Rienzo A, Modrusan Z, et al. Comprehensive genomic analysis of malignant pleural mesothelioma identifies recurrent mutations, gene fusions and splicing alterations. *Nat Genet*. (2016) 48:407–16. doi: 10.1038/ng.3520
5. Hmeljak J, Sanchez-Vega F, Hoadley KA, Shih J, Stewart C, Heiman D, et al. Integrative molecular characterization of malignant pleural mesothelioma. *Cancer Discov*. (2018) 8:1548–65. doi: 10.1158/2159-8290.CD-18-0804
6. Cheng JQ, Jhanwar SC, Klein WM, Bell DW, Lee WC, Altomare DA, et al. p16 alterations and deletion mapping of 9p21-p22 in malignant mesothelioma. *Cancer Res*. (1994) 54:5547–51.
7. Jongsma J, van Montfort E, Vooijs M, Zevenhoven J, Krimpenfort P, van der Valk M, et al. A conditional mouse model for malignant mesothelioma. *Cancer Cell*. (2008) 13:261–71. doi: 10.1016/j.ccr.2008.01.030
8. Jennings CJ, Murer B, O'Grady A, Hearn LM, Harvey BJ, Kay EW, et al. Differential p16/INK4A cyclin-dependent kinase inhibitor expression correlates with chemotherapy efficacy in a cohort of 88 malignant pleural mesothelioma patients. *Br J Cancer*. (2015) 113:69–75. doi: 10.1038/bjc.2015.187
9. Stott FJ, Bates S, James MC, McConnell BB, Starborg M, Brookes S, et al. The alternative product from the human CDKN2A locus, p14(ARF), participates in a regulatory feedback loop with p53 and MDM2. *EMBO J*. (1998) 17:5001–14. doi: 10.1093/emboj/17.17.5001
10. Bonelli MA, Digiacomo G, Fumarola C, Alfieri R, Quaini F, Falco A, et al. Combined inhibition of CDK4/6 and PI3K/AKT/mTOR pathways induces a synergistic anti-tumor effect in malignant pleural mesothelioma cells. *Neoplasia*. (2017) 19:637–48. doi: 10.1016/j.neo.2017.05.003
11. Delaunay T, Achard C, Boisgerault N, Grard M, Petithomme T, Chatelain C, et al. Frequent homozygous deletions of type I interferon genes in pleural mesothelioma confer sensitivity to oncolytic measles virus. *J Thorac Oncol*. (2020) 15:827–42. doi: 10.1016/j.jtho.2019.12.128
12. Pease DF, Kratzke RA. Oncolytic viral therapy for mesothelioma. *Front Oncol*. (2017) 7:179. doi: 10.3389/fonc.2017.00179
13. Nishikawa H, Wu W, Koike A, Kojima R, Gomi H, Fukuda M, et al. BRCA1-associated protein 1 interferes with BRCA1/BARD1 RING heterodimer activity. *Cancer Res*. (2009) 69:111–9. doi: 10.1158/0008-5472.CAN-08-3355
14. Carbone M, Yang H, Pass HI, Krausz T, Testa JR, Gaudino G. BAP1 and cancer. *Nat Rev Cancer*. (2013) 13:153–9. doi: 10.1038/nrc3459
15. Bott M, Brevet M, Taylor BS, Shimizu S, Ito T, Wang L, et al. The nuclear deubiquitinase BAP1 is commonly inactivated by somatic mutations and 3p21.1 losses in malignant pleural mesothelioma. *Nat Genet*. (2011) 43:668–72. doi: 10.1038/ng.855
16. Yu H, Pak H, Hammond-Martel I, Ghram M, Rodrigue A, Daou S, et al. Tumor suppressor and deubiquitinase BAP1 promotes DNA double-strand break repair. *Proc Natl Acad Sci USA*. (2014) 111:285–90. doi: 10.1073/pnas.1309085110
17. Eletr ZM, Wilkinson KD. An emerging model for BAP1's role in regulating cell cycle progression. *Cell Biochem Biophys*. (2011) 60:3–11. doi: 10.1007/s12013-011-9184-6
18. Parrotta R, Okonska A, Ronner M, Weder W, Stahel R, Penengo L, et al. A novel BRCA1-associated protein-1 isoform affects response of mesothelioma cells to drugs impairing BRCA1-mediated DNA repair. *J Thorac Oncol*. (2017) 12:1309–19. doi: 10.1016/j.jtho.2017.03.023
19. Srinivasan G, Sidhu GS, Williamson EA, Jaiswal AS, Najmunnisa N, Wilcoxen K, et al. Synthetic lethality in malignant pleural mesothelioma with PARP1 inhibition. *Cancer Chemother Pharmacol*. (2017) 80:861–7. doi: 10.1007/s00280-017-3401-y
20. Rathkey D, Khanal M, Murai J, Zhang J, Sengupta M, Jiang Q, et al. Sensitivity of mesothelioma cells to PARP inhibitors is not dependent on BAP1 but is enhanced by temozolomide in cells with high-Schlafen 11and low-MGMT expression. *J Thorac Oncol*. (2020) 15:843–59. doi: 10.1016/j.jtho.2020.01.012
21. Kolluri KK, Alifrangis C, Kumar N, Ishii Y, Price S, Michaut M, et al. Loss of functional BAP1 augments sensitivity to TRAIL in cancer cells. *eLife*. (2018) 7:e30224. doi: 10.7554/eLife.30224
22. Bononi A, Yang H, Giorgi C, Patergnani S, Pellegrini L, Su M, et al. Germline BAP1 mutations induce a Warburg effect. *Cell Death Differ*. (2017) 24:1694–704. doi: 10.1038/cdd.2017.95
23. Dai F, Lee H, Zhang Y, Zhuang L, Yao H, Xi Y, et al. BAP1 inhibits the ER stress gene regulatory network and modulates metabolic stress response. *Proc Natl Acad Sci USA*. (2017) 114:3192–7. doi: 10.1073/pnas.1619588114
24. Zhang Y, Shi J, Liu X, Feng L, Gong Z, Koppula P, et al. BAP1 links metabolic regulation of ferroptosis to tumour suppression. *Nat Cell Biol*. (2018) 20:1181–92. doi: 10.1038/s41556-018-0178-0
25. Campagne A, Lee MK, Zielinski D, Michaud A, Le Corre S, Dingli F, et al. BAP1 complex promotes transcription by opposing PRC1-mediated H2A ubiquitylation. *Nat Commun*. (2019) 10:348. doi: 10.1038/s41467-018-08255-x
26. Sacco JJ, Kenyani J, Butt Z, Carter R, Chew HY, Cheeseman LP, et al. Loss of the deubiquitylase BAP1 alters class I histone deacetylase expression and sensitivity of mesothelioma cells to HDAC inhibitors. *Oncotarget*. (2015) 6:13757–71. doi: 10.18632/oncotarget.3765
27. Krug LM, Kindler HL, Calvert H, Manegold C, Tsao AS, Fennell D, et al. Vorinostat in patients with advanced malignant pleural mesothelioma who have progressed on previous chemotherapy (VANTAGE-014): a phase 3, double-blind, randomised, placebo-controlled trial. *Lancet Oncol*. (2015) 16:447–56. doi: 10.1016/S1470-2045(15)70056-2
28. LaFave LM, Beguelin W, Koche R, Teater M, Spitzer B, Chramiec A, et al. Loss of BAP1 function leads to EZH2-dependent transformation. *Nat Med*. (2015) 21:1344–9. doi: 10.1038/nm.3947
29. Marchesi I, Bagella L. Targeting Enhancer of Zeste Homolog 2 as a promising strategy for cancer treatment. *World J Clin Oncol*. (2016) 7:135–48. doi: 10.5306/wjco.v7.i2.135
30. Zauderer MG, Szlosarek PW, Moulec SL, Popat S, Taylor P, Planchard D, et al. Safety and efficacy of tazemetostat, an enhancer of zeste-homolog 2 inhibitor, in patients with relapsed or refractory malignant mesothelioma. *J Clin Oncol*. (2020) 38:9058. doi: 10.1200/JCO.2020.38.15_suppl.9058
31. Schoumacher M, Le Corre S, Houy A, Mulugeta E, Stern MH, Roman-Roman S, et al. Uveal melanoma cells are resistant to EZH2 inhibition regardless of BAP1 status. *Nat Med*. (2016) 22:577–8. doi: 10.1038/nm.4098
32. Arzt L, Quehenberger F, Halbwedl I, Mairinger T, Popper HH. BAP1 protein is a progression factor in malignant pleural mesothelioma. *Pathol Oncol Res*. (2014) 20:145–51. doi: 10.1007/s12253-013-9677-2
33. Baumann F, Flores E, Napolitano A, Kanodia S, Taioli E, Pass H, et al. Mesothelioma patients with germline BAP1 mutations have 7-fold improved long-term survival. *Carcinogenesis*. (2015) 36:76–81. doi: 10.1093/carcin/bgu227
34. Broz ML, Binnewies M, Boldajipour B, Nelson AE, Pollack JL, Erle DJ, et al. Dissecting the tumor myeloid compartment reveals rare activating antigen-presenting cells critical for T cell immunity. *Cancer Cell*. (2014) 26:638–52. doi: 10.1016/j.ccell.2014.09.007
35. Li W, Cooper J, Karajannis MA, Giancotti FG. Merlin: a tumour suppressor with functions at the cell cortex and in the nucleus. *EMBO Rep*. (2012) 13:204–15. doi: 10.1038/sj.embor.2012.11
36. Yu F-X, Zhao B, Guan K-L. Hippo pathway in organ size control, tissue homeostasis, and cancer. *Cell*. (2015) 163:811–28. doi: 10.1016/j.cell.2015.10.044
37. Li W, Cooper J, Zhou L, Yang C, Erdjument-Bromage H, Zagzag D, et al. Merlin/NF2 loss-driven tumorigenesis linked to CRL4(DCAF1)-mediated inhibition of the hippo pathway kinases Lats1 and 2 in the nucleus. *Cancer Cell*. (2014) 26:48–60. doi: 10.1016/j.ccr.2014.05.001
38. Harvey KF, Zhang X, Thomas DM. The Hippo pathway and human cancer. *Nat Rev Cancer*. (2013) 13:246–57. doi: 10.1038/nrc3458
39. Tranchant R, Quetel L, Tallet A, Meiller C, Renier A, de Koning L, et al. Co-occurring mutations of tumor suppressor genes, LATS2 and NF2, in malignant pleural mesothelioma. *Clin Cancer Res*. (2017) 23:3191–202. doi: 10.1158/1078-0432.CCR-16-1971
40. Benhamouche S, Curto M, Saotome I, Gladden AB, Liu CH, Giovannini M, et al. Nf2/Merlin controls progenitor homeostasis and tumorigenesis in the liver. *Genes Dev*. (2010) 24:1718–30. doi: 10.1101/gad.1938710
41. Zhang WQ, Dai YY, Hsu PC, Wang H, Cheng L, Yang YL, et al. Targeting YAP in malignant pleural mesothelioma. *J Cell Mol Med*. (2017) 21:2663–76. doi: 10.1111/jcmm.13182
42. Dasari VR, Mazack V, Feng W, Nash J, Carey DJ, Gogoi R. Verteporfin exhibits YAP-independent anti-proliferative and cytotoxic

effects in endometrial cancer cells. *Oncotarget*. (2017) 8:28628–40. doi: 10.18632/oncotarget.15614
43. Tranchant R, Quetel L, Montagne F, De Wolf J, Meiller C, De Koning L, et al. Assessment of signaling pathway inhibitors and identification of predictive biomarkers in malignant pleural mesothelioma. *Lung Cancer*. (2018) 126:15–24. doi: 10.1016/j.lungcan.2018.10.015
44. White SM, Avantaggiati ML, Nemazanyy I, Di Poto C, Yang Y, Pende M, et al. YAP/TAZ inhibition induces metabolic and signaling rewiring resulting in targetable vulnerabilities in NF2-deficient tumor cells. *Dev Cell*. (2019) 49:425–43e9. doi: 10.1016/j.devcel.2019.04.014
45. Poulikakos PI, Xiao GH, Gallagher R, Jablonski S, Jhanwar SC, Testa JR. Re-expression of the tumor suppressor NF2/merlin inhibits invasiveness in mesothelioma cells and negatively regulates FAK. *Oncogene*. (2006) 25:5960–8. doi: 10.1038/sj.onc.1209587
46. Seguin L, Desgrosellier JS, Weis SM, Cheresh DA. Integrins and cancer: regulators of cancer stemness, metastasis, and drug resistance. *Trends Cell Biol*. (2015) 25:234–40. doi: 10.1016/j.tcb.2014.12.006
47. Shapiro IM, Kolev VN, Vidal CM, Kadariya Y, Ring JE, Wright Q, et al. Merlin deficiency predicts FAK inhibitor sensitivity: a synthetic lethal relationship. *Sci Transl Med*. (2014) 6:237ra68. doi: 10.1126/scitranslmed.3008639
48. Kato T, Sato T, Yokoi K, Sekido Y. E-cadherin expression is correlated with focal adhesion kinase inhibitor resistance in Merlin-negative malignant mesothelioma cells. *Oncogene*. (2017) 36:5522–31. doi: 10.1038/onc.2017.147
49. Soria JC, Gan HK, Blagden SP, Plummer R, Arkenau HT, Ranson M, et al. A phase I, pharmacokinetic and pharmacodynamic study of GSK2256098, a focal adhesion kinase inhibitor, in patients with advanced solid tumors. *Ann Oncol*. (2016) 27:2268–74. doi: 10.1093/annonc/mdw427
50. Fennell DA, Baas P, Taylor P, Nowak AK, Gilligan D, Nakano T, et al. Maintenance defactinib versus placebo after first-line chemotherapy in patients with merlin-stratified pleural mesothelioma: COMMAND-A double-blind, randomized, phase II study. *J Clin Oncol*. (2019) 37:790–8. doi: 10.1200/JCO.2018.79.0543
51. Quetel L, Meiller C, Assie JB, Blum Y, Imbeaud S, Montagne F, et al. Genetic alterations of malignant pleural mesothelioma: association with tumor heterogeneity and overall survival. *Mol Oncol*. (2020) 14:1207–23. doi: 10.1002/1878-0261.12651
52. Krug LM, Wozniak AJ, Kindler HL, Feld R, Koczywas M, Morero JL, et al. Randomized phase II trial of pemetrexed/cisplatin with or without CBP501 in patients with advanced malignant pleural mesothelioma. *Lung Cancer*. (2014) 85:429–34. doi: 10.1016/j.lungcan.2014.06.008
53. Xu D, Liang SQ, Yang H, Bruggmann R, Berezowska S, Yang Z, et al. CRISPR screening identifies WEE1 as a combination target for standard chemotherapy in malignant pleural mesothelioma. *Mol Cancer Ther*. (2020) 19:661–72. doi: 10.1158/1535-7163.MCT-19-0724
54. Joseph NM, Chen YY, Nasr A, Yeh I, Talevich E, Onodera C, et al. Genomic profiling of malignant peritoneal mesothelioma reveals recurrent alterations in epigenetic regulatory genes BAP1, SETD2, and DDX3X. *Mod Pathol*. (2017) 30:246–54. doi: 10.1038/modpathol.2016.188
55. Ding H, Zhao J, Zhang Y, Yu J, Liu M, Li X, et al. Systematic analysis of drug vulnerabilities conferred by tumor suppressor loss. *Cell Rep*. (2019) 27:3331–44e6. doi: 10.1016/j.celrep.2019.05.043
56. Tallet A, Nault JC, Renier A, Hysi I, Galateau-Salle F, Cazes A, et al. Overexpression and promoter mutation of the TERT gene in malignant pleural mesothelioma. *Oncogene*. (2014) 33:3748–52. doi: 10.1038/onc.2013.351
57. Pirker C, Bilecz A, Grusch M, Mohr T, Heidenreich B, Laszlo V, et al. Telomerase reverse transcriptase promoter mutations identify a genomically defined and highly aggressive human pleural mesothelioma subgroup. *Clin Cancer Res*. (2020) 26:3819–30. doi: 10.1158/1078-0432.CCR-19-3573
58. Solimini NL, Luo J, Elledge SJ. Non-oncogene addiction and the stress phenotype of cancer cells. *Cell*. (2007) 130:986–8. doi: 10.1016/j.cell.2007.09.007
59. Luo J, Solimini NL, Elledge SJ. Principles of cancer therapy: oncogene and non-oncogene addiction. *Cell*. (2009) 136:823–37. doi: 10.1016/j.cell.2009.02.024
60. Mezzapelle R, Miglio U, Rena O, Paganotti A, Allegrini S, Antona J, et al. Mutation analysis of the EGFR gene and downstream signalling pathway in histologic samples of malignant pleural mesothelioma. *Br J Cancer*. (2013) 108:1743–9. doi: 10.1038/bjc.2013.130
61. Garland LL, Rankin C, Gandara DR, Rivkin SE, Scott KM, Nagle RB, et al. Phase II study of erlotinib in patients with malignant pleural mesothelioma: a Southwest oncology group study. *J Clin Oncol*. (2007) 25:2406–13. doi: 10.1200/JCO.2006.09.7634
62. Mak G, Soria JC, Blagden SP, Plummer R, Fleming RA, Nebot N, et al. A phase Ib dose-finding, pharmacokinetic study of the focal adhesion kinase inhibitor GSK2256098 and trametinib in patients with advanced solid tumours. *Br J Cancer*. (2019) 120:975–81. doi: 10.1038/s41416-019-0452-3
63. Zhou S, Liu L, Li H, Eilers G, Kuang Y, Shi S, et al. Multipoint targeting of the PI3K/mTOR pathway in mesothelioma. *Br J Cancer*. (2014) 110:2479–88. doi: 10.1038/bjc.2014.220
64. Hartman ML, Esposito JM, Yeap BY, Sugarbaker DJ. Combined treatment with cisplatin and sirolimus to enhance cell death in human mesothelioma. *J Thorac Cardiovasc Surg*. (2010) 139:1233–40. doi: 10.1016/j.jtcvs.2009.06.027
65. Hoda MA, Mohamed A, Ghanim B, Filipits M, Hegedus B, Tamura M, et al. Temsirolimus inhibits malignant pleural mesothelioma growth in vitro and in vivo: synergism with chemotherapy. *J Thorac Oncol*. (2011) 6:852–63. doi: 10.1097/JTO.0b013e31820e1a25
66. Ou SH, Moon J, Garland LL, Mack PC, Testa JR, Tsao AS, et al. SWOG S0722: phase II study of mTOR inhibitor everolimus (RAD001) in advanced malignant pleural mesothelioma (MPM). *J Thorac Oncol*. (2015) 10:387–91. doi: 10.1097/JTO.0000000000000360
67. Cipriani NA, Abidoye OO, Vokes E, Salgia R. MET as a target for treatment of chest tumors. *Lung Cancer*. (2009) 63:169–79. doi: 10.1016/j.lungcan.2008.06.011
68. Ou WB, Corson JM, Flynn DL, Lu WP, Wise SC, Bueno R, et al. AXL regulates mesothelioma proliferation and invasiveness. *Oncogene*. (2011) 30:1643–52. doi: 10.1038/onc.2010.555
69. Marek LA, Hinz TK, von Massenhausen A, Olszewski KA, Kleczko EK, Boehm D, et al. Nonamplified FGFR1 is a growth driver in malignant pleural mesothelioma. *Mol Cancer Res*. (2014) 12:1460–9. doi: 10.1158/1541-7786.MCR-14-0038
70. Jacobson BA, De A, Kratzke MG, Patel MR, Jay-Dixon J, Whitson BA, et al. Activated 4E-BP1 represses tumourigenesis and IGF-I-mediated activation of the eIF4F complex in mesothelioma. *Br J Cancer*. (2009) 101:424–31. doi: 10.1038/sj.bjc.6605184
71. Kothmaier H, Quehenberger F, Halbwedl I, Morbini P, Demirag F, Zeren H, et al. EGFR and PDGFR differentially promote growth in malignant epithelioid mesothelioma of short and long term survivors. *Thorax*. (2008) 63:345–51. doi: 10.1136/thx.2007.085241
72. Strizzi L, Catalano A, Vianale G, Orecchia S, Casalini A, Tassi G, et al. Vascular endothelial growth factor is an autocrine growth factor in human malignant mesothelioma. *J Pathol*. (2001) 193:468–75. doi: 10.1002/path.824
73. Bertino P, Porta C, Barbone D, Germano S, Busacca S, Pinato S, et al. Preliminary data suggestive of a novel translational approach to mesothelioma treatment: imatinib mesylate with gemcitabine or pemetrexed. *Thorax*. (2007) 62:690–5. doi: 10.1136/thx.2006.069872
74. Bertino P, Piccardi F, Porta C, Favoni R, Cilli M, Mutti L, et al. Imatinib mesylate enhances therapeutic effects of gemcitabine in human malignant mesothelioma xenografts. *Clin Cancer Res*. (2008) 14:541–8. doi: 10.1158/1078-0432.CCR-07-1388
75. Scherpereel A, Wallyn F, Albelda SM, Munck C. Novel therapies for malignant pleural mesothelioma. *Lancet Oncol*. (2018) 19:e161–72. doi: 10.1016/s1470-2045(18)30100-1
76. Buikhuisen WA, Burgers JA, Vincent AD, Korse CM, van Klaveren RJ, Schramel FM, et al. Thalidomide versus active supportive care for maintenance in patients with malignant mesothelioma after first-line chemotherapy (NVALT 5): an open-label, multicentre, randomised phase 3 study. *Lancet Oncol*. (2013) 14:543–51. doi: 10.1016/S1470-2045(13)70125-6
77. Scagliotti GV, Gaafar R, Nowak AK, Nakano T, van Meerbeeck J, Popat S, et al. Nintedanib in combination with pemetrexed and cisplatin for chemotherapy-naive patients with advanced malignant pleural mesothelioma (LUME-Meso): a double-blind, randomised, placebo-controlled phase 3 trial. *Lancet Respir Med*. (2019) 7:569–80. doi: 10.1016/s2213-2600(19)30139-0
78. Yadav RK, Chae SW, Kim HR, Chae HJ. Endoplasmic reticulum stress and cancer. *J Cancer Prev*. (2014) 19:75–88. doi: 10.15430/JCP.2014.19.2.75

79. Senft D, Ronai ZA. UPR, autophagy, and mitochondria crosstalk underlies the ER stress response. *Trends Biochem Sci*. (2015) 40:141–8. doi: 10.1016/j.tibs.2015.01.002
80. Hetz C. The unfolded protein response: controlling cell fate decisions under ER stress and beyond. *Nat Rev Mol Cell Biol*. (2012) 13:89–102. doi: 10.1038/nrm3270
81. Clarke HJ, Chambers JE, Liniker E, Marciniak SJ. Endoplasmic reticulum stress in malignancy. *Cancer Cell*. (2014) 25:563–73. doi: 10.1016/j.ccr.2014.03.015
82. Hetz C, Chevet E, Oakes SA. Proteostasis control by the unfolded protein response. *Nat Cell Biol*. (2015) 17:829–38. doi: 10.1038/ncb3184
83. Dalton LE, Clarke HJ, Knight J, Lawson MH, Wason J, Lomas DA, et al. The endoplasmic reticulum stress marker CHOP predicts survival in malignant mesothelioma. *Br J Cancer*. (2013) 108:1340–7. doi: 10.1038/bjc.2013.66
84. Xu D, Liang SQ, Yang H, Luthi U, Riether C, Berezowska S, et al. Increased sensitivity to apoptosis upon endoplasmic reticulum stress-induced activation of the unfolded protein response in chemotherapy-resistant malignant pleural mesothelioma. *Br J Cancer*. (2018) 119:65–75. doi: 10.1038/s41416-018-0145-3
85. Xu D, Yang H, Yang Z, Berezowska S, Gao Y, Liang SQ, et al. Endoplasmic reticulum stress signaling as a therapeutic target in malignant pleural mesothelioma. *Cancers (Basel)*. (2019) 11:1502. doi: 10.3390/cancers11101502
86. Juin P, Geneste O, Gautier F, Depil S, Campone M. Decoding and unlocking the BCL-2 dependency of cancer cells. *Nat Rev Cancer*. (2013) 13:455–65. doi: 10.1038/nrc3538
87. Montero J, Letai A. Why do BCL-2 inhibitors work and where should we use them in the clinic? *Cell Death Differ*. (2018) 25:56–64. doi: 10.1038/cdd.2017.183
88. Merino D, Kelly GL, Lessene G, Wei AH, Roberts AW, Strasser A. BH3-mimetic drugs: blazing the trail for new cancer medicines. *Cancer Cell*. (2018) 34:879–91. doi: 10.1016/j.ccell.2018.11.004
89. Fennell DA, Rudd RM. Defective core-apoptosis signalling in diffuse malignant pleural mesothelioma: opportunities for effective drug development. *Lancet Oncol*. (2004) 5:354–62. doi: 10.1016/S1470-2045(04)01492-5
90. Mohiuddin I, Cao X, Fang B, Nishizaki M, Smythe WR. Significant augmentation of pro-apoptotic gene therapy by pharmacologic Bcl-xL down-regulation in mesothelioma. *Cancer Gene Ther*. (2001) 8:547–54. doi: 10.1038/sj.cgt.7700332
91. Barbone D, Ryan JA, Kolhatkar N, Chacko AD, Jablons DM, Sugarbaker DJ, et al. The Bcl-2 repertoire of mesothelioma spheroids underlies acquired apoptotic multicellular resistance. *Cell Death Dis*. (2011) 2:e174. doi: 10.1038/cddis.2011.58
92. Cao X, Yap JL, Newell-Rogers MK, Peddaboina C, Jiang W, Papaconstantinou HT, et al. The novel BH3 alpha-helix mimetic JY-1-106 induces apoptosis in a subset of cancer cells (lung cancer, colon cancer and mesothelioma) by disrupting Bcl-xL and Mcl-1 protein-protein interactions with Bak. *Mol Cancer*. (2013) 12:42. doi: 10.1186/1476-4598-12-42
93. Jackson MR, Ashton M, Koessinger AL, Dick C, Verheij M, Chalmers AJ. Mesothelioma cells depend on the anti-apoptotic protein Bcl-xL for survival and are sensitized to ionizing radiation by BH3-mimetics. *Int J Radiat Oncol Biol Phys*. (2019) 106:867–77. doi: 10.1016/j.ijrobp.2019.11.029
94. Kim MC, Hwang SH, Kim NY, Lee HS, Ji S, Yang Y, et al. Hypoxia promotes acquisition of aggressive phenotypes in human malignant mesothelioma. *BMC Cancer*. (2018) 18:819. doi: 10.1186/s12885-018-4720-z
95. Kaira K, Serizawa M, Koh Y, Takahashi T, Hanaoka H, Oriuchi N, et al. Relationship between 18F-FDG uptake on positron emission tomography and molecular biology in malignant pleural mesothelioma. *Eur J Cancer*. (2012) 48:1244–54. doi: 10.1016/j.ejca.2012.01.016
96. Nabavi N, Bennewith KL, Churg A, Wang Y, Collins CC, Mutti L. Switching off malignant mesothelioma: exploiting the hypoxic microenvironment. *Genes Cancer*. (2016) 7:340–54. doi: 10.18632/genesandcancer.124
97. Bristow RG, Hill RP. Hypoxia and metabolism. Hypoxia, DNA repair and genetic instability. *Nat Rev Cancer*. (2008) 8:180–92. doi: 10.1038/nrc2344
98. Tsherniak A, Vazquez F, Montgomery PG, Weir BA, Kryukov G, Cowley GS, et al. Defining a cancer dependency map. *Cell*. (2017) 170:564–76e16. doi: 10.1016/j.cell.2017.06.010
99. Shibue T, Weinberg RA. EMT, CSCs, and drug resistance: the mechanistic link and clinical implications. *Nat Rev Clin Oncol*. (2017) 14:611–29. doi: 10.1038/nrclinonc.2017.44
100. Abdullah LN, Chow EK. Mechanisms of chemoresistance in cancer stem cells. *Clin Transl Med*. (2013) 2:3. doi: 10.1186/2001-1326-2-3
101. Pasdar EA, Smits M, Stapelberg M, Bajzikova M, Stantic M, Goodwin J, et al. Characterisation of mesothelioma-initiating cells and their susceptibility to anti-cancer agents. *PLoS One*. (2015) 10:e0119549. doi: 10.1371/journal.pone.0119549
102. Wu L, Blum W, Zhu CQ, Yun Z, Pecze L, Kohno M, et al. Putative cancer stem cells may be the key target to inhibit cancer cell repopulation between the intervals of chemoradiation in murine mesothelioma. *BMC Cancer*. (2018) 18:471. doi: 10.1186/s12885-018-4354-1
103. Cortes-Dericks L, Froment L, Boesch R, Schmid RA, Karoubi G. Cisplatin-resistant cells in malignant pleural mesothelioma cell lines show ALDH(high)CD44(+) phenotype and sphere-forming capacity. *BMC Cancer*. (2014) 14:304. doi: 10.1186/1471-2407-14-304
104. Jackson SP, Bartek J. The DNA-damage response in human biology and disease. *Nature*. (2009) 461:1071–8. doi: 10.1038/nature08467
105. Curtin NJ. DNA repair dysregulation from cancer driver to therapeutic target. *Nat Rev Cancer*. (2012) 12:801–17. doi: 10.1038/nrc3399
106. Lord CJ, Ashworth A. The DNA damage response and cancer therapy. *Nature*. (2012) 481:287–94. doi: 10.1038/nature10760
107. Hassan R, Morrow B, Thomas A, Walsh T, Lee MK, Gulsuner S, et al. Inherited predisposition to malignant mesothelioma and overall survival following platinum chemotherapy. *Proc Natl Acad Sci USA*. (2019) 116:9008–13. doi: 10.1073/pnas.1821510116
108. Roe OD, Anderssen E, Sandeck H, Christensen T, Larsson E, Lundgren S. Malignant pleural mesothelioma: genome-wide expression patterns reflecting general resistance mechanisms and a proposal of novel targets. *Lung Cancer*. (2010) 67:57–68. doi: 10.1016/j.lungcan.2009.03.016
109. Romagnoli S, Fasoli E, Vaira V, Falleni M, Pellegrini C, Catania A, et al. Identification of potential therapeutic targets in malignant mesothelioma using cell-cycle gene expression analysis. *Am J Pathol*. (2009) 174:762–70. doi: 10.2353/ajpath.2009.080721
110. Indovina P, Marcelli E, Di Marzo D, Casini N, Forte IM, Giorgi F, et al. Abrogating G(2)/M checkpoint through WEE1 inhibition in combination with chemotherapy as a promising therapeutic approach for mesothelioma. *Cancer Biol Ther*. (2014) 15:380–8. doi: 10.4161/cbt.27623
111. Yang Z, Klionsky DJ. Eaten alive: a history of macroautophagy. *Nat Cell Biol*. (2010) 12:814–22. doi: 10.1038/ncb0910-814
112. Liu B, Wen X, Cheng Y. Survival or death: disequilibrating the oncogenic and tumor suppressive autophagy in cancer. *Cell Death Dis*. (2013) 4:e892. doi: 10.1038/cddis.2013.422
113. Echeverry N, Ziltener G, Barbone D, Weder W, Stahel RA, Broaddus VC, et al. Inhibition of autophagy sensitizes malignant pleural mesothelioma cells to dual PI3K/mTOR inhibitors. *Cell Death Dis*. (2015) 6:e1757. doi: 10.1038/cddis.2015.124
114. Sui X, Chen R, Wang Z, Huang Z, Kong N, Zhang M, et al. Autophagy and chemotherapy resistance: a promising therapeutic target for cancer treatment. *Cell Death Dis*. (2013) 4:e838. doi: 10.1038/cddis.2013.350
115. Levy JM, Thompson JC, Griesinger AM, Amani V, Donson AM, Birks DK, et al. Autophagy inhibition improves chemosensitivity in BRAF(V600E) brain tumors. *Cancer Discov*. (2014) 4:773–80. doi: 10.1158/2159-8290.CD-14-0049
116. Follo C, Cheng Y, Richards WG, Bueno R, Broaddus VC. Inhibition of autophagy initiation potentiates chemosensitivity in mesothelioma. *Mol Carcinog*. (2018) 57:319–32. doi: 10.1002/mc.22757
117. Whittaker SR, Theurillat JP, Van Allen E, Wagle N, Hsiao J, Cowley GS, et al. A genome-scale RNA interference screen implicates NF1 loss in resistance to RAF inhibition. *Cancer Discov*. (2013) 3:350–62. doi: 10.1158/2159-8290.CD-12-0470
118. Linton A, Cheng YY, Griggs K, Kirschner MB, Gattani S, Srikaran S, et al. An RNAi-based screen reveals PLK1, CDK1 and NDC80 as potential therapeutic

targets in malignant pleural mesothelioma. *Br J Cancer*. (2014) 110:510–9. doi: 10.1038/bjc.2013.731
119. Okonska A, Buhler S, Rao V, Ronner M, Blijlevens M, van der Meulen-Muileman IH, et al. Functional genomic screen in mesothelioma reveals that loss of function of BRCA1-associated protein 1 induces chemoresistance to ribonucleotide reductase inhibition. *Mol Cancer Ther*. (2020) 19:552–63. doi: 10.1158/1535-7163.MCT-19-0356
120. Li L, Ng SR, Colon CI, Drapkin BJ, Hsu PP, Li Z, et al. Identification of DHODH as a therapeutic target in small cell lung cancer. *Sci Transl Med*. (2019) 11:eaaw7852. doi: 10.1126/scitranslmed.aaw7852
121. Wang C, Vegna S, Jin H, Benedict B, Lieftink C, Ramirez C, et al. Inducing and exploiting vulnerabilities for the treatment of liver cancer. *Nature*. (2019) 574:268–72. doi: 10.1038/s41586-019-1607-3
122. Hart T, Chandrashekhar M, Aregger M, Steinhart Z, Brown KR, MacLeod G, et al. High-resolution CRISPR screens reveal fitness genes and genotype-specific cancer liabilities. *Cell*. (2015) 163:1515–26. doi: 10.1016/j.cell.2015.11.015
123. Wang T, Yu H, Hughes NW, Liu B, Kendirli A, Klein K, et al. Gene essentiality profiling reveals gene networks and synthetic lethal interactions with oncogenic Ras. *Cell*. (2017) 168:890–903e15. doi: 10.1016/j.cell.2017.01.013
124. Ruiz S, Mayor-Ruiz C, Lafarga V, Murga M, Vega-Sendino M, Ortega S, et al. A genome-wide CRISPR screen identifies CDC25A as a determinant of sensitivity to ATR inhibitors. *Mol Cell*. (2016) 62:307–13. doi: 10.1016/j.molcel.2016.03.006
125. Manguso RT, Pope HW, Zimmer MD, Brown FD, Yates KB, Miller BC, et al. In vivo CRISPR screening identifies Ptpn2 as a cancer immunotherapy target. *Nature*. (2017) 547:413–8. doi: 10.1038/nature23270
126. Blum Y, Meiller C, Quetel L, Elarouci N, Ayadi M, Tashtanbaeva D, et al. Dissecting heterogeneity in malignant pleural mesothelioma through histo-molecular gradients for clinical applications. *Nat Commun*. (2019) 10:1333. doi: 10.1038/s41467-019-09307-6
127. Oehl K, Vrugt B, Opitz I, Meerang M. Heterogeneity in malignant pleural mesothelioma. *Int J Mol Sci*. (2018) 19:1603. doi: 10.3390/ijms19061603
128. Boj SF, Hwang CI, Baker LA, Chio II, Engle DD, Corbo V, et al. Organoid models of human and mouse ductal pancreatic cancer. *Cell*. (2015) 160:324–38. doi: 10.1016/j.cell.2014.12.021
129. Italiano A, Soria JC, Toulmonde M, Michot JM, Lucchesi C, Varga A, et al. Tazemetostat, an EZH2 inhibitor, in relapsed or refractory B-cell non-Hodgkin lymphoma and advanced solid tumours: a first-in-human, open-label, phase 1 study. *Lancet Oncol*. (2018) 19:649–59.
130. Walter RFH, Sydow SR, Berg E, Kollmeier J, Christoph DC, Christoph S, et al. Bortezomib sensitivity is tissue dependent and high expression of the 20S proteasome precludes good response in malignant pleural mesothelioma. *Cancer Manag Res*. (2019) 11:8711–20. doi: 10.2147/CMAR.S194337
131. Fennell DA, Danson S, Woll PJ, Forster M, Talbot D, Child J, et al. Ganetespib in combination with pemetrexed-platinum chemotherapy in patients with pleural mesothelioma (MESO-02): a phase Ib trial. *Clin Cancer Res*. (2020):doi: 10.1158/1078-0432.CCR-20-1306 [Epub ahead of print].

Conflict of Interest: The authors declare that the research was conducted in the absence of any commercial or financial relationships that could be construed as a potential conflict of interest.

frontiers in Oncology

ORIGINAL RESEARCH
published: 13 November 2020
doi: 10.3389/fonc.2020.588563

The Impact on Outcome by Adding Bevacizumab to Standard Induction Chemotherapy Prior to Mesothelioma Surgery: A Retrospective Single Center Analysis

*Olivia Lauk[1], Karina Bruestle[1], Thomas Neuer[1], Bianca Battilana[1], Thi Dan Linh Nguyen[2], Thomas Frauenfelder[2], Rolf Stahel[3], Walter Weder[1], Alessandra Curioni-Fontecedro[3] and Isabelle Opitz[1]**

[1] Department of Thoracic Surgery, University Hospital Zurich, Zurich, Switzerland, [2] Institute of Diagnostic and Interventional Radiology, University Hospital Zurich, Zurich, Switzerland, [3] Department of Medical Oncology and Hematology, University Hospital Zurich, Zurich, Switzerland

OPEN ACCESS

Edited by:
Marco Lucchi,
University of Pisa, Italy

Reviewed by:
Jan P. Van Meerbeeck,
Ghent University, Belgium
Marcello Migliore,
University of Catania, Italy

***Correspondence:**
Isabelle Opitz
isabelle.schmitt-opitz@usz.ch

Specialty section:
This article was submitted to Thoracic Oncology, a section of the journal Frontiers in Oncology

Received: 29 July 2020
Accepted: 05 October 2020
Published: 13 November 2020

Citation:
Lauk O, Bruestle K, Neuer T, Battilana B, Nguyen TDL, Frauenfelder T, Stahel R, Weder W, Curioni-Fontecedro A and Opitz I (2020) The Impact on Outcome by Adding Bevacizumab to Standard Induction Chemotherapy Prior to Mesothelioma Surgery: A Retrospective Single Center Analysis. Front. Oncol. 10:588563. doi: 10.3389/fonc.2020.588563

Objectives: Adding bevacizumab, an anti-Vascular Endothelial Growth Factor (VEGF), to platinum-based chemotherapy/pemetrexed in 1st line treatment of advanced malignant pleural mesothelioma (MPM), significantly improved overall survival. However, increased high grade bleeding after operation was reported in patients with colorectal cancer who previously received bevacizumab. In the present analysis, we assessed for the first time the impact of adding bevacizumab to induction chemotherapy prior to surgery for mesothelioma patients.

Methods: Two hundred twenty-seven MPM patients, intended to be treated with induction chemotherapy followed by surgery at the University Hospital of Zurich between 2002 and December 2018, were included in the present analysis. After propensity score matching for gender, histology and age (1:3 ratio), data from 88 patients were analyzed. Sixty-six patients underwent induction chemotherapy (with cis-/carboplatin and pemetrexed: control group) alone and 22 patients underwent induction chemotherapy with the addition of bevacizumab (bevacizumab group) prior macroscopic complete resection (MCR). Perioperative and long-term outcome variables were analyzed.

Results: Patients undergoing combination treatment with bevacizumab had a significantly better response than with chemotherapy alone as assessed by modified RECIST (p=0.046). Intraoperative complications in the bevacizumab group (one patient), or in the control group (three patients) were not related to intraoperative bleeding. Postoperative transfusion of blood products occurred in a larger amount in the control group than in the bevacizumab group (p=0.047). Overall survival was not statistically different between both groups.

Conclusion: These initial data demonstrate that MCR can be performed safely after triple induction chemotherapy with bevacizumab without increased intra- and postoperative

bleeding complications. Response rates were significantly improved by the addition of bevacizumab.

Keywords: malignant pleural mesothelioma, anti-angiogenic therapy, bevacizumab, induction chemotherapy, macroscopic complete resection, pleurectomy/decortication

INTRODUCTION

Malignant pleural mesothelioma (MPM) is an aggressive cancer with poor outcome despite multimodality treatment (1, 2). The Mesothelioma Avastin Cisplatin Pemetrexed Study (MAPS)—a multicenter, randomized, controlled, clinical phase III trial-showed the improvement of survival by the addition of bevacizumab to standard chemotherapy cisplatin/carboplatin/pemetrexed in first line treatment for advanced MPM (survival 18.8 months [95% CI 15.9-22.6] vs. 16.1 months [95% CI 14.0–17.9]) (3).

Vascular endothelial growth factor (VEGF) represents a target for cancer treatment as anti-VEGF agents can induce a direct toxicity by decreasing neoplastic cell viability. Moreover they induce structural changes on tumor vasculature with increase in stability, perfusion and permeability leading to an augmented distribution of chemotherapeutic agents at the tumor site (4). A previous meta-analysis of 20 randomized controlled trials reported an overall increase in high grade bleeding in colorectal, renal and non-small cell lung cancer, as well as an increase in thrombotic events (5–7) in patients undergoing treatment with anti-VEGF agents.

OBJECTIVES

In the present analysis, we report for the first time, the perioperative and long-term outcome as well as chemotherapy response when bevacizumab is added to current standard platinum based induction chemotherapy for MPM patients undergoing subsequent macroscopic complete resection (MCR).

PATIENTS AND METHODS

This is an observational study of retrospective nature. The institutional database was searched for patients intended to be treated with induction chemotherapy followed by surgery (n=227) during the period 2002–2018. Some patients in both groups (bevacizumab and control group) were treated within our phase I and II trials of intracavitary application of cisplatin bound to a fibrin carrier (NCT01644994). Sixty-six patients were excluded due to missing data (n=35) or palliative therapy only (n=31). Propensity score matching (1:3 ratio), was performed in 161 patients based on age, gender, and histotype (see **Table 1**) between patients receiving induction chemotherapy (cisplatin/carboplatin/pemetrexed) with bevacizumab and induction chemotherapy (cisplatin/carboplatin/pemetrexed) (control group) followed by surgery. Follow-up was performed with computed tomography (CT) and positron emission tomography/computed tomography (PET/CT) scans in an alternating manner according to our institutional guidelines. This means a post-surgery quarterly clinical and radiological follow-up within the 1st year, bi-annual in the 2nd year, and from there on annually. A logistic regression model was fitted to obtain the propensity score with the application of bevacizumab as outcome and the three explanatory variables mentioned above to reduce potential sources of bias. The standardized mean difference was used to estimate the group differences, which is preferred over the sample size dependent t-test (see **Table 1**). The matching was performed without repetition of controls and a caliper distance within 0.2 times the standard deviation of the propensity scores was accepted as a match. For all cases obtaining bevacizumab three appropriate matches were found.

For statistical analysis, R-software version 3.5.3 was used. Continuous variables were analyzed with paired t-test and conditional logistic regression was performed for binary variables. A p value of <0.05 was considered as statistically significant. Missing data are reflected in the overall column in each table. Throughout the manuscript, due to the missing adjustment for multiple testing in this analysis, p values should be interpreted as descriptive.

Local ethics committee approval was given for analysis of the mesothelioma database (StV 29-2009, EK-ZH 2012-0094).

Staging and Induction Chemotherapy

Mesothelioma was diagnosed and staged as described previously (8). After completion of staging, patients received between two and seven cycles of induction chemotherapy either with cisplatin/carboplatin or carboplatin/pemetrexed with the addition of bevacizumab in 22 cases. In case of only two cycles applied, the chemotherapy was interrupted due to side effects and the patient proceeded to surgery. In case of seven cycles (n=1), the patient did not want to undergo surgery at first and decided at a later point to have surgery. The last cycle prior to surgery was conducted without bevacizumab. The decision for induction chemotherapy with the addition of bevacizumab was individually discussed for each patient at our interdisciplinary tumor-board based on the comorbidity profile of the patient (e.g. coagulation disorders).

Surgery and Intraoperative Blood Loss

Thirty-one patients underwent (extended) pleurectomy/decortication [(E)PD), 35 extrapleural pneumonectomy (EPP)] in the control group whereas in the bevacizumab group 21 patients underwent (E)PD and one patient EPP. P/D only was performed in four patients in the control group and none in the bevacizumab group. EPP and (E)PD were performed as already

TABLE 1 | Covariates before 1:3 matching (left) and after 1:3 matching (right).

Before 1:3 matching					After 1:3 matching				
Covariate	**Overall**	**Control group**	**Bevacizumab group**	**SMD**	**Covariate**	**Overall**	**Control group**	**Bevacizumab group**	**SMD**
n	**161**	**139**	**22**		**n**	**88**	**66**	**22**	
Gender, male (%)	139 (86.3)	121 (87.1)	18 (81.8)	0.145	**Gender, male (%)**	71 (80.7)	53 (80.3)	18 (81.8)	0.039
Histotype, epithelioid (%)	133 (82.6)	115 (82.7)	18 (81.8)	0.024	**Histotype, epithelioid (%)**	73 (83.0)	55 (83.3)	18 (81.8)	0.04
Age (median [range])	63 (33–76)	63 [33-76]	64.5 [50-76]	0.275	**Age (median [range])**	65 [40-76]	65 [40-76]	64.5 [50-76]	0.031

SMD, Standard mean difference. Sample size independent measure of group discrepancy.

described previously (8). The difference between EPD and P/D was that in EPD pericardium and/or diaphragm are additionally resected depending on the tumor spread. In uncertain cases this was decided under guidance of intraoperatively taken fresh frozen sections.

Blood loss during surgery as well as the amount of substituted erythrocyte concentrates were documented.

Further, hemoglobin, hematocrit and thrombocytes were measured on postoperative day (POD) 1 to 6; not all values were available for each day. Thirty- and 90-day mortality was reported as well as postoperative morbidity. Postoperative major morbidity included: complications necessitating reoperation, chylothorax, patch failure, empyema, bronchopleural fistula, thromboembolic events, and acute respiratory distress syndrome (ARDS). The number of thromboembolic events for each patient are reported in detail, in particular the time point of the events (before chemotherapy, after chemotherapy but before surgery, post-surgery and after adjuvant chemo-/radiotherapy).

mRECIST

Chemotherapy response was assessed by mRECIST in a restaging CT scan (9). The p-value was calculated *via* a McNemar test.

OS and PFS

Overall survival (OS) and progression free survival (PFS) probabilities were calculated with Kaplan Meier analysis and the difference between treatment groups was evaluated with a conditional long rank test. The median and 95% confidence interval were also determined using the Kaplan-Meier method. OS was calculated from start of induction chemotherapy until death or lost to follow up.

RESULTS

88 patients, receiving either induction chemotherapy (cisplatin/carboplatin/pemetrexed + bevacizumab) or induction chemotherapy (platinum based/pemetrexed) only, followed by surgery, were analyzed (**Figure 1**): 66 patients in the control group and 22 patients in the bevacizumab group [(see **Table 1**) after propensity score matching (1:3 ratio)]. Additionally, intracavitary chemotherapy was applied in nine patients of the control group and six patients of the bevacizumab group. Patient`s characteristics are shown in **Table 2**.

The overall median age in this present cohort was 65 years (range 40–76 years) and did not differ significantly between both groups. All patients underwent surgery in a median time of 41.5 days (6 weeks, range 15–155 days) after the last cycle of induction chemotherapy. The median number of cycles applied for all patients was 3 (range 2–7). One patient had surgery <20 days following the last cycle of chemotherapy based on his own wish. Two patients underwent surgery after >100 days; one due to other surgery and the other based on patient's wishes.

mRECIST

According to mRECIST criteria (9) there were no patients with progressive disease (PD) in the bevacizumab group

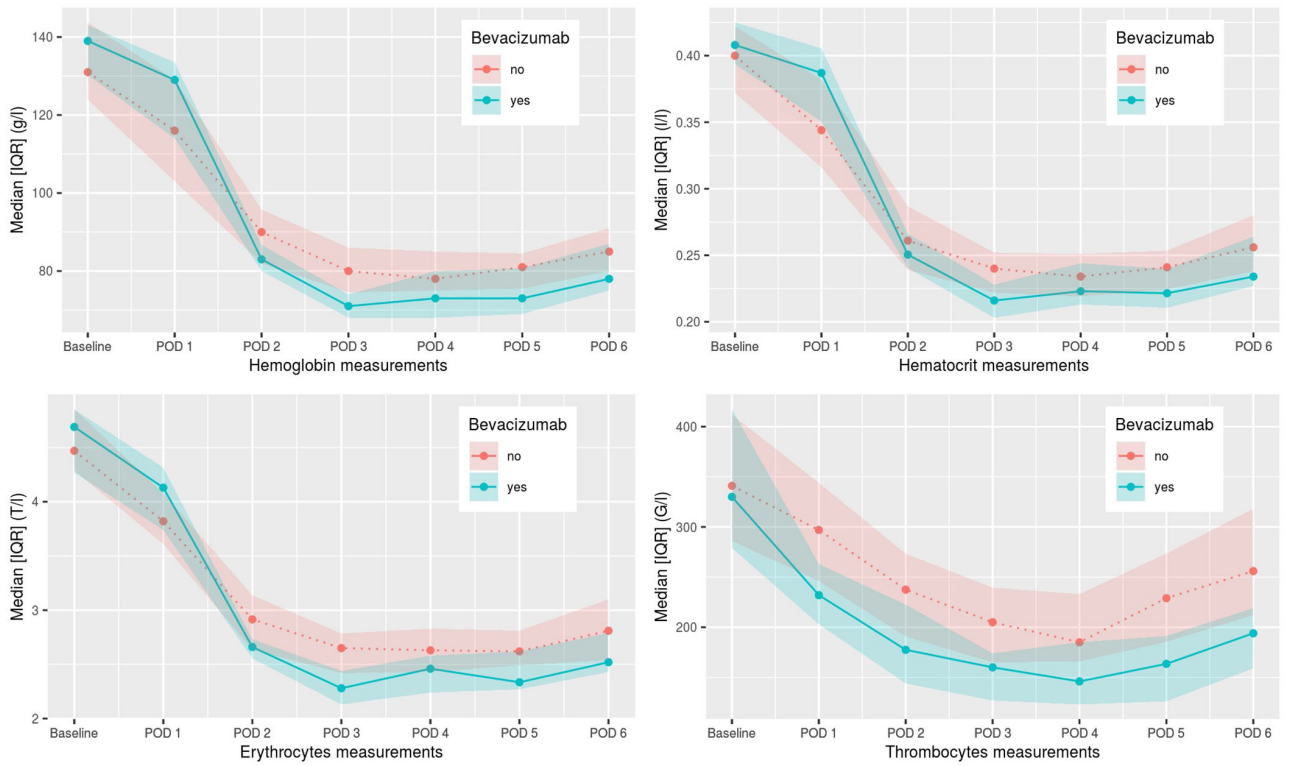

FIGURE 1 | Postoperative hemoglobin, hematocrit, erythrocyte, and thrombocyte values from day 1–6. POD, postoperative day.

TABLE 2 | Patients' characteristics.

Covariate n	Overall 88	Control group 66	Bevacizumab group 22	p-value
Age (median [range])	65 [40-76]	65 [40-76]	64.5 [50-76]	NS
Gender, male (%)	71 (80.7)	53 (80.3)	18 (81.8)	NS
Laterality of MPM, right (%)	53 (60.2)	37 (56.1)	16 (72.7)	NS
Epithelioid histotype (%)	73 (83.0)	55 (83.3)	18 (81.8)	NS
Induction chemotherapy				
Cisplatin (%)	78 (88.6)	60 (90.9)	18 (81.8)	NS
Carboplatin (%)	18 (20.5)	11 (16.7)	7 (31.8)	NS
Pemetrexed (%)	87 (98.9)	65 (98.5)	22 (100.0)	NS
Bevacizumab (%)	22 (25.0)	0 (0.0)	22 (100.0)	**<0.001**
Other (%)	1 (1.1)	1 (1.5)	0 (0.0)	NS
IMIG (%)	12 (13.6)	5 (7.6)	7 (31.8)	NS
IA	17 (19.3)	14 (21.2)	3 (13.6)	
IB	37 (42.0)	28 (42.4)	9 (40.9)	
II	11 (12.5)	10 (15.2)	1 (4.5)	
IIIA	9 (10.2)	8 (12.1)	1 (4.5)	
IIIB	2 (2.3)	1 (1.5)	1 (4.5)	
Type of surgery (%)				**<0.001**
EPD	52 (59.1)	31 (47.91)	21 (95.5)	
EPP	36 (40.9)	35 (53.0)	1 (4.5)	
P/D	4 (4.5)	4 (6.1)	0 (0.0)	

IMIG, International Mesothelioma Interest Group, (E)PD, extended pleurectomy/decortication; EPP, extrapleural pneumonectomy; P/D, pleurectomy/decortication. Bold, statistically significant with a p-value <0.05.

compared to 15 patients (22.7%) with PD in the control group following induction chemotherapy. Partial remission (PR) was observed in 23 cases in the control group (34.8%) and nine cases (40.9%) in the bevacizumab group. 28 cases (42.4%) in the control and 13 cases (59.1%) in the bevacizumab group, had stable disease (SD). The overall response rate was significantly better in the bevacizumab group with a p-value of 0.046.

Intraoperative complication rate and postoperative 30-day and 90-day mortality rate was not higher in the patient group undergoing induction chemotherapy with bevacizumab in comparison to the control group. Three patients in the control group and one patient in the bevacizumab group had intraoperative complications, none due to intraoperative bleeding. The number of postoperative transfusions of blood products was statistically different (p=0.047) in the two groups, with 68.2% of patients in the control group receiving postoperative blood products including mainly erythrocyte concentrates compared to 21 patients (95.5%) in the bevacizumab group (see **Table 3**). In few cases factor concentrate substitution, fresh frozen plasma, and thrombocyte concentrates were given as well. The postoperative hemoglobin, hematocrit, and thrombocyte values for both groups are shown in **Figure 1**. A statistically significant difference between the two groups was seen for hemoglobin values on POD 1-5, for hematocrit value on POD 5, for erythrocyte values on POD 2-6, for thrombocyte values on POD 1-6, and for hematocrit value on POD 1. For all these values, the bevacizumab group did better, except for the hematocrit value on POD 1. Additionally, no patient showed major pathological response and all patient still had microscopically vital tumor tissue in the definitive pathological tumor specimen.

Postoperative morbidity did not differ between the two groups with seven (32%) events in the bevacizumab group compared to 19 (29%) in the control group. Pulmonary embolism (PE) occurred in six patients in both groups (control 9.1% and bevacizumab group 27.3%; p=0.09). Three patients in each group had a thromboembolic event after induction therapy and one patient in each, for both groups, had a thromboembolic event either before chemotherapy started or after surgery, or after adjuvant chemo-/radiotherapy. There was no statistically significant difference in the occurrence of pulmonary embolism between the two groups in terms of time of occurrence and number of events. Occurrence of thromboembolic events according to the surgical procedure was as follow: EPP (n=1 for bevacizumab group vs n=1 for control group), EPD (n=5 vs. n=3), and P/D (n=0 vs. n=2).

Thirty-day mortality [control group n=1 (1.5%) and bevacizumab group n=1 (4.5%)] was not statistically different among the two groups as well as the 90-day mortality [control group n=4 (6.1%) and n=1 (4.5%, bevacizumab group)].

OS and PFS

At the time point of analysis, 17 patients in the control group and nine patients in the bevacizumab group were still alive (two lost to follow up in the control group). Overall median follow up time was 41 months.

Median OS was 23 months (95% CI: 17.3–33.5) in patients undergoing induction chemotherapy only and 22.4 months in patients receiving induction chemotherapy and bevacizumab (95% CI: 13.5 – not applicable; p = 0.55) with no censored cases. Median PFS was 11.5 months (95% CI: 11.1–14.5) for the control group and 11.4 months (95% CI: 10.1–18.2) in the bevacizumab group. No statistical difference in the two groups was observed in terms of OS and PFS. OS and PFS are shown in **Figure 2**.

DISCUSSION

In this propensity score matched retrospective analysis, 22 patients with malignant pleural mesothelioma were treated with induction chemotherapy consisting of platinum-based/pem with bevacizumab prior to surgery compared to 66 patients receiving standard induction chemotherapy with platinum-based/pemetrexed alone. Whereas the concept of a multimodality treatment is widely accepted and recommended for this disease, the timing of chemotherapy before or after surgery is discussed controversially (1, 10, 11) and currently investigated in a multicenter randomized phase II trial by the

TABLE 3 | Surgery dependent variables.

Covariate n	Overall 88	Control group 66	Bevacizumab group 22	p-value
Blood loss during surgery (ml, median [range])	1000 [200–5000]	1000 [200–5000]	850 [400–3000]	NS
Intraoperative blood products applied (pack) (%)	32 (36.4)	26 (39.4)	6 (27.3)	NS
Intraoperative ECs applied (ml, median [range])	300 [0–1500]	600 [0–1500]	300 [300–600]	NS
Intraoperative complications n (%)	4 (4.5)	3 (4.5)	1 (4.5)	NS
30 Day Mortality (%)	2 (2.3)	1 (1.5)	1 (4.5)	NS
90 Day Mortality (%)	5 (5.7)	4 (6.1)	1 (4.5)	NS
Postoperative hemorrhage necessitating reoperation (%)	3 (3.4)	2 (3.0)	1 (4.5)	NS
Postoperative morbidities (%)	87 (98.9)	65 (98.5)	22 (100)	NS
Postoperative transfusion of blood products (pack) (%)	66 (75.0)	45 (68.2)	21 (95.5)	**0.047**

NS, Not statistically significant. Bold, statistically significant with a p-value <0.05.

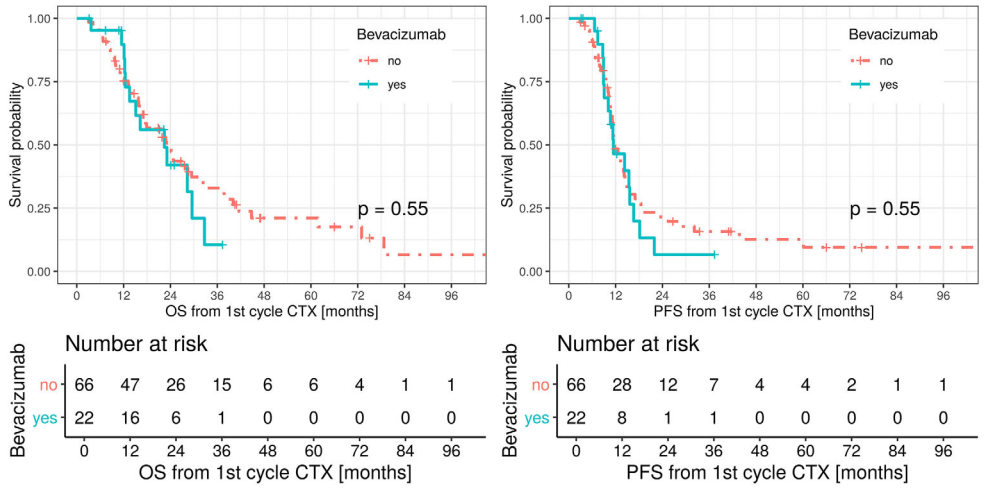

FIGURE 2 | Overall survival (OS, left figure), red line patients treated with platinum-based/pemetrexed for induction chemotherapy and green line patients treated with triplet induction chemotherapy including bevacizumab. Median OS in the bevacizumab group 22.4 months (LCL 95%, 13.5, UCL 95%, not applicable). Median OS in the control group 23 months (LCL 95%, 17.3, UCL 95%, 33.5). Progression free survival (PFS, right figure), red line patients treated with platinum-based/pemetrexed for induction chemotherapy and green line patients treated with triplet induction chemotherapy including bevacizumab.

EORTC [The European Organization for Research and Treatment of Cancer (NCT 02436733)].

In the present analysis, adding bevacizumab to standard induction chemotherapy did not significantly increase perioperative, in particular not bleeding, complications, although the proportional number of postoperative blood products and PE were higher compared to the control group. The small sample size and the lack of randomization do not allow to draw any conclusion to fully answer this question as well as the fact that PE is in general a known side effect of also the other chemotherapeutic agents. As known in other settings, these data suggest that a careful monitoring of embolic events in patients undergoing bevacizumab is warranted.

Bevacizumab is a well-known and potent VEGF inhibitor and has been mostly used as an additional chemotherapeutic agent, especially, in solid tumors including malignant mesothelioma, non-small cell lung cancer, colorectal cancer, renal cancer, and breast cancer. In malignant pleural mesothelioma patients, anti-VEGF has already been investigated in several studies for its safety and efficacy (7, 12). One of the main side effects is an increased risk of bleeding ranging from minor epistaxis to fatal hemorrhage (7, 13).

Despite evidence of an increased bleeding risk with bevacizumab, surgery was demonstrated to be safe in our cohort with negligible intra- and postoperative bleeding complications and even less intraoperative blood loss (750 ml vs. 900 ml) in the bevacizumab group, if a time interval of 2–7 weeks after induction chemotherapy, and the exclusion of bevacizumab in the last cycle prior to surgery, was respected. By recommendation of the Food and Drug Administration (FDA), bevacizumab should not be administered less than 28 days before and after a surgical intervention (14).

Numerical wise, in the bevacizumab group, more postoperative bleeding complications occurred although without statistical significance compared to the control group. Two cases in the control group necessitated reoperation due to hemorrhage after EPP and one case in the bevacizumab group. One hypothesis might be of a greater postoperative bleeding risk after EPP compared to (E)PD (8, 15, 16), but the risk for intra- or postoperative bleeding complications arise from the big bleeding surface after parietal pleurectomy part (being part of both procedures) (8).

Thirty-day- and 90-day mortality in the bevacizumab group was very low with one case each compared to the control group with one and four cases, respectively. The reasons for postoperative mortality were postoperative empyema, patch failure with gastric herniation, global respiratory insufficiency after EPP and necrotizing pancreatitis most probably related to the surgical procedure itself.

Due to the long observation period, there have been more EPP performed in the control group than in the (E)PD group. The learning curve for a better patient selection, the procedures and complication management might also play a significant role for the minor postoperative bleeding complication in the EPD/bevacizumab group. Additionally, preoperative selection criteria improved over the past years. On restaging imaging by contrast enhanced CT scan or even PET/CT after induction chemotherapy, there is a routine assessment of mRECIST, whereby patients are classified to their tumor response to induction chemotherapy.

A marginal statistically significant difference in terms of a better response was seen for the bevacizumab group. This improved response did not translate into a survival benefit.

There have been controversial debates on the efficacy and overall benefit of bevacizumab treatment, both for single agent use and for additive use (17–19). Several studies failed to show a clear benefit in OS or PFS when adding bevacizumab to standard therapy regimens for patients with malignant pleural mesothelioma. This may be due to the small sample sizes in the

cohorts (17–19). This holds true for our analysis, as PFS and OS in this cohort did not show a statistically significant improvement when bevacizumab was added to standard chemotherapy.

Our results are in line with the first randomized double blind placebo-controlled phase II trial by Kindler et al. where bevacizumab was added to gemcitabine and cisplatin and both PFS and OS did not differ statistically significant [PFS of 6.9 months compared to 6.0 months without bevacizumab (p=0.88) and an OS of 15.6 months compared to 14.7 months, respectively (p=0.91)] (17).

However, the MAPS trial, the first phase III trial investigated the addition of bevacizumab to standard chemotherapy regime proofed the beneficial effect of bevacizumab as the primary outcome of OS was significantly extended [median OS 18.8 months vs. 16.1 months without bevacizumab (p=0.0167)] (3).

We are aware of the limitations of this study mostly related to the retrospective nature, even though we performed a 1:3 propensity score match. Further stratification for more homogenous distribution of patients in each treatment group was not applicable due to the limited number of patients treated with additional bevacizumab and next to the rarity of this disease and the novel and not yet standardized use of bevacizumab. The outcomes overall survival, progression free survival, postoperative morbidity and mortality as well as response to chemotherapy given as mRECIST may be influenced by potential cofounders in this propensity score matched analysis. Due to the retrospective nature of this analysis, there might have been an improvement in patient management over the time, especially regarding the general learning curve and a transition from EPP to (E)PD, on top of the lower mortality rate in the latter group per se, in parallel to the patient allocation to bevacizumab in the later period.

The missing impact on overall survival additionally may be due to this antiangiogenic drug being newly used as an addition to standard induction chemotherapy (17–19). Secondly, the bevacizumab group was the one with more patients still alive, this was in the majority given to the fact, that those were the more recently treated patients. The scarce statistically significant difference in terms of response was seen in the bevacizumab group, as well as the missing benefit of overall survival underlies again that these results must been taken with caution due to the small sample size.

Despite all these new therapy approaches further trials are warranted to find an ideal therapy regimen balancing toxicity and efficacy. Although, increased bleeding risk with bevacizumab is a known common side effect, mesothelioma surgery can still be performed safely if appropriate time intervals are respected. We conclude, this therapy approach, including bevacizumab, warrants further investigation into a larger number of patients in order to finally characterize safety and outcome for patients with mesothelioma.

MEETING PRESENTATION

This work was presented at the 27th ESTS annual meeting in Dublin, Ireland on Tuesday 11th of June in the Chest Wall/ Diaphragm/Pleura Session XIII (2pm–3pm).

DATA AVAILABILITY STATEMENT

The raw data supporting the conclusions of this article will be made available by the authors, without undue reservation.

ETHICS STATEMENT

Local ethics committee approval was given for analysis of the mesothelioma database (StV 29-2009, EK-ZH 2012-0094). The patients/participants provided their written informed consent to have their anonymized data collected.

AUTHOR CONTRIBUTIONS

OL: Creation and presentation of the published work, specifically writing the initial draft (including substantive translation), Conceived and designed the analysis. KB: Drafted and provided critical revision of the article. TN: Performed the analysis, Conceived and designed the analysis. BB: Collected the data. TDLN: Drafted and provided critical revision of the article. TF: Drafted and provided critical revision of the article. AC-F: Drafted and provided critical revision of the article. RS: Drafted and provided critical revision of the article. WW: Drafted and provided critical revision of the article. IO: Oversight and leadership responsibility for the research activity planning and execution, including mentorship external to the core team. All authors contributed to the article and approved the submitted version.

FUNDING

This work was partially funded by the Swiss National Science Foundation (PP00P3_133657 and PP00P3_159269).

ACKNOWLEDGMENTS

We thank Dr. Chloe Spichiger for support in the formatting of the article.

REFERENCES

1. Baas P, Fennell D, Kerr KM, Van Schil PE, Haas RL, Peters S, et al. Malignant pleural mesothelioma: ESMO Clinical Practice Guidelines for diagnosis, treatment and follow-up. *Ann Oncol* (2015) 26 Suppl 5:v31–9. doi: 10.1093/annonc/mdv199
2. van Zandwijk N, Clarke C, Henderson D, Musk AW, Fong K, Nowak A, et al. Guidelines for the diagnosis and treatment of malignant pleural mesothelioma. *J Thorac Dis* (2013) 5:E254–307. doi: 10.3978/j.issn.2072-1439.2013.11.28
3. Zalcman G, Mazieres J, Margery J, Greillier L, Audigier-Valette C, Moro-Sibilot D, et al. Bevacizumab for newly diagnosed pleural mesothelioma in the

Mesothelioma Avastin Cisplatin Pemetrexed Study (MAPS): a randomised, controlled, open-label, phase 3 trial. *Lancet* (2016) 387:1405–14. doi: 10.1016/S0140-6736(15)01238-6
4. Fuso Nerini I, Cesca M, Bizzaro F, Giavazzi R. Combination therapy in cancer: effects of angiogenesis inhibitors on drug pharmacokinetics and pharmacodynamics. *Chin J Cancer* (2016) 35:61. doi: 10.1186/s40880-016-0123-1
5. Hang XF, Xu WS, Wang JX, Wang L, Xin HG, Zhang RQ, et al. Risk of high-grade bleeding in patients with cancer treated with bevacizumab: A meta-analysis of randomized controlled trials. *Eur J Clin Pharmacol* (2011) 67:613–23. doi: 10.1007/s00228-010-0988-x
6. Saltz LB. Bevacizumab in colorectal cancer: it should have worked. *Lancet Oncol* (2016) 17:1469–70. doi: 10.1016/S1470-2045(16)30213-3
7. Hapani S, Sher A, Chu D, Wu S. Increased risk of serious hemorrhage with bevacizumab in cancer patients: a meta-analysis. *Oncology* (2010) 79:27–38. doi: 10.1159/000314980
8. Kostron A, Friess M, Inci I, Hillinger S, Schneiter D, Gelpke H, et al. Propensity matched comparison of extrapleural pneumonectomy and pleurectomy/decortication for mesothelioma patients. *Interact Cardiovasc Thorac Surg* (2017) 24:740–6. doi: 10.1093/icvts/ivw422
9. Byrne MJ, Nowak AK. Modified RECIST criteria for assessment of response in malignant pleural mesothelioma. *Ann Oncol* (2004) 15:257–60. doi: 10.1093/annonc/mdh059
10. Vogelzang NJ, Rusthoven JJ, Symanowski J, Denham C, Kaukel E, Ruffie P, et al. Phase III study of pemetrexed in combination with cisplatin versus cisplatin alone in patients with malignant pleural mesothelioma. *J Clin Oncol* (2003) 21:2636–44. doi: 10.1200/JCO.2003.11.136
11. Voigt SL, Raman V, Jawitz OK, Bishawi M, Yang CJ, Tong BC, et al. The Role of Neoadjuvant Chemotherapy in Patients with Resectable Malignant Pleural Mesothelioma - An Institutional and National Analysis. *J Natl Cancer Inst* (2020) Online ahead of print.
12. Levin PA, Dowell JE. Spotlight on bevacizumab and its potential in the treatment of malignant pleural mesothelioma: the evidence to date. *Onco Targets Ther* (2017) 10:2057–66. doi: 10.2147/OTT.S113598
13. Gordon MS, Margolin K, Talpaz M, Sledge GW Jr, Holmgren E, Benjamin R, et al. Phase I safety and pharmacokinetic study of recombinant human anti-vascular endothelial growth factor in patients with advanced cancer. *J Clin Oncol* (2001) 19:843–50. doi: 10.1200/JCO.2001.19.3.843
14. Gordon CR, Rojavin Y, Patel M, Zins JE, Grana G, Kann B, et al. A review on bevacizumab and surgical wound healing: an important warning to all surgeons. *Ann Plast Surg* (2009) 62:707–9. doi: 10.1097/SAP.0b013e3181828141
15. Magouliotis DE, Tasiopoulou VS, Athanassiadi K. Updated meta-analysis of survival after extrapleural pneumonectomy versus pleurectomy/decortication in mesothelioma. *Gen Thorac Cardiovasc Surg* (2019) 67:312–20. doi: 10.1007/s11748-018-1027-6
16. Opitz I, Friess M, Kestenholz P, Schneiter D, Frauenfelder T, Nguyen-Kim TD, et al. A New Prognostic Score Supporting Treatment Allocation for Multimodality Therapy for Malignant Pleural Mesothelioma: A Review of 12 Years' Experience. *J Thorac Oncol* (2015) 10(11):1634–41. doi: 10.1097/JTO.0000000000000661
17. Kindler HL, Karrison TG, Gandara DR, Lu C, Krug LM, Stevenson JP, et al. Multicenter, double-blind, placebo-controlled, randomized phase II trial of gemcitabine/cisplatin plus bevacizumab or placebo in patients with malignant mesothelioma. *J Clin Oncol* (2012) 30:2509–15. doi: 10.1200/JCO.2011.41.5869
18. Ceresoli GL, Zucali PA, Mencoboni M, Botta M, Grossi F, Cortinovis D, et al. Phase II study of pemetrexed and carboplatin plus bevacizumab as first-line therapy in malignant pleural mesothelioma. *Br J Cancer* (2013) 109:552–8. doi: 10.1038/bjc.2013.368
19. Dowell JE, Dunphy FR, Taub RN, Gerber DE, Ngov L, Yan J, et al. A multicenter phase II study of cisplatin, pemetrexed, and bevacizumab in patients with advanced malignant mesothelioma. *Lung Cancer* (2012) 77:567–71. doi: 10.1016/j.lungcan.2012.05.111

Conflict of Interest: The authors declare that the research was conducted in the absence of any commercial or financial relationships that could be construed as a potential conflict of interest.

frontiers in Oncology

ORIGINAL RESEARCH
published: 10 March 2021
doi: 10.3389/fonc.2021.603223

BAP1-Altered Malignant Pleural Mesothelioma: Outcomes With Chemotherapy, Immune Check-Point Inhibitors and Poly(ADP-Ribose) Polymerase Inhibitors

Elizabeth Dudnik[1,2†], Jair Bar[2,3†], Assaf Moore[1], Teodor Gottfried[3], Mor Moskovitz[4], Julia Dudnik[5], Tzippy Shochat[6], Aaron M. Allen[1,2], Alona Zer[1,2], Ofer Rotem[1], Nir Peled[5,7], Damien Urban[2,3] and on behalf of the Israel Lung Cancer Group*

[1] Thoracic Cancer Service, Davidoff Cancer Center, Rabin Medical Center, Petah Tikva, Israel, [2] Sackler Faculty of Medicine, Tel Aviv University, Tel Aviv, Israel, [3] Thoracic Oncology Service, Institute of Oncology, Sheba Medical Center, Ramat Gan, Israel, [4] Thoracic Cancer Service, Rambam Health Care Campus, Haifa, Israel, [5] The Legacy Heritage Oncology Center, Soroka Medical Center, Beersheba, Israel, [6] Statistical Consulting Unit, Rabin Medical Center, Petah Tikva, Israel, [7] Ben Gurion University of Negev, Beersheba, Israel

OPEN ACCESS

Edited by:
Ticiana A. Leal,
University of Wisconsin-Madison,
United States

Reviewed by:
Luisella Righi,
University of Turin, Italy
Luciano Mutti,
Temple University, United States

***Correspondence:**
Elizabeth Dudnik
elizabetadu@clalit.org.il;
elizabeth.dudnik1603@gmail.com

†These authors have contributed equally to this work

Specialty section:
This article was submitted to Thoracic Oncology, a section of the journal Frontiers in Oncology

Received: 05 September 2020
Accepted: 05 January 2021
Published: 10 March 2021

Citation:
Dudnik E, Bar J, Moore A, Gottfried T, Moskovitz M, Dudnik J, Shochat T, Allen AM, Zer A, Rotem O, Peled N and Urban D (2021) BAP1-Altered Malignant Pleural Mesothelioma: Outcomes With Chemotherapy, Immune Check-Point Inhibitors and Poly(ADP-Ribose) Polymerase Inhibitors. Front. Oncol. 11:603223. doi: 10.3389/fonc.2021.603223

Objectives: Little is known regarding the outcomes of systemic treatments in BAP1-altered malignant pleural mesothelioma (MPM).

Materials and Methods: Forty five patients with MPM [group A: eight MPM patients with BAP1 inactivating mutation/copy number loss (FoundationOne® CDx/TEMPUSxT), selected from the electronic databases of four Israeli cancer centers (ICC); group B: 37 consecutive (years 2016–2018) MPM patients selected from the electronic databases of two ICC—of those six patients without a BAP1 alteration (group B1) and 31 patients not tested for BAP1 (group B2)] were analyzed for ORR, PFS (mRECIST), and OS with 1st-line platinum/pemetrexed+/−antiangiogenic drug (CT, n-28), immune check-point inhibitors (ICPi, n-16) and poly (ADP-ribose) polymerase inhibitors (PARPi, n-4). OS since diagnosis (OSDx) was assessed.

Results: There were no differences in ORR or mPFS with CT between the groups: ORR-50% *vs*. 47% *vs*. 50% *vs*. 47% (p>0.9), mPFS-9.1mo (95% CI, 1.2–16.1) *vs*. 9.2mo (95% CI, 2.9–13.3) *vs*. 7.2mo (95% CI, 2.3-NR) *vs*. 10.9mo (95% CI, 2.9–20.3) (p>0.8) in groups A, B, B1, and B2, respectively. There were no differences in ORR or mPFS with ICPi between the groups: ORR-0% *vs*. 27% *vs*. 33% *vs*. 25% (p>0.2), mPFS-2.5mo (95% CI, 1.4–3.7) *vs*. 3.0mo (95% CI, 1.3–10.5) *vs*. 2.0mo (95% CI, 1.9-NR) *vs*. 4.5mo (95% CI, 0.3–10.5) (p>0.3) in groups A, B, B1, and B2, respectively. In group A, no responses were seen with PARPi; mPFS with PARPi was 1.8mo (95% CI, 1.8-NR). OSDx was 98.3mo (95% CI, 9.7–98.3) *vs*. 19.4mo (95% CI, 9.7–47.3) *vs*. 18.8mo (95% CI, 8.5-NR) *vs*. 19.5mo (95% CI, 8.3–82.2) in groups A, B, B1, and B2, respectively (p>0.3).

Conclusions: BAP1-altered MPM, as compared to non-selected MPM, is characterized by similar efficacy of CT and ICPi. Numerically longer OS in BAP1-altered MPM may reflect favorable tumor biology. No responses were observed with PARPi.

Keywords: mesothelioma, BAP1, immune check-point inhibitors, PARP inhibitors, chemotherapy

INTRODUCTION

Mesothelioma is a rare malignancy that originates from mesothelial cells, mostly from the pleura [malignant pleural mesothelioma (MPM)], with an incidence rate of 1.4 cases per 100,000 population in the United States (1, 2). The median OS (mOS) of patients with MPM is in the range of 5.9–12.6 months, 1-year survival is 21–55%, and 5-year survival is about 10% (2–5).

The recommended 1st-line regimen for advanced MPM is a combination of cisplatin and pemetrexed (6). The addition of bevacizumab to cisplatin and pemetrexed results in a moderate survival improvement (7), and it is recommended for use in selected patients (8). Carboplatin-pemetrexed is also appropriate when cisplatin is contraindicated (8–12). This therapy is associated with an objective response rate (ORR) of 34–41%, median progression-free survival (mPFS) of 5.7–9.2 months, and mOS of 12.1–18.8 months (6, 7).

Immune checkpoint inhibitors (ICPi) in MPM were initially assessed after progression on platinum/pemetrexed. In this clinical scenario, therapy with programmed cell death-1 (PD-1) inhibitors or programmed cell death ligand-1 (PD-L1) inhibitors is associated with an ORR of 9–29%, mPFS of 2.6–4.1 months, and mOS of 11.5–12 months (13–17). Numerically better results have been demonstrated with the combination of a PD-1/PD-L1 inhibitor with a cytotoxic T-lymphocyte-associated protein 4 (CTLA-4) inhibitor (ORR of 25%, mPFS of 5.6–5.7 months, mOS of 16–16.6 months) (18, 19). Recently, the combination of nivolumab, a PD-1-inhibitor, with ipilimumab, a CTLA-4 inhibitor, in treatment-naïve MPM, resulted in better OS as compared to therapy with platinum/pemetrexed (20).

BRCA1 associated protein-1 (BAP1) is responsible for de-ubiquitination of histones and, as a result, protein transcription and cell cycle regulation (21), it also acts as a homologous recombination deoxyribonucleic acid (DNA) repair component found in the BRCA1/BARD1 complex (22). Pathogenic germline variants of BAP1 are associated with various malignancies, including mesothelioma (23–25); 1–7% of malignant mesotheliomas are attributable to a germline mutation in BAP1 (26–28). Additionally, between 20 and 64% of MPM harbor somatic inactivating aberrations in BAP1, including point mutations, copy number loss, and rearrangements (22, 26, 29–38). In MPM, the presence of either germline or somatic BAP1 aberration has been associated with prolonged OS in most of the genomic analyses performed (23, 27, 31, 34–37, 39, 40).

Little is known about the value of BAP1 alterations as potential predictive biomarkers and as targets for various systemic treatments in MPM. It has been hypothesized that BAP1-altered MPM are characterized by extremely high sensitivity to platinum-based chemotherapy—similarly to BRCA2-mutant ovarian cancer (41). This hypothesis was based on the assumption that BAP1-altered MPM cells cannot efficiently repair platinum-induced DNA cross-links. It has also been suggested that BAP1-altered MPM might be susceptible to poly (ADP-ribose) polymerase inhibitors (PARPi) (22, 42, 43). Mesotheliomas harboring BAP1 aberrations are characterized by elevated immune signaling and inflammatory tumor microenvironment (36, 44), and, therefore, may predict long-term responses with ICPi.

However, llittle is known regarding the clinical outcomes of the above-mentioned systemic treatments in BAP1-mutant MPM. We conducted this retrospective analysis, aiming to compare the clinical outcomes with platinum/pemetrexed+/−antiangiogenic drugs, ICPi and PARPi in patients with BAP1-altered MPM to outcomes in BAP1-wild type or non-selected MPM patients.

Abbreviations: AJCC, American Joint Committee on Cancer; BAP1, BRCA1 associated protein-1; CALGB, Cancer and leukemia group B; CI, confidence interval; CT, platinum/pemetrexed+/−antiangiogenic drug; CR, complete response; CTCAE, v. 4.03, Common Terminology Criteria for Adverse Events, version 4.03; CTLA-4, cytotoxic T-lymphocyte-associated protein 4; DNA, deoxyribonucleic acid; ECOG PS, Eastern Cooperative Oncology Group performance status; ed, electronic databases; EORTC, European Organization for Research and Treatment of Cancer; EPP, extra-pleural pneumonectomy; EZH2i, enhancer of zeste homolog 2 inhibitors; HDACi, histone deacetylase inhibitors; HR, hazard ratio; ICC, Israeli cancer centers; ICPi, immune check-point inhibitors; IHC, immunohistochemistry; IQR, interquartile range; MMR, mismatch repair; (m)OS, (median) overall survival; (m)PFS, (median) progression-free survival; MPM, malignant pleural mesothelioma; mRECIST, Modified Revised Response Evaluation Criteria in Solid Tumors; MSI, microsatellite instability; mut/Mb, mutations per megabase; NA, not determined/not available/not applicable; NR, not reached; ORR, objective response rate; OSDx, OS since diagnosis; PARPi, poly (ADP-ribose) polymerase inhibitors; PD, progressive disease; PD-1, programmed cell death-1; PD-L1, programmed cell death ligand-1; PR, partial response; SD, stable disease; SEER, States Surveillance Epidemiology and End Results; TMB, tumor mutational burden; TPS, tumor proportion score.

MATERIALS AND METHODS

Patient Selection and Group Assignment

Forty-three consecutive patients with histologically confirmed MPM diagnosed in January 2016–December 2018 were identified through electronic databases of two Israeli cancer centers (Davidoff Cancer Center, Rabin Medical Center, Beilinson Campus and Institute of Oncology, Sheba Medical Center, Tel HaShomer). Of the selected patients, 12 patients (28%) underwent next-generation sequencing of their tumors, and BAP1 tumor status has been determined. The selected patients were divided into group A (n-6; tumors with a BAP1

inactivating mutation/copy number loss) [BAP1 status was determined using FoundationOne® CDx (n-5) (45), or TEMPUSxT (n-1) (46)], and group B (n-37; tumors without a BAP1 alteration or tumors not tested for the presence of a BAP1 alteration). Patients in group B were further divided into group B1 (n-6; tumors without a BAP1 alteration) [BAP1 status was determined using FoundationOne® CDx (n-3) (45), FoundationOne® Liquid (n-1) (47), TEMPUSxT (n-1) (46), and GPS Cancer™ (n-1) (48)], and group B2 (n-31; tumors not tested for the presence of a BAP1 alteration). A search aiming at identifying additional patients with a BAP1-mutant MPM was performed within the Israeli Lung Cancer Group, and two additional patients meeting the above-mentioned criteria for inclusion in group A were identified [BAP1 mutation was diagnosed by FoundationOne® CDx in both cases (45)]. After adding these 2 patients, the study cohort reached 45 patients overall, of those: 8 patients in group A and 37 patients in group B (6 patients in group B1 and 31 patients in group B2).

Study Design and Assessments

Baseline demographic (including asbestos exposure and family history of MPM), clinical [including European Organization for Research and Treatment of Cancer (EORTC) prognostic score (3), Cancer and Leukemia Group B

(CALGB) prognostic score (4, 5), surgery and radiotherapy type, systemic treatment type] and pathologic characteristics [including histological type, PD-L1 expression, tumor mutational burden (TMB), MSI status/mismatch repair status (MMR)] were collected and compared between the groups.

PD-L1 assessment was done by immunohistochemistry (IHC) using 22C3 PharmDx antibody on either Dako 22C3 PD-L1 IHC platform (Dako, Carpinteria, CA) or Ventana's BenchMark XT platform (Ventana Medical Systems, Tucson, AZ) (49, 50). PD-L1 tumor proportion score (TPS), which is the percentage of tumor cells showing partial or complete membrane staining, was determined and classified as negative, intermediate, or high (TPS of <1%, 1–49%, and >=50%, respectively) (49). TMB was calculated according to either the FoundationOne® CDx algorithm (45, 47), TEMPUSxT algorithm (46), or GPS Cancer™ algorithm (48)—according to the next-generation sequencing platform used in each case. MSI status was determined using either the FoundationOne® CDx algorithm (45, 47), or TEMPUSxT algorithm (46), and reported as "MSI-high" and "MSI-stable." MMR status was assessed by IHC staining for MLH-1 (mouse, clone M1 Ventana), MSH-2 (mouse, G-219-1129 Ventana), MSH-6 (mouse, clone 44 Ventana or SP93 Cell Marque), and PMS-2 (rabbit, EPR 3947 Ventana) proteins on Ventana's BenchMark XT platform (Ventana Medical Systems, Tucson, AZ), and reported as "MMR deficient" or "MMR proficient."

ORR, PFS, and OS were assessed and compared for each different systemic treatment modality administered (platinum/pemetrexed chemotherapy, ICPi). For that purpose, only therapies administered for the treatment of advanced-stage disease were considered (neo-adjuvant/adjuvant systemic therapies were excluded from the analysis); for platinum-based combinations only 1st line treatments were analyzed (re-challenge with platinum-based combination were not included in the comparison). Additionally, OS since disease diagnosis (OSDx) was compared between the groups. In group A, ORR, PFS, and safety with PARPi were assessed. Univariate analyses of PFS and OS with platinum/pemetrexed+/−antiangiogenic drug, ICPi, and OSDx were performed using Cox proportional-hazards regression model.

ORR and PFS were assessed using Modified Revised Response Evaluation Criteria in Solid Tumors (mRECIST) used for response assessment in MPM (51); radiological assessment was done by the investigators. PFS was calculated from treatment initiation until disease progression or death; the outcome was censored if a patient was alive without known progression of the disease at the time of last follow-up. OS was calculated from the day of treatment initiation until death; the outcome was censored if a patient was alive at the time of last follow-up. OSDx was calculated similarly, since MPM diagnosis. Adverse events were graded using Common Terminology Criteria for Adverse Events, version 4.03 (CTCAE, v. 4.03) (52).

The study was conducted in accordance with the principles of good clinical practice, and institutional review board approval was obtained before the study initiation.

Statistical Analysis

The sample size was determined by the available patients meeting the inclusion criteria. The statistical analysis was generated using SAS Software, version 9.4 (53).

Categorical variables were presented by numbers and percentiles, medians and ranges were reported for continuous variables. Fisher's exact test and T-test were used to compare the baseline demographic, clinical, and pathologic characteristics. PFS and OS were assessed by the Kaplan-Meier method, with the log-rank test for the comparison. The Cox proportional-hazards regression model was used for univariate and multivariate OS analysis. All reported p-values are based on two-sided hypothesis tests.

RESULTS

Patient and Tumor Characteristics

Baseline demographic and clinical characteristics of patients are presented in **Table 1**. The vast majority of patients were mid-aged males, tumors with epithelioid histology predominated; the majority of tumors were "good-prognosis" by EORTC and CALGB prognostic scoring systems. Patients in group A were younger as compared to patients in group B1 (p-0.02). Patents in group A were more likely to have a family history of malignancy (including breast cancer, gastric cancer, cancer of ovary, lung cancer, colorectal cancer, and CNS tumors), and less likely to have an asbestos exposure—these differences were not statistically significant. Interestingly, 1 patient appearing to have no BAP1 alteration in his tumor (using GPS Cancer™) had a family history of MPM in two brothers. More patients in group A, as opposed to group B, received platinum-based

TABLE 1 | Baseline and treatment characteristics of patients with malignant pleural mesothelioma in Group A (BAP1 inactivating mutation/copy number loss, n-8) and Group B (without a BAP1 alteration/not tested, n-37).

	Group A (n-8)	Group B (n-37)	Group B1 (n-6)	Group B2 (n-31)	p value (between A and B)	p value (between A and B1)
Age at diagnosis, years (median, range)	65 (25-76)	69 (30-93)	77 (71-90)	66 (30-93)	0.2	0.02
Sex, n (%)					0.7	0.6
Female	3 (37)	11(30)	1 (17)	10 (32)		
Male	5 (63)	26 (70)	5 (83)	21 (68)		
Asbestos exposure, n (%)					0.4	1.0
Yes	2 (25)	15 (41)	2 (33)	13 (42)		
No	5 (63)	15 (41)	4 (67)	11 (35)		
NA	1 (12)	7(18)	0 (0)	7 (23)		
Family history of malignancy, n (%)	2 (25)	4 (11)	1 (17)	3 (10)	1.0	1.0
Histology, n (%)					0.6	1.0
Epithelioid	7 (88)	31 (85)	6 (100)	25 (82)		
Sarcomatoid	0 (0)	2 (5)	0 (0)	2 (6)		
Biphasic	1 (12)	2 (5)	0 (0)	2 (6)		
NA	0 (0)	2 (5)	0 (0)	2 (6)		
PD-L1 TPS, n (%)					0.03	0.08
>50%	2 (25)	0 (0)	0 (0)	0 (0)		
1-50%	0 (0)	5 (14)	3 (50)	2 (6)		
<1%	1 (12)	2 (5)	1 (17)	1 (3)		
NA	5 (63)	30 (81)	2 (33)	28 (91)		
MSI high/MMR deficient, n (%)	0 (0)*	0 (0)**	0 (0)	0 (0)	0.4	0.6
TMB, mut/Mb, (median, range)	3 (0.8-5)¥	1.5 (0-2)¥¥	1.5 (0-2)¥¥	NA	0.2	0.2
Stage at diagnosis (AJCC Cancer Staging, 8th edition), n (%)					0.5	0.5
I/II	1 (12)	9 (24)	2 (33)	7 (22.5)		
III	3 (38)	19 (51)	3 (50)	16 (52)		
IV	3 (38)	8 (22)	1 (17)	7 (22.5)		
NA	1 (12)	1 (3)	0 (0)	1 (3)		
ECOG PS at diagnosis, n (%)					1.0	1.0
0/1	7 (88)	30 (81)	6 (100)	24 (78)		
2/3/4	1 (12)	5 (14)	0 (0)	5 (16)		
NA	0 (0)	2 (5)	0 (0)	2 (6)		
EORTC prognostic scoring system					0.6	1.0
Good-prognosis	5 (63)	22 (59)	5 (83)	17 (55)		
Poor-prognosis	1 (12)	11 (30)	0 (0)	11 (35)		
NA	2 (25)	4 (11)	1 (17)	3 (10)		
CALGB prognostic scoring system					0.7	0.5
1/2	2 (25)	12 (32)	3 (50)	9 (29)		
3/4	2 (25)	18 (49)	2 (33)	16 (51)		
5/6	1 (12)	3 (8)	0 (0)	3 (10)		
NA	3 (38)	4 (11)	1 (17)	3 (10)		
Surgery, n (%)					1.0	1.0
EPP	1 (12)	6 (16)	1 (17)	5 (16)		
Decortication	1 (12)	1 (3)	0 (0)	1 (3)		
Pleurodesis	1 (12)	7 (18)	3 (50)	4 (13)		
Chest radiotherapy, n (%)					0.4	1.0
Definitive	2 (25)	9 (24)	1 (17)	8 (26)		
Palliative	3 (38)	7 (18)	2 (33)	5 (16)		
Platinum/pemetrexed+/-antiangiogenic agents (as a 1st-line treatment for advanced-stage disease), n (%)	8 (100)	20 (54)	4 (67)	16 (52)	0.02	0.2
ICPi, n (%)	3 (38)	13 (35)	4 (67)	9 (29)	1.0	0.6
PARPi, n (%)	4 (50)	0 (0)	0 (0)	0 (0)	0.0005	0.0005

AJCC, American Joint Committee on Cancer; CALGB, Cancer and Leukemia Group B; BAP1, BRCA1 associated protein-1; ECOG PS, Eastern Cooperative Oncology Group performance status score; EORTC, European Organization for Research and Treatment of Cancer; EPP, extra-pleural pneumonectomy; ICPi, immune check-point inhibitors; MMR, mismatch repair; MSI, microsatellite instability; mut/Mb, mutations per megabase; NA, not available/not applicable; PARPi, poly (ADP-ribose) polymerase inhibitors; PD-L1, programmeddeath ligand 1; TMB, tumor mutational burden; TPS, tumor proportion score.

**n-8; **n-6; ¥n-5; ¥¥n-4.*

chemotherapy as a 1st-line treatment for advanced disease (p-0.02); as expected, only patients in group A received PARPi. No other imbalances in terms of clinical baseline and treatment characteristics between the groups were observed.

From the molecular perspective, the proportion of tumors with TPS ≥50% was higher in group A as opposed to group B (25 *vs.* 0%, p-0.03); no significant differences in terms of tumor PD-L1 expression between groups A and B1 were observed. None of the 14 tumors tested (8 in group A, and 6 in group B) had an MSI-high or MMR-deficient status. Median TMB was low in either group and comprised three mutations per megabase (mut/Mb) (range, 0.8–5), 1.5 mut/Mb (range, 0–2), and 1.5 mut/Mb (range, 0–2) in 5, 4, and 4 tumors tested in groups A, B, and B1, respectively, without significant differences between the groups (**Table 1**). The BAP1 alterations diagnosed in patients in group A (all predicted to be associated with loss of BAP1 function(were as follows: BAP1 Q684 mutation, BAP1 F660fs*32 mutation, BAP1 loss exons 9-17 mutation, BAP1 E198fs*45 mutation, BAP1 splice site 375 + 2T>C mutation, BAP1 loss exons 13-17, BAP1 loss, BAP1 copy number loss. The co-existing alterations observed in BAP1-altered tumors are listed in **Table 2**. No matched normal DNA was available for the analysis. Upon our request, in seven out of eight cases included in group A, an additional review of the molecular data has been done by Foundation Medicine, however, no differentiation could be made with regards to somatic or germline nature of the BAP1 alterations (**Table 2**).

ORR, PFS, and OS With Platinum/Pemetrexed+/–Antiangiogenic Agents

Median follow-up since diagnosis of MPM was 18.7 months [interquartile range (IQR), 10.2–31.8], 12.4 months (IQR, 7.8–29.5), 14.7 months (IQR, 8.5–18.8), and 11.2 months (IQR, 7.5–31.2) in groups A, B, B1, and B2, respectively.

Twenty-eight patients [8 patients (100%) in group A, 20 patients (54%) in group B, 4 patients (67%) in group B1, and 16 patients (52%) in group B2] were treated with 1st-line platinum/pemetrexed chemotherapy. Of those, nine patients [five patients (62% of receiving platinum/pemetrexed) in group A and four patients (20% of receiving platinum/pemetrexed) in group B (including 1 patient in group B1 and three patients in group B2)] received chemotherapy in combination with bevacizumab. Two additional patients in group B (of those, 1 patient in group B1 and 1 patient in group B2) received 1st-line platinum/pemetrexed chemotherapy+/– nintedanib within the LUME-Meso clinical trial (ClinicalTrials.gov Identifier: NCT01907100).

In group A, four patients (50%) had a partial response (PR), three patients (38%) had stable disease (SD), and one patient (12%) had disease progression (PD). In group B, one patient (5%) developed complete response (CR), eight patients (42%) developed PR, seven patients (37%) experienced SD, three patients (16%) had PD, and one patient was not evaluable for response assessment (the treatment was stopped before radiological assessment was done). In group B1, two patients

TABLE 2 | BAP1 alterations and co-existing genomic alterations, TMB and MSI status in patients with advanced BAP1 - altered MPM.

Patients	BAP1 alteration	Somatic/germline nature of BAP1 alteration	Co-existing genomic alterations	TMB, muts/Mb	MSI
#1	BAP1 Q684	NA	CDKN2A/B loss; NOTCH3 R1893	4	MS-stable
#2	BAP1 F660fs*32	NA The sample failed the copy BAP1 number quality metrics for SGZ calling, whereas somatic/germline calling was still unavailable with manual review	MLL2 splice site 14382+1G>T	NA	NA
#3	BAP1 loss exons 9-17	NA Somatic/germline calling is not available for copy number alteration events	NF2 W74; CDKN2A p16INK4a R80* and p14ARF P94L; CREBBP complex rearrangement	3	MS-stable
#4	BAP1 E198fs*45	NA The sample failed the copy number quality metrics for SGZ calling, whereas somatic/germline calling was still unavailable with manual review	DNMT3A D529fs*16	NA	NA
#5	BAP1 splice site 375+2T>C	NA	HGF amplification; CDKN2A/B loss; PBRM1 deletion exons 8-12	5	MS-stable
#6	BAP1 loss exons 13-17	NA Somatic/germline calling is not available for copy number alteration events	TP53 splice site 9209_993+70del153	1	MS-stable
#7	BAP1 loss	NA Somatic/germline calling is not available for copy numberalteration events	KDM6A loss; PBRM1 loss exons 23-30	NA	NA
#8	BAP1 copy number loss	NA Somatic/germline calling is not available for copy number stable alteration events	PBRM1 copy number loss	0.8	MS-stable

BAP1, BRCA1 associated protein-1; MSI, microsatellite instability; mut/Mb, mutations per megabase; NA, not determined; TMB, tumor mutational burden.

(50%) developed PR, and two patients (50%) experienced SD. In group B2, one patient (7%) developed CR, six patients (40%) developed PR, five patients (33%) experienced SD, three patients (20%) had PD, and one patient was not evaluable for response assessment. ORR with 1st-line platinum/pemetrexed chemotherapy+/− antiangiogenic agents comprised 50 and 47% in groups A and B, respectively (p-0.97). In groups A, B1, and B2, ORR was 50, 50, and 47%, respectively (p-1.0).

Of patients treated with 1st-line platinum/pemetrexed chemotherapy+/− antiangiogenic agents, 7 patients (87%) in group A, 17 patients (85%) in group B, 4 patients (100%) in group B1, and 13 patients (81%) in group B2 had progressed or died. Median PFS comprised 9.1 months [95% confidence interval (CI), 1.2–16.1] and 9.2 months (95% CI, 2.9–13.3) in groups A and B, respectively (p-0.96; **Figure 1**). Median PFS comprised 9.1 months (95% CI, 1.2–16.1), 7.2 months [95% CI, 2.3-not reached (NR)], and 10.9 months (95% CI, 2.9-20.3) in groups A, B1, and B2, respectively (p>0.8 for each comparison; **Figure 1**).

Of patients treated with 1st-line platinum/pemetrexed chemotherapy+/− antiangiogenic agents, 4 (50%), 14 (70%), 1 (25%), and 13 (93%) patients had died in groups A, B, B1, and B2, respectively. Median OS with 1st-line platinum/pemetrexed chemotherapy+/− antiangiogenic agents comprised 32.2 months (95% CI, 6.6-NR) and 17.4 months (95% CI, 5.4–46.3) in groups A and B, respectively (p-0.45; **Figure 1**). Median OS comprised 32.2 months (95% CI, 6.6-NR), NR (95% CI, 16.6-NR), and 17.4 months (95% CI, 4.2–46.3) in groups A, B1, and B2, respectively (p>0.4 for each comparison; **Figure 1**).

In the univariate analysis, the only variables which correlated with PFS and OS with 1st-line platinum/pemetrexed chemotherapy+/− antiangiogenic agents were tumor histology and EORTC risk score (**Table 3**). Presence or absence of BAP1 alteration did not affect PFS or OS with 1st-line platinum/pemetrexed chemotherapy+/− antiangiogenic agents in a significant manner.

ORR, PFS, and OS With ICPi

A total of 16 patients were treated with ICPi: 3 patients (38%) in group A and 13 patients (35%) in group B [including 4 patients (67%) in group B1 and 9 patients (29%) in group B2]. Of these, 12 patients [2 patients (67% of receiving ICPi) in group A and 10 patients (77% of receiving ICPi) in group B] received PD-1/PD-L1 inhibitors, and 4 patients [1 patient [33% of receiving ICPi] in group A and 3 patients (23% of receiving ICPi) in group B] received a combination of a PD-1/PD-L1 inhibitor with another ICPi (mostly, CTLA-4 inhibitor). In group B1, all four patients (100% of receiving ICPi) were treated with PD-1/PD-L1 inhibitors, whereas in group B2, six patients (67% of receiving ICPi) were treated with PD-1/PD-L1 inhibitors, and three additional patients (33% of receiving ICPi) received a combination of a PD-1/PD-L1 inhibitor with another ICPi.

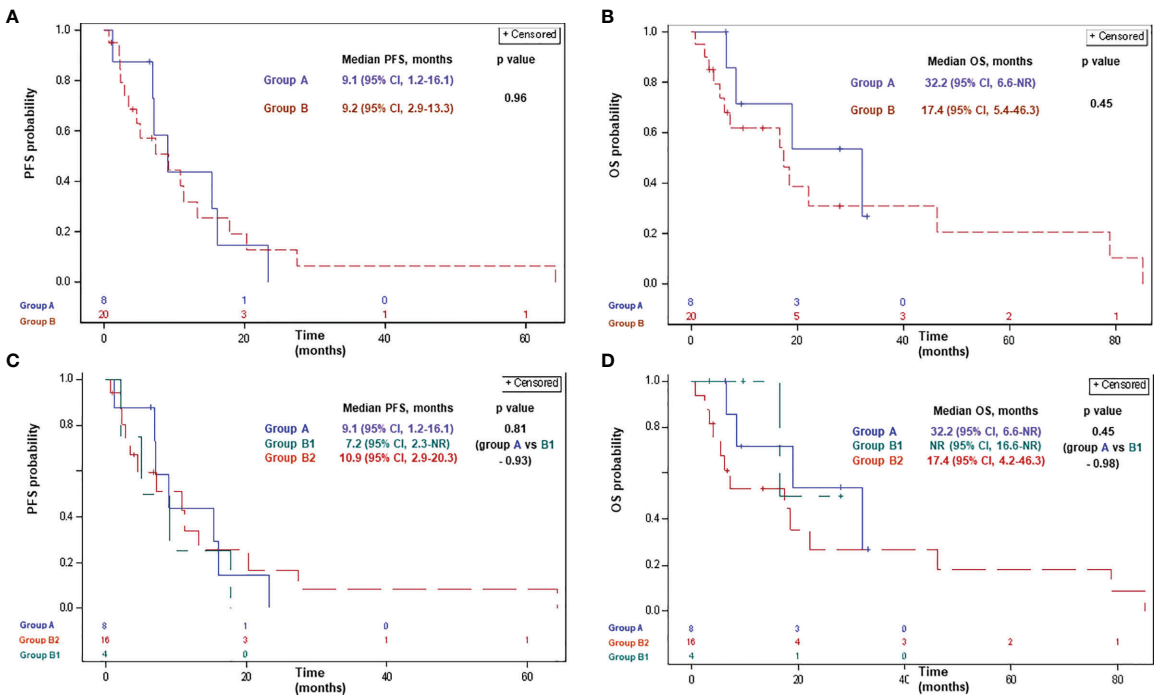

FIGURE 1 | Progression-free survival **(A, C)** and overall survival **(B, D)** with platinum-based chemotherapy in patients with advanced MPM according to BAP1 mutation status. Group A: MPM with a BAP1 inactivating mutation/copy number loss; group B: MPM without a BAP1 alteration/not tested; group B1: MPM without a BAP1 alteration; group B2: MPM not tested for a BAP1 alteration. BAP1, BRCA1 associated protein-1; CI, confidence interval; MPM, malignant pleural mesothelioma; NR, not reached; OS, overall survival; PFS, progression-free survival.

TABLE 3 | Univariate analysis of PFS and OS with platinum/pemetrexed+/antiangiogenic agent (A), ICPi (B) and OS since diagnosis of malignant pleural mesothelioma (C) by the Cox proportional-hazards regression model.

A	PFS				OS			
Parameter	**HR**	**95% HR CI**		**p value**	**HR**	**95% HR CI**		**p value**
Platinum/pemetrexed+/-antiangiogenic agent								
Age	1.01	0.99	1.04	0.25	1.03	0.99	1.07	0.08
Sex (male *vs* female)	2.64	0.88	7.78	0.08	3.63	0.88	14.98	0.07
Histology (sarcomatoid *vs* epithelioid)	13.02	2.01	84.30	0.007	11.22	1.84	68.44	0.008
Histology (biphasic *vs* epithelioid)	12.12	2.02	72.83	0.006	5.62	1.04	30.26	0.04
No BAP1 mutation/not tested vs BAP1 mutation present	0.99	0.40	2.42	0.97	1.44	0.46	4.45	0.53
ECOG PS at chemotherapy initiation (2-4 *vs* 0/1)	10.48	0.65	167.75	0.10	3.41	0.54	21.41	0.19
EORTC prognostic scale (poor risk *vs* good-risk)	8.96	2.01	39.88	0.004	9.33	2.13	40.83	0.003
CALGB prognostic scale (3/4 *vs* 1/2)	1.07	0.39	2.93	0.90	2.08	0.64	6.82	0.23
CALGB prognostic scale (5/6 *vs* 1/2)	1.49	0.33	6.78	0.60	2.34	0.44	12.45	0.32
B		ICPi						
Age	0.97	0.92	1.03	0.37	0.95	0.89	1.03	0.21
Sex (male *vs* female)	0.86	0.22	3.32	0.83	0.96	0.21	4.42	0.96
Histology (biphasic *vs* epithelioid)	12.40	1.17	131.77	0.04	7.14	0.99	51.53	0.05
No BAP1 mutation/not tested vs BAP1 mutation present	0.44	0.09	2.08	0.30	1.07	0.23	4.92	0.93
ECOG PS at ICPi initiation (2-4 *vs* 0/1)	3.56	0.47	27.19	0.22	2.21	0.31	15.93	0.43
EORTC prognostic scale (poor risk *vs* good-risk)	12.96	0.81	207.57	0.07	12.41	0.77	199.35	0.07
CALGB prognostic scale (3/4 *vs* 1/2)	1.92	0.41	9.01	0.41	3.61	0.43	30.23	0.24
CALGB prognostic scale (5/6 *vs* 1/2)	2.63	0.28	25.12	0.40	1.20	0.10	14.51	0.88
C	OS since diagnosis							
Age				1.02	0.99	1.05	0.07	1.02
Sex (male *vs* female)					2.93	1.11	7.75	0.03
Histology (sarcomatoid *vs* epithelioid)					13.98	2.68	73.01	0.002
Histology (biphasic *vs* epithelioid)					3.24	0.79	13.32	0.10
No BAP1 mutation/not tested vs BAP1 mutation present					1.56	0.55	4.41	0.40
ECOG PS at diagnosis (2-4 *vs* 0/1)					3.53	1.11	11.19	0.03
Surgery (EPP/decortication) *vs* none					0.42	0.14	1.19	0.10
Radiotherapy *vs* none					0.77	0.36	1.67	0.51
Platinum-based chemotherapy *vs* none					1.54	0.57	4.16	0.39
ICPi *vs* none					0.80	0.37	1.76	0.58
EORTC prognostic scale (poor risk *vs* good-risk)					2.80	1.19	6.59	0.02
CALGB prognostic scale (3/4 *vs* 1/2)					1.55	0.63	3.83	0.34
CALGB prognostic scale (5/6 *vs* 1/2)					1.91	0.49	7.53	0.35

BAP1, BRCA1 associated protein-1; CALGB, Cancer and Leukemia Group B; CI, confidence interval; ECOG PS, Eastern Cooperative Oncology Group performance status score; EORTC, European Organization for Research and Treatment of Cancer; EPP, extra-pleural pneumonectomy; HR, hazard ratio; ICPi, immune check-point inhibitors; OS, median overall survival; PFS, median progression-free survival.

In group A, two patients (100%) had PD, and one patient was not evaluable for response assessment. In group B, three patients (27%) achieved PR, four patients (36.5%) experienced SD, four patients (36.5%) had PD, and two patients were not evaluable for response assessment. In group B1, one patient (33%) achieved PR, two patients (67%) had PD, and one patient was not evaluable for response assessment. In group B2, two patients (25%) achieved PR, four patients (50%) experienced SD, two patients (25%) had PD, and one patient was not evaluable for response assessment. ORR with ICPi comprised 0 and 27% in groups A and B, respectively (p-0.28), and 0, 33, and 25% in groups A, B1, and B2, respectively (p-0.35).

Of patients receiving ICPi, two (67%), nine (69%), two (50%), and seven (78%) patients had progressed or died in groups A, B, B1, and B2, respectively. Median PFS with ICPi comprised 2.5 months (95% CI, 1.4–3.7) and 3.0 months (95% CI, 1.3–10.5) in groups A and B, respectively (p-0.39; **Figure 2**). Median PFS was 2.5 months (95% CI, 1.4–3.7), 2.0 months (95% CI, 1.9-NR), and 4.5 months (95% CI, 0.3–10.5) in groups A, B1, and B2, respectively (p>0.5 for each comparison; **Figure 2**).

Of patients receiving ICPi, 2 (67%), 8 (61%), 1 (25%), and 7 (78%) patients had died in groups A, B, B1, and B2, respectively. Median OS with ICPi comprised 10.4 months (95% CI, 4.0–16.8) and 5.8 months (95% CI, 2.2–13.2) in groups A and B,

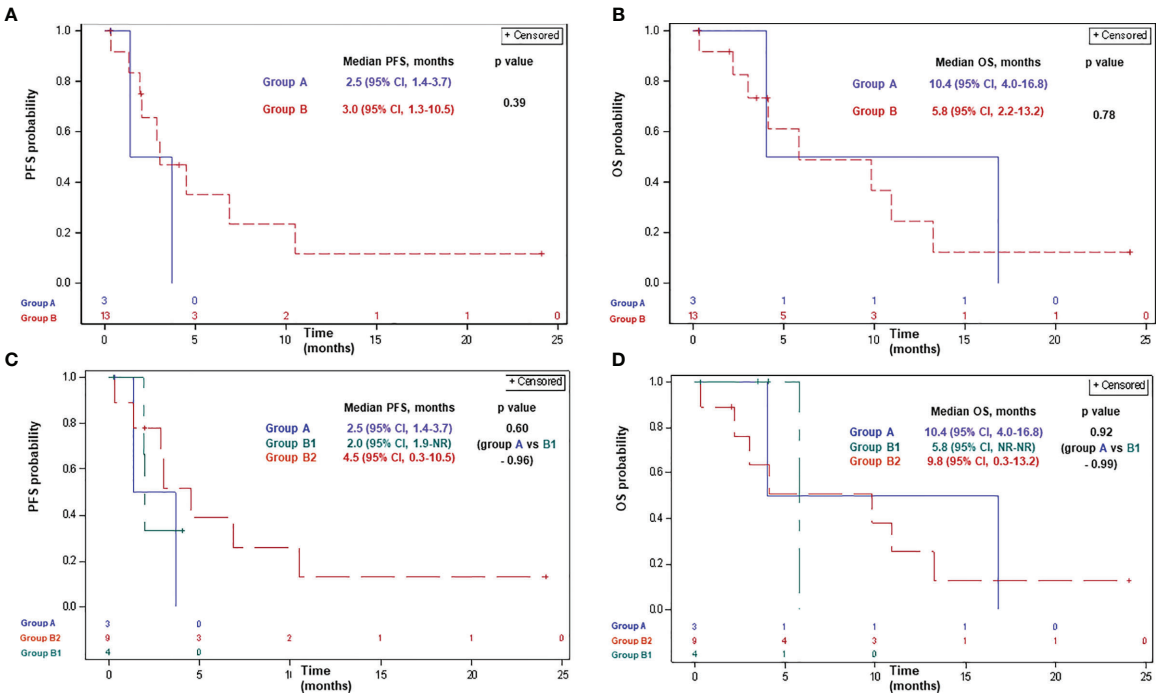

FIGURE 2 | Progression-free survival **(A, C)** and overall survival **(B, D)** with ICPi in patients with advanced MPM according to BAP1 mutation status. Group A: MPM with a BAP1 inactivating mutation/copy number loss; group B: MPM without a BAP1 alteration/not tested; group B1: MPM without a BAP1 alteration; group B2: MPM not tested for a BAP1 alteration. BAP1, BRCA1 associated protein-1; CI, confidence interval; ICPi, immune check-point inhibitors; MPM, malignant pleural mesothelioma; NR, not reached; OS, overall survival; PFS, progression-free survival.

respectively (p-0.78; **Figure 2**). Median OS was 10.4 months (95% CI, 4.0–16.8), 5.8 months (95% CI, NR-NR), and 9.8 months (95% CI, 0.3–13.2) in groups A, B1, and B2, respectively (p>0.9 for each comparison; **Figure 2**).

In the univariate analysis, the only variable which correlated with PFS and OS with ICPi was tumor histology (**Table 3**). Presence or absence of BAP1 alteration did not affect PFS or OS with ICPi.

ORR, PFS With PARPi

Four patients in group A were treated with PARPi: two patients received veliparib, two patients received olaparib, and one patient was also treated with the combination of carboplatin and olaparib after olaparib failure. Olaparib was administered at a dose of 300 mg #2/d; veliparib was administered at a dose of 200 mg#2/d; the combination included carboplatin AUC-2 weekly and olaparib 300 mg #2/d. No objective responses with PARPi occurred; three patients had PD, and one patient achieved SD for 3.4+ months (SD is ongoing at the time of the analysis). PFS with PARPi comprised 3.4+, 1.9, 1.8, and 1.8 months; median PFS was 1.8 months (95% CI, 1.8-NR). The patient treated with the combination of carboplatin and olaparib after olaparib failure demonstrated PD 1.5 months after the initiation of the combined treatment.

One patient developed grade 3 thrombocytopenia during olaparib treatment; one patient developed grade 3 fatigue and grade 3 anorexia during veliparib treatment. The combined treatment was not associated with any treatment-related adverse events.

OS Since MPM Diagnosis

Of 45 patients included in the analysis, 4 (50%), 23 patients (62%), 3 (50%), and 20 (64%) patients in groups A, B, B1, and B2, respectively, had died. Median OSDx was 98.3 months (95% CI, 9.7–98.3) and 19.4 months (95% CI, 9.7–47.3) in groups A and B, respectively (p-0.31; **Figure 3**). Median OSDx was 98.3 months (95% CI, 9.7–98.3), 18.8 months (95% CI, 8.5-NR), and 19.5 months (95% CI, 8.3–82.2) in groups A, B1, and B2, respectively (p>0.5 for each comparison; **Figure 3**).

In the univariate analysis, the variables which significantly correlated with OSDx were sex, tumor histology, Eastern Cooperative Oncology Group performance status (ECOG PS) at diagnosis, and EORTC prognostic risk score (**Table 3**). Presence or absence of BAP1 alteration did not demonstrate a statistically significant correlation with OSDx.

DISCUSSION

To the best of our knowledge, our series represents one of the first one reporting on different systemic treatment outcomes in BAP1-altered MPM patients. According to our observation, 1st-

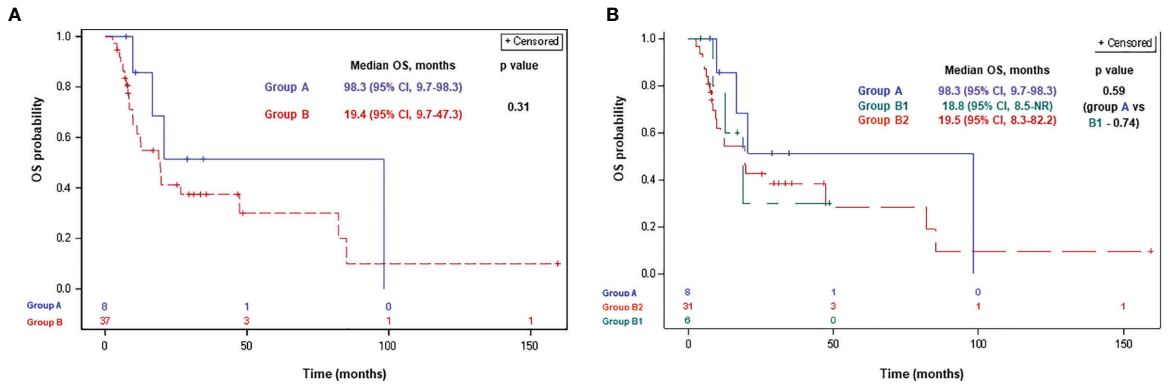

FIGURE 3 | Overall survival since MPM diagnosis according to BAP1 mutation status for groups A, B **(A)** and A, B1, B2 **(B)**. Group A: MPM with a BAP1 inactivating mutation/copy number loss; group B: MPM without a BAP1 alteration/not tested; group B1: MPM without a BAP1 alteration; group B2: MPM not tested for a BAP1 alteration. BAP1, BRCA1 associated protein-1; CI, confidence interval; ICPi, immune check-point inhibitors; MPM, malignant pleural mesothelioma; NR, not reached; OS, overall survival.

line platinum/pemetrexed chemotherapy in this category of patients was associated with an ORR of 50% and mPFS of 9.1 months (95% CI, 1.2–16.1). These results were similar to the results observed in non-selected MPM patients [ORR of 47%, p-0.97 and mPFS of 9.2 months (95% CI, 2.9–13.3), p-0.96]—despite the fact, that higher proportion of patients with BAP1-mutant MPM (62%), as compared to non-selected MPM patients (20%), received the treatment in combination with bevacizumab. Moreover, similar ORR (50%, p-1.0) and mPFS [7.2 months (95% CI, 2.3-NR), p-0.93] were seen in wild-type BAP1 tumors. These results are also in line with the previously reported in the literature with platinum/pemetrexed-bevacizumab in non-selected MPM patients [mPFS of 9.2 months (95% CI, 8.5–10.5)] (7). Furthermore, the results of univariate analysis of outcomes with platinum/pemetrexed did not indicate that BAP1 alterations have any predictive ability in association with this type of treatment. These observations, overall, do not support the assumption regarding the extreme sensitivity of BAP1-mutant MPM to platinum-based chemotherapy. Importantly, Kumar *et al.* did not observe an association between the loss of nuclear BAP1 expression and outcomes with platinum-based chemotherapy in MPM either (54). In another retrospective analysis assessing the predictive value of different genomic aberrations in MPM performed by Lo Iacono et al., PIK3CA and TP53 mutations, but not BAP1 mutations, predicted time-to-tumor progression and OS with platinum/pemetrexed (38). With regards to predictive value of BAP1 aberrations with another chemotherapy regimens, a non-significant trend toward improved OS with vinorelbine in MPM with loss of nuclear BAP1 expression was observed by Kumar *et al.*, suggesting a potential modulatory effect of BAP1 on microtubule organization and, as a result, response to vinorelbine (54). In addition, non-functional BAP1 has been associated with resistance to gemcitabine in cell lines (55, 56).

In our series, the presence of BAP1 aberrations did not seem to modify response to ICPi. Indeed, treatment with ICPi, mainly PD-1/PD-L1 inhibitors, resulted in similar ORR and mPFS of 0 and 27% (p-0.28), and 2.5 months (95% CI, 1.4–3.7) and 3.0 months (95% CI, 1.3–10.5) (p-0.39) in BAP1-altered and non-selected MPM patients, respectively. Again, similar ORR (33%, p-0.35) and mPFS [2.0 months (95% CI, 1.9-NR), p-0.96] with ICPi were seen in wild-type BAP1 tumors. The outcomes in both groups were in line with the reported in the literature with PD-1/PD-L1 inhibitors in similar clinical scenario (ORR of 9–29%, mPFS of 2.6–4.1 months) (13–17). Furthermore, univariate analysis of outcomes with ICPi did not demonstrate a correlation between the presence of BAP1 alteration and ICPi efficacy.

The presence of BAP1 aberration in our cohort was associated with numerically longer OS since MPM diagnosis of 98.3 months (95% CI, 9.7–98.3), as compared to 19.4 months (95% CI, 9.7–47.3) in non-selected MPM and 18.8 months (95% CI, 8.5-NR) in wild-type BAP1 MPM—despite the lack of striking inter-group differences in other baseline patient and tumor characteristics. The inter-group differences in proportion of patients receiving platinum/pemetrexed and PARPi are less likely to explain such a big numerical difference in OS. Similar ORR and PFS with platinum/pemetrexed and ICPi, but numerically longer OS since MPM diagnosis in the BAP1-altered group, in our opinion, reflected favorable natural history and indolent character of the disease, and not necessarily better responsiveness to systemic treatments. Giving the higher frequency of family history of malignancy in the BAP1-mutant cohort (24), we can hypothesize, that in some patients in our cohort BAP1 mutation reflected germline abnormalities, which are known to be associated with longer OS (39, 40). Every attempt to elucidate the nature of the BAP1 genomic alterations in our cohort, unfortunately, was unsuccessful. However, considering the low prevalence of germline BAP1 mutations in MPM [1–7% (25–28)], such an explanation for the longer OS in the BAP1-altered group seems less likely.

In our series, none of the four patients with BAP1-altered MPM demonstrated an objective response with PARPi; three

patients demonstrated progressive disease at the first radiological response evaluation. This represents an early lack-of-activity signal of PARPi in the BAP1-altered MPM, however, the response evaluation in our series has been done retrospectively, and no central radiological revision has been performed. PARPi are currently being evaluated in two ongoing phase 2 trials: one trial assessing niraparib in BAP1-altered malignant mesothelioma and other DNA damage response-deficient neoplasms (NCT03207347), and another trial evaluating olaparib in separate cohorts of patients with malignant mesothelioma in accordance with the BAP1 status (NCT03531840); no results have been presented so far. One of the promising biological agents in BAP1—altered MPM is enhancer of zeste homolog 2 inhibitor (EZH2i) tazemetostat. This is based on its selective *in vivo* activity in BAP1-mutant MPM (57), and positive results obtained in a phase 2 trial conducted in BAP1-altered MPM (the study met its primary end point demonstrating a disease-control rate of 51% at 12 weeks) (58). The role of histone deacetylase inhibitors (HDACi) in MPM with BAP1 alterations warrants further exploration as well. BAP1 downregulation increases the sensitivity to HDACi in mesothelioma cell lines (59), and therefore, it would be important to see whether BAP1 aberrations modulate response to vorinostat in VANTAGE 014 study (60).

One of the major limitations of our series, in addition to its retrospective nature, small sample size, and lack of central radiological assessment, is the absence of routine molecular profiling for all MPM patients resulting in a significant chance of contamination of one of the comparator groups (group B, representing the "non-selected" MPM) by the BAP1-altered tumors. Whereas the prevalence of BAP1 somatic alterations (including point mutations, deletions, splice alterations, chromosomal alterations, and copy number loss) in MPM ranges between 20 and 64%—depending on the technology used (22, 26, 29–38), most large series implementing next-generation sequencing or Sanger sequencing report on the prevalence of 20–25% (30, 34, 37). Based on the latter estimation and considering performance of genomic testing for some of the patients in the comparator group, the proportion of BAP1-altered tumors in the comparator group (group B) in our cohort is expected to be around 20-25%. Moreover, the estimation of prevalence of BAP1 somatic alterations of 50% results in the proportion of BAP1-altered tumors in the comparator group (group B) of 43%. Overall, the significant chance of contamination of the "non-selected" comparator group by the BAP1-altered tumors represents an additional important limitation of our analysis. This limitation, at least partially, was addressed by the comparative analysis of BAP1-altered and wild-type BAP1 MPM which demonstrated similar outcomes in both groups. Inability to differentiate between the germline and somatic aberrations in the BAP1 gene represents an additional weakness of the analysis. Finally, although patients in the selected cohort were consecutive patients, these appeared to be mainly "good prognosis" by EORTC and CALGB prognostic scoring systems, reflecting the typical patient population treated at tertiary cancer centers. As a result of this selection bias, there is an uncertainty regarding the representability of the selected cohort. Noteworthy, many of the recent clinical trials assessing novel treatment strategies in MPM have selection bias, which misleads the understanding of these novel treatments' efficacy in the real-world setting.

Since loss of BAP1 nuclear staining correlates with BAP1 loss-of-function mutations with a sensitivity and specificity of 88 and 97% respectively (61), it would be interesting to assess its predictive value on the clinical outcomes of different systemic treatments. Considering the involvement of several oncological centers, and the absence of formal guidelines for IHC BAP1 assessment, a centralized pathological testing was essential for such analysis. Such a centralized pathological testing, however, was not feasible—which represents an additional important limitation of our analysis.

CONCLUSIONS

According to our retrospective analysis, the presence of BAP1 genomic aberration in MPM does not seem to modulate responses to platinum/pemetrexed or ICPi. Numerically longer OS since diagnosis in BAP1-altered MPM has been observed probably reflecting favorable natural history of this disease subset. In four BAP1-altered MPM patients treated with PARPi no responses have been seen. The clinical research to identify effective biological agents in BAP1-mutant MPM is ongoing.

DATA AVAILABILITY STATEMENT

The raw data supporting the conclusions of this article will be made available by the authors, without undue reservation.

ETHICS STATEMENT

The studies involving human participants were reviewed and approved by 0391-14-RMC. Written informed consent for participation was not required for this study in accordance with the national legislation and the institutional requirements.

AUTHOR CONTRIBUTIONS

Conceptualization: ED, DU, and JB. Methodology: ED, DU, and JB. Validation: ED and DU. Formal Analysis: TS. Investigation: ED and DU. Resources: ED, DU, JB, AM, TG, MM, JD, AA, AZ, OR, and NP. Data curation: ED, DU, and TS. Writing-original draft: ED, AM, DU, and JB. Writing-review and editing: ED, DU, JB, AM, TG, MM, JD, AA, AZ, OR, and NP. Visualization: JD, AM, DU, and JB. Supervision: ED and DU. Project administration: ED. Funding acquisition: NA. All authors contributed to the article and approved the submitted version.

ACKNOWLEDGMENTS

The paper was presented as a poster during the WCLC 2019 congress (62). Since this publication, the manuscript was updated, and additional analyses have been done.

SUPPLEMENTARY MATERIAL

The Supplementary Material for this article can be found online at: https://www.frontiersin.org/articles/10.3389/fonc.2021.603223/full#supplementary-material

REFERENCES

1. Lanphear BP, Buncher CR. Latent period for malignant mesothelioma of occupational origin. *J Occup Med* (1992) 34(7):718–21.
2. American Cancer Society, Cancer Facts & and 017. Special Section: Rare Cancers in Adults. *Cancer Facts Fig 2017 Spec Sect Rare Cancers Adults* (2017), 30–9.
3. Curran BD, Sahmoud T, Therasse P, Van Meerbeeck J, Postmus PE, Giaccone G. Prognostic Factors in Patients With Pleural Mesothelioma: The European Organization for Research and Treatment of Cancer Experience. *Society* (1998) 16(1):145–52. doi: 10.1200/JCO.1998.16.1.145
4. Herndon JE, Green MR, Chahinian AP, Corson JM, Suzuki Y, Vogelzang NJ. Factors predictive of survival among 337 patients with mesothelioma treated between 1984 and 1994 by the Cancer and Leukemia Group B. *Chest* (1998) 113(3):723–31. doi: 10.1378/chest.113.3.723
5. Edwards JG, Leverment JN, Spyt TJ, Waller DA, O'Byrne KJ. Prognostic factors for malignant mesothelioma in Leicester: Validation of EORTC and CALGB scores. *Thorax* (1999) 54(SUPPL. 3):731–5. doi: 10.1136/thorax.55.9.731
6. Vogelzang NJ, Rusthoven JJ, Symanowski J, Denham C, Kaukel E, Ruffie P, et al. Phase III study of pemetrexed in combination with cisplatin versus cisplatin alone in patients with malignant pleural mesothelioma. *J Clin Oncol* (2003) 21(14):2636–44. doi: 10.1200/JCO.2003.11.136
7. Zalcman G, Mazieres J, Margery J, Greillier L, Audigier-Valette C, Moro-Sibilot D, et al. Bevacizumab for newly diagnosed pleural mesothelioma in the Mesothelioma Avastin Cisplatin Pemetrexed Study (MAPS): A randomised, controlled, open-label, phase 3 trial. *Lancet* (2016) 387(10026):1405–14. doi: 10.1016/S0140-6736(15)01238-6
8. Kindler HL, Ismaila N, Hassan R. Treatment of Malignant Pleural Mesothelioma: American Society of Clinical Oncology Clinical Practice Guideline Summary. *J Oncol Pract* (2018) 14(4):256–64. doi: 10.1200/jop.17.00012
9. Ceresoli GL, Zucali PA, Mencoboni M, Botta M, Grossi F, Cortinovis D, et al. Phase II study of pemetrexed plus carboplatin in malignant pleural mesothelioma. *J Clin Oncol* (2006) 24(9):1443–8. doi: 10.1200/JCO.2005.04.3190
10. Castagneto B, Botta M, Aitini E, Spigno F, Degiovanni D, Alabiso O, et al. Phase II study of pemetrexed in combination with carboplatin in patients with malignant pleural mesothelioma (MPM). *Ann Oncol Off J Eur Soc Med Oncol* (2008) 19(2):370–3. doi: 10.1093/annonc/mdm501
11. Baas P, Fennell D, Kerr KM, van Schil PE, Haas RL, Peters S. Malignant pleural mesothelioma: ESMO Clinical Practice Guidelines for diagnosis, treatment and follow-up. *Ann Oncol* (2015) 26:v31–9. doi: 10.1093/annonc/mdv199
12. Santoro A, O'Brien ME, Stahel RA, Nackaerts K, Baas P, Karthaus M, et al. Pemetrexed plus cisplatin or pemetrexed plus carboplatin for chemonaïve patients with malignant pleural mesothelioma: Results of the international expanded access program. *J Thorac Oncol* (2008) 3(7):756–63. doi: 10.1097/JTO.0b013e31817c73d6
13. Quispel-Janssen J, van der Noort V, de Vries JF, Zimmerman M, Lalezari F, Thunnissen E, et al. rogrammed Death 1 Blockade With Nivolumab in Patients With Recurrent Malignant Pleural Mesothelioma. *J Thorac Oncol* (2018) 13(10):1569–76. doi: 10.1016/j.jtho.2018.05.038
14. Okada M, Kijima T, Aoe K, Kato T, Fujimoto N, Nakagawa K, et al. Clinical Efficacy and Safety of Nivolumab: Results of a Multicenter, Open-label, Single-arm, Japanese Phase II study in Malignant Pleural Mesothelioma (MERIT). *Clin Cancer Res* (2019) 25(18):5485–92. doi: 10.1158/1078-0432.CCR-19-0103
15. Desai A, Karrison T, Rose B, Tan Y, Hill B, Pemberton E, et al. OA08.03 Phase II Trial of Pembrolizumab (NCT02399371) In Previously-Treated Malignant Mesothelioma (MM): Final Analysis. *J Thorac Oncol* (2018) 13(10):S339. doi: 10.1016/j.jtho.2018.08.277
16. Alley EW, Lopez J, Santoro A, Morosky A, Saraf S, Piperdi B, et al. Clinical safety and activity of pembrolizumab in patients with malignant pleural mesothelioma (KEYNOTE-028): preliminary results from a non-randomised, open-label, phase 1b trial. *Lancet Oncol* (2017) 18(5):623–30. doi: 10.1016/S1470-2045(17)30169-9
17. Hassan R, Thomas A, Nemunaitis JJ, Patel MR, Bennouna J, Chen FL, et al. Efficacy and Safety of Avelumab Treatment in Patients with Advanced Unresectable Mesothelioma: Phase 1b Results from the JAVELIN Solid Tumor Trial. *JAMA Oncol* (2019) 5(3):351–7. doi: 10.1001/jamaoncol.2018.5428
18. Scherpereel A, Mazieres J, Greillier L, Lantuejoul S, Dô P, Bylicki O, et al. Nivolumab or nivolumab plus ipilimumab in patients with relapsed malignant pleural mesothelioma (IFCT-1501 MAPS2): a multicentre, open-label, randomised, non-comparative, phase 2 trial. *Lancet Oncol* (2019) 20 (2):239–53. doi: 10.1016/S1470-2045(18)30765-4
19. Callabrò L, Morra A, Giannarelli D, Amato G, D'Incecco A, Covre A, et al. Tremelimumab combined with durvalumab in patients with mesothelioma (NIBIT-MESO-1): an open-label, non-randomised, phase 2 study. *Lancet Respir Med* (2018) 6(6):451–60. doi: 10.1016/S2213-2600(18)30151-6
20. Baas P, Scherpereel A, Nowak AK, Fujimoto N, Peters S, Tsao AS, et al. First-line nivolumab plus ipilimumab in unresectable malignant pleural mesothelioma (CheckMate 743): a multicentre, randomised, open-label, phase 3 trial. *Lancet*. (2021) 397(10272):375–386. doi: 10.1016/S0140-6736(20)32714-8.
21. Scheuermann J, de Ayala Alonso AG, Oktaba K, Ly-Hartig N, McGinty RK, Fraterman S, et al. Histone H2A deubiquitinase activity of the Polycomb repressive complex PR-DUB. *Nature* (2010) 465:243–7.
22. Srinivasan G, Sidhu GS, Williamson EA, Jaiswal AS, Najmunnisa N, Wilcoxen K, et al. Synthetic lethality in malignant pleural mesothelioma with PARP1 inhibition. *Cancer Chemother Pharmacol* (2017) 80(4):861–7. doi: 10.1007/s00280-017-3401-y
23. Walpole S, Pritchard AL, Cebulla CM, Pilarski R, Stautberg M, Davidorf FH, et al. Comprehensive Study of the Clinical Phenotype of Germline BAP1 Variant-Carrying Families Worldwide. *J Natl Cancer Inst* (2018) 110 (12):1328–41. doi: 10.1093/jnci/djy171
24. Carbone M, Ferris LK, Baumann F, Napolitano A, Lum CA, Flores EG, et al. BAP1 cancer syndrome: malignant mesothelioma, uveal and cutaneous melanoma, and MBAITs. *J Transl Med* (2012) 10(1):1–7. doi: 10.1186/1479-5876-10-179
25. Testa JR, Cheung M, Pei J, Below JE, Tan Y, Sementino E, et al. Germline BAP1 mutations predispose to malignant mesothelioma. *Nat Genet* (2011) 43 (10):1022–5. doi: 10.1038/ng.912.Germline
26. Panou V, Gadiraju M, Wolin A, Weipert CM, Skarda E, Husain AN, et al. Frequency of germline mutations in cancer susceptibility genes in malignant mesothelioma. *J Clin Oncol* (2018) 36(28):2863–71. doi: 10.1200/JCO.2018.78.5204
27. Hassan R, Morrow B, Thomas A, Walsh T, Lee MK, Gulsuner S, et al. Inherited predisposition to malignant mesothelioma and overall survival following platinum chemotherapy. *Proc Natl Acad Sci USA* (2019) 116 (18):9008–13. doi: 10.1073/pnas.1821510116
28. Rusch A, Ziltener G, Nackaerts K, Weder W, Stahel RA, Felley-Bosco E. Prevalence of BRCA-1 associated protein 1 germline mutation in sporadic malignant pleural mesothelioma cases. *Lung Cancer* (2015) 87(1):77–9. doi: 10.1016/j.lungcan.2014.10.017
29. Guo G, Chmielecki J, Goparaju C, Heguy A, Dolgalev I, Carbone M, et al. Whole-exome sequencing reveals frequent genetic alterations in BAP1, NF2, CDKN2A, and CUL1 in malignant pleural mesothelioma. *Cancer Res* (2015) 75(2):264–9. doi: 10.1158/0008-5472.CAN-14-1008
30. Bott M, Brevet M, Taylor BS, Shimizu S, Ito T, Wang L, et al. The nuclear deubiquitinase BAP1 is commonly inactivated by somatic mutations and 3p21.1 losses in malignant pleural mesothelioma. *Nat Genet* (2011) 43 (7):668–72. doi: 10.1038/ng.855
31. Leblay N, Leprêtre F, Le Stang N, Gautier-Stein A, Villeneuve L, Isaac S, et al. BAP1 Is Altered by Copy Number Loss, Mutation, and/or Loss of Protein Expression in More Than 70% of Malignant Peritoneal Mesotheliomas. *J Thorac Oncol* (2017) 12(4):724–33. doi: 10.1016/j.jtho.2016.12.019

32. Bueno R, Stawiski EW, Goldstein LD, Durinck S, De Rienzo A, Modrusan Z, et al. Comprehensive genomic analysis of malignant pleural mesothelioma identifies recurrent mutations, gene fusions and splicing alterations. *Nat Genet* (2016) 48(4):407–16. doi: 10.1038/ng.3520
33. Nasu M, Emi M, Pastorino S, Tanji M, Powers A, Luk H, et al. High incidence of somatic BAP1 alterations in sporadic malignant mesothelioma. *J Thorac Oncol* (2015) 10(4):565–76. doi: 10.1097/JTO.0000000000000471
34. Zauderer MG, Bott M, McMillan R, Sima CS, Rusch V, Krug LM, et al. Clinical characteristics of patients with malignant pleural mesothelioma (MPM) harboring somatic BAP1 mutations. *J Thorac Oncol* (2013) 8 (11):1430–3. doi: 10.1097/JTO.0b013e31829e7ef9
35. De Reynies A, Jaurand MC, Renier A, Couchy G, Hysi I, Elarouci N, et al. Molecular classification of malignant pleural mesothelioma: Identification of a poor prognosis subgroup linked to the epithelial-to-mesenchymal transition. *Clin Cancer Res* (2014) 20(5):1323–34. doi: 10.1158/1078-0432.CCR-13-2429
36. Hmeljak J, Sanchez-Vega F, Hoadley KA, Shih J, Stewart C, Heiman D, et al. Integrative molecular characterization of malignant pleural mesothelioma. *Cancer Discovery* (2018) 8(12):1549–65. doi: 10.1158/2159-8290.CD-18-0804
37. Quetel L, Meiller C, Assié JB, Blum Y, Imbeaud S, Montagne F, et al. Genetic alterations of malignant pleural mesothelioma: association with tumor heterogeneity and overall survival. *Mol Oncol* (2020). doi: 10.1002/1878-0261.12651
38. Lo Iacono M, Monica V, Righi L, Grosso F, Libener R, Vatrano S, et al. Targeted next-generation sequencing of cancer genes in advanced stage malignant pleural mesothelioma: A retrospective study. *J Thorac Oncol* (2015) 10(3):492–9. doi: 10.1097/JTO.0000000000000436
39. Pastorino S, Yoshikawa Y, Pass HI, Emi M, Nasu M, Pagano I, et al. A subsetof mesotheliomas with improved survival occurring in carriers of BAP1 andother germline mutations. *J Clin Oncol* (2018) 36(35):3485–94. doi: 10.1200/JCO.2018.79.0352
40. Baumann F, Flores E, Napolitano A, Kanodia S, Taioli E, Pass H, et al. Mesothelioma patients with germline BAP1 mutations have 7-fold improved long-term survival. *Carcinogenesis* (2015) 36(1):76–81. doi: 10.1093/carcin/bgu227
41. Yang D, Brca B, Entrez N, Kanodia S, Taioli E, Pass H, et al. Association of BRCA1 and BRCA2 Mutations With Survival, Chemotherapy Sensitivity , and Gene Mutator Phenotype. *Jama* (2013) 306(14):1557–65. doi: 10.1001/jama.2011.1456
42. Yu H, Pak H, Hammond-Martel I, Ghram M, Rodrigue A, Daou S, et al. Tumor suppressor and deubiquitinase BAP1 promotes DNA double-strand break repair. *Proc Natl Acad Sci USA* (2014) 111(1):285–90. doi: 10.1073/pnas.1309085110
43. Parrotta R, Okonska A, Ronner M, Weder W, Stahel R, Penengo L, et al. A Novel BRCA1-Associated Protein-1 Isoform Affects Response of Mesothelioma Cells to Drugs Impairing BRCA1-Mediated DNA Repair. *J Thorac Oncol* (2017) 12(8):1309–19. doi: 10.1016/j.jtho.2017.03.023
44. Shrestha R, Nabavi N, Lin YY, Mo F, Anderson S, Volik S, et al. BAP1 haploinsufficiency predicts a distinct immunogenic class of malignant peritoneal mesothelioma. *Genome Med* (2019) 11(1):1–12. doi: 10.1186/s13073-019-0620-3
45. Chalmers ZA, Connelly CF, Fabrizio D, Gay L, Ali SM, Ennis R, et al. Analysis of 100,000 human cancer genomes reveals the landscape of tumor mutational burden. *Genome Med* (2017) 9(1):34. doi: 10.1186/s13073-017-0424-2
46. https://www.tempus.com/tempus-unveils-tempus-xt-595-gene-panel-aimed-at-empowering-data-driven-cancer-care/.
47. . https://www.foundationmedicine.com/genomic-testing/foundation-one-cdx.
48. . https://nanthealth.com/products/precision-insights/.
49. Garon EB, Rizvi NA, Hui R, Leighl N, Balmanoukian AS, Eder JP, et al. Pembrolizumab for the treatment of non-small-cell lung cancer. *N Engl J Med* (2015) 372(21):2018–28. doi: 10.1056/NEJMoa1501824
50. Neuman T, London M, Kania-Almog J, Litvin A, Zohar Y, Fridel L, et al. A harmonization study for the use of 22C3 PD-L1 immunohistochemical staining on ventana's platform. *J Thorac Oncol* (2016) 11(11):1863–8. doi: 10.1016/j.jtho.2016.08.146
51. Byrne MJ, Nowak AK. Modified RECIST criteria for assessment of response in malignant pleural mesothelioma. *Ann Oncol* (2004) 15(2):257–60. doi: 10.1093/annonc/mdh059
52. *Common Terminology Criteria for Adverse Events (CTCAE) Version 4.0* (2009). Available at: https://www.eortc.be/services/doc/ctc/CTCAE_4.03_2010-06-14_QuickReference_5x7.pdf (Accessed June 15, 2019). (v4.03: June 14, 2010).
53. *SAS® 9.4 statistical software* . Available at: https://www.sas.com/en_us/software/sas9.html.%0A (Accessed February 2, 2019).
54. Kumar N, Alrifai D, Kolluri KK, Sage EK, Ishii Y, Guppy N, et al. Retrospective response analysis of BAP1 expression to predict the clinical activity of systemic cytotoxic chemotherapy in mesothelioma. *Lung Cancer* (2019) 127(October 2018):164–6. doi: 10.1016/j.lungcan.2018.12.004
55. Guazzelli A, Meysami P, Bakker E, Demonacos C, Giordano A, Krstic-Demonacos M, et al. BAP1 status determines the sensitivity of malignant mesothelioma cells to gemcitabine treatment. *Int J Mol Sci* (2019) 20(2). doi: 10.3390/ijms20020429
56. Okonska A, Bühler S, Rao V, Ronner M, Blijlevens M, der Meulen-Muileman IV. Genome-wide silencing screen in mesothelioma cells reveals that loss of function of BAP1 induces chemoresistance to ribonucleotide reductase inhibition: implication for therapy. *bioRxiv* (2018) 381533. doi: 10.1101/381533
57. Kemp CD, Rao M, Xi S, Inchauste S, Mani H, Fetsch P, et al. Polycomb Repressor Complex-2 is a Novel Target for Mesothelioma Therapy. *Clin Cancer Res* (2012) 18(1):77–90. doi: 10.1158/1078-0432.CCR-11-0962
58. Zauderer MG, Szlosarek P, Le Moulec S, Popat S, Taylor P, et al. Phase 2, multicenter study of the EZH2 inhibitor tazemetostat as monotherapy in adults with relapsed or refractory (R/R) malignant mesothelioma (MM) with BAP1 inactivation. *J Clin Oncol* (2018) 36(15_suppl):8515–5.
59. Sacco JJ, Kenyani J, Butt Z, Carter R, Chew HY, Cheeseman LP, et al. Loss of the deubiquitylase BAP1 alters class I histone deacetylase expression and sensitivity of mesothelioma cells to HDAC inhibitors. *Oncotarget* (2015) 6 (15):13757–71. doi: 10.18632/oncotarget.3765
60. Krug LM, Kindler HL, Calvert H, Manegold C, Tsao AS, Fennell D, et al. Vorinostat in patients with advanced malignant pleural mesothelioma who have progressed on previous chemotherapy (VANTAGE-014): a phase 3, double-blind, randomised, placebo-controlled trial. *Lancet Oncol* (2015) 16 (4):447–56.
61. Shah AA, Bourne TD, Murali R. BAP1 protein loss by immunohistochemistry: A potentially useful tool for prognostic prediction in patients with uveal melanoma. *Pathology* (2013) 45(7):651–6. doi: 10.1097/PAT.0000000000000002
62. Dudnik E, Bar J, Kuznetsov T, Moskovitz M, Dudnik J, Shochat T, et al. BAP1 Mutant Malignant Pleural Mesothelioma (MPM): Outcomes with Chemotherapy, ICPi and PARPi. *J Thorac Oncol* (2019) 14(10):S760. doi: 10.1016/j.jtho.2019.08.1632

Conflict of Interest: ED reported grants from Boehringer Ingelheim, personal fees for consulting or advisory services from Boehringer Ingelheim, Roche, Astra Zeneca, Pfizer, MSD, BMS, Novartis, Takeda. JB reported grants from MSD, Roche, Boehringer Ingelheim, AstraZeneca and Pfizer, and personal fees for consulting or advisory services from MSD, Roche, Boehringer Ingelheim, AstraZeneca, Pfizer, BMS, Novartis, Takeda, Bayer, Vascular Biogenics, and Abbvie. AM reported honoraria from Merck, Roche. MM reported personal fees for consulting or advisory services from Boehringer Ingelheim, Roche, Astra Zeneca, MSD, BMS, and Takeda. AZ reported grants from BMS, personal fees for consulting or advisory services from Roche, MSD, BMS, Astra Zeneca. NP reported grants and personal fees for consulting or advisory services from Astra Zeneca, Boehringer Ingelheim, BMS, Eli Lilly, MSD, Roche, Pfizer, Novartis, NovellusDx, FMI, Gaurdant360. DU reported personal fees for consulting or advisory services from Boehringer Ingelheim, Roche, Astra Zeneca, MSD, BMS, Takeda.

The remaining authors declare that the research was conducted in the absence of any commercial or financial relationships that could be construed as a potential conflict of interest.

frontiers in Oncology

ORIGINAL RESEARCH
published: 23 April 2021
doi: 10.3389/fonc.2021.615234

Combined Analysis of RNA Sequence and Microarray Data Reveals a Competing Endogenous RNA Network as Novel Prognostic Markers in Malignant Pleural Mesothelioma

Weicheng Duan[1†], *Kang Wang*[1†], *Yijie Duan*[1], *Xiuyi Chen*[2], *Xufeng Chu*[1], *Ping Hu*[2*] and *Bo Xiong*[1*]

[1] Department of Forensic Medicine, Tongji Medical College, Huazhong University of Science and Technology, Wuhan, China, [2] Key Laboratory of Environment and Health (HUST), Ministry of Education, School of Public Health, Tongji Medical College, Huazhong University of Science and Technology, Wuhan, China

Malignant pleural mesothelioma (MPM) is a highly aggressive cancer with short survival time. Unbalanced competing endogenous RNAs (ceRNAs) have been shown to participate in the tumor pathogenesis and served as biomarkers for the clinical prognosis. However, the comprehensive analyses of the ceRNA network in the prognosis of MPM are still rarely reported. In this study, we obtained the transcriptome data of the MPM and the normal samples from TCGA, EGA, and GEO databases and identified the differentially expressed (DE) mRNAs, lncRNAs, and miRNAs. The functions of the prognostic genes and the overlapped DEmRNAs were further annotated by the multiple enrichment analyses. Then, the targeting relationships among lncRNA–miRNA and miRNA–mRNA were predicted and calculated, and a prognostic ceRNA regulatory network was established. We included the prognostic 73 mRNAs and 13 miRNAs and 26 lncRNAs into the ceRNA network. Moreover, 33 mRNAs, three miRNAs, and seven lncRNAs were finally associated with prognosis, and a model including seven mRNAs, two lincRNAs, and some clinical factors was finally established and validated by two independent cohorts, where CDK6 and SGMS1-AS1 were significant to be independent prognostic factors. In addition, the identified co-expressed modules associated with the prognosis were overrepresented in the ceRNA network. Multiple enrichment analyses showed the important roles of the extracellular matrix components and cell division dysfunction in the invasion of MPM potentially. In summary, the prognostic ceRNA network of MPM was established and analyzed for the first time and these findings shed light on the function of ceRNAs and revealed the potential prognostic and therapeutic biomarkers of MPM.

Keywords: ceRNA, mesothelioma, lncRNA, biomarker, overall survival, microenvironment

OPEN ACCESS

Edited by:
Nicholas Syn, National University of Singapore, Singapore

Reviewed by:
Luciano Mutti, Temple University, United States
Suman Ghosal, National Institutes of Health (NIH), United States

***Correspondence:**
Ping Hu
pinghu@hust.edu.cn
Bo Xiong
bxiong@hust.edu.cn

[†] These authors have contributed equally to this work

Specialty section:
This article was submitted to Thoracic Oncology, a section of the journal Frontiers in Oncology

Received: *08 October 2020*
Accepted: *15 February 2021*
Published: *23 April 2021*

Citation:
Duan W, Wang K, Duan Y, Chen X, Chu X, Hu P and Xiong B (2021) Combined Analysis of RNA Sequence and Microarray Data Reveals a Competing Endogenous RNA Network as Novel Prognostic Markers in Malignant Pleural Mesothelioma. Front. Oncol. 11:615234. doi: 10.3389/fonc.2021.615234

INTRODUCTION

Malignant pleural mesothelioma (MPM), which is mainly associated with the asbestos exposure and derived from the pleural or peritoneal mesothelial cell surfaces, is an aggressive tumor with very poor prognosis (median survival time < 12 months after diagnosis) (1). According to epidemiological investigations, the number of patients has been increasing in recent years, especially in developing countries, which leads to ca. 40,000 deaths per year worldwide (2). Currently, it is difficult to differentially diagnose MPM, since inclusion of more biomarkers based on the latest research would likely increase the accuracy and efficiency of prognosis. It is therefore essential and urgent to identify new prognostic biomarkers and therapeutic targets and to understand its molecular mechanisms.

The competing endogenous RNA (ceRNA) theory illustrates a novel regulatory mechanism for gene regulation, by which one transcript (e.g., an lncRNA) can control and modulate the expression of another transcript (e.g., an mRNA) by competitive interactions with an miRNA (3). It has been demonstrated that ceRNAs are widely involved in the occurrence and progression of various cancers (4–6). Moreover, some ceRNAs have been shown to be valuable targets for the treatment and prognosis of multiple cancers (7, 8). With the development of high-throughput sequencing technologies, more and more ceRNA networks have been constructed and analyzed in multiple cancers, such as gastric cancer and breast cancer (9, 10). However, there are few studies focused on the function of ceRNA networks in MPM. Some recent studies implicated that non-coding RNA (ncRNA) dysfunction is closely associated with the properties of MPM cells (11–13). Therefore, it is highly likely that certain ceRNA networks may also be involved in the pathogenesis of MPM.

In this study, we analyzed the differential expression of mRNAs, lncRNAs, and miRNAs (DEmRNAs, DElncRNAs, and DEmiRNAs) based on the RNA-Seq and miRNA-Seq data in different subgroups of the MPM patients categorized according to the overall survival of the MPM patients. The DEGs related to the overall survival were further compared with the DEGs between the MPM and the normal tissues in the microarray data. Then, we constructed a ceRNA network of the overlapped DERNAs based on their interactions obtained from multiple databases. Furthermore, Kaplan–Meier survival analyses and univariate, lasso, and multivariate Cox regression analyses were conducted to explore the mRNA, miRNA, and lncRNA biomarkers in the ceRNA network. Accordingly, the risk assessment model combined with the multiple clinical factors and the screened RNAs based on regression coefficients were established, evaluated, and validated based on the two independent MPM datasets. Weighted gene co-expression network analysis (WGCNA) was used to further explore the reliability of the ceRNA network as a prognostic marker as well as its potential mechanism. This study provides new insights on the biological functions related to the lncRNA in MPM patients and the additional biomarkers for the prognosis of MPM.

MATERIALS AND METHODS

TCGA MPM Dataset

Data for patients with MPM collected from the TCGA database was regarded as a training group. The criteria of exclusion were set as follows: (1) patients without lncRNA and mRNA information; (2) survival time of patients was unavailable or survival time of alive patients was <30 months. Overall, 80 MPM patients were included in our study. Next, the 80 patients were further screened to be included into two groups according to the survival time: high-risk group and low-risk group. The criteria of grouping were set as follows: patients with overall survival <12 months were included into high-risk group, and patients with overall survival >30 months were included in the low-risk group. Finally, the expression profiles of the patients in the two groups were used for the differential expression gene (DEG) analyses. In addition, the clinical information and the expression profiles of all 80 patients were used for the univariate, the lasso and multivariate Cox regression analyses, and WGCNA. Similarly, another study from the EGA database including 211 MPM patients was used to validate the RNA expression results. The GSE12345 (four normal tissues and nine MPM tissues) and GSE42977 (nine normal tissues and 39 MPM tissues) datasets were downloaded from the GEO database to explore the DEGs between the normal tissues and the MPM tissues for cross comparison of DEG associated with overall survival.

Data Processing

The normalized read-count data and the Fragments Per Kilobase of transcript per Million fragments of RNA-Seq by RNASeqV2 were obtained from the TCGA database as well as the STAD level 3 microRNA sequencing (miRNA-seq) data. The cleaned fastq files were downloaded from the EGA database. According to the protocol in the TCGA database, the STAR software was used to align the fastq files to the human GRCh38 genome file, and the Htseq-Count software was used to count the reads. Next, the Edge R package was applied to analyze the gene expression profiles to identify the DEmRNAs, DElincRNAs, and DEmiRNAs ($\log_2$-fold change > 1.0, false discovery rate (FDR) < 0.05). The TPM (Transcripts Per Million) were calculated for the subsequent analyses and validation. The GSE12345 dataset obtained from the Affymetrix Human Genome U133 Plus 2.0 Array was annotated by GPL570. The GSE42977 dataset based on the Illumina HumanRef-6 v2.0 expression beadchip was annotated by GPL6790. The two microarray datasets were normalized by the robust multi-array average algorithm. When multiple probes were mapped to the same gene, the mean of the probe intensities will be used. After that, the differential expression analyses of the microarray data were performed using limma package [fold change > 2.0, false discovery rate (FDR) < 0.05].

Functional Enrichment Analysis

The functional enrichment analyses of the DEGs, including GO function analyses and KEGG pathway analyses, were carried out by the clusterProfiler package. For the GO analyses, cellular component (CC), biological

process (BP), and molecular function (MF) terms were analyzed. FDR < 0.05 was used as the statistically significant cutoff in these analyses. Besides, we also performed the gene set enrichment analysis (GSEA) for all the mRNAs using the clusterProfiler package with the c2.all.v6.2.entrez.gmt and c5.all.v6.2.entrez.gmt gene set collections. Gene sets with FDR < 0.05 were considered to be significantly enriched.

TABLE 1 | The characteristics of the included MPM patients.

Characteristic		TCGA		EGA	
		All case numbers	Case numbers used in DEG analysis	All case numbers	Case numbers used in DEG analysis
Sample type	MESO	80	30	211	128
Age	Median	64.5	62.5	65.4	64.15
	Range [years]	28–81	28–81	18.8–86	27.3–86
Sex	Male	65	27	176	108
	Female	15	3	35	20
Vital status	Alive	8	0	48	0
	Dead	72	30	163	128
Survival time	Median	15.06	8.32	12.6	7.8
	Range [months]	0.65–91.73	0.65–91.73	0.24–132.6	0.24–132.6

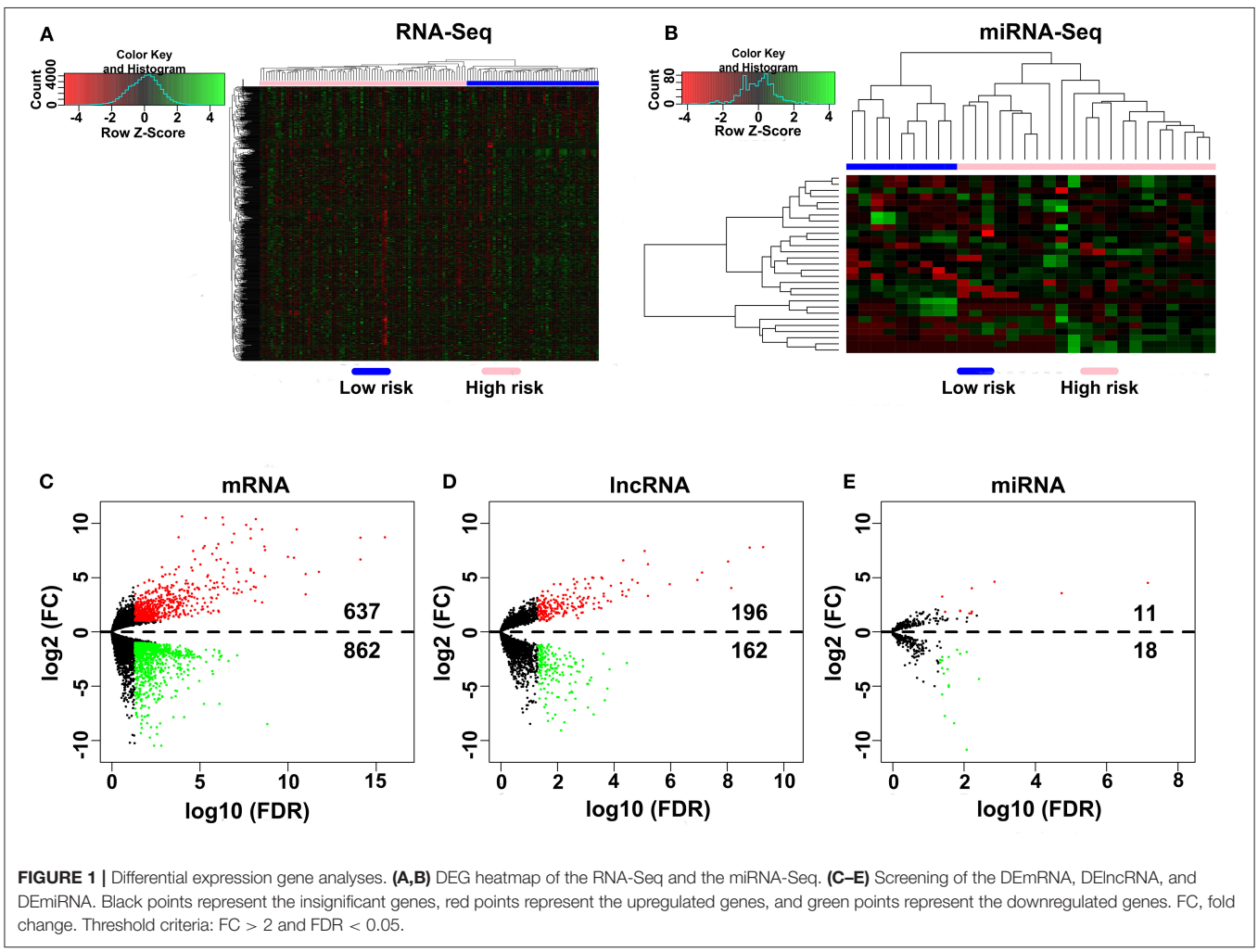

FIGURE 1 | Differential expression gene analyses. **(A,B)** DEG heatmap of the RNA-Seq and the miRNA-Seq. **(C–E)** Screening of the DEmRNA, DElncRNA, and DEmiRNA. Black points represent the insignificant genes, red points represent the upregulated genes, and green points represent the downregulated genes. FC, fold change. Threshold criteria: FC > 2 and FDR < 0.05.

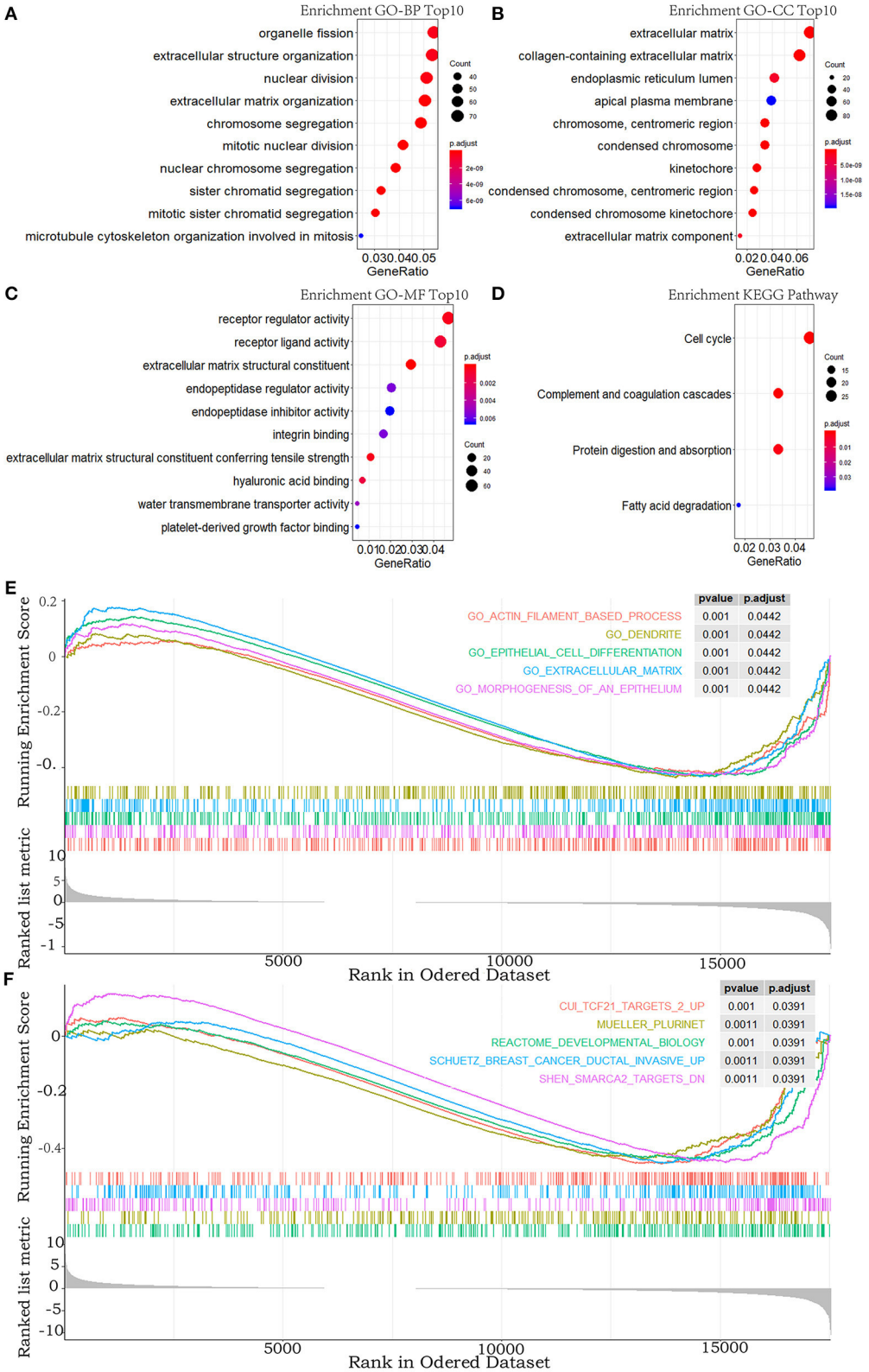

FIGURE 2 | GO, KEGG pathway, and GSEA enrichment analyses. **(A–C)** Top 10 enriched terms in GO-BP, GO-CC, and GO-MF. **(D)** The significant terms in the KEGG pathway. **(E,F)** TOP 5 enriched terms of GSEA in the c5.all.v6.2.entrez.gmt gene sets and the c2.all.v6.2.entrez.gmt gene sets. *P*-value adjusted by FDR < 0.05.

Construction of an lncRNA-Related ceRNA Network

The overlapped DEGs between the RNA-Seq and the microarray were used for the construction of the prognostic ceRNA network. We used starBase v3.0 (http://starbase.sysu.edu.cn/) to retrieve the lncRNA–miRNA interactions and then used miRBase targets (http://mirdb.org/miRDB/), miRTarBase (http://mirtarbase.mbc.nctu.edu.tw/), and TargetScan (http://www.targetscan.org/) to predict lmiRNA–mRNA interactions (14–17). To increase the reliability of the results, only the miRNA–mRNA interactions

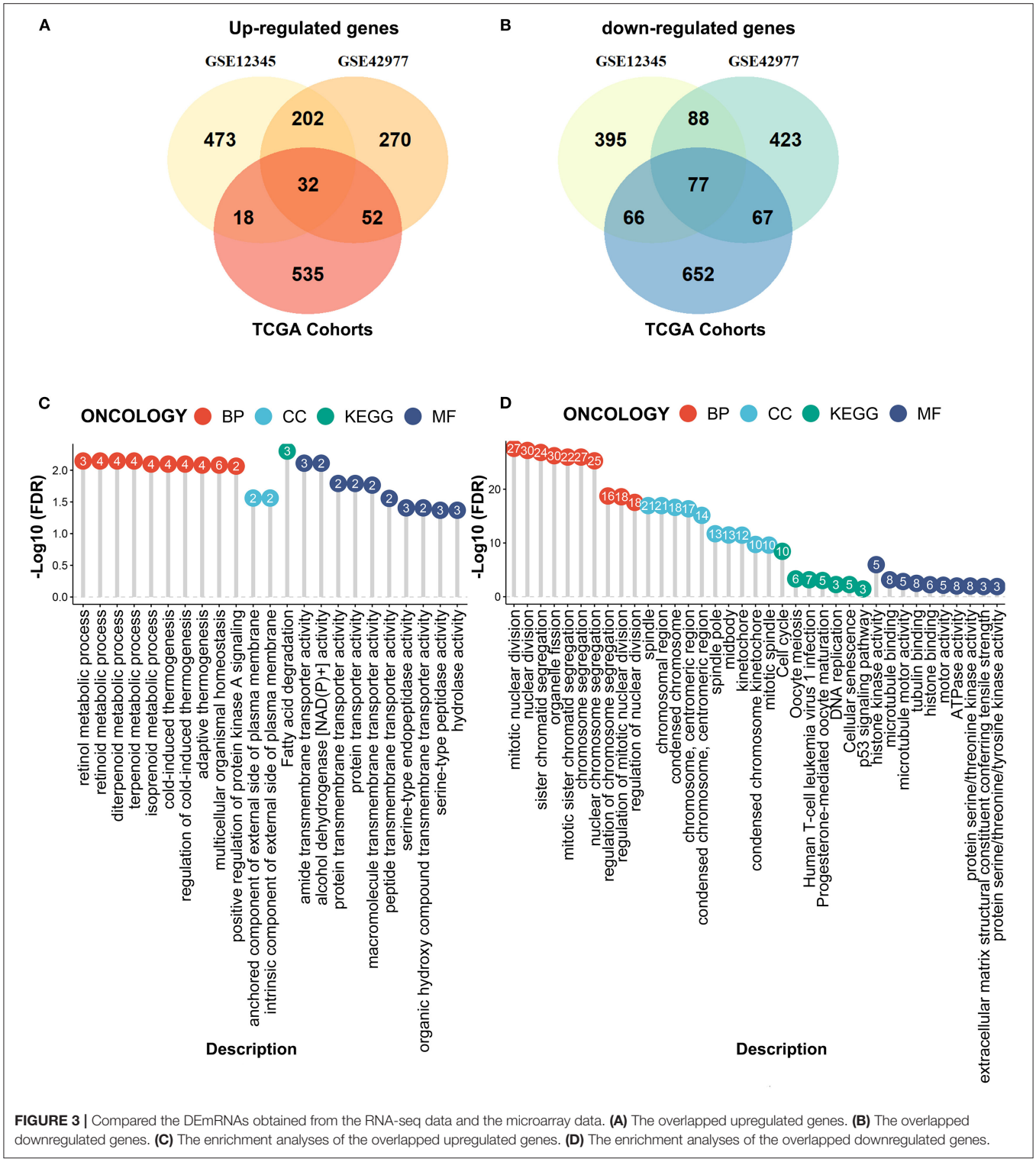

FIGURE 3 | Compared the DEmRNAs obtained from the RNA-seq data and the microarray data. **(A)** The overlapped upregulated genes. **(B)** The overlapped downregulated genes. **(C)** The enrichment analyses of the overlapped upregulated genes. **(D)** The enrichment analyses of the overlapped downregulated genes.

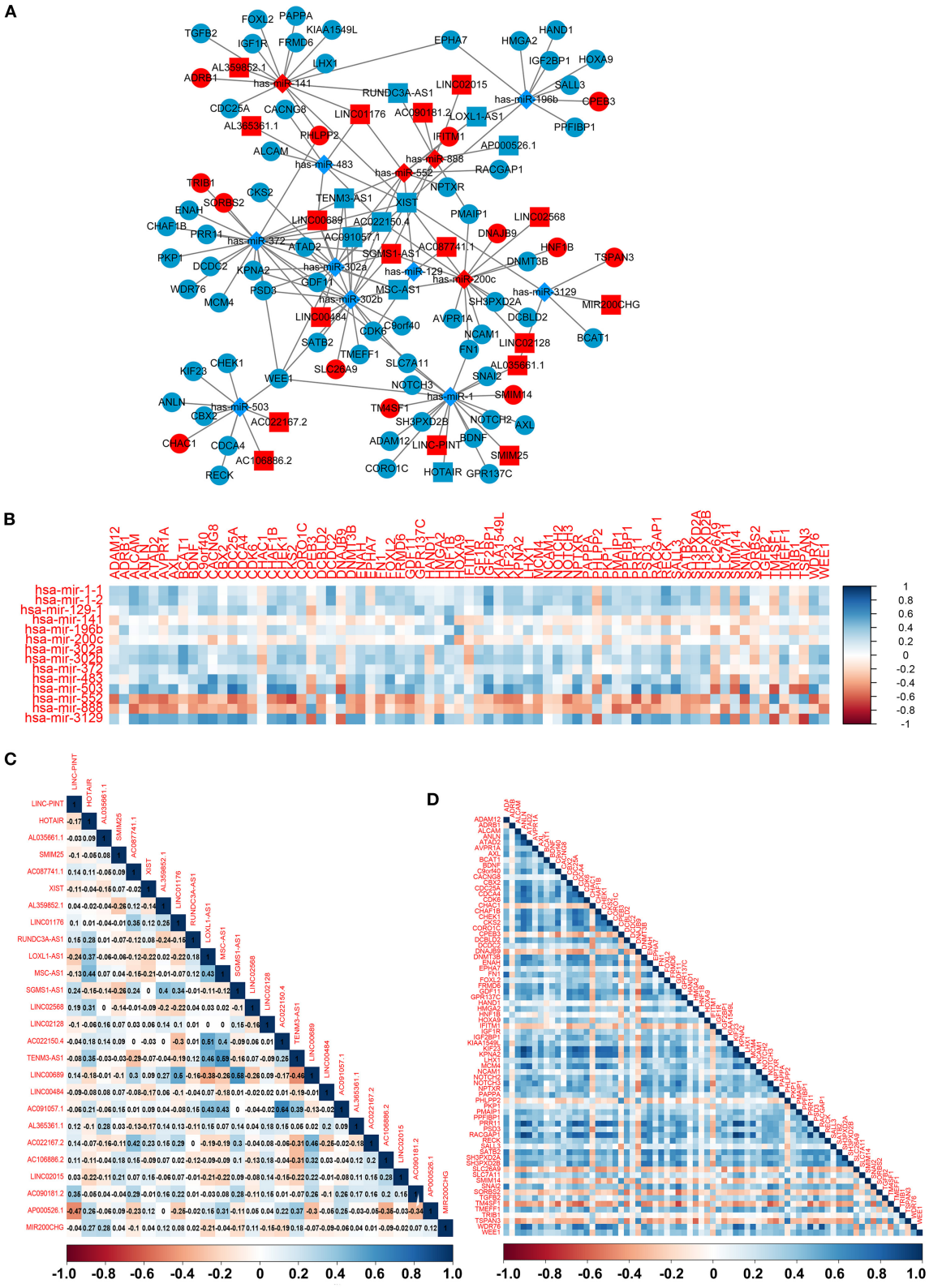

FIGURE 4 | The construction of the ceRNA network among the 26 lncRNAs, 13 miRNAs, and 73 mRNAs. **(A)** The ceRNA network among lncRNA–miRNA–mRNA. Ellipse represents mRNA. Rectangle represents lncRNA. Diamond represents miRNA. Red represents upregulation, and blue represents downregulation. **(B–D)** The Pearson correlation analyses among the miRNA–mRNA, 26 lncRNAs, and 73 mRNAs.

intersecting in all three databases were included into the ceRNA network. Moreover, the Pearson correlations of the pairs between miRNAs and mRNAs were calculated and the absolute values of the pairs more than 0.4 were regarded as interacted pairs. Finally, a ceRNA network was constructed and visualized by Cytoscape v3.7.1.

Survival Prediction Model Construction and Evaluation

The mRNAs, miRNAs, and lncRNAs from the ceRNA network were used for the univariable Cox regression analyses to screen for the RNAs associated with overall survival, and only the RNAs with $P < 0.05$ were enrolled into the followed Kaplan–Meier survival analyses based on the log-rank test according to the grouping by the median value of the expression quantities. After Kaplan–Meier survival analyses, the mRNAs and lncRNAs with $P < 0.05$ were included into the lasso Cox regression analyses to further screen the variables. Accordingly, the survival prediction model was constructed through the regression coefficients of the multivariable Cox regression analysis, as described in the following equation: risk score = R1G1 + R2G2 + R3G3 + ... RnGn (R is the regression coefficient obtained from the final multivariable Cox analysis and L is the expression value of each gene or the type of different clinical factor). Then, the patients were divided into two groups (high-risk-score group and low-risk-score group) according to the cutoff value obtained from the OptimalCutpoints package, and the Kaplan–Meier survival analyses were performed between the two groups. Moreover, the receiver-operating characteristic (ROC) curve analyses were performed to estimate the efficiencies of the model under the same grouping; only AUC values > 70% were regarded as efficient models.

Identification and Annotation of Gene Modules Related to the Risk Model According to WGCNA

The WGCNA algorithm was used to construct the gene co-expression network (18). We first conducted the WGCNA analysis to identify the gene modules closely related to the overall survival and the risk scores. Then the significant modules were further selected for further analyses, and the mRNAs of the ceRNA network co-expressed in the significant modules were further input in the String database (string.org) to predict the protein–protein interaction (PPI) relationship. The PPI network was then visualized by Cytoscape v3.7.1, and the hub genes were identified using 12 algorithms of the CytoHubba plugin. Then, the results were cross-compared to generate a final list of hub genes. Besides, the genes enrolled into these significant modules were used for GO-BP, GO-MF, and KEGG pathway enrichment analyses by clusterProfiler package.

Evaluation of the Tumor Infiltrating Immune Cells With the Risk Model

To infer the infiltrating immune cells of MPM associated with the ceRNA axes, we used the mRNAs in the ceRNA network to estimate the proportions of the 22 types of infiltrating immune cells by deconvolution of the CIBERSORT algorithm (19). According to the grouping, we obtained the significant changes of the immune cell types between the high- and low-risk-score groups using Student's *t*-test.

TABLE 2 | The concrete interactions among the lncRNAs, miRNAs, and mRNAs in the ceRNA network.

miRNA	lncRNA	mRNA
hsa-miR-1	LINC-PINT, HOTAIR, AL035661.1, SMIM25, AC087741.1	NOTCH2, FN1, TM4SF1, SMIM14, SLC7A11, SH3PXD2B, CDK6, SNAI2, ADAM12, WEE1, BDNF, CORO1C, GPR137C, NOTCH3, AXL
hsa-miR-129	AC087741.1, XIST	CDK6
hsa-miR-141	AL359852.1, LINC01176, RUNDC3A-AS1, XIST	TGFB2, CDC25A, FOXL2, EPHA7, PAPPA, ADRB1, KIAA1549L, FRMD6, IGF1R, PHLPP2, LHX1
hsa-miR-196b	LOXL1-AS1, XIST	HAND1, EPHA7, HOXA9, CPEB3, PPFIBP1, HMGA2, IGF2BP1, SALL3
hsa-miR-200c	MSC-AS1, SGMS1-AS1, LINC02568, LINC02128, AC022150.4, XIST	FN1, DCBLD2, DNAJB9, SH3PXD2A, NCAM1, AVPR1A, HNF1B, PMAIP1, DNMT3B
hsa-miR-302a	TENM3-AS1, LINC00689, MSC-AS1, LINC00484, SGMS1-AS1, AC091057.1, AC022150.4, XIST	PSD3, ATAD2, CKS2, WEE1, GDF11, KPNA2
hsa-miR-302b	TENM3-AS1, LINC00689, MSC-AS1, LINC00484, SGMS1-AS1, AC091057.1, AC022150.4, XIST	SLC26A9, SATB2, SLC7A11, CDK6, PSD3, ATAD2, C9orf40, TMEFF1, WEE1, GDF11, KPNA2
hsa-miR-372	TENM3-AS1, LINC00689, MSC-AS1, LINC00484, SGMS1-AS1, AC091057.1, AC022150.4, XIST	PKP1, ENAH, SORBS2, DCDC2, CDK6, PSD3, MCM4, ATAD2, TRIB1, WEE1, GDF11, WDR76, PHLPP2, PRR11, KPNA2, CHAF1B
hsa-miR-483	AL365361.1, LINC01176, LINC00689, AC022150.4, XIST	ALCAM, CACNG8
hsa-miR-503	AC022167.2, AC106886.2	ANLN, RECK, WEE1, CHEK1, CDCA4, CHAC1, KIF23, CBX2
hsa-miR-552	TENM3-AS1, LINC01176, AC091057.1, AC022150.4, XIST, LOXL1-AS1	IFITM1, RACGAP1, NPTXR
hsa-miR-888	LINC02015, SGMS1-AS1, AC090181.2, RUNDC3A-AS1, AP000526.1, XIST	PMAIP1
hsa-miR-3129	MIR200CHG, AL035661.1, XIST	BCAT1, TSPAN3

Statistical Analysis

The differential expression gene analyses of the RNA-seq data were performed by the R package "edge R." The differential expression gene analyses of the microarray data were conducted by the R package "limma." The enrichment analyses were performed by R package "clusterProfiling." All of these analyses involved in the multiple-hypothesis test were finally corrected by the FDR method. The univariate and the multivariate Cox regression analyses were performed by R package "survival." The lasso regression analyses were performed by the R package "glmet." Moreover, the Kaplan–Meier analyses were carried out by R package "survival," whose statistical significances were assessed by the two-sided log-rank test. The statistical analyses between the clinical traits and the risk model were performed by the chi-square test or Fisher exact test according to the distribution of the data. The R software version 3.6.3 was used for the study. All statistical tests were two-sided.

RESULTS

Screening of Patients and Identification of DEGs

A total of 80 patients with MPM were downloaded from the TCGA database. Thereinto, the RNA expression profiles of 21 low-risk (overall survival > 30 months) samples and nine high-risk (overall survival < 12 months) samples were used to explore the DEmRNAs, DElncRNAs, and DEmiRNAs. The clinical and pathological characteristics of MPM patients are shown in **Table 1**. According to the results of the DEGs, the patients were clearly clustered into two groups, indicating that the overall gene expression patterns are significantly different in the two groups (**Figures 1A,B**). A total of 1,499 DEmRNAs, 358 DElncRNAs, and 29 DEmiRNAs were obtained according to the criteria ($P < 0.05$ and fold change > 2, **Figures 1C–E**).

To explore the functional features of these DEGs related to overall survival, we performed GO and KEGG enrichment analyses (FDR-corrected $P < 0.05$). The top 10 significant GO terms are mainly involved in the processes and the components related to the extracellular matrix, the cell division, and the receptor regulator activity (**Figures 2A–C**). Four pathways were enriched in the KEGG analysis (**Figure 2D**). These results all suggested that abnormal extracellular matrix components, cell cycle, and immune-response components are potentially important causes in the progression of MPM, which have been closely associated with growth and metastasis of other cancer cells (20).

In addition, to explore the changes of the overall gene expression levels of MPM, 17746 mRNAs were input to implement GSEA based on the fold change order using the gene sets of c2.all.v6.2.entrez.gmt and c5.all.v6.2.entrez.gmt. One hundred eighty terms in c5.all.v6.2.entrez.gmt gene set and 188 terms in the c2.all.v6.2.entrez.gmt gene set were enriched (FDR < 0.05), the top five of which were exhibited in **Figures 2E,F**. Morphogenesis and differentiation of epithelium, cell movement, and extracellular matrix were significantly enriched in the c5.all.v6.2.entrez.gmt gene set (**Figure 2E**), supporting the role of the extracellular matrix in the progression of MPM and indicating the convergence between the invasion of MPM and the morphogenesis and differentiation of the epithelium. Some specific targets and pathways were mainly enriched in the c2.all.v6.2.entrez.gmt gene set (**Figure 2F**), suggesting that progression of MPM may partly be involved in the invasive

TABLE 3 | Statistical analyses associated with the OS of the mRNAs and lncRNAs in the ceRNA network.

Gene symbol	Univariate analysis			(Kaplan–Meier survival curves, log-rank test)
	HR	CI95	*P*-value	*P*-value
KPNA	1.02	1.01–1.02	<0.0001	3.53e-10
PRR11	1.25	1.16–1.34	<0.0001	4.82e-08
CDC25A	2.14	1.68–2.73	<0.0001	9.28e-08
KIF23	1.19	1.12–1.23	<0.0001	1.92e-07
ANLN	1.06	1.04–1.09	<0.0001	6.64e-07
CHAF1B	1075	1.46–2.1	<0.0001	1.20e-06
RACGAP1	1.21	1.14–1.29	<0.0001	4.29e-06
CHEK1	1.20	1.1–1.31	0.00001	4.30e-06
SATB2	1.58	1.19–2.11	<0.0019	4.35e-06
DNMT3B	3.01	1.85–4.49	<0.0001	5.10e-06
MCM	1.11	1.06–1.16	<0.0001	8.06e-06
CORO1C	10.4	1.03–1.05	<0.0001	2.21e-05
AXL	1.01	1.01–1.02	<0.0001	2.48e-05
CDCA4	1.14	1.08–1.2	<0.0001	3.35e-05
TMEFF1	129.56	4.61–3643.52	0.043	4.54e-05
WEE1	1.17	1.07–1.28	0.0006	5.15e-05
CKS2	1.03	1.02–1.04	<0.0001	7.01e-05
CDK6	1.13	1.08–1.18	<0.0001	9.47e-05
C9orf40	1.78	1.46–2.16	<0.0001	0.000147
ENAH	1.11	1.06–1.16	<0.0001	0.000354
GDF11	1.64	1.26–2.12	<0.0001	0.000413
WDR76	1.45	1.24–1.71	<0.0001	0.001005
ATAD2	1.26	1.14–1.39	<0.0001	0.00202
CPEB3	0.50	0.34–0.74	<0.0001	0.002249
NPTXR	1.25	1.12–1.39	<0.0001	0.002846
PAPPA	1.19	1.08–1.3	<0.0002	0.004774
SNAI2	1.07	1.04–1.1	<0.0001	0.006123
DCDC2	1.12	1.05–1.2	0.0014	0.006189
DNAJB9	0.98	0.96–0.99	0.0027	0.006755
AC026470.1	0.75	0.69–0.88	0.0001	0.008526
DCBLD2	1.03	1.01–1.05	0.0007	0.01441
FRMD6	1.10	1.05–1.15	0.0001	0.035087
SMIM14	0.93	0.9–0.97	0.0007	0.041198
hsa-miR-302a	1.02	1–1.04	0.0118	0.000125
hsa-miR-302b	1.01	1–1.02	0.0109	0.000134
hsa-miR-503	1.01	1–1.01	0.0062	0.007793
AC091057.1	3.92	2.21–6.97	<0.0001	0.000565
AC022150.4	3.99	2.1–7.6	<0.0001	0.000763
SGMS1.AS1	0.03	0–0.19	2.00E-04	3.56E-05
LINC00689	0.4	0.23–0.71	0.0017	0.030472
AC087741.1	0.58	0.41–0.83	0.0025	0.036343
MSC.AS1	1.26	1.08–1.48	0.0031	0.00131
RUNDC3A.AS1	10.26	1.98–53.1	0.0055	0.010718

Bold: the genes in the survival model.

pathways of breast cancer and pathways related to TCF21 and SMARCA2 targets.

We next performed the differential expression analyses to explore the DEGs between the MPM tissues and the normal tissues by the limma algorithm based on the microarray data. A total of 1351 DEGs (725 upregulated genes and 626 downregulated genes) were obtained from the GSE12345 dataset, and 1211 DEGs (556 upregulated genes and 655 downregulated genes) were obtained from the GSE42977 dataset (**Figures 3A,B**). To screen the DEGs associated with the development of the MPM, we further compared the DEGs related to the overall survival from the RNA-Seq dataset with the DEGs related to MPM obtained from the two microarray datasets, which showed the 32 overlapped upregulated DEGs and the 77 downregulated DEGs (**Figures 3A,B**). Similar to the above results, the enrichment analyses of the overlapped downregulated

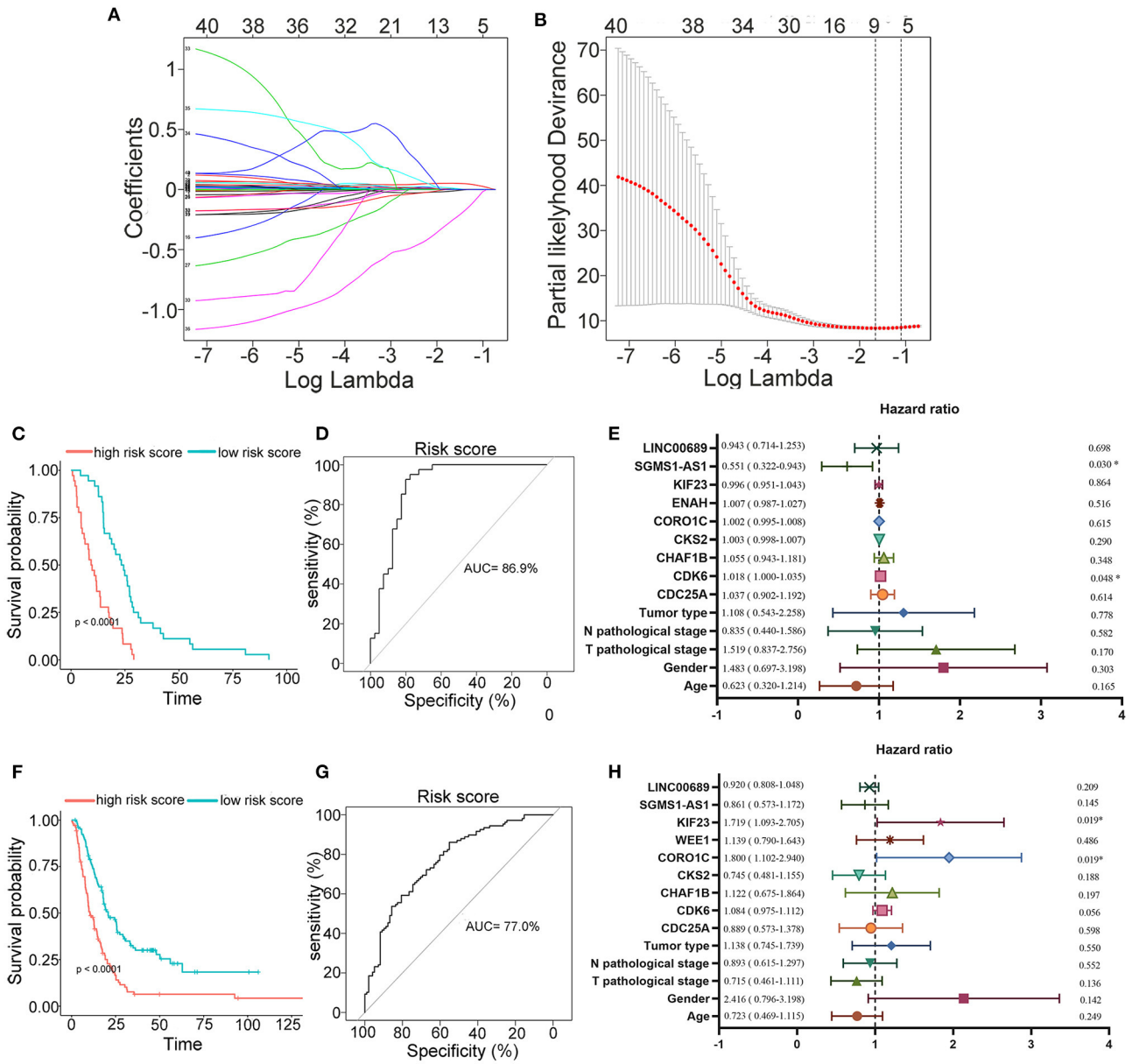

FIGURE 5 | Construction, estimation, and validation of the risk model. **(A)** Least absolute shrinkage and selection operator (LASSO) coefficient profiles of the 40 genes. The value was chosen by 10-fold cross-validation. **(B)** The numbers above the graph represent the number of genes involved in the LASSO model. **(C,D)** Survival curve and ROC curve of the risk model according to the dataset of EGA. **(E)** Forest plot showing associations between the selected nine genes, the reported clinical factors, and the overall survival in the model. **(F–H)** Validation of the risk model based on the survival curve, the ROC curve, and the multivariate Cox analysis according to the EGA dataset. The significances of the survival curves were calculated by log-rank test. Also, the AUC values of ROC curves > 70% were regarded as efficient models.

TABLE 4 | Statistical analyses between the clinical traits and the risk model.

Subgroup	Low score	High score	*P*-value
Age			
<60	12	11	0.8049
≥60	28	29	
Sex			
Male	32	33	0.7745
Female	8	7	
Tumor grade			
STAGE I	3	6	0.4638
STAGE II+STAGE III+STAGE IV	37	34	
Histological types			
Biphasic mesothelioma	5	17	***0.003296***
Diffuse malignant mesothelioma (NOS)	2	3	
Epithelioid mesothelioma	33	20	

Bold: the types of clinical traits.
Italic and bold: significant value.

DEGs also revealed the abnormal roles of the cell division in the development of the MPM (**Figure 3C**). Moreover, the overlapped upregulated DEGs were mainly involved in the regulation of the metabolic processes (**Figure 3D**).

Construction of an lncRNA–miRNA–mRNA ceRNA Network

To construct the credible ceRNA network among the lncRNAs–miRNAs–mRNAs, we input the 29 DEmiRNAs and the 358 DElncRNAs to get the interaction data between miRNAs and lncRNAs from the starBase v3.0 database. We next performed target prediction for miRNAs–mRNAs among the 29 miRNAs and the 109 overlapped mRNAs in the three databases (miRTarBase, miRDB, and TargetScan) and cross-compared the results to retain the miRNA–mRNA interactions that are consistent in all three databases. As a result, 26 lncRNAs, 13 miRNAs, and 73 mRNAs were predicted to have close interaction (**Figure 4A**, **Table 2**). To further explore the reliability of the ceRNA network, the Pearson correlations among the miRNAs–mRNAs, lncRNAs, and mRNAs were calculated based on the 80 expression profiles. The interacted miRNAs–mRNAs almost have relative high correlations with $|r| > 0.4$ (**Figure 4B**). Similar to the scattered distributions of the lncRNAs in the ceRNA network, the correlations among the lncRNAs were relatively weak, which suggested the accuracy of our ceRNA network (**Figure 4C**). Moreover, the majority of the mRNAs in the ceRNA network have positive correlations; the same with that many of the mRNAs in the ceRNA network are downregulated genes (**Figure 4D**). These results suggested the validity of the prognostic ceRNA network.

Construction and Evaluation of Survival Prediction Model

To further determine the association between the expression levels of the 73 mRNAs, 13 miRNAs, and 26 DElncRNAs in the ceRNA network and the overall survival of MPM patients, we performed the univariate Cox regression analyses in the 80 patients from TCGA (**Table 3**). Next, 52 mRNAs, six miRNAs, and 12 lncRNA were analyzed by the Kaplan–Meier survival analyses according to the grouping by the median value of expression quantities. Thirty-three mRNAs, three miRNAs, and seven lncRNAs were significant in the Kaplan–Meier survival analyses, and the significant mRNAs and lncRNAs were further screened to avoid overfitting by lasso Cox regression analyses (**Figure 5A**). As a result, CDC25A, CDK6, CHAF1B, CKS2, CORO1C, WEE1, KIF23, SGMS1-AS1, and LINC00689 were enrolled into the survival model (**Figure 5B**, **Table 3**). Interestingly, WEE1 and KIF23 were also identified as hub genes in the co-expressed PPI network, highlighting the importance of them related to the prognosis and the progression of MPM and the reliability of the model. Besides, the lncRNAs, WEE1, CKS2, and KIF23 included in the model were interacted with the miRNAs associated with survival time, suggesting that the model possessed high efficiency by integrating the information of mRNAs, lncRNAs, and miRNAs. Next, several clinical factors related to prognosis were also enrolled into the model, including age (≤60 or > 60), gender (female, male), T pathological stage (T1 + T2 or T3 + T4), N pathological stage (N0 + N1 or N2 + N3), and tumor type (epithelioid mesothelioma or non-epithelioid mesothelioma). According to the result of multivariate analysis, a risk model was constructed: Risk score = −0.472*age + 0.400*gender + 0.418*(T pathological stage)−0.180*(N pathological stage) + 0.102* (tumor type) + 0.036* CDC25A(exp) + 0.017*CDK6(exp) + 0.054* CHAF1B(exp) + 0.003* CKS2(exp) + 0.002* CORO1C(exp) + 0.0237* WEE1(exp)−0.004* KIF23(exp)−0.0597* SGMS1-AS1(exp)−0.056* LINC00689(exp). The cutoff value was determined by the sensitivity equal to the specificity method from the OptimalCutpoints package, which showed the best sensitivity and specificity for prognostic prediction (AUC values = 86.9%, **Figure 5D**). The Kaplan–Meier survival curves showed that the overall survival of patients with high-risk scores ($n = 32$) were significantly lower than those with the low-risk scores in the three models ($p < 0.001$, **Figure 5C**). The results showed that the model is of value for prognostic prediction (**Figures 5C,D**). In this risk model, CDK6 and SGMS1-AS1 were significant as potential independent prognostic factors (**Figure 5E**). Interestingly, the histological types of MPM were associated with the risk score after the statistical analyses between the clinical traits and the risk score, similar to the previous report about the correlation between the histological types and the overall survival (**Table 4**). Furthermore, another dataset of MPM patients was used to validate our results. According to the TPM values of 128 patients in the EGA database, the expression of the nine DEGs in our risk model were further confirmed to be significant based on Student's *t*-test with or without Welch correction (low risk: 40 patients, high risk: 88 patients, **Figure 6**). Moreover, the Kaplan–Meier survival analyses of the nine DEGs in our risk model based on the data of the 211 patients from EGA also showed that all of them are closely related to the survival time of the MPM patients (**Figure 7**). Likewise, the Kaplan–Meier survival

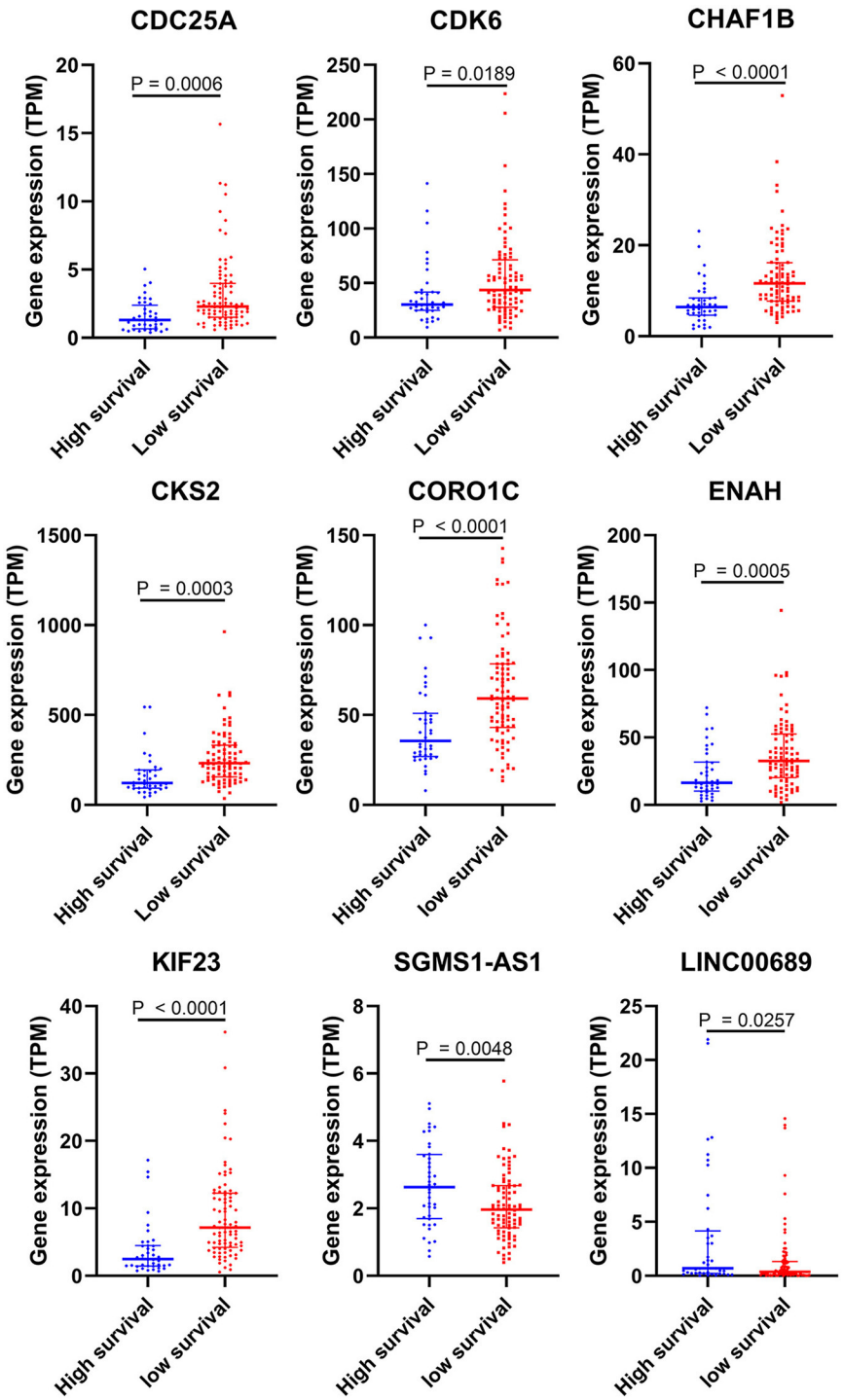

FIGURE 6 | Validation of DEGs in the risk model based on the EGA MPM dataset. The statistical analyses were performed by Students' *t*-test with or without Welch correction according to the TPM of genes.

analyses and the ROC curves showed that the risk model has great values to estimate the prognosis of MPM ($P < 0.001$, AUC values = 77.0%, **Figures 5F,G**). Also, the multivariate Cox analysis was performed to verify the identified potential independent prognostic factors according to the variates from the survival model in the EGA data, which showed that CDK6 had marginal significance and KIF23 and CORO1C were significant in the model (**Figure 5H**). In summary, all of these results using the EGA data validated the effectiveness of the risk model.

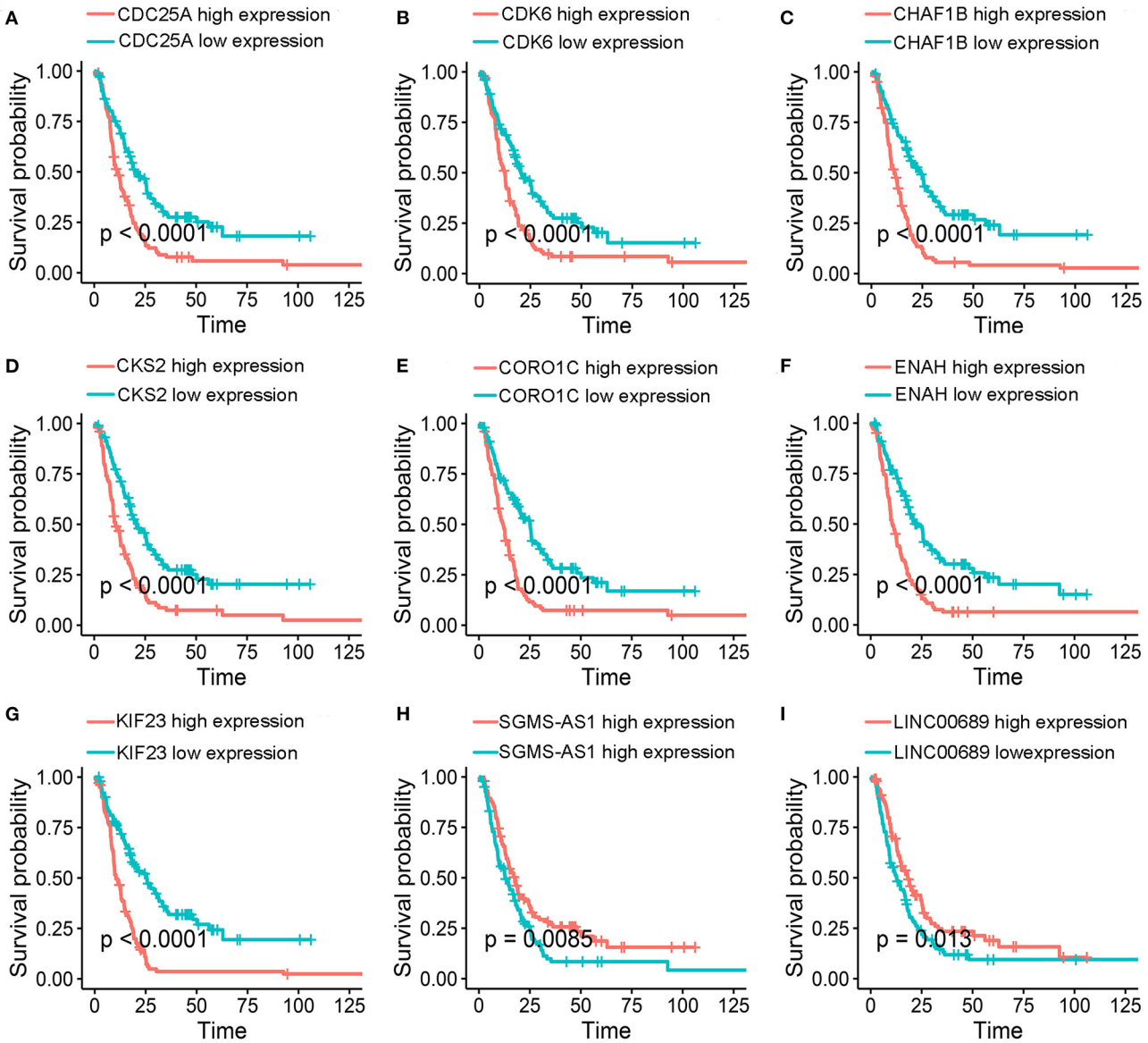

FIGURE 7 | Kaplan–Meier survival analyses. **(A-I)** Validation of of the nine genes in the model based on the EGA MPM dataset. The statistical significances were determined by the log-rank test.

Identification of Gene Modules and Functional Analyses According to WGCNA

To investigate the potential biological function of the ceRNA network, we used the WGCNA method to cluster the DEmRNAs based on the 80 expression profiles obtained from the TCGA database. Except the non-co-expression module (gray), we identified nine co-expression modules (**Figure 8A**) and associated the clinical traits with the identified modules, including the tumor stage, survival time, and risk score (**Figure 8B**). We found that the turquoise module and the blue module were the top two most significant modules associated with the risk scores and the survival time (**Figure 8B**). We then performed the Pearson analyses based on the genes in the two modules and further revealed that the turquoise module was positively correlated with the risk scores and the blue module was negatively correlated with the risk scores (turquoise module—risk score: cor = 0.9, P = 1e-200; blue module—risk score: cor = 0.81, P = 6e-59; **Figures 8C,D**). Notably, 7 of 73 mRNAs in the ceRNA network co-expressed in the blue module and 42 of 73 mRNAs in the ceRNA network co-expressed in the turquoise module (turquoise module: 513 genes, blue module: 195 genes), which showed that the genes in the turquoise co-expression modules associated with survival were overrepresented in the ceRNA network and indicated the reliability of the ceRNA network (P = 2.458e-05). We then input the genes in the turquoise module into the String database to

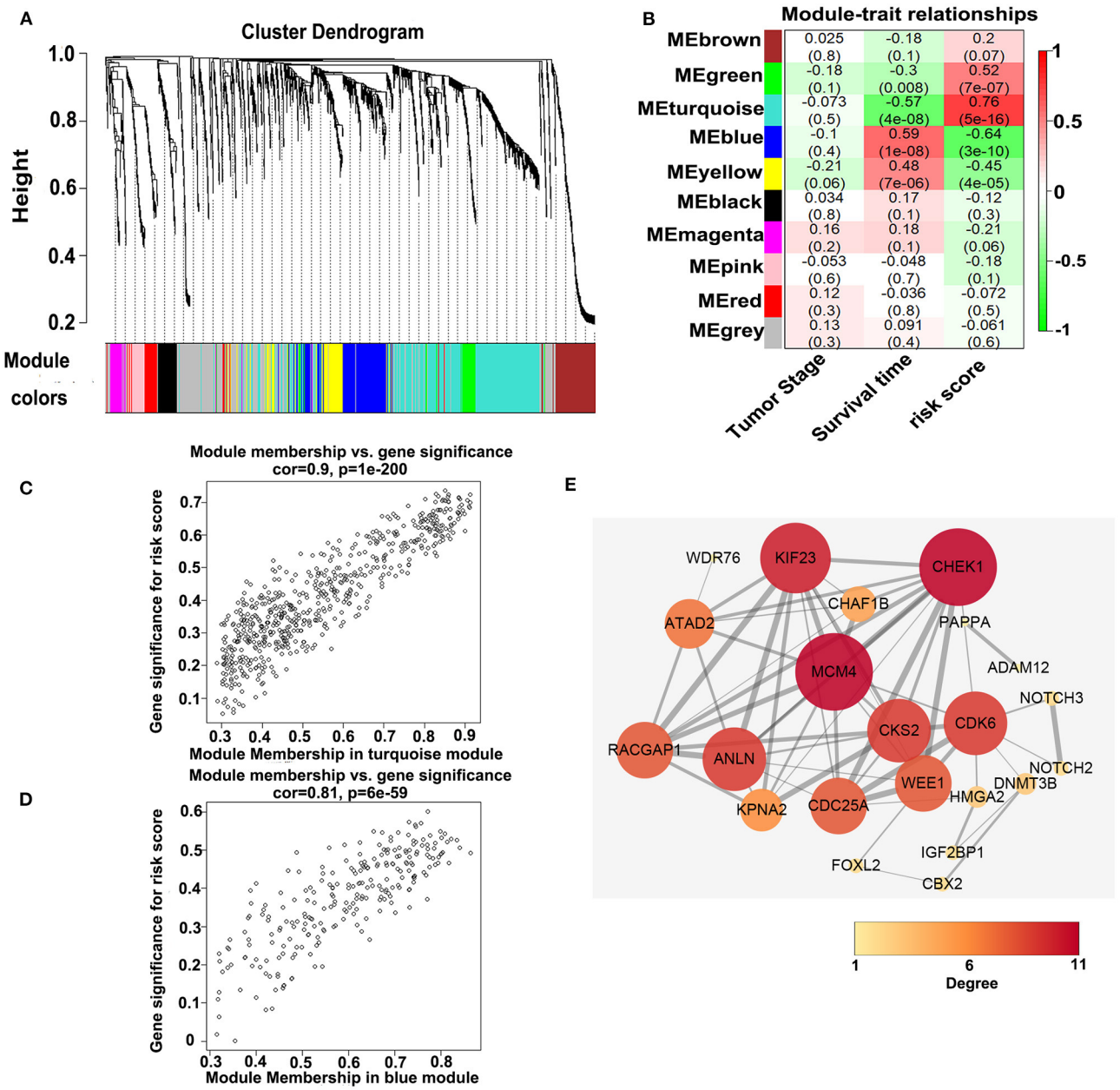

FIGURE 8 | WGCNA analyses of the DEmRNAs. **(A)** Identification of the co-expression modules. **(B)** Association between the modules and the traits. **(C)** Pearson correlations between the genes in the turquoise module and the risk score. **(D)** Pearson correlations between the genes in the blue module and the risk model. **(E)** Protein–protein interaction network analysis of the overlapped mRNAs in the ceRNA network and the turquoise module. The size and color of the round represent the number of links of the protein (gene).

predict the PPI relationship (**Figure 8E**). We further analyzed the topical structure of the PPI network by 12 methods to obtain the hub genes. According to the degrees among the genes, WEE1 and KIF23 were finally selected as the hub genes in the ceRNA PPI network, suggesting that they play important roles in the MPM.

The top 10 results of GO-BP, GO-MF, and KEGG pathway enrichment analyses using the genes included into the blue module and the turquoise module are shown in **Figure 9**. In the blue module, GO terms are mainly involved in the constituent of extracellular matrix (**Figures 9A,B**). As for pathways, they may be associated with the terminal symptoms of cancer patients (**Figure 9C**).

In the turquoise module, multiple processes related to the cell division were enriched (**Figures 9D,E**). Moreover, the markedly enriched pathways are associated with the cell cycle, the homologous recombination, the microRNAs in cancer, the p53 signaling pathway, etc. **Figure 9F**), which

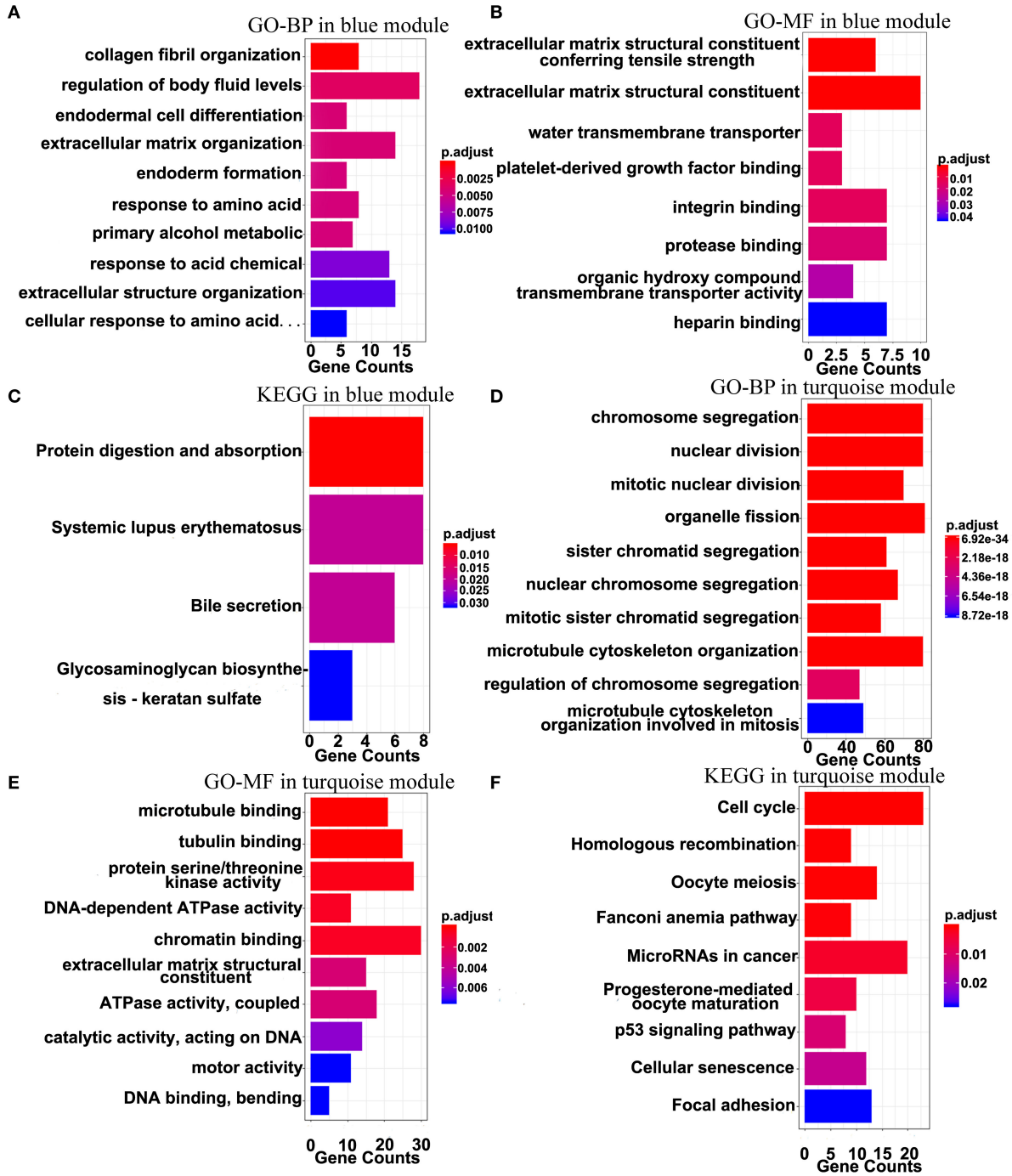

FIGURE 9 | Gene-enrichment analyses of genes in the blue module and the turquoise module. **(A)** Top 10 GO-BP terms in the blue module. **(B,C)** Significant GO-MF and KEGG pathway terms in the blue module. **(D,E)** Top 10 GO-BP and GO-MF terms in the turquoise module. **(F)** Significant KEGG terms in the turquoise module. *P*-value was adjusted by the FDR method and $p < 0.05$ was significant.

have been reported to participate in multiple levels of the tumorigenesis and the invasion. Overall, the results of the enrichment analyses demonstrated that the genes in the turquoise module are mainly involved in the abnormal process of cell division.

The Immune Cell Infiltration Analysis in the ceRNA Network

The tumor microenvironment involves the extracellular matrix components, the immune cells, and the other cellular components, which have partly been highlighted in multiple

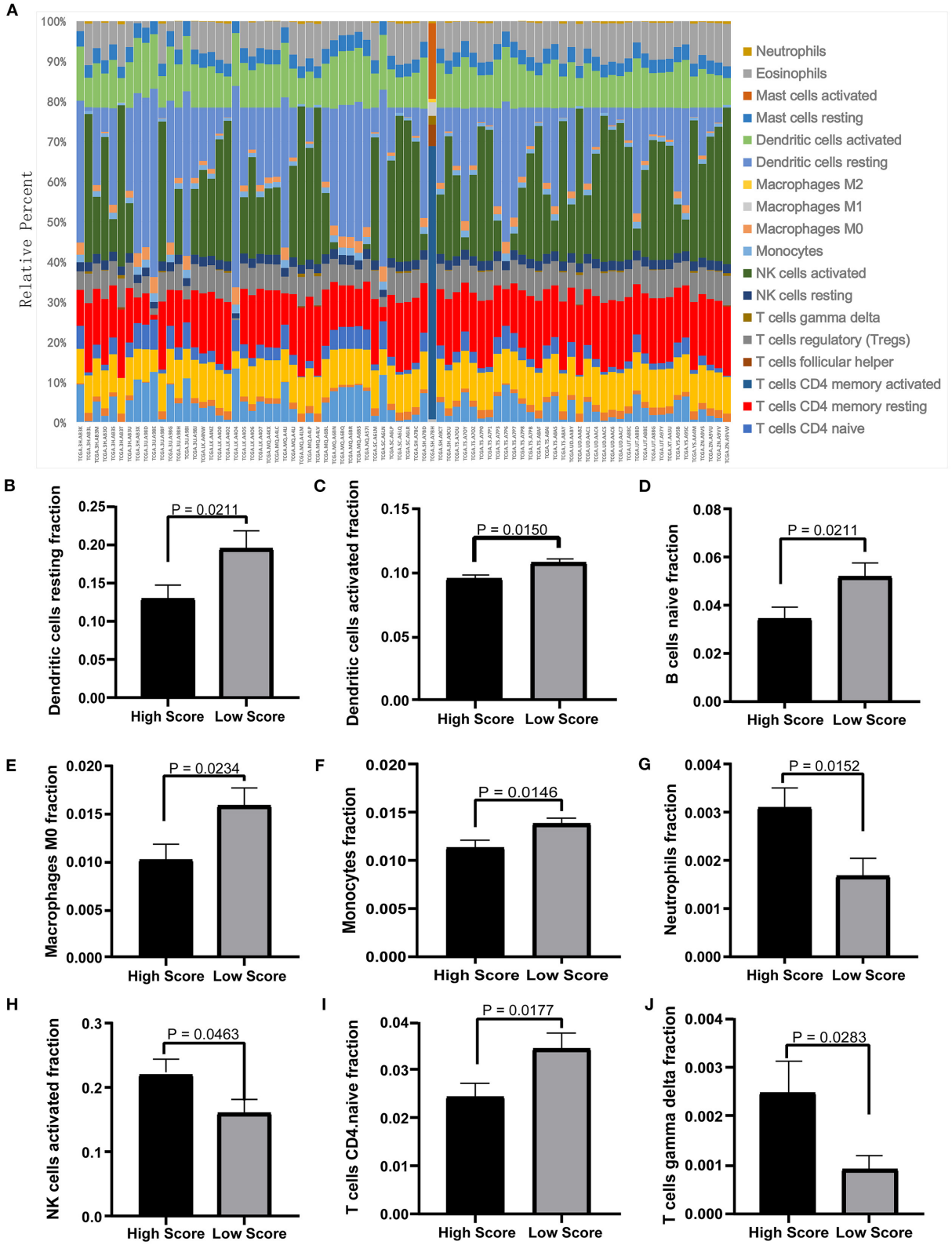

FIGURE 10 | Twenty-two types of immune-cell infiltration analyses. **(A)** The overall changes of 22 types of immune cells in the MPM tissues of the 80 patients. **(B–J)** The significant differences of the immune cells between the high- and low-score groups based on the Student's *t*-test.

analyses above. To further investigate the biological function of the ceRNA network regarding the tumor microenvironment, we utilized the CIBERSORT algorithm to study the changes of tumor-infiltrating immune cells between the high- and low-risk-score groups according to the DEmRNAs in the ceRNA network (73 mRNA). We calculated the variations of the 22 types of immune cells among the 80 patients (**Figure 10A**) and found that the components of the nine immune cell subtypes exhibited obvious variations between the high- and low-risk groups. Compared to the low-risk group, the high-risk group possesses a higher proportion for the neutrophils, the NK cells activated, and the T cell gamma delta, while the dendritic cell resting, the dendritic cells activated, the naïve B cells, the macrophages M0, the monocytes, and the CD4-naive T cells decreased (**Figures 10B–J**). These results suggested that the ceRNA network may be involved in the regulation of the tumor-related microenvironment partly by changing the immune infiltration, which is potentially important for the subsequent targeted intervention.

DISCUSSION

MPM is a highly aggressive cancer. In the past years, great progress has been made in the knowledge of the occurrence and the development of MPM, and some target molecules and pathways were identified, including BAP1 and YAP/TAZ/TEAD oncogenic axis (21, 22). However, the pathomechanism of MPM is still largely unknown, and the clinical outcomes are highly heterogeneous. Thus, the pathogenesis of MPM requires further study, and more effective biomarkers and predictive models need to be established to satisfy the clinical setting.

Up to now, the studies aimed at screening the potential diagnostic and therapeutic targets of MPM mainly focused on the protein-coding genes (23). However, the biological processes of MPM are very complicated, which are involved in the complex interactions of the multiple types of components rather than regulation of individual molecules. Thus, it is necessary to understand the mechanism of tumor progression based on the regulatory networks. In this study, we comprehensively analyzed the expression and function of aberrant RNAs and established a ceRNA network of MPM to screen the prognostic biomarkers and construct a survival prediction model.

We firstly identified the DEGs closely related to overall survival and then annotated the abnormal function. We found that extracellular matrix organization, chromosome structure, and cell cycle were mainly involved in MPM progression. It has been well-established that the chromosome structure and the cell-cycle regulation are closely related to the cancer. Interestingly, recent studies also suggest that the tumor microenvironment is mainly formed by extracellular matrix organization, which plays an important role in the invasion and metastasis of tumor (24–26). As tumor cells proliferate, the surrounding extracellular matrix dynamically interacts with resident cells to change the architecture of the microenvironment (27). Our findings supported the importance of the extracellular matrix in MPM. In addition, the GSEA analyses based on the expressional changes of all genes also suggested anomalous morphogenesis and differentiation of epithelium and the invasive process of breast cancer partly shared the processed with the MPM development. The pathways related to oncogenes TCF21 and SMARCA2 were also enriched in the GSEA analyses. TCF21 and SMARCA2 have been reported to participate in the multiple steps of the invasion of several cancers, such as proliferation, chemoresistance, and migration (28–30), suggesting the convergence of targets among the different cancers. Besides, the overlapped DEmRNAs between the RNA-seq data and the microarray data were also identified. The function of the overlapped DEmRNAs further suggested the dysfunction of the cell division in the development of MPM.

Next, multiple databases were simultaneously used to predict the interaction among the lncRNA–miRNA-overlapped mRNAs. Finally, 26 lncRNAs, 13 miRNAs, and 73 target mRNAs were included to construct the ceRNA network. Thirty-three mRNAs, three miRNAs, and seven lncRNAs are finally identified as the genes associated with overall survival by univariate Cox regression analyses and Kaplan–Meier survival analyses. Seven mRNAs and two lncRNAs were finally selected and further used to establish survival predictive models (mRNAs: CDC25A, CDK6, CHAF1B, CKS2, CORO1C, WEE1, and KIF23; lncRNAs: SGMS1-AS1 and LINC00689). Besides, after reviews of these genes in the model, we found that all of the seven genes have been associated with multiple processes of tumor, where CDC25A, CDK6, and KIF23 have been reported to directly participate in the pathophysiological process of MPM (31–33). The expression of CDC25A has been reported to correlate with lymph-node spread of MPM (33). CDK6, WEE1, and KIF23 are thought as potential therapeutic targets, which are closely related to the prognosis of the MPM patients (31, 34). Similarly, it is noteworthy that CDK6 is also significant or marginal significant in the multivariate Cox analysis of the model according to both TCGA and EGA data, which indicated that CDK6 may be an important target and an independent prognostic factor. Although the other four genes have not been directly linked to MPM, they are widely involved in the development of cancers. CHAF1B plays a considerable role in leukemia pathogenesis and proliferation of the lung cancer and the prognosis of some cancers (32, 33). CKS2 and CORO1C participate in the growth, invasion, and prognosis of several types of cancers (35–38). Therefore, it is possible that they are also involved in the progression of MPM. LINC00689 and SGMS1-AS1 have not been extensively studied. However, there are some hints that they may be genuine tumor factors. It has been reported that LINC00689 can promote the growth, metastasis, and glycolysis of the glioma cells by completing with miR-338-3p (39). The abnormal expression of SGMS1 has been reported to regulate the epithelial-to-mesenchymal transition in several tumors (40–42). Moreover, SGMS1-AS1 may be an independent prognostic factor, which needs more data to verify. Thus, the two lncRNAs are likely to participate in the invasive process of MPM. The functions of all these genes are worth further studying, especially the concrete validation of the lncRNA–miRNA–mRNA axis. The genes included in the

model exhibited high efficiency by integrating the information of mRNAs, lncRNAs, and miRNAs. The other genes may also have high clinical significance. Interestingly, some of these genes out of the models were also directly associated with the MPM, which were mainly regarded as potential therapeutic targets, including CHEK1, DNMT3B, AXL, PAPPA, and miR-302b. Previous studies suggested that these genes are involved in the multiple antineoplastic processes of MPM, such as relief of chemo- and radioresistance, anti-proliferation, inhibition of growth and migration, and induction of apoptosis (31, 43–48). Only two small-molecule drugs aiming to target the identified genes have been preliminarily evaluated, including palbociclib targeting CDK6 and AZD1775 targeting WEE1. Therefore, more preclinical experiments should be conducted to screen the drugs targeting the corresponding genes and assess the antitumor effect of these identified targets before the clinical studies, especially for these identified lncRNAs, in consideration of their central roles in the ceRNA network.

We next clustered the nine co-expression modules from the 1500 DEmRNAs based on the method of WGCNA and found that the blue module and the turquoise module were significantly associated with the overall survival and the risk model. Importantly, the two hub genes WEE1 and KIF23 in the turquoise co-expression PPI network have been previously reported to play important roles in the aggressive property of MPM, whose inhibition was previously regarded as the promising therapeutic targets (49, 50). Interestingly, WEE1 and KIF23 are also included into the survival model, which indicated the validity of the model and the ceRNA network. Besides, KIF23 was identified as an independent survival predictor in EGA data, but not in the TCGA data, possibly due to insufficient data. As for the biological functions of KIF23 and WEE1 in MPM, they remain largely unknown. The ceRNA mechanisms of the two genes in MPM also have not been assessed, which may be important for the growth and metastasis of the MPM cells. Similarly, the gene enrichment analyses further suggested that the blue module mainly regulates the function of the extracellular matrix, indicating that the ceRNA network could affect the tumor microenvironment and consequently contribute to MPM progression. Moreover, the functions of the turquoise module were mainly involved in the process of cell division and in the structure of cells, whose dysfunction is widely regarded as the initiation and the invasive factor of cancer. In other words, we deduce that the ceRNA network mainly regulates the invasion of MPM by regulating the extracellular matrix and the cell division.

The tumor-related microenvironment also includes the immune cells, the fibroblasts, and the endothelial cells, which could inhibit the development of tumor. However, with the progression of tumor, the inhibitory signals and the immune cells could be circumvented by changing the tumor microenvironment (51). Therefore, there is a complex relationship between the tumor cells and the immune cells, which plays important roles in either elimination of tumor cells or invasion of rumors. Thus, we calculated the proportions of the 22 types of immune cells by the deconvolution of the DEmRNAs from the ceRNA network, whose result suggested that the ceRNA network may also be involved in the infiltration of multiple immune cells and the regulation of the microenvironment of MPM.

To conclude, we have identified a number of potential prognostic genes and analyzed their functions related to the progression of the MPM. A ceRNA regulatory network was accordingly constructed, where 33 mRNAs, three miRNAs, and seven lncRNAs are finally identified as the genes associated with the overall survival. Then an efficient risk score assessment system based on two lncRNAs, seven mRNAs, and five clinical factors were accordingly established and validated to predict the overall survival of MPM patients by two independent MPM case–control studies. Besides, the influence of the ceRNA network on the tumor microenvironment has also been assessed from several perspectives, providing a further understanding of the mechanisms of MPM progression. The follow-up clinical and experimental researches are needed to further optimize the models and concretely clarify the role that these genes play in the MPM.

DATA AVAILABILITY STATEMENT

The original contributions presented in the study are included in the article/supplementary materials, further inquiries can be directed to the corresponding author/s.

ETHICS STATEMENT

Ethical approval was not provided for this study on human participants because the human datasets were obtained from the public database including TCGA, EGA and GEO, which have been approved by the ethical reviews. The patients/participants provided their written informed consent to participate in this study.

AUTHOR CONTRIBUTIONS

WD, BX, and PH: conceptualization. WD and KW: methodology, software, and writing—original draft preparation. WD, YD, and XYC: validation. WD and XFC: formal analysis. BX and PH: writing—review and editing, supervision, and project administration. WD: visualization. BX: funding acquisition. All authors have read and agreed to the published version of the manuscript.

ACKNOWLEDGMENTS

We sincerely thank Dr. Steffen Durinck for their permission of the EAG dataset. We profusely thank Dona Shaju for the instruction of downloading, who is a helper in the EGA database.

REFERENCES

1. Odgerel CO, Takahashi K, Sorahan T, Driscoll T, Fitzmaurice C, Yoko-O M, et al. Estimation of the global burden of mesothelioma deaths from incomplete national mortality data. *Occup Environ Med.* (2017) 74:851–8. doi: 10.1136/oemed-2017-104298
2. Stayner L, Welch LS, Lemen R. The worldwide pandemic of asbestos-related diseases. *Annu Rev Public Health.* (2013) 34:205–16. doi: 10.1146/annurev-publhealth-031811-124704
3. Salmena L, Poliseno L, Tay Y, Kats L, Pandolfi PP. A ceRNA hypothesis: the Rosetta Stone of a hidden RNA language? *CELL.* (2011) 146:353–8. doi: 10.1016/j.cell.2011.07.014
4. Credendino SC, Bellone ML, Lewin N, Amendola E, Sanges R, Basu S, et al. A ceRNA circuitry involving the long noncoding RNA Klhl14-AS, Pax8, and Bcl2 drives thyroid carcinogenesis. *Cancer Res.* (2019) 79:5746–57. doi: 10.1158/0008-5472.CAN-19-0039
5. Wang Y, Yang L, Chen T, Liu X, Guo Y, Zhu Q, et al. A novel lncRNA MCM3AP-AS1 promotes the growth of hepatocellular carcinoma by targeting miR-194-5p/FOXA1 axis. *Mol Cancer.* (2019) 18:28. doi: 10.1186/s12943-019-0957-7
6. Song YX, Sun JX, Zhao JH, Yang YC, Shi JX, Wu ZH, et al. Non-coding RNAs participate in the regulatory network of CLDN4 via ceRNA mediated miRNA evasion. *Nat Commun.* (2017) 8:289. doi: 10.1038/s41467-017-00304-1
7. Li R, Yang YE, Jin J, Zhang MY, Liu X, Liu XX, et al. Identification of lncRNA biomarkers in lung squamous cell carcinoma using comprehensive analysis of lncRNA mediated ceRNA network. *Artif Cells Nanomed Biotechnol.* (2019) 47:3246–58. doi: 10.1080/21691401.2019.1647225
8. Li X, Dai D, Wang H, Wu B, Wang R. Identification of prognostic signatures associated with long-term overall survival of thyroid cancer patients based on a competing endogenous RNA network. *Genomics.* (2020) 112:1197–1207. doi: 10.1016/j.ygeno.2019.07.005
9. Chen X, Chen Z, Yu S, Nie F, Yan S, Ma P, et al. Long Noncoding RNA LINC01234 functions as a competing endogenous RNA to regulate CBFB expression by sponging miR-204-5p in gastric cancer. *Clin Cancer Res.* (2018) 24:2002–14. doi: 10.1158/1078-0432.CCR-17-2376
10. Zheng L, Xiang C, Li X, Guo Q, Gao L, Ni H, et al. STARD13-correlated ceRNA network-directed inhibition on YAP/TAZ activity suppresses stemness of breast cancer via co-regulating Hippo and Rho-GTPase/F-actin signaling. *J Hematol Oncol.* (2018) 11:72. doi: 10.1186/s13045-018-0613-5
11. Felley-Bosco E, Rehrauer H. Non-coding transcript heterogeneity in mesothelioma: insights from asbestos-exposed mice. *INT J MOL SCI.* (2018) 19:1163. doi: 10.3390/ijms19041163
12. Renganathan A, Kresoja-Rakic J, Echeverry N, Ziltener G, Vrugt B, Opitz I, et al. GAS5 long non-coding RNA in malignant pleural mesothelioma. *Mol Cancer.* (2014) 13:119. doi: 10.1186/1476-4598-13-119
13. Huang R, Wu J, Zheng Z, Wang G, Song D, Yan P, et al. The construction and analysis of ceRNA network and patterns of immune infiltration in mesothelioma with bone metastasis. *Front Bioeng Biotechnol.* (2019) 7:257. doi: 10.3389/fbioe.2019.00257
14. Chou CH, Chang NW, Shrestha S, Hsu SD, Lin YL, Lee WH, et al. miRTarBase 2016: updates to the experimentally validated miRNA-target interactions database. *Nucleic Acids Res.* (2016) 44:D239–47. doi: 10.1093/nar/gkv1258
15. Agarwal V, Bell GW, Nam JW, Bartel DP. Predicting effective microRNA target sites in mammalian mRNAs. *Elife.* (2015) 4:5005. doi: 10.7554/eLife.05005
16. Li JH, Liu S, Zhou H, Qu LH, Yang JH. starBase v2.0: decoding miRNA-ceRNA, miRNA-ncRNA and protein-RNA interaction networks from large-scale CLIP-Seq data. *Nucleic Acids Res.* (2014) 42:D92–7. doi: 10.1093/nar/gkt1248
17. Kozomara A, Griffiths-Jones S. miRBase: annotating high confidence microRNAs using deep sequencing data. *Nucleic Acids Res.* (2014) 42:D68–73. doi: 10.1093/nar/gkt1181
18. Langfelder P, Horvath S. WGCNA: an R package for weighted correlation network analysis. *BMC Bioinformatics.* (2008) 9:559. doi: 10.1186/1471-2105-9-559
19. Newman AM, Liu CL, Green MR, Gentles AJ, Feng W, Xu Y, et al. Robust enumeration of cell subsets from tissue expression profiles. *Nat Methods.* (2015) 12:453–7. doi: 10.1038/nmeth.3337
20. Yang L, Lin PC. Mechanisms that drive inflammatory tumor microenvironment, tumor heterogeneity, and metastatic progression. *Semin Cancer Biol.* (2017) 47:185–95. doi: 10.1016/j.semcancer.2017.08.001
21. Zhang WQ, Dai YY, Hsu PC, Wang H, Cheng L, Yang YL, et al. Targeting YAP in malignant pleural mesothelioma. *J Cell Mol Med.* (2017) 21:2663–76. doi: 10.1111/jcmm.13182
22. Cigognetti M, Lonardi S, Fisogni S, Balzarini P, Pellegrini V, Tironi A, et al. BAP1 (BRCA1-associated protein 1) is a highly specific marker for differentiating mesothelioma from reactive mesothelial proliferations. *Mod Pathol.* (2015) 28:1043–57. doi: 10.1038/modpathol.2015.65
23. Zhou JG, Zhong H, Zhang J, Jin SH, Roudi R, Ma H. Development and validation of a prognostic signature for malignant pleural mesothelioma. *Front Oncol.* (2019) 9:78. doi: 10.3389/fonc.2019.00078
24. Walker C, Mojares E, Del RHA. Role of extracellular matrix in development and cancer progression. *Int J Mol Sci.* (2018) 19:3028. doi: 10.3390/ijms19103028
25. Zhou Z, Lu ZR. Molecular imaging of the tumor microenvironment. *Adv Drug Deliv Rev.* (2017) 113:24–48. doi: 10.1016/j.addr.2016.07.012
26. Insua-Rodriguez J, Oskarsson T. The extracellular matrix in breast cancer. *Adv Drug Deliv Rev.* (2016) 97:41–55. doi: 10.1016/j.addr.2015.12.017
27. Grossman M, Ben-Chetrit N, Zhuravlev A, Afik R, Bassat E, Solomonov I, et al. Tumor cell invasion can be blocked by modulators of collagen fibril alignment that control assembly of the extracellular matrix. *Cancer Res.* (2016) 76:4249–58. doi: 10.1158/0008-5472.CAN-15-2813
28. Gooskens SL, Klasson TD, Gremmels H, Logister I, Pieters R, Perlman EJ, et al. TCF21 hypermethylation regulates renal tumor cell clonogenic proliferation and migration. *Mol Oncol.* (2018) 12:166–79. doi: 10.1002/1878-0261.12149
29. Sun W, Li S, Yu Y, Jin H, Xie Q, Hua X, et al. MicroRNA-3648 is upregulated to suppress TCF21, resulting in promotion of invasion and metastasis of human bladder cancer. *Mol Ther Nucleic Acids.* (2019) 16:519–30. doi: 10.1016/j.omtn.2019.04.006
30. Xue Y, Meehan B, Fu Z, Wang X, Fiset PO, Rieker R, et al. SMARCA4 loss is synthetic lethal with CDK4/6 inhibition in non-small cell lung cancer. *Nat Commun.* (2019) 10:557. doi: 10.1038/s41467-019-08380-1
31. Walter RF, Vollbrecht C, Werner R, Mairinger T, Schmeller J, Flom E, et al. Screening of pleural mesotheliomas for dna-damage repair players by digital gene expression analysis can enhance clinical management of patients receiving platin-based chemotherapy. *J Cancer.* (2016) 7:1915–25. doi: 10.7150/jca.16390
32. Duan Y, Liu T, Li S, Huang M, Li X, Zhao H, et al. CHAF1B promotes proliferation and reduces apoptosis in 95D lung cancer cells and predicts a poor prognosis in nonsmall cell lung cancer. *ONCOL REP.* (2019) 41:2518–28. doi: 10.3892/or.2019.6994
33. Volk A, Liang K, Suraneni P, Li X, Zhao J, Bulic M, et al. A CHAF1B-dependent molecular switch in hematopoiesis and leukemia pathogenesis. *Cancer Cell.* (2018) 34:707–23.e7. doi: 10.1016/j.ccell.2018.10.004
34. Bonelli MA, Digiacomo G, Fumarola C, Alfieri R, Quaini F, Falco A, et al. Combined inhibition of CDK4/6 and PI3K/AKT/mTOR pathways induces a synergistic anti-tumor effect in malignant pleural mesothelioma cells. *NEOPLASIA.* (2017) 19:637–648. doi: 10.1016/j.neo.2017.05.003
35. Chen D, Xu L, Li X, Chu Y, Jiang M, Xu B, et al. Enah overexpression is correlated with poor survival and aggressive phenotype in gastric cancer. *Cell Death Dis.* (2018) 9:998. doi: 10.1038/s41419-018-1031-x
36. Qi J, Yu Y, Akilli OO, Holland JD, Besser D, Fritzmann J, et al. New Wnt/beta-catenin target genes promote experimental metastasis and migration of colorectal cancer cells through different signals. *GUT.* (2016) 65:1690–701. doi: 10.1136/gutjnl-2014-307900
37. Mataki H, Enokida H, Chiyomaru T, Mizuno K, Matsushita R, Goto Y, et al. Downregulation of the microRNA-1/133a cluster enhances cancer cell migration and invasion in lung-squamous cell carcinoma via regulation of Coronin1C. *J Hum Genet.* (2015) 60:53–61. doi: 10.1038/jhg.2014.111
38. Wang J, Tsouko E, Jonsson P, Bergh J, Hartman J, Aydogdu E, et al. miR-206 inhibits cell migration through direct targeting of the actin-binding protein coronin 1C in triple-negative breast cancer. *Mol Oncol.* (2014) 8:1690–702. doi: 10.1016/j.molonc.2014.07.006
39. Liu X, Zhu Q, Guo Y, Xiao Z, Hu L, Xu Q. LncRNA LINC00689 promotes the growth, metastasis and glycolysis of glioma cells by

targeting miR-338-3p/PKM2 axis. *Biomed Pharmacother.* (2019) 117:109069. doi: 10.1016/j.biopha.2019.109069
40. Bilal F, Montfort A, Gilhodes J, Garcia V, Riond J, Carpentier S, et al. Sphingomyelin Synthase 1 (SMS1) downregulation is associated with sphingolipid reprogramming and a worse prognosis in melanoma. *Front Pharmacol.* (2019) 10:443. doi: 10.3389/fphar.2019.00443
41. Liu S, Hou H, Zhang P, Wu Y, He X, Li H, et al. Sphingomyelin synthase 1 regulates the epithelialtomesenchymal transition mediated by the TGFbeta/Smad pathway in MDAMB231 cells. *Mol Med Rep.* (2019) 19:1159–67. doi: 10.3892/mmr.2018.9722
42. Moorthi S, Burns TA, Yu GQ, Luberto C. Bcr-Abl regulation of sphingomyelin synthase 1 reveals a novel oncogenic-driven mechanism of protein up-regulation. *Faseb J.* (2018) 32:4270–83. doi: 10.1096/fj.201701016R
43. Song W, Wang H, Lu M, Ni X, Bahri N, Zhu S, et al. AXL inactivation inhibits mesothelioma growth and migration via regulation of p53 expression. *Cancers (Basel).* (2020) 12:2757. doi: 10.3390/cancers12102757
44. Baird AM, Easty D, Jarzabek M, Shiels L, Soltermann A, Klebe S, et al. When RON MET TAM in Mesothelioma: All Druggable for One, and One Drug for All? *Front Endocrinol (Lausanne).* (2019) 10:89. doi: 10.3389/fendo.2019.00089
45. Khodayari N, Mohammed KA, Lee H, Kaye F, Nasreen N. MicroRNA-302b targets Mcl-1 and inhibits cell proliferation and induces apoptosis in malignant pleural mesothelioma cells. *Am J Cancer Res.* (2016) 6:1996–2009.
46. Cartron PF, Blanquart C, Hervouet E, Gregoire M, Vallette FM. HDAC1-mSin3a-NCOR1, Dnmt3b-HDAC1-Egr1 and Dnmt1-PCNA-UHRF1-G9a regulate the NY-ESO1 gene expression. *Mol Oncol.* (2013) 7:452–63. doi: 10.1016/j.molonc.2012.11.004
47. Huang J, Tabata S, Kakiuchi S, The VT, Goto H, Hanibuchi M, et al. Identification of pregnancy-associated plasma protein A as a migration-promoting gene in malignant pleural mesothelioma cells: a potential therapeutic target. *Oncotarget.* (2013) 4:1172–84. doi: 10.18632/oncotarget.1126
48. Roe OD, Anderssen E, Sandeck H, Christensen T, Larsson E, Lundgren S. Malignant pleural mesothelioma: genome-wide expression patterns reflecting general resistance mechanisms and a proposal of novel targets. *Lung Cancer.* (2010) 67:57–68. doi: 10.1016/j.lungcan.2009.03.016
49. Indovina P, Marcelli E, Di Marzo D, Casini N, Forte IM, Giorgi F, et al. Abrogating G(2)/M checkpoint through WEE1 inhibition in combination with chemotherapy as a promising therapeutic approach for mesothelioma. *Cancer Biol Ther.* (2014) 15:380–8. doi: 10.4161/cbt.27623
50. Kato T, Lee D, Wu L, Patel P, Young AJ, Wada H, et al. Kinesin family members KIF11 and KIF23 as potential therapeutic targets in malignant pleural mesothelioma. *Int J Oncol.* (2016) 49:448–56. doi: 10.3892/ijo.2016.3566
51. Quail DF, Joyce JA. Microenvironmental regulation of tumor progression and metastasis. *Nat Med.* (2013) 19:1423–37. doi: 10.1038/nm.3394

Conflict of Interest: The authors declare that the research was conducted in the absence of any commercial or financial relationships that could be construed as a potential conflict of interest.

frontiers in Oncology

ORIGINAL RESEARCH
published: 08 December 2021
doi: 10.3389/fonc.2021.789244

Aurora Kinase A as a Diagnostic and Prognostic Marker of Malignant Mesothelioma

Zhenying Guo[1,2,3,4,5], *Li Shen*[6], *Ningning Li*[3,4], *Xiaoxiao Wu*[3,4], *Canming Wang*[3,4], *Zheng Gu*[7], *Zhongjian Chen*[4,8], *Junping Liu*[4,8], *Weimin Mao*[4,5,8] *and Yuchen Han*[1,2*]

[1] *Department of Pathology, Shanghai Chest Hospital, Shanghai Jiao Tong University, Shanghai, China,* [2] *School of Medicine, Shanghai Jiao Tong University, Shanghai, China,* [3] *Department of Pathology, Cancer Hospital of the University of Chinese Academy of Sciences (Zhejiang Cancer Hospital), Hangzhou, China,* [4] *Institute of Basic Medicine and Cancer, Chinese Academy of Sciences, Hangzhou, China,* [5] *Zhejiang Key Laboratory of Diagnosis and Treatment Technology on Thoracic Oncology, Zhejiang Cancer Hospital, Hangzhou, China,* [6] *Office of Education, Sir Run Run Shaw Hospital, Zhejiang University School of Medicine, Hangzhou, China,* [7] *Department of Clinical Medicine Engineering, Second Affiliated Hospital of Zhejiang University, School of Medicine, Hangzhou, China,* [8] *Cancer Hospital of University of Chinese Academy of Sciences, Zhejiang Cancer Hospital, Hangzhou, China*

OPEN ACCESS

Edited by:
Glen Reid,
University of Otago, New Zealand

Reviewed by:
Sk. Kayum Alam,
University of Minnesota Twin Cities, United States
Jorg Kobarg,
State University of Campinas, Brazil
Diletta Rosati,
University of Siena, Italy

****Correspondence:***
Yuchen Han
ychan@cmu.edu.cn

Specialty section:
This article was submitted to Thoracic Oncology, a section of the journal Frontiers in Oncology

Received: *04 October 2021*
Accepted: *19 November 2021*
Published: *08 December 2021*

Citation:
Guo Z, Shen L, Li N, Wu X, Wang C, Gu Z, Chen Z, Liu J, Mao W and Han Y (2021) Aurora Kinase A as a Diagnostic and Prognostic Marker of Malignant Mesothelioma. Front. Oncol. 11:789244. doi: 10.3389/fonc.2021.789244

Background: Malignant mesothelioma (MM) is a highly aggressive cancer with a poor prognosis. Despite the use of several well-known markers, the diagnosis of MM is still challenging in some cases. we applied bioinformatics to identify key genes and screen for diagnostic and prognostic markers of MM.

Methods: The expression profiles of GSE2549 and GSE112154 microarray datasets from the Gene Expression Omnibus database contained 87 cases of MM tissue and 8 cases of normal mesothelial tissue in total. The GEO2R tool was used to detect differentially expressed genes (DEGs). Gene ontology (GO) and Kyoto Encyclopedia of Genes and Genomes (KEGG) pathway enrichment analyses of DEGs were performed using DAVID Bioinformatics Resources. The DEGs protein-protein interaction networks were constructed from the STRING database. Cytoscape was used to identify significant modules and hub genes. The GEPIA database was used to explore relationships between hub genes and prognosis of MM. Immunohistochemistry was used to analyze protein expression in tissue microarrays with 47 Chinese MM tissues. Statistical analyses diagnostic and prognostic values.

Results: 346 DEGs were identified: 111 genes upregulated, and 235 downregulated. GO analysis showed that the primary biological processes of these DEGs were cell adhesion, leukocyte migration, and angiogenesis. The main cellular components included the extracellular space, extracellular exosome, and extracellular region. The molecular functions were integrin binding, heparin binding, and calcium ion binding. KEGG pathway analysis showed that DEGs are primarily involved in PPAR signaling pathway, extracellular matrix–receptor interactions, and regulation of lipolysis in adipocytes. Survival analysis showed that seven genes—*AURKA, GAPDH, TOP2A, PPARG, SCD, FABP4*, and *CEBPA*—may be potential prognostic markers for MM. Immunohistochemical studies showed that Aurora kinase A (*AURKA* gene encode, Aurora-A) and GAPDH were highly

expressed in MM tissue in comparison with normal mesothelial tissue. Kaplan-Meier analysis confirmed a correlation between Aurora-A protein expression and overall survival but did not confirm a correlation with GAPDH. The receiver operating characteristic curves of Aurora-A protein expression suggested acceptable accuracy (AUC = 0.827; 95% CI [0.6686 to 0.9535]; $p = 0.04$). The sensitivity and specificity of Aurora-A were 83.33% and 77.78%, respectively.

Conclusion: Aurora-A could be an optimal diagnostic biomarker and a potential prognostic marker for MM.

Keywords: malignant mesothelioma, bioinformatics, biomarkers, tissue microarray, Aurora kinase A

INTRODUCTION

Malignant mesothelioma (MM) is an aggressive cancer that arises from the mesothelial cells lining the pleura, peritoneum, pericardium, and tunica vaginalis. MM primarily affects older people who have been occupationally exposed to asbestos (1). The median survival of patients with MM is less than one year, and their 5-year survival rate is less than 5%. Although the development of multidisciplinary treatment, including surgical resection, radiotherapy, chemotherapy and targeted immunotherapy, the diagnosis and treatment of malignant mesothelioma is still a big challenge. Therefore, it is important to identify the diagnostic and prognostic value of markers that can aid in selecting patients who will benefit from treatments (2).

Genomic studies have been conducted on pleural MM subsets using microarray-based comparative genomic hybridization, fluorescence *in situ* hybridization, and targeted DNA sequencing with the ultimate goal of finding new molecular targets. genetic alterations (*BAP1*, *NF2*, *TP53*, and *CDKN2A* mutations and/or copy number alterations) commonly found in pleural mesothelioma are also present in diffuse peritoneal MM, although their frequencies vary according to the anatomical localization (3–5).

Integrating and reanalyzing these genomic data offer possibilities for identifying specific disease-related biomarkers. Recently, two studies used bioinformatics methods to analyze MM microarrays based on the Gene Expression Omnibus (GEO) dataset GSE51024 for the identification of differentially expressed genes (DEGs) between pleural MM tissues and normal lung tissues (6, 7). However, MM is derived from mesothelial cells on the surface of the pleura and peritoneum. Therefore, using pleural or peritoneal tissue as a negative control can obtain more accurate data. In this study, we identified robust and stable DEGs between MM tissues and normal pleural or peritoneal tissues from GEO microarray datasets and assessed potential functions of the genes. Seven hub genes were selected with prognostic value for MM. Subsequently, tissue microarray (TMA) was used to validate protein expression encoded by DEGs and evaluate the diagnostic and prognostic value. Finally, Aurora-A was identified as an optimal diagnostic biomarker and a potential prognostic marker for MM. In conclusion, these results provide a novel biomarker for diagnosis and prognosis, as well as potential therapeutic targets for MM.

MATERIAL AND METHODS

Microarray Data

Using the keywords "malignant mesothelioma [Accession]" to search the GEO database (https://www.ncbi.nlm.nih.gov/geo/), we downloaded the gene expression profiles of GSE2549 (8, 9) and GSE112154 (10). The platform for GSE2549 is GPL96 Affymetrix Human Genome U133A Array (HG-U133A), which includes pleural MM surgical tissues (n = 42), normal pleura tissues (n = 5). The platform for GSE112154 is GPL10558 Illumina HumanHT-12 V4.0 expression bead chip, which includes 45 frozen surgical tissues of diffuse malignant peritoneal mesothelioma, 3 normal peritoneal tissues. The dataset information is shown in **Table 1**. In addition, MM RNA-sequencing and clinical data were downloaded from The Cancer Genome Atlas database (https://cancergenome.nih.gov/) and used in the study.

DEGs Screening

The GEO2R tool (https://www.ncbi.nlm.nih.gov/geo/geo2r) was used to detect DEGs between MM and normal pleural or peritoneal tissues. the cut-off criteria was ($p < 0.01$ and $|\log FC| \geq 1$). Statistical analysis was carried out for each dataset, and the intersecting part was identified using the Venn diagram web tool (bioinformatics.psb.ugent.be/webtools/Venn). Heatmap was drawn on the normalized expression matrix using the pheatmap package in R software Volcano plot was drawn using the ggplot2 package in R software

Functional DEGs Enrichment Analyses

Gene ontology (GO) functional annotations and Kyoto Encyclopedia of Genes and Genomes (KEGG) pathway analysis of DEGs were performed using the DAVID Bioinformatics Resources 6.8 database (https://david.ncifcrf.gov/home.jsp).

Gene set enrichment analysis (GSEA) was performed using Gene Set Enrichment Analysis (GSEA, version 4.1.0, http://www.gsea-msigdb.org/gsea/index.jsp) to reveal the critical signaling pathways involving MM.

Construction and Module Analysis of PPI Network

The STRING database (version 11.0, http://string-db.org) was used to build a protein-protein interaction (PPI) network. a

TABLE 1 | Characteristics of the included datasets.

GEO Dataset ID	GSE2549	GSE112154
Platform	GPL96	GPL10558
Number of Rows per platform	22283	48107
Country	USA	Italy
Tumor Site	Pleura	Peritoneum
Number of samples		
Tumor tissue	42	45
Normal pleural mesothelium	5	/
Normal peritoneal mesothelium	/	3
Reference	Gordon GJ et al. (8)	Sciarrillo R et al. (10)

comprehensive Gt score greater than 0.4 was considered statistically significant. Analysis of functional interactions between proteins can be helpful for understanding mechanisms related to disease occurrence and development. Cytoscape (version 3.8.2) was used to visualize and analyze the interaction network. The most important module in the PPI network was identified by the MCODE of Cytoscape. The selection criteria were as follows: MCODE score greater than 5, cut-off value of 2, node cut-off value of 0.2, maximum depth of 100, and k-score of 2.

Identification of Hub Genes

The CytoHubba plugin of the Cytoscape software was used to select the hub genes and can predict and explore important nodes and subnetworks using several topological algorithms. The Maximal Clique Centrality algorithm was selected to explore hub genes.

Validation and Survival Analysis of Hub Genes

The GEPIA database (http://gepia.cancer-pku.cn) includes 9736 tumor and 8587 normal tissue samples from The Cancer Genome Atlas database (TCGA) and the Genotype-Tissue Expression (GTEx) projects. Initial survival analysis was conducted with the gene expression profiles and clinical information of 87 MM patients who were diagnosed between 1999 and 2013 in the GEPIA database. Single-gene analysis was used to create plots in MM and normal mesothelium. The threshold was selected as the default value.

Patient Material

Patients diagnosed with MM between 2002 and 2020 in the Cancer Hospital of the University of Chinese Academy of Sciences (Zhejiang Cancer Hospital) were selected. Corresponding H&E slides and immunochemistry slides were reviewed by three pathologists (Z.Guo, N.Li and Y.Han) for confirmation of the diagnosis. Clinical records were accessed: sex, age at diagnosis, family and personal history of cancer, asbestos exposure, lymph node or systemic metastases, and the date of last follow-up or death. Data on histologic type, the presence of vascular invasion and lymph node metastases was extracted from the surgical pathology reports. Follow-up time was calculated as months between the date of the diagnosis and the date of the last follow-up. Patients were considered to be lost to follow-up if no medical information was obtainable beyond the original surgery. The Institutional Review Board at the Cancer Hospital of the University of Chinese Academy of Sciences (Zhejiang Cancer Hospital) approved this study. 10 normal peritoneal mesothelium (NP) were obtained from patients who underwent surgery for gastric or colon carcinomas as control.

Tissue Microarray

Formalin-fixed, paraffin-embedded tissue blocks of 47 MM specimens were selected according to tissue availability for the construction of TMA. The TMA consisted of triplicate 1.0-mm cores made using a manual tissue microarray (Beecher Instrument, Sun Prairie, WI, USA). The selection of regions in the tissue block for the cores included two cores from the periphery of the lesion and one core from the center of the lesion. Sections of 4 μm were cut for subsequent immunohistochemical analysis.

Immunohistochemical Staining

Immunohistochemical staining of the TMA was conducted with the following antibodies: anti-SCD1 (1:250 dilution; Abcam, CD.E10, ab19862), anti-FABP4 (1:10000 dilution; Abcam, EPR3580, ab92501), anti-topoisomerase II alpha (1:5000 dilution; Abcam, EP1102Y, ab52934), anti-C/EBPα (1:200 dilution; CST, D56F10, No. 8178), anti-phospho-Aurora-A (Thr288) (1:800 dilution; CST, C39D8, No. 3079), anti-Aurora-A (1:200 dilution; Abcam, 35C1, ab13824), anti-PPARγ (1:250 dilution; Santa Cruz Biotechnology, E-8, sc-7273), anti-GAPDH (1:800 dilution; CST, 14C10, No. 2118). Negative control slides consisted of substituting normal serum for the primary antibody. A whole section of a MM was used as a positive control. Immunohistochemical staining was scored semi-quantitatively by three pathologists (Z.Guo, N.Li, Y.Han), which is obtained by multiplying the proportion of cells showing staining and the intensity of staining (0, no staining; 1, weak; 2, moderate; and 3, strong). A case was considered to show positive staining when at least 1% of tumor cells showed staining.

Statistical Analysis

Immunohistochemical data between the MM group and NP group were compared using the Mann-Whitney *U* test. The Kaplan-Meier method was used to estimate survival. The receiver operating curve (ROC) was used to test for diagnostic factors. All statistical analyses were performed using Prism (version 9.2; GraphPad Inc.). A p value (two-tail) of less than 0.05 was considered to be statistically significant.

RESULTS

Identification and Functional Enrichment Analysis of DEGs in MM

The MM expression microarray datasets GSE2549 and GSE112154 were used in this study. GSE2549 contained 42 pleural MM samples and 5 normal pleural tissues, and GSE112154 included 45 peritoneal MM tissues and 3 normal peritoneal tissues (**Table 1**). Overall, 346 DEGs were identified: 111 upregulated genes and 235 downregulated genes (**Figure 1A**). Hierarchical heatmap revealed distinct clusters of MM and Normal mesothelial tissues (**Figure 1B**). Volcano plot displayed significantly downregulated (green) or upregulated (red) genes (**Figure 1C**).

Biological annotation of the DEGs in MM was performed using the DAVID online analysis tool, and the 346 DEGs were chosen to perform GO and KEGG analyses (**Figure 2**). We detected enrichment in biological process (BP) GO terms such as cell adhesion, leukocyte migration, and angiogenesis. Regarding cell composition (CC), enrichment areas included the extracellular space, extracellular exosome, extracellular region, and extracellular matrix. In terms of molecular function (MF), enrichment was found in integrin binding, heparin binding, calcium ion binding, and protein binding (**Figure 2A**). KEGG pathway analysis showed that the DEGs were mostly associated with the PPAR signaling pathway, regulation of lipolysis in adipocytes, ECM-receptor interaction, AMPK signaling pathway, and cell adhesion molecules (**Table 2**). These results indicate that most of the DEGs are significantly enriched in the extracellular matrix, cell cycle adhesion, and the PPAR signaling pathway. Chord plot depicting the relationship between genes and GO terms of the top 100 DEGs (**Figure 2B**). Gene set enrichment analysis (GSEA) analysis revealed that genes involved in Ubiquitin mediated proteolysis and cell cycle were significantly enriched in MM compared to normal mesothelial tissues (**Figure 2C**).

PPI Network Construction and Module Analysis

Protein interactions among a network of DEGs were constructed using STRING. A total of 305 nodes and 1217 edges were involved in the PPI network (**Figure 1D**) and the top 2 significant modules were obtained using Cytoscape (**Figure 3**). The functional analyses of genes involved in this module were analyzed using DAVID. Based on MCODE score, we identified two modules in the network with a setting k-score greater than 6. Module 1 included 35 nodes and 148 edges. Module 2 consisted of 19 nodes and 60 edges. The DEGs of modules 1 and 2 were significantly enriched in cell adhesion, angiogenesis, and protein phosphatase binding (**Table 3**). Cell adhesion molecules included *CD36, PECAM1, MSLN, MCAM, SELP, SELE*. Protein phosphatase binding included *CDH5, PPARG, NEK2* Angiogenesis included *JAG1, ANGPT2, ANGPT1, LEP, MCAM, PDE3B, PECAM1, MFGE8*.

Hub Gene Selection and Survival Analysis

The top 20 genes of the PPI network were identified as hub genes with the Maximal Clique Centrality analysis method (**Table 4**). Subsequently, the overall survival analysis and disease-free survival analysis of the hub genes were performed using the GEPIA based on TCGA database. MM patients with higher expressions in *GAPDH*, *AURKA*, *TOP2A, SCD, and FABP4* showed worse overall survival than lower expressions (**Figure 4**). Nonetheless, MM patients with higher alterations in *GAPDH*, *AURKA*, *TOP2A*, and *SCD* showed worse disease-free survival than lower expressions (**Figure 4**). However, MM patients with higher *PPARG* expressions showed better disease-free survival. Moreover, high alteration of *CEBPA* was associated with more prolonged disease-free survival and better overall survival of MM (**Figure 4**). *GAPDH* has both glyceraldehyde-3-phosphate dehydrogenase and nitrosylase activities, thereby playing a role in glycolysis and nuclear functions, respectively. Aurora Kinase A encoded by *AURKA* is a mitotic serine/threonine kinase that contributes to the regulation of cell cycle progression. *TOP2A* encodes a DNA topoisomerase, an enzyme that controls and alters the topologic states of DNA during transcription. *SCD* encodes an enzyme involved in fatty acid biosynthesis, primarily the synthesis of oleic acid. *FABP4* roles include fatty acid uptake, transport, and metabolism. *PPARG* encodes a member of the peroxisome proliferator-activated receptor (PPAR) subfamily of nuclear receptors It's a key regulator of adipocyte differentiation and glucose homeostasis. *CEBPA* gene encodes a transcription factor that contains a basic leucine zipper domain and recognizes the CCAAT motif inthe promoters of target genes. *CEBPA* coordinates proliferation arrest and the differentiation of myeloid progenitors, adipocytes, hepatocytes, and cells of the lung and the placenta

Clinicopathological Characteristics

The demographic and follow-up information about the patients whose MM tissues were analyzed on the TMA are shown in **Table 5**. In total, 47 diagnosed cases of MM were analyzed: 44 in the peritoneum, 3 in the pleura. The mean age of the patients at diagnosis was 47 (range, 21-73) years; 18 patients were men, and 29 were women. Twenty-two of the 47 MM cases (20 in the peritoneum, 2 in the pleura) occurred in patients who were exposed to asbestos. The mean follow-up period ranged from 1 to 70 months. MM samples were subclassified as epithelioid (n = 42), biphasic (n = 3), or sarcomatoid (n = 2).

Immunohistochemistry

Immunohistochemistry was performed on the TMA with antibodies summarized in **Table 6**. The staining analysis is summarized in **Table 7**. GAPDH staining was primarily in the cytoplasm and found in 97% (44/47) of MM samples (**Figure 5**). The expression of GAPDH was significantly higher in MM than normal mesothelial cells ($p < 0.0001$). Additionally, GAPDH immunostaining was noted in some stromal fibroblasts in the TMA. Cytoplasm staining for GAPDH was present in 4 of 10 normal mesothelial tissue samples. Aurora-A membrane and cytoplasm staining was expressed in 76.7% (36/47) MM samples (**Figure 5**). Focal week cytoplasmic staining for Aurora-A was present in 2 of 10 normal mesothelial samples but was absent in all other NP cases. The expression of Aurora-A was significantly

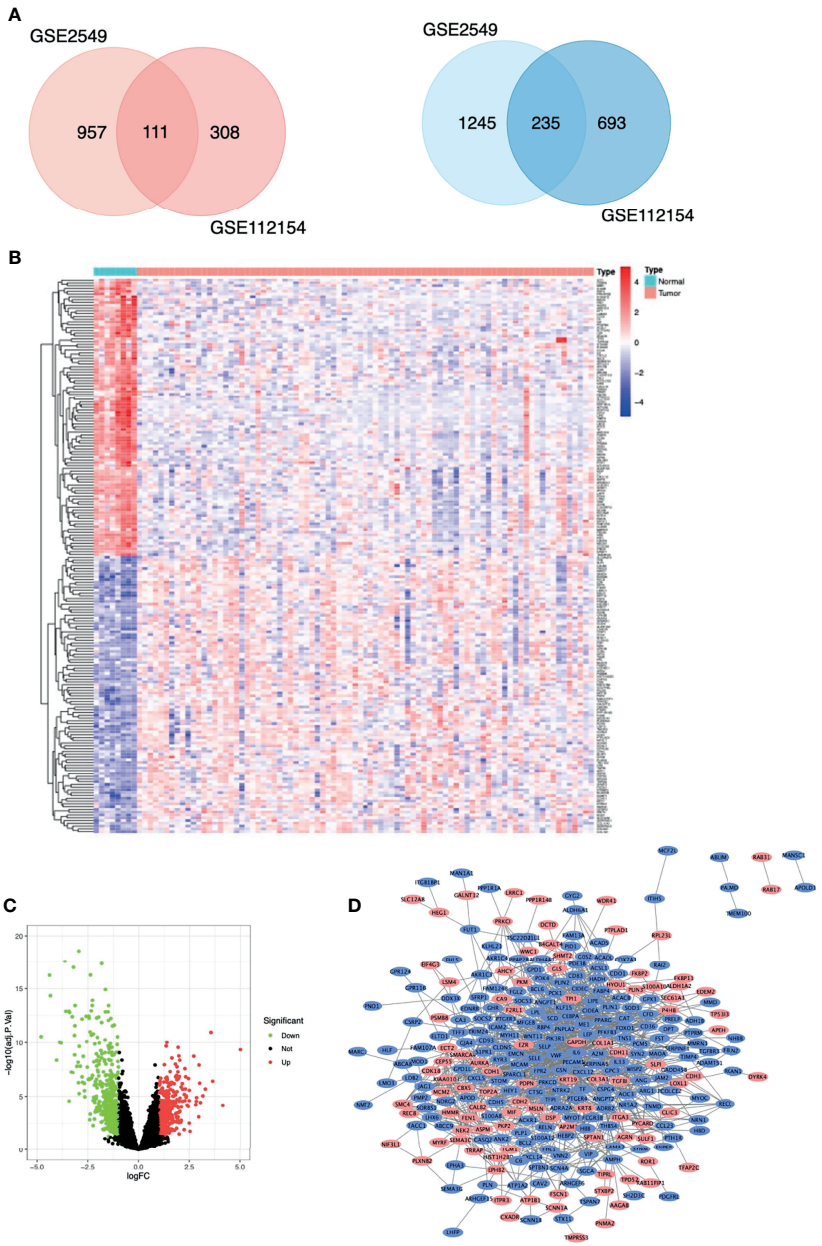

FIGURE 1 | Differentially expressed genes (DEGs) in patients with malignant mesothelioma. **(A)** Venn diagram of DEGs among the mRNA expression profiling sets GSE2549 and GSE112154. Blue denotes downregulated genes, and red denotes upregulated genes showed. **(B)** Hierarchical heat map of TOP100 DEGs between malignant mesothelioma and normal mesothelial tissues. **(C)** Volcano plot of all DEGs between malignant mesothelioma and normal mesothelial tissues. **(D)** Protein-protein interaction network constructed with DEGs using Cytoscape. Red nodes represent upregulated genes, and blue nodes represent downregulated genes.

higher in MM samples than in NP samples ($p < 0.0001$). DNA topoisomerase II alpha (TOPIIA) expression was found in the nuclei of 19.1% (9/47) MM tissues but not in those of normal mesothelial samples; however, this difference was not statistically significant (**Figure 5**). SCD1 was expressed in the cytoplasm of 89.4% (42/47) MM tissues and 80% (8/10) NP tissues ($p > 0.05$); some stromal fibroblasts and endovascular cells expressed SCD1 as well. FABP4 was weakly expressed in the cytoplasm of 12.8% (6/47) MM tissues but no NP tissues ($p > 0.05$). Additionally, FABP4 immunostaining was noted in some fat stromal cells and endovascular cells in the TMA. All MM cases were negative for CEBPA and PPARG.

Kaplan-Meier analysis showed that MM cases with Aurora-A expression had significantly poorer overall survival rates (**Figure 6A**). The ROC curve of Aurora-A demonstrated diagnostic accuracy (area under the curve, 0.81; $p = 0.04$) (**Figure 6B**). However, GAPDH expression was not associated with overall survival and diagnostic accuracy in MM tissues

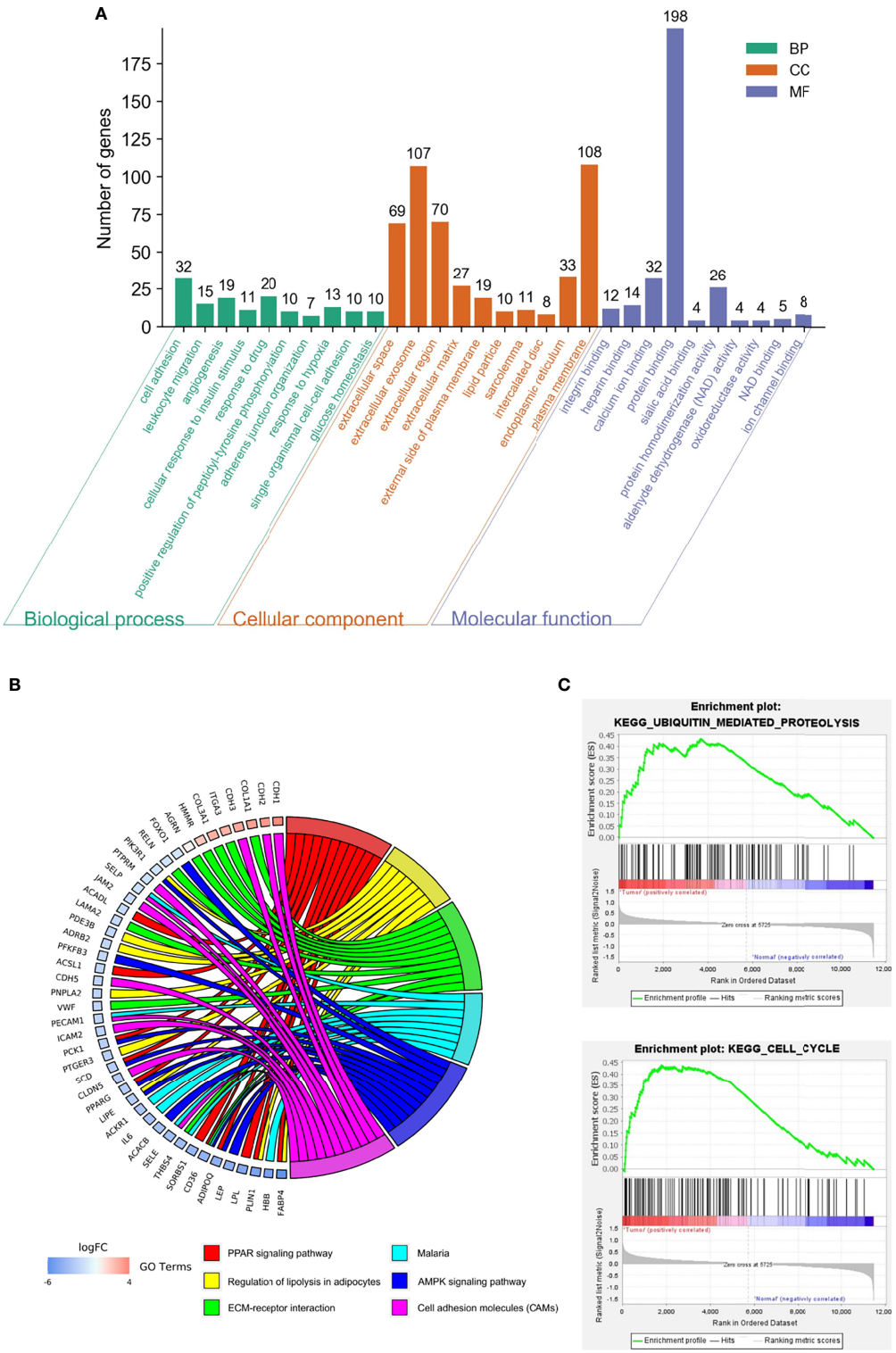

FIGURE 2 | Functional analysis of differentially expressed genes (DEGs). **(A)** Gene ontology (GO) function and Kyoto Encyclopedia of Genes and Genomes (KEGG) pathway enrichment analysis for DEGs were performed using DAVID Bioinformatics Resources. The enriched GO terms were divided into CC, BP, and MF ontologies. **(B)** Chord plot depicting the relationship between genes and GO terms of the top 100 DEGs. **(C)** Gene set enrichment analysis (GSEA) analysis of DEGs.

TABLE 2 | KEGG pathway enrichment analysis of DEGs.

Category	Term	Count	PValue	Genes
Upregulated genes	ECM-receptor interaction	5	4.67E-03	*COL1A1, COL3A1, ITGA3, HMMR, AGRN*
	Arrhythmogenic right ventricular cardiomyopathy	4	1.54E-02	*DSP, CDH2, ITGA3, PKP2*
	Biosynthesis of amino acids	4	1.86E-02	*PKM, TPI1, SHMT2, GAPDH*
	Protein processing in endoplasmic reticulum	5	4.30E-02	*SEC61A1, EIF2AK1, EDEM2, HYOU1, P4HB*
Downregulated genes	PPAR signaling pathway	11	2.08E-07	*FABP4, ACADL, ACSL1, SCD, ADIPOQ, LPL, PPARG, PLIN1, SORBS1, CD36, PCK1*
	Malaria	8	2.04E-05	*SELP, IL6, PECAM1, HBB, CD36, ACKR1, SELE, THBS4*
	Regulation of lipolysis in adipocytes	8	4.97E-05	*LIPE, FABP4, PDE3B, PTGER3, PLIN1, ADRB2, PIK3R1, PNPLA2*
	AMPK signaling pathway	11	5.49E-05	*LIPE, PFKFB3, SCD, LEP, ADIPOQ, PPARG, CD36, PIK3R1, PCK1, ACACB, FOXO1*
	Adipocytokine signaling pathway	7	1.37E-03	*SOCS3, ACSL1, LEP, ADIPOQ, CD36, PCK1, ACACB*

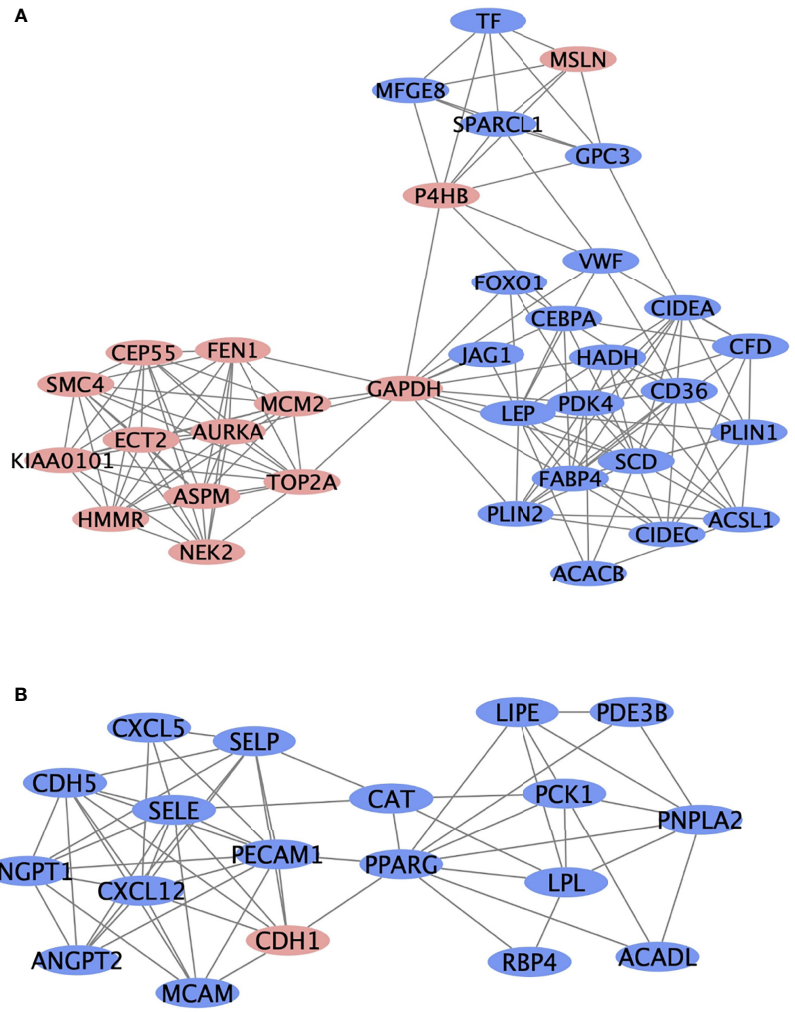

FIGURE 3 | The top two most significant modules of DEGs. The top two significant modules **(A, B)** are selected from the PPI network. Red nodes represent upregulated genes, and blue nodes represent downregulated genes.

(**Figures 6A, B**). The results suggested that Aurora-A could be an optimal diagnostic biomarker for identifying MM from benign mesothelial hyperplasia and it could be a potential prognostic marker for MM.

DISCUSSION

MM is a highly aggressive cancer with a poor prognosis for patients who receive multimodal treatment, including surgical

TABLE 3 | The Top 2 significantly modules.

Cluster	Score	Nodes	Edges	Node IDs
1	8.706	35	148	*VWF, LEP, ASPM, SPARCL1, AURKA, MCM2, KIAA0101, FEN1, TF, MFGE8, GPC3, SMC4, CFD, NEK2, HMMR, GAPDH, CEP55, ECT2, TOP2A, CEBPA, CIDEA, ACACB, PDK4, ACSL1, SCD, JAG1, PLIN2, CIDEC, HADH, MSLN, FABP4, P4HB, FOXO1, PLIN1, CD36*
2	6.667	19	60	*ACADL, LIPE, PPARG, PCK1, PNPLA2, ANGPT2, PECAM1, ANGPT1, CDH1, LPL, SELP, MCAM, SELE, CXCL5, CDH5, CXCL12, PDE3B, CAT, RBP4*

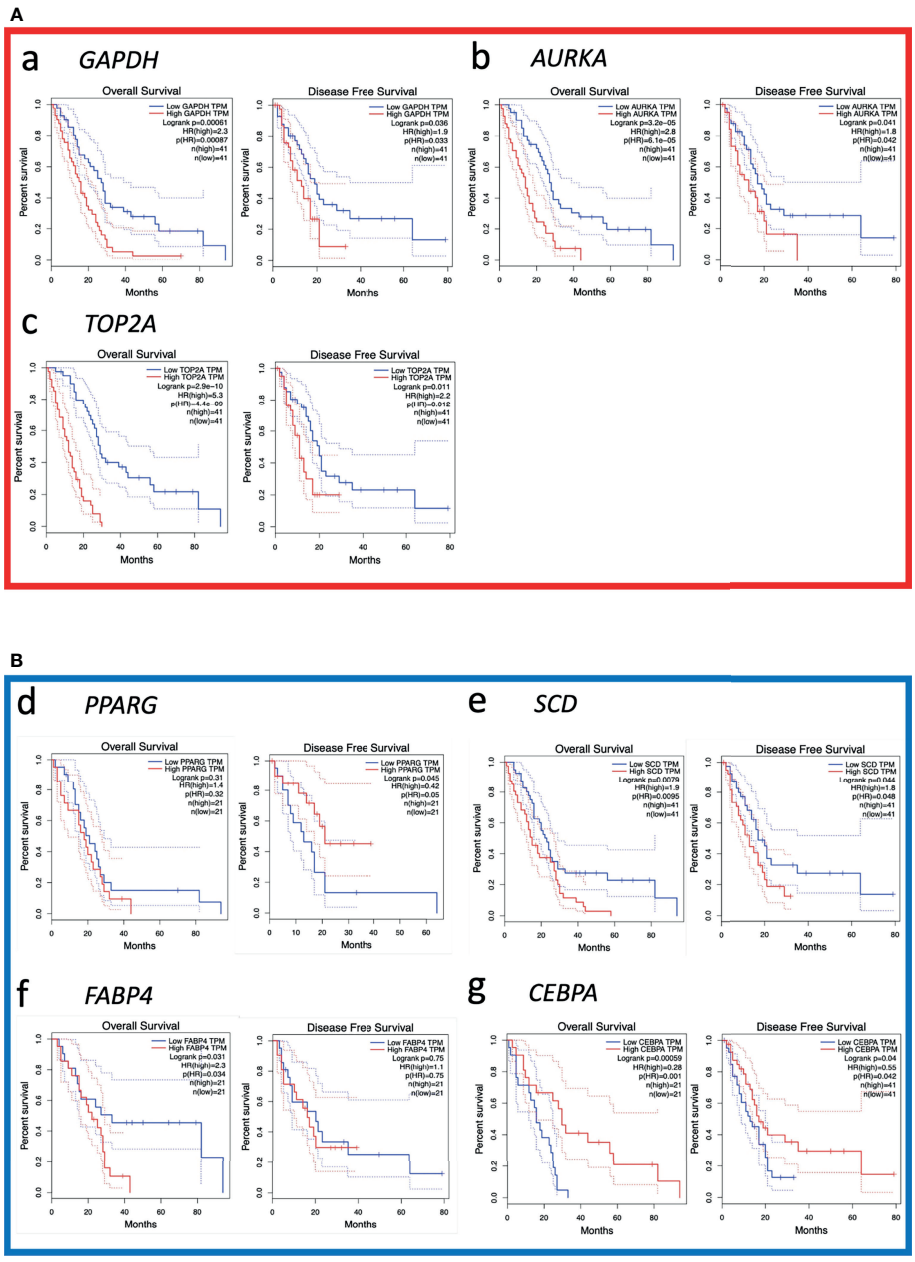

FIGURE 4 | Kaplan-Meier survival analyses for the top 20 hub genes expressed in malignant mesothelioma patients. **(A)** Upregulated genes are significantly associated with overall survival (OS) and/or disease-free survival (DFS; red square). **(B)** Downregulated genes are significantly associated with OS and/or DFS (blue square). The other 13 genes without significant associations with OS and DFS are shown in **Supplemental Data**.

TABLE 4 | Top 20 Hub gene in PPI network ranked by MCC method.

Rank	Name	Score	Degree
1	*PPARG*	3741564	39
2	*PNPLA2*	3726405	33
3	*LIPE*	3725389	26
4	*LPL*	3724044	28
5	*SCD*	3601850	24
6	*FABP4*	3443890	24
7	*LEP*	3128788	44
8	*PDK4*	2107470	19
9	*PLIN2*	1815265	16
10	*GAPDH*	1257609	83
11	*CIDEA*	1134028	16
12	*CIDEC*	1129272	15
13	*PCK1*	1020601	21
14	*PLIN1*	857570	18
15	*CD36*	766099	19
16	*ACSL1*	576013	18
17	*IL6*	491836	67
18	*CEBPA*	453645	17
19	*AURKA*	161314	15
20	*TOP2A*	161312	13

TABLE 5 | Patient and tumor Characteristics of MM cases.

Characteristics	MM
Number of cases	47
Gender	18 M/29 F
Site	3 pleura/44 peritoneum
Age, median (range)	47 (21-73)
Histologic type	42 epithelioid/3 biphasic/2 sarcomatoid
Asbestos exposure (%)	22 (46.8%)
Alive with disease	4
Died of disease	43

resection, radiation therapy, chemotherapy, and immunotherapy (11, 12). Identifying molecular biomarkers is critically important for early diagnosis, prognosis prediction, and personalized therapy. Mesothelioma primarily arises from mesothelial cells in the thoracic and abdominal cavities. During embryogenesis, mesothelial cells are a single layer of mesodermal cells resting on a basement membrane that covers the celomic cavity. During the second month of human gestation, the celomic cavity is divided by the septum transversum into what will become the thoracic and abdominal cavities. Pleural and peritoneal mesothelioma has the same origin, similar histology and immunophenotypes. In this study, we analyzed the genes expression in GSE2549 and GSE112154 microarray datasets to identify common differentially expressed genes between pleural and peritoneal MM and verified them in TMA. To the best of our knowledge, this is the first report to demonstrate the differential expressed gene involvement of diagnostic-and prognosis-related genes in pleural and peritoneal MM.

A total of 346 DEGs were identified in the two GEO datasets, of which 111 genes were upregulated and 235 genes were downregulated. Subsequently, we utilized bioinformatics methods to deeply explore these DEGs, including GO term enrichment, signaling pathway enrichment, PPI network construction, hub genes selection, and survival analysis. Functional enrichment analysis of DEGs revealed primary involvement of cell adhesion, leukocyte migration, extracellular matrix, integrin binding, heparin binding, and calcium ion binding. KEGG pathway analysis showed that these genes were primarily associated with the PPAR signaling pathway, ECM-receptor interaction, regulation of lipolysis in adipocytes, AMPK signaling pathway, and cell adhesion molecules. GSEA analysis revealed that genes involved in Ubiquitin mediated proteolysis and cell cycle were significantly enriched in MM compared to normal mesothelial tissues

In our previous research, compared with Europe and the United States, the incidence of malignant mesothelioma in China has unique characteristics: 1) women have a high incidence; 2) peritoneal site is more common than pleural; 3) the age of onset is less than 50 years old (13, 14). In most industrialized countries, pleural MM characteristically occurs in a setting of asbestos exposure. Because men are most often involved in trades that expose them to asbestos, pleural MM is typically higher in men, with a male to female ratio of approximately 4:1 (15). However, among Chinese patients with pleural MM, 80% were women, and only 42% had been exposed to asbestos, underscoring the unusual prevalence of MM in Chinese women (13). These findings present a unique opportunity to investigate other causes of peritoneal MM in the Chinese population, aside from asbestos. In the United States and Europe, an increasing number of peritoneal MM cases do not seem to be associated with asbestos (16), leading some researchers to speculate that a subgroup of peritoneal MM cases may have a different pathogenesis.

Then, initial survival analysis was conducted with the gene expression profiles and clinical information from The Cancer Genome Atlas database of 87 patients who were diagnosed as having MM between 1999 and 2013. Seven key genes associated

TABLE 6 | Characteristics of antibodies used for IHC.

Protein (clone)	Antibody	Origin	Pretreatment	Dilution	Location of staining
SCD1(CD.E10)	Mouse mAb	Abcam	Dako 3 in 1 AR buffers EDTA pH 9.0	1:250	Cytoplasm
FABP4(EPR3579)	Rabbit mAb	Abcam	Tris/EDTA buffer, pH 9.0	1:10000	Cytoplasm
Topoisomerase II alpha (EP1102Y)	Rabbit mAb	Abcam	Tris/EDTA buffer, pH 9.0	1:5000	Nucleus
C/EBPα(D56F10)	Rabbit mAb	CST	Citrate Unmasking Solution	1:200	Cytoplasm
Phospho-Aurora-A (Thr288) (C39D8)	Rabbit mAb	CST	Citrate Unmasking Solution	1:800	Cytoplasm
Aurora-A(35C1)	Mouse mAb	Abcam	Tris/EDTA buffer, pH 9.0	1:200	Cytoplasm
PPARγ(E-8)	Mouse mAb	Santa Cruz Biotechnology	Citrate Unmasking Solution	1:250	Nucleus
GAPDH (14C10)	Rabbit mAb	CST	Citrate Unmasking Solution	1:800	Cytoplasm

mAb-monoclonal antibody.

TABLE 7 | IHC staining in MM.

Specimens	Positive/Total, (%)						
	GAPDH	Aurora-A	TOPⅡA	SCD1	FABP4	CEBPA	PPARG
MM	44/47(93.6%)	36/47(75.6%)	9/47(19.1%)	42/47(89.4%)	6/47(12.8%)	0/47(0%)	0/47(0%)
Epithelioid	39/42(92.9%)	33/42(78.6%)	6/42(14.3%)	39/42(92.9%)	6/42(14.3%)	0/42(0%)	0/42(0%)
biphasic	3/3(100%)	2/3(66.7%)	2/3(66.7%)	2/3(66.7%)	0/3(0%)	0/3(0%)	0/3(0%)
sarcomatoid	2/2(100%)	1/2(50%)	1/2(50%)	1/2(50%)	0/2(0%)	0/2(0%)	0/2(0%)
normal peritoneum	4/10(40%)	2/10(20%)	0/10(0%)	8/10(80%)	0/10(0%)	0/10(0%)	0/10(0%)

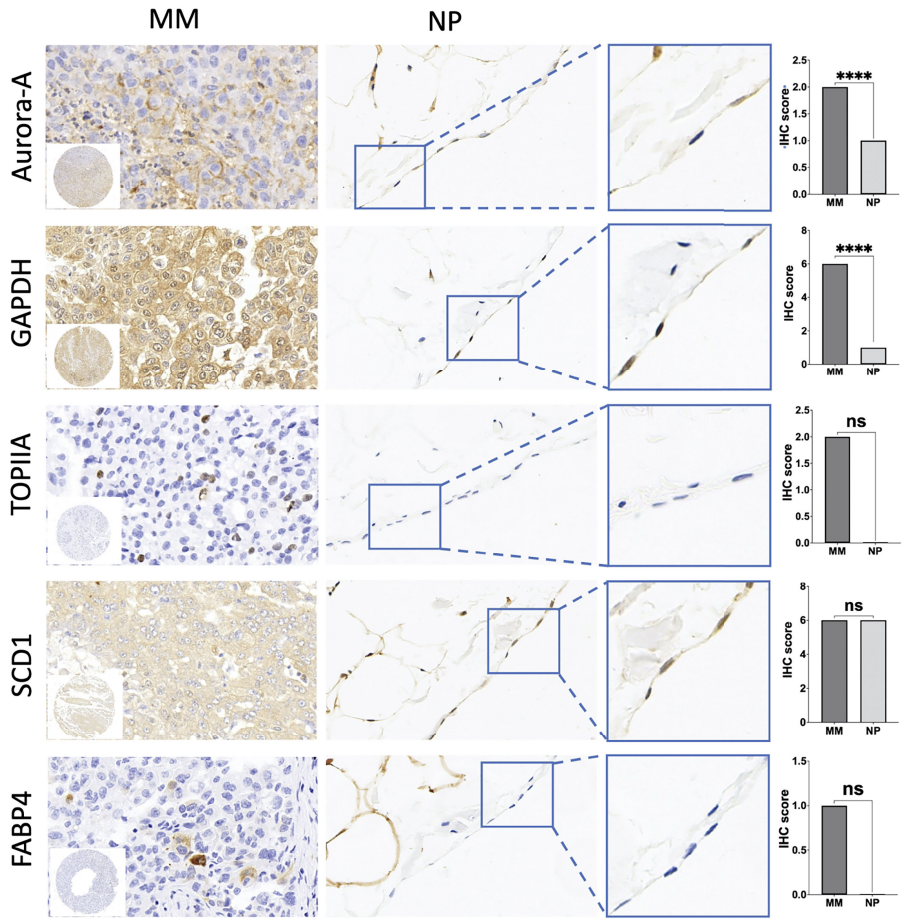

FIGURE 5 | Immunohistochemical (IHC) staining of tissue microarrays (TMA) of malignant mesothelioma (MM) and normal peritoneal (NP) samples to identify the expression of hub genes. Amplification of IHC images of representative mesothelial cells in NP tissue was shown in the blue box. Significant differences are shown in Aurora-A and GAPDH. Quantification of IHC results of aforementioned key genes is shown in the box plot. ****$p < 0.0001$; ns, not statistically significant.

with prognosis—including *GAPDH*, *AURKA*, *TOP2A*, *SCD*, *FABP4*, *CEBPA*, and *PPARG*—were selected. To evaluate the diagnostic and prognostic value of seven key genes, we constructed a TMA consisting of 47 MM tissue samples and performed immunohistochemistry to verify the proteins encoded by those seven genes. GAPDH and Aurora-A expression were significantly higher in MM samples than in normal mesothelial samples ($p < 0.0001$). Kaplan-Meier analysis identified that only Aurora-A (encoded by *AURKA*) is associated with a poor prognosis.

As a pathologist, we identify malignant mesothelioma not only from other source cancer in pathological diagnostic work but also from benign mesothelial hyperplasia, especially in the case of pleural biopsies, abdominal biopsies, hydrothorax, and ascites specimens. How to distinguish between benign mesothelial hyperplasia and malignant mesothelioma has become particularly important. The commonly used mesothelioma markers such as Calretinin and WT-1 are not useful to identify mesothelioma from mesothelial hyperplasia.

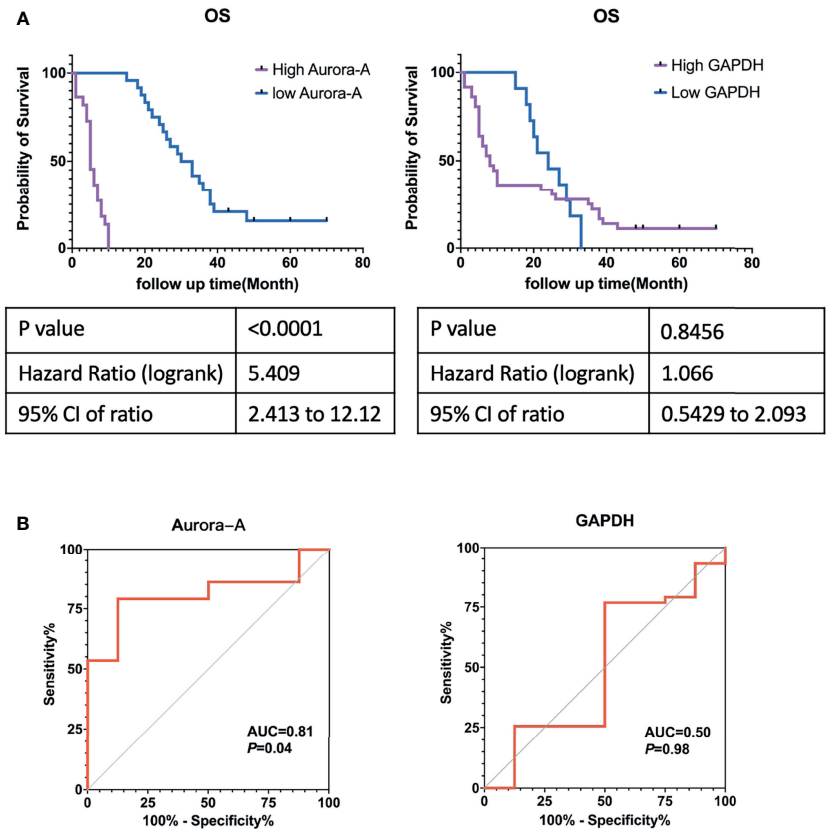

FIGURE 6 | Aurora-A and GAPDH protein expression in tissue microarrays from patients with malignant mesothelioma. **(A)** Kaplan-Meier survival curves. **(B)** Receiver operating curves.

In this study, the expression of Aurora-A was significantly higher in MM samples than in Normal mesothelial samples. ROC curve analysis identified that Aurora-A has a diagnostic value. Aurora-A is a useful marker for identifying benign mesothelial hyperplasia and malignant mesothelioma.

Three members of the Aurora kinase family have been identified in mammals: Aurora-A, Aurora-B, and Aurora-C (17). Both Aurora-A and Aurora-B play essential roles in regulating cell division during mitosis, whereas Aurora-C has a unique physiological role in spermatogenesis. Aurora-A is a cell cycle-regulated serine/threonine-protein kinase that appears to be involved in crucial cancer-related signaling pathways such as the p53, Hippo, FOXO, PI3K-Akt, and Wnt pathways. Aurora-A has been a popular target for cancer therapy with nearly 50 clinical trials using specific Aurora-A kinase inhibitors (AKIs) (18). Aurora-A promotes tumorigenesis by participating in the cancer cell proliferation, apoptosis, epithelial-mesenchymal transition, self-renewal of cancer stem cells, and metastasis. Aurora-A interacts with numerous tumor suppressors and oncogenes, such as YBX1, Merlin, LDHB, ALDH1A1, Twist, YAP, GSK-3β, β-catenin, and ERα. In recent years, several selectively target Aurora-A small molecules have been identified with anticancer activity in preclinical studies, including BPR1K0609S1 (19, 20), LY3295668 (21), MK-8745 (22, 23), LDD970 (24), CYC3 (25), and AKI603 (26).

A phase 2 study for MLN8237 (alisertib), a selective Aurora-A kinase inhibitor, found an overall response rate of 27% in patients with relapsed and refractory aggressive B- and T-cell non-Hodgkin lymphomas (27). Alisertib seems to be clinically active in both B- and T-cell aggressive lymphomas. Based on these results, confirmatory single-agent and combination studies have been initiated. However, in an open-label, first-in-setting, randomized phase 3 trial to evaluate the efficacy of alisertib, in patients with relapsed/refractory peripheral T-cell lymphoma, alisertib was not significantly superior to the placebo comparator arm (28). A single-arm phase 2 study assessed single-agent efficacy and safety of alisertib in patients with platinum-refractory or -resistant epithelial ovarian, fallopian tube, or primary peritoneal carcinoma. Sixteen (52%) patients achieved stable disease with a mean response duration of 2.86 months, and 6 (19%) reached three or more months. Median progression-free survival and the time to progression were 1.9 months (29). In a multicenter phase 1/2 study, an objective response was noted in 9 (18%) of 49 women with breast cancer and 10 (21%) of 48 patients with small-cell lung cancer (30). In a phase 2 trial of patients with castration-resistant and neuroendocrine prostate cancer, a subset of patients with advanced prostate cancer and molecular features supporting Aurora-A and N-myc activation achieved significant clinical benefit from single-agent alisertib (31).

Alisertib plus cytarabine and idarubicin induction are effective and safe in acute myeloid leukemia patients (32, 33). 60 mg/m^2 alisertib per dose for seven days shows antitumor activity, particularly in neuroblastoma patients with MYCN-nonamplified tumors (34, 35). EGFR-mutant lung adenocarcinoma cells with acquired resistance to third-generation EGFR inhibitors are sensitive to AKIs. Furthermore, combination treatment with AKIs and EGFR inhibitors was found to robustly decrease tumor growth in an EGFR-mutant lung adenocarcinoma PDX model (36). alisertib facilitates an anticancer immune microenvironment with decreased numbers of myeloid-derived suppressor cells and increased numbers of active CD8+ and CD4+ T lymphocytes (37). More importantly, the combined administration of alisertib and a PD-L1 antibody demonstrated synergistic efficacy for treating breast cancer cell 4T1 xenografts (37).

In this study, we identified common differentially expressed genes between pleural and peritoneal MM. Functional enrichment analysis of DEGs revealed primary involvement of cell adhesion, leukocyte migration, extracellular matrix, integrin binding, heparin binding, and calcium ion binding. KEGG pathway analysis showed that these genes were primarily associated with the PPAR signaling pathway, ECM-receptor interaction, regulation of lipolysis in adipocytes, and AMPK signaling pathway. Through TCGA database and immunochemistry analysis on Chinese MM TMA, Aurora-A expression was significantly higher in MM samples than in normal mesothelial samples ($p < 0.0001$). and Kaplan-Meier analysis and ROC curve analysis identified that only Aurora-A (encoded by *AURKA*) is associated with poor prognosis and has diagnostic value. At the same time, it may also be a potential therapeutic target.

CONCLUSION

We identified Aurora-A as a prognostic and diagnostic marker for MM. This protein may predict the survival of patients with MM and play a role as a biomarker of diagnosis and sensitivity to target therapy. Moreover, we validated these results in tissue samples of patients with MM in China. However, due to the low incidence of mesothelioma, larger samples are needed to verify our results in the future. Taken together, Aurora-A shows promise as a diagnostic and prognostic marker for MM.

DATA AVAILABILITY STATEMENT

Publicly available datasets were analyzed in this study. This data can be found here: GSE2549 and GSE112154 in GEO database (https://www.ncbi.nlm.nih.gov/geo/).

ETHICS STATEMENT

The studies involving human participants were reviewed and approved by The Institutional Review Board at the Cancer Hospital of the University of Chinese Academy of Sciences (Zhejiang Cancer Hospital). Written informed consent for participation was not required for this study in accordance with the national legislation and the institutional requirements.

AUTHOR CONTRIBUTIONS

ZGuo and YH guaranteed the manuscript's integrity and were involved in the conceptualization and design of the study. ZGuo, LS, NL, and ZGu contributed to the data collection, analysis, and interpretation. ZGuo, XW, CW, ZC, JL, WM, and YH contributed to administrative, technical, or material support. All the authors contributed to writing and revising the manuscript. The final manuscript has been read and approved by all authors.

FUNDING

This work was supported by grants from the National Natural Science Foundation of China (Grant No. 82072577), Natural Science Foundation of Zhejiang Province of China (Grant No. LY21H160002), Medical and Health Science and Technology Project of Zhejiang Province (No. 2020RC047), Key R&D Program Projects in Zhejiang Province (No. 2018C04009), National Natural Science Foundation of China (No .81672315), Clinical Research Fund of Zhejiang Medical Association (No. 2019ZYC-A77), International Cooperation Project of Zhejiang Basic Public Technology Research Program (No. LGJ20H010001), Projects of Zhejiang Province Medical and Health Science and Technology Plan (No. 2017KY256), Medical and Health Science and Technology Project of Zhejiang Province (No. 2021KY543), Medical and Health Science and Technology Plan Project of Zhejiang Province (No. 2019PY033), Research Program of Department of Science and Technology of Zhejiang Province (No. LGF19H180019), and Research Program of Zhejiang University 2018 Zhejiang Provincial Department of Education General Research Project (Natural Science) (No. Y201840845).

SUPPLEMENTARY MATERIAL

The Supplementary Material for this article can be found online at: https://www.frontiersin.org/articles/10.3389/fonc.2021.789244/full#supplementary-material

Supplementary Figure 1 | Kaplan-Meier survival analyses for the top 20 hub genes expressed in malignant mesothelioma patients without statistical significance. **(A)** *PNPLA2*, **(B)** *LIPE*, **(C)** *LPL*, **(D)** *LEP*, **(E)** *PDK4*, **(F)** *PLIN2*, **(G)** *CIDEA*, **(H)** *CIDEC*, **(I)** *PCK1*, **(J)** *PLIN1*, **(K)** *CD36*, **(L)** *ACSL*, **(M)** *IL6*.

Supplementary Figure 2 | IHC staining of PPARG and CEBPA in TMA of malignant mesothelioma (MM) and normal peritoneal (NP) samples. Amplification of IHC images of representative mesothelial cells in NP tissue was shown in the blue box.

REFERENCES

1. Carbone M, Adusumilli PS, Alexander HR, Baas P, Bardelli F, Bononi A, et al. Mesothelioma: Scientific Clues for Prevention, Diagnosis, and Therapy. *CA Cancer J Clin* (2019) 69:402–29. doi: 10.3322/caac.21572
2. Lapidot M, Freyaldenhoven S, Bueno R. New Concepts in the Treatment of Malignant Pleural Mesothelioma. *J Thorac Dis* (2018) 10:1283–5. doi: 10.21037/jtd.2018.02.75
3. Joseph NM, Chen Y-YY, Nasr A, Yeh I, Talevich E, Onodera C, et al. Genomic Profiling of Malignant Peritoneal Mesothelioma Reveals Recurrent Alterations in Epigenetic Regulatory Genes BAP1, SETD2, and DDX3X. *Mod Pathol* (2017) 30:246–54. doi: 10.1038/modpathol.2016.188
4. Chirac P, Maillet D, Leprêtre F, Isaac S, Glehen O, Figeac M, et al. Genomic Copy Number Alterations in 33 Malignant Peritoneal Mesothelioma Analyzed by Comparative Genomic Hybridization Array. *Hum Pathol* (2016) 55:72–82. doi: 10.1016/j.humpath.2016.04.015
5. Takeda M, Kasai T, Enomoto Y, Takano M, Morita K, Nakai T, et al. Comparison of Genomic Abnormality in Malignant Mesothelioma by the Site of Origin. *J Clin Pathol* (2014) 67:1038–43. doi: 10.1136/jclinpath-2014-202465
6. Xu X, Cheng L, Fan Y, Mao W. Tumor Microenvironment-Associated Immune-Related Genes for the Prognosis of Malignant Pleural Mesothelioma. *Front Oncol* (2020) 10:544789. doi: 10.3389/fonc.2020.544789
7. Xu D, Yang H, Yang Z, Berezowska S, Gao Y, Liang SQ, et al. Endoplasmic Reticulum Stress Signaling as a Therapeutic Target in Malignant Pleural Mesothelioma. *Cancers (Basel)* (2019) 11:1502. doi: 10.3390/cancers11101502
8. Gordon GJ, Rockwell GN, Jensen RV, Rheinwald JG, Glickman JN, Aronson JP, et al. Identification of Novel Candidate Oncogenes and Tumor Suppressors in Malignant Pleural Mesothelioma Using Large-Scale Transcriptional Profiling. *Am J Pathol* (2005) 166:1827–40. doi: 10.1016/S0002-9440(10)62492-3
9. Bueno R, de Rienzo A, Dong L, Gordon GJ, Hercus CF, Richards WG, et al. Second Generation Sequencing of the Mesothelioma Tumor Genome. *PloS One* (2010) 5:e10612. doi: 10.1371/journal.pone.0010612
10. Sciarrillo R, Wojtuszkiewicz A, El Hassouni B, Funel N, Gandellini P, Lagerweij T, et al. Splicing Modulation as Novel Therapeutic Strategy Against Diffuse Malignant Peritoneal Mesothelioma. *EBioMedicine* (2019) 39:215–25. doi: 10.1016/j.ebiom.2018.12.025
11. Nicholson AG, Sauter JL, Nowak AK, Kindler HL, Gill RR, Remy-Jardin M, et al. EURACAN/IASLC Proposals for Updating the Histologic Classification of Pleural Mesothelioma: Towards a More Multidisciplinary Approach. *J Thorac Oncol* (2019) 15:29–49. doi: 10.1016/j.jtho.2019.08.2506
12. Yap TA, Aerts JG, Popat S, Fennell DA. Novel Insights Into Mesothelioma Biology and Implications for Therapy. *Nat Rev Cancer* (2017) 17:475–88. doi: 10.1038/nrc.2017.42
13. Mao W, Zhang X, Guo Z, Gao Z, Pass HIHI, Yang H, et al. Association of Asbestos Exposure With Malignant Mesothelioma Incidence in Eastern China. *JAMA Oncol* (2017) 3:562–4. doi: 10.1001/jamaoncol.2016.5487
14. Guo Z, Carbone M, Zhang X, Su D, Sun W, Lou J, et al. Improving the Accuracy of Mesothelioma Diagnosis in China. *J Thorac Oncol* (2017) 12:714–23. doi: 10.1016/j.jtho.2016.12.006
15. Carbone M, Kanodia S, Chao A, Miller A, Wali A, Weissman D, et al. Consensus Report of the 2015 Weinman International Conference on Mesothelioma. *J Thorac Oncol* (2016) 11:1246–62. doi: 10.1016/j.jtho.2016.04.028
16. Sugarbaker PH. Update on the Management of Malignant Peritoneal Mesothelioma. *Transl Lung Cancer Res* (2018) 7:599–608. doi: 10.21037/tlcr.2018.08.03
17. Du R, Huang C, Liu K, Li X, Dong Z. Targeting AURKA in Cancer: Molecular Mechanisms and Opportunities for Cancer Therapy. *Mol Cancer* (2021) 20:1–27. doi: 10.1186/s12943-020-01305-3
18. Mou PK, Yang EJ, Shi C, Ren G, Tao S, Shim JS. Aurora Kinase A, a Synthetic Lethal Target for Precision Cancer Medicine. *Exp Mol Med* (2021) 53:835–47. doi: 10.1038/s12276-021-00635-6
19. Coumar MS, Chu CY, Lin CW, Shiao HY, Ho YL, Reddy R, et al. Fast-Forwarding Hit to Lead: Aurora and Epidermal Growth Factor Receptor Kinase Inhibitor Lead Identification. *J Med Chem* (2010) 53:4980–8. doi: 10.1021/jm1000198
20. Shionome Y, Lin WH, Shiao HY, Hsieh HP, Hsu JTA, Ouchi T. A Novel Aurora-A Inhibitor, BPR1K0609S1, Sensitizes Colorectal Tumor Cells to 5-Fluorofracil (5-FU) Treatment. *Int J Biol Sci* (2013) 9:403–11. doi: 10.7150/ijbs.5806
21. Du J, Yan L, Torres R, Gong X, Bian H, Marugan C, et al. Aurora A–selective Inhibitor LY3295668 Leads to Dominant Mitotic Arrest, Apoptosis in Cancer Cells, and Shows Potent Preclinical Antitumor Efficacy. *Mol Cancer Ther* (2019) 18:2207–19. doi: 10.1158/1535-7163.MCT-18-0529
22. Nair JS, Ho AL, Schwartz GK. The Induction of Polyploidy or Apoptosis by the Aurora A Kinase Inhibitor MK8745 Is P53-Dependent. *Cell Cycle* (2012) 11:807–17. doi: 10.4161/cc.11.4.19323
23. Shionome Y, Yan L, Liu S, Saeki T, Ouchi T. Integrity of P53 Associated Pathways Determines Induction of Apoptosis of Tumor Cells Resistant to Aurora-A Kinase Inhibitors. *PloS One* (2013) 8:4–11. doi: 10.1371/journal.pone.0055457
24. Ndolo KM, Park KR, Lee HJ, Yoon KB, YC K, Han SY. Characterization of the Indirubin Derivative LDD970 as a Small Molecule Aurora Kinase a Inhibitor in Human Colorectal Cancer Cells. *Immune Netw* (2017) 17:110–5. doi: 10.4110/in.2017.17.2.110
25. Lin Y, Richards FM, Krippendorff BF, Bramhall JL, Harrington JA, Bapiro TE, et al. Paclitaxel and CYC3, an Aurora Kinase A Inhibitor, Synergise in Pancreatic Cancer Cells But Not Bone Marrow Precursor Cells. *Br J Cancer* (2012) 107:1692–701. doi: 10.1038/bjc.2012.450
26. Zheng FM, Long ZJ, Hou ZJ, Luo Y, Xu LZ, Xia JL, et al. A Novel Small Molecule Aurora Kinase Inhibitor Attenuates Breast Tumor-Initiating Cells and Overcomes Drug Resistance. *Mol Cancer Ther* (2014) 13:1991–2003. doi: 10.1158/1535-7163.MCT-13-1029
27. Friedberg JW, Mahadevan D, Cebula E, Persky D, Lossos I, Agarwal AB, et al. Phase Ii Study of Alisertib, a Selective Aurora a Kinase Inhibitor, in Relapsed and Refractory Aggressive B- And T-Cell non-Hodgkin Lymphomas. *J Clin Oncol* (2014) 32:44–50. doi: 10.1200/JCO.2012.46.8793
28. O'Connor OA, Ozcan M, Jacobsen ED, Roncero JM, Trotman J, Demeter J, et al. Randomized Phase III Study of Alisertib or Investigator's Choice (Selected Single Agent) in Patients With Relapsed or Refractory Peripheral T-Cell Lymphoma. *J Clin Oncol* (2019) 37:613–23. doi: 10.1200/JCO.18.00899
29. Matulonis UA, Sharma S, Ghamande S, Gordon MS, Del Prete SA, Ray-Coquard I, et al. Phase II Study of MLN8237 (Alisertib), an Investigational Aurora A Kinase Inhibitor, in Patients With Platinum-Resistant or -Refractory Epithelial Ovarian, Fallopian Tube, or Primary Peritoneal Carcinoma. *Gynecol Oncol* (2012) 127:63–9. doi: 10.1016/j.ygyno.2012.06.040
30. Melichar B, Adenis A, Lockhart AC, Bennouna J, Dees EC, Kayaleh O, et al. Safety and Activity of Alisertib, an Investigational Aurora Kinase A Inhibitor, in Patients With Breast Cancer, Small-Cell Lung Cancer, non-Small-Cell Lung Cancer, Head and Neck Squamous-Cell Carcinoma, and Gastro-Oesophageal Adenocarcinoma: A Five-Arm Phase 2 Study. *Lancet Oncol* (2015) 16:395–405. doi: 10.1016/S1470-2045(15)70051-3
31. Beltran H, Oromendia C, Danila DC, Montgomery B, Hoimes C, Szmulewitz R, et al. A Phase II Trial of the Aurora Kinase A Inhibitor Alisertib for Patients With Castration Resistant and Neuroendocrine Prostate Cancer: Efficacy and Biomarkers. *Clin Cancer Res* (2019) 25:43–51. doi: 10.1158/1078-0432.CCR-18-1912.A
32. Brunner AM, Blonquist TM, DeAngelo DJ, McMasters M, Fell G, Hermance NM, et al. Alisertib Plus Induction Chemotherapy in Previously Untreated Patients With High-Risk, Acute Myeloid Leukaemia: A Single-Arm, Phase 2 Trial. *Lancet Haematol* (2020) 7:e122–33. doi: 10.1016/S2352-3026(19)30203-0
33. Kelly KR, Friedberg JW, Park SI, McDonagh K, Hayslip J, Persky D, et al. Phase I Study of the Investigational Aurora A Kinase Inhibitor Alisertib Plus Rituximab or Rituximab/Vincristine in Relapsed/Refractory Aggressive B-Cell Lymphoma. *Clin Cancer Res* (2018) 24:6150–9. doi: 10.1158/1078-0432.CCR-18-0286
34. DuBois SG, Marachelian A, Fox E, Kudgus RA, Reid JM, Groshen S, et al. Phase I Study of the Aurora A Kinase Inhibitor Alisertib in Combination With Irinotecan and Temozolomide for Patients With Relapsed or Refractory Neuroblastoma: A Nant (New Approaches to Neuroblastoma Therapy) Trial. *J Clin Oncol* (2016) 34:1368–75. doi: 10.1200/JCO.2015.65.4889
35. DuBois SG, Mosse YP, Fox E, Kudgus RA, Reid JM, McGovern R, et al. Phase II Trial of Alisertib in Combination With Irinotecan and Temozolomide for Patients With Relapsed or Refractory Neuroblastoma. *Clin Cancer Res* (2018) 24:6142–9. doi: 10.1158/1078-0432.CCR-18-1381

36. Shah KN, Bhatt R, Rotow J, Rohrberg J, Olivas V, Wang VE, et al. Aurora Kinase A Drives the Evolution of Resistance to Third Generation EGFR Inhibitors in Lung Cancer. *Nat Med* (2019) 25:111–8. doi: 10.1038/s41591-018-0264-7.Aurora
37. Yin T, Zhao ZB, Guo J, Wang T, Yang JB, Wang C, et al. Aurora A Inhibition Eliminates Myeloid Cell- Mediated Immunosuppression and Enhances the Efficacy of Anti-PD-L1 Therapy in Breast Cancer. *Cancer Res* (2019) 79:3431–44. doi: 10.1158/0008-5472.CAN-18-3397

Conflict of Interest: The authors declare that the research was conducted in the absence of any commercial or financial relationships that could be construed as a potential conflict of interest.

Publisher's Note: All claims expressed in this article are solely those of the authors and do not necessarily represent those of their affiliated organizations, or those of the publisher, the editors and the reviewers. Any product that may be evaluated in this article, or claim that may be made by its manufacturer, is not guaranteed or endorsed by the publisher.

frontiers in Oncology

ORIGINAL RESEARCH
published: 19 January 2022
doi: 10.3389/fonc.2021.795467

Insulin-Like Growth Factor 2 mRNA Binding Protein 3 Promotes Cell Proliferation of Malignant Mesothelioma Cells by Downregulating $p27^{Kip1}$

*Ihiro Endo, Vishwa Jeet Amatya, Kei Kushitani, Takahiro Kambara, Tetsuya Nakagiri, Yutaro Fujii and Yukio Takeshima**

Department of Pathology, Hiroshima University Graduate School of Biomedical and Health Sciences, Hiroshima, Japan

Malignant mesothelioma is a tumor with a poor prognosis, mainly caused by asbestos exposure and with no adequate treatment yet. To develop future therapeutic targets, we analyzed the microarray dataset GSE 29370 of malignant mesothelioma and reactive mesothelial hyperplasia, downloaded from the Gene Expression Omnibus (GEO) database. We identified insulin-like growth factor 2 mRNA binding protein 3 (IGF2BP3) as one of the significantly upregulated genes in malignant mesothelioma. IGF2BP3 functions as an oncoprotein in many human cancers; however, to our knowledge, this is the first study on the biological function of IGF2BP3 in malignant mesothelioma cells. The knockdown of IGF2BP3 in malignant mesothelioma cells resulted in the suppression of cell proliferation with an increase in the proportion of cells in the G1 phase of the cell cycle. Furthermore, knockdown of IGF2BP3 inhibited cell migration and invasion. We focused on the cell cycle assay to investigate the role of IGF2BP3 in cell proliferation in malignant mesothelioma. Among the various proteins involved in cell cycle regulation, the expression of p27 Kip1 (p27) increased significantly upon IGF2BP3 knockdown. Next, p27 siRNA was added to suppress the increased expression of p27. The results showed that p27 knockdown attenuated the effects of IGF2BP3 knockdown on cell proliferation and G1 phase arrest. In conclusion, we found that IGF2BP3 promotes cell proliferation, a critical step in tumorigenesis, by suppressing the expression of p27 in malignant mesothelioma.

Keywords: mesothelioma, IGF2BP3, siRNA, p27, cell line, proliferation

OPEN ACCESS

Edited by:
Marco Lucchi,
University of Pisa, Italy

Reviewed by:
Luis E. Arias-Romero,
National Autonomous University of Mexico, Mexico
Loredana Urso,
University of Padua, Italy

***Correspondence:**
Yukio Takeshima
ykotake@hiroshima-u.ac.jp

Specialty section:
This article was submitted to Thoracic Oncology, a section of the journal Frontiers in Oncology

Received: *15 October 2021*
Accepted: *31 December 2021*
Published: *19 January 2022*

Citation:
Endo I, Amatya VJ, Kushitani K, Kambara T, Nakagiri T, Fujii Y and Takeshima Y (2022) Insulin-Like Growth Factor 2 mRNA Binding Protein 3 Promotes Cell Proliferation of Malignant Mesothelioma Cells by Downregulating $p27^{Kip1}$. Front. Oncol. 11:795467. doi: 10.3389/fonc.2021.795467

INTRODUCTION

Malignant mesothelioma is a highly aggressive tumor that is mainly caused by occupational and environmental exposure to asbestos. The incidence of malignant mesothelioma is increasing worldwide, especially in developing countries, and the mortality rate in Japan is expected to peak by 2030 (1, 2). Although multidisciplinary therapies, including surgery, chemotherapy, and

radiation therapy, are used to treat malignant mesothelioma, sufficiently effective treatments have not yet been established (3, 4). The molecular mechanisms of mesothelioma carcinogenesis are not fully understood, and it is important to evaluate potential new therapeutic targets for the development of new therapies.

Insulin-like growth factor 2 mRNA-binding protein 3 (IGF2BP3) is a member of the IGF2BP family (5) and plays a vital role in the transport, stabilization, and translational regulation of multiple mRNAs (6, 7). IGF2BP3, an oncofetal protein, is not expressed in normal adult tissues (8). IGF2BP3 is highly expressed in human cancers, including lung cancer (9), melanoma (10), colorectal cancer (11), liver cancer (12), and squamous cell carcinoma of the head and neck (13). The expression of IGF2BP3 has a significant influence on biological functions related to tumorigenesis, such as cell proliferation and migration in various human cancers, including esophageal cancer (14), breast cancer (15), colorectal cancer (16), and prostate cancer (17). IGF2BP3 also contributes to tumorigenesis in many human organs and its malignant progression.

There are a few studies on IGF2BP3 expression in malignant mesothelioma. IGF2BP3 has been reported as a prognostic biomarker of malignant mesothelioma, and its reduced expression has a positive effect on life expectancy (18). Furthermore, IGF2BP3 has been used as a differential diagnostic marker to distinguish malignant mesothelioma from reactive mesothelial hyperplasia (19–21). These studies suggest that IGF2BP3 has diagnostic and prognostic value in malignant mesothelioma. However, biological studies have not yet been conducted. In this study, we conducted a functional analysis of IGF2BP3 in malignant mesothelioma cell lines and the regulation of downstream genes.

MATERIALS AND METHODS

Analysis of Gene Expression Data

Microarray data were downloaded from GEO datasets. The GSE 29370 (22) was used to analyze 11 malignant mesothelioma and 2 reactive mesothelioma hyperplasia samples; the differentially expressed genes were examined based on those that showed more than 1.5-fold change, using the Subio Platform software (Subio, Amami-shi, Japan). The histological types of 11 malignant mesothelioma samples used were as follows: MM26-P (epithelioid), MM34-P (epithelioid), MM35-P (epithelioid), MM45-P (epithelioid), MM46-P (sarcomatoid), MM16-P (biphasic), MM30-P (biphasic), H28 (epithelioid), H2452 (epithelioid), HMMME (epithelioid), MSTO-211H (biphasic).

Mesothelioma Cell Lines

Two human mesothelioma cell lines were used in this study. The ACC-MESO1 mesothelioma cell line was purchased from RIKEN BioResource Research Center (Tsukuba, Japan), and the CRL-5915 mesothelioma cell line was purchased from the American Type Culture Collection (Manassas, VA, USA). The cell lines used were sampled from malignant pleural mesothelioma, and the histological types are ACC-MESO1 for fibroblast-like type and CRL-5915 for epithelioid type. Cells were cultured in Roswell Park Memorial Institute 1640 medium (RPMI-1640) supplemented with kanamycin, amphotericin B, and 5% fetal bovine serum (Thermo Fisher Scientific, Tokyo, Japan). Cells were maintained in culture dishes at 37°C in a humidified incubator with 5% CO_2.

Transfection of Mesothelioma Cells

IGF2BP3 siRNA (#s20919), p27 Kip1 siRNA (#s2837), and negative control (NC) siRNA were purchased from Thermo Fisher Scientific (Tokyo, Japan). Mesothelioma cells at 60%–80% confluence were transfected with IGF2BP3, p27, or NC siRNA using Lipofectamine RNAiMAX (Thermo Fisher Scientific) in Opti-MEM Reduced Serum Medium (Thermo Fisher Scientific) according to the manufacturer's recommended protocols.

Quantitative Reverse-Transcription Polymerase Chain Reaction

Mesothelioma cell lines (3×10^5) were transfected with 25 pmol of IGF2BP3 or NC siRNA in 6-well plates for 72 h. RNA was extracted from the cells using Maxwell RSC RNA Cells Kits using the Maxwell RSC Instrument (Promega KK, Tokyo, Japan) according to the manufacturer's protocols. The extracted RNA was reverse transcribed with SuperScript IV VILO Master Mix (Thermo Fisher Scientific) and amplified using the PowerUp SYBR Green Master Mix (Thermo Fisher Scientific) on an AriaMax Real-Time PCR System (Agilent Technologies, Tokyo, Japan). The relative expression levels were calculated using the comparative Cq method. Expression levels were normalized to that of glyceraldehyde 3-phosphate dehydrogenase (GAPDH). The primer sequences used for quantitative reverse-transcription polymerase chain reaction (qRT-PCR) were as follows:

IGF2BP3 forward: 5′-AGT TGT TGT CCC TCG TGA CC-3′
IGF2BP3 reverse: 5′-GTC CAC TTT GCA GAG CCT TC-3′
GAPDH forward: 5′-ACA ACT TTG GTA TCG TGG AAG G-3′
GAPDH reverse: 5′-GCC ATC ACG CCA CAG TTT C-3′

Cell Proliferation Assay

Mesothelioma cell lines (3×10^3 cells) were incubated with 1 pmol IGF2BP3 siRNA, p27 siRNA, or NC siRNA in 96-well plates for 72 or 96 h. The proliferation rate was determined at 24, 48, 72, and 96 h using the Cell Titer Glo 2.0 reagent (Promega) and the GloMax Explorer microplate reader (Promega) according to the manufacturer's recommended protocols, by measuring the ATP level relative to the number of viable cells.

Cell Cycle Assay

Mesothelioma cell lines (1×10^5 cells) were transfected with 5 pmol IGF2BP3, p27, or NC siRNA in 24-well plates for 72 h, following which the cells were collected and fixed in 70% ethanol in 15 mL centrifuge tubes for approximately 1 h. After centrifugation and ethanol removal, the Guava Cell Cycle Reagent (Luminex, Austin, TX, USA) was added. This reagent contains propidium iodide, which allows for discrimination between cells at different stages of the cell cycle by labeling the cellular DNA. The signal intensity of the DNA labelling was measured using a Guava EasyCyte Mini flow cytometer (Guava

Technologies, Hayward, CA, USA) according to the manufacturer's protocol. Cell cycle data were analyzed using FCS Express 5.0 (DeNovo, Los Angeles, USA).

Cell Migration Assay

Mesothelioma cell lines were incubated overnight with 5 pmol IGF2BP3, p27, or NC siRNAs in collagen-coated 24-well plates. A wound was created by scratching each well with a 1 mL micropipette tip. The wells were washed twice to remove floating cells and subsequently incubated. The gap area (wound) was photographed every 12 h using a CKX53 inverted microscope equipped with a DP21 digital camera (Olympus, Tokyo, Japan), and the gap area was further analyzed using ImageJ software (https://imagej.nih.gov/ij/index.html).

Cell Invasion Assay

ACC-MESO1 (1×10^5 cells) and CRL-5915 (3×10^5 cells) were incubated with 5 pmol siRNA in BD FluoroBlok culture inserts (BD Biosciences, Franklin Lakes, NJ, USA) with 8 μm pores. The ACC-MESO1 and CRL-5915 cells were analyzed 48 h and 72 h after transfection, respectively. Infiltrating cells were stained with Hoechst 33342 (Thermo Fisher Scientific) for 10 min, and images of the infiltrating cells were acquired using an IX81 inverted fluorescence microscope equipped with a DP80 digital camera (Olympus, Tokyo, Japan). Fluorescence images were analyzed using ImageJ software (https://imagej.nih.gov/ij/index.html), and the total number of infiltrating cells was determined.

Western Blot Analysis

Mesothelioma cell lines (3×10^5) were transfected with 25 pmol IGF2BP3, p27, or NC siRNA in 6-well plates for 72 h. Cell lysates were prepared using the RIPA Lysis Buffer System (Santa Cruz Biotechnologies, Dallas, TX, USA), and the total protein was quantified using a Qubit Fluorometer (Thermo Fisher Scientific). The total protein (20 μg) was separated on a Bolt 4%–12% Bis-Tris Plus Gel (Thermo Fisher Scientific) with lithium dodecyl sulfate (LDS) electrophoresis at 165 V for 35 min. It was then transferred onto a polyvinylidene difluoride (PVDF) membrane using a Mini Blot Module (Thermo Fisher Scientific) at 20 V for 60 min. After blocking with 5% bovine serum albumin in TBS-T, the membranes were incubated overnight with primary antibodies. Anti-IGF2BP3 antibody (1:2000, polyclonal, #14642-1-AP) was purchased from Proteintech (Rosemont, IL, USA). p27 Kip1(1:3000, #3686), CDK2 (1:3000, #2546), cyclin E1 (1:3000, #20808), phospho-RB (1:3000, #8516), and GAPDH (1:5000, #2118) were purchased from Cell Signaling Technology (Danvers, MA, USA). The membrane was then incubated with secondary antibody. The secondary antibody used was anti-rabbit IgG-HRP (1:2000, #7074, Cell Signaling Technology). The membrane was stained with ImmunoStar LD (Wako Pure Chemical Industries, Osaka, Japan) and captured using a c-Digit Blot Scanner (LICOR, Lincoln, NE, USA).

Statistical Analysis

The experiments were performed in triplicate, and the data are expressed as the mean ± the standard deviation. The difference between the two groups was analyzed using an unpaired Student's t-test. The statistical significance was set at $p < 0.05$.

RESULTS

IGF2BP3 Is Upregulated in Malignant Mesothelioma Tissue and Cell Lines

Using the GSE29370 dataset from the GEO database, we analyzed 11 malignant mesothelioma samples and 2 reactive mesothelial hyperplasia samples. We identified 378 upregulated transcripts and 256 downregulated transcripts with more than 1.5-fold change in malignant mesothelioma compared to those in reactive mesothelial hyperplasia, as shown by the hierarchical clustering (**Figure 1A**). The mean transcript level of IGF2BP3 in mesothelioma increased by approximately 2-fold as shown in the scatter plot (**Figure 1B**). All seven mesothelioma tissues and four mesothelioma cell lines showed high expression of IGF2BP3 compared with two reactive mesothelial hyperplasia tissues (**Figure 1C**).

IGF2BP3 Knockdown Reduces Proliferation With G1 Phase Arrest, Migration, and Invasion of Mesothelioma Cell

IGF2BP3 siRNA was transfected into malignant mesothelioma cells to knock down IGF2BP3, and the efficiency of transfection was evaluated by western blotting and RT-PCR. IGF2BP3 mRNA expression was suppressed by 86.9% in ACC-MESO1 cells and 85.7% in CRL-5915 cells transfected with IGF2BP3 siRNA, as compared with those transfected with NC siRNA (**Figure 2A**). Furthermore, IGF2BP3 protein expression was suppressed by 77.4% in ACC-MESO1 and by 64.5% in CRL-5915, compared with that in the negative control (**Figure 2B**).

IGF2BP3 siRNA transfection suppressed the proliferation of ACC-MESO1 cells by 47.2% and CRL-5915 cells by 47.5% after 72 h, when compared with that of cells transfected with NC siRNA (**Figure 3A**). Given that the IGF2BP3 knockdown suppressed cell proliferation, we further investigated the effect of IGF2BP3 on cell cycle progression. The proportion of ACC-MESO1 and CRL-5915 cells in the G1 phase of the cell cycle was higher with IGF2BP3 siRNA transfection (69.9% and 75.4%, respectively) than with NC siRNA transfection (57.3% and 62.5%, respectively) (**Figure 3B**).

IGF2BP3 siRNA transfection decreased the wound gap area more slowly than NC siRNA transfection in both mesothelial cell lines. Transfection with IGF2BP3 siRNA significantly reduced the migration of both ACC-MESO1 and CRL-5915 cells, by 23.9% and 36.0%, respectively, as compared with that by NC siRNA transfection (**Figure 3C**).

IGF2BP3 knockdown significantly reduced cell invasion in both mesothelial cell lines Transfection with IGF2BP3 siRNA reduced the number of invading cells by 16.0% in ACC-MESO1 cells and 36.5% in CRL-5915 cells as compared with the cell numbers after NC siRNA transfection (**Figure 3D**).

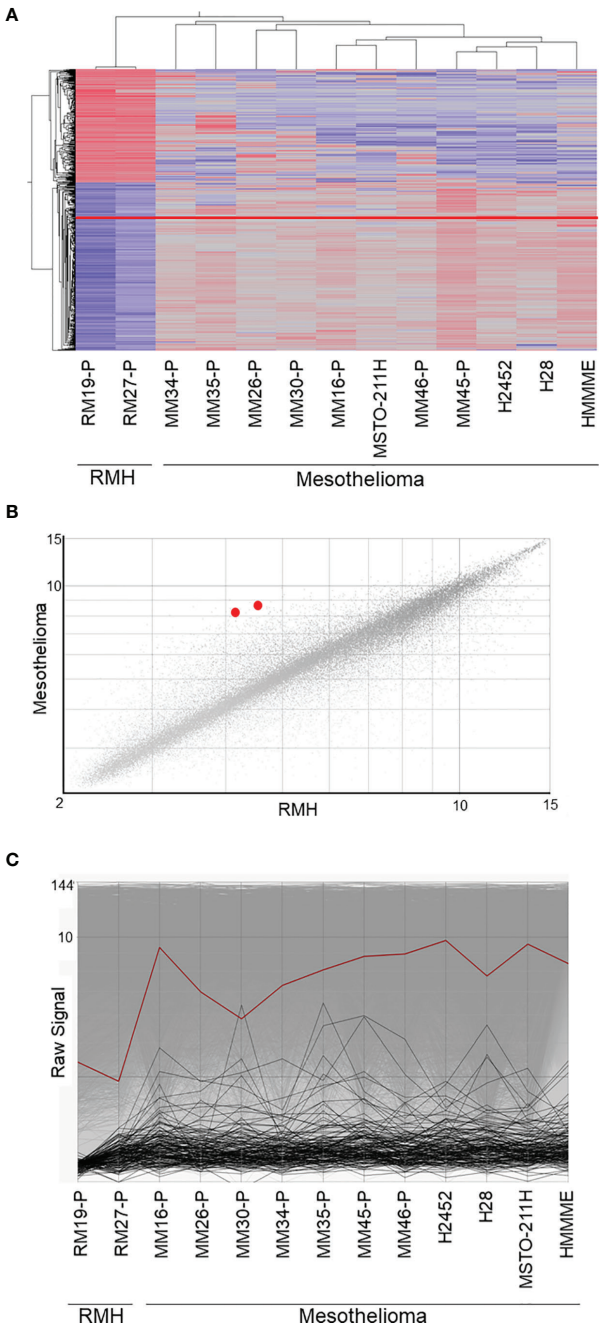

FIGURE 1 | Microarray data analysis. **(A)** Supervised hierarchical clustering of 11 malignant mesothelioma samples and 2 reactive mesothelial hyperplasia samples. IGF2BP3, presented as a red line, is upregulated in malignant mesothelioma, as compared with its expression in reactive mesothelioma hyperplasia. **(B)** The scatter plot showing the correlation between gene expression in malignant mesothelioma and reactive mesothelial hyperplasia. The two IGF2BP3 transcripts, shown as red dots, were upregulated in malignant mesothelioma when compared against expression in reactive mesothelial hyperplasia. **(C)** Line graph showing the gene expression in malignant mesothelioma and reactive mesothelial hyperplasia; IGF2BP3 expression, represented by the red line, is higher in malignant mesothelioma than in reactive mesothelial hyperplasia. RMH, reactive mesothelial hyperplasia.

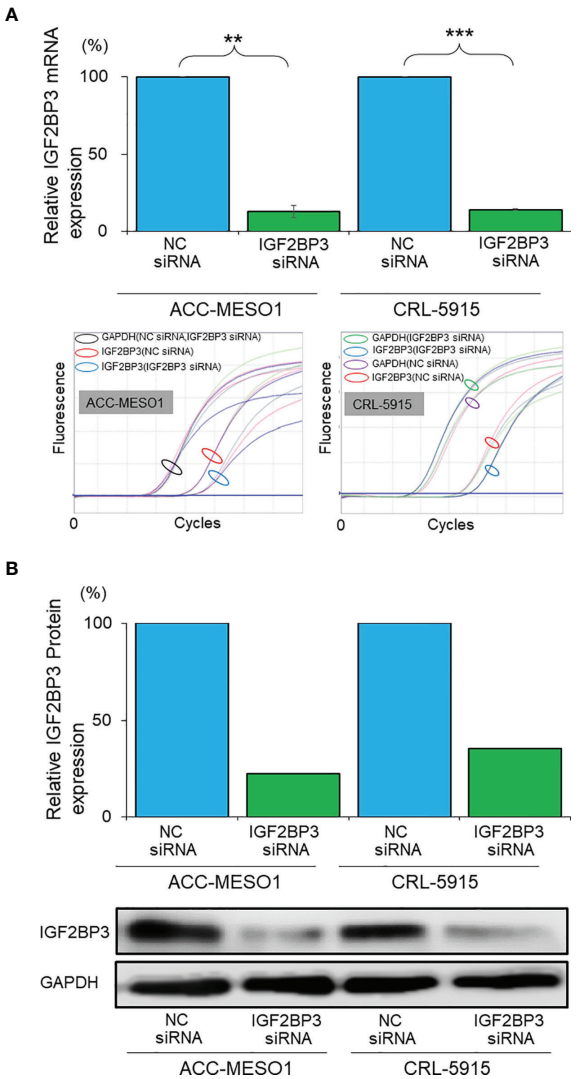

FIGURE 2 | Validation of IGF2BP3 knockdown. **(A)** Bar graph showing the relative IGF2BP3 mRNA expression in mesothelioma cell lines transfected with IGF2BP3 siRNA as compared with those transfected with NC siRNA (the lower panel represents the amplification curves of real time PCR experiments). **(B)** Bar graph showing the relative IGF2BP3 protein expression in mesothelioma cell lines transfected with IGF2BP3 siRNA as compared with those transfected with the NC siRNA (lower panel is an image of the western blot). NC, negative control; $^{**}p < 0.01$; $^{***}p < 0.001$.

IGF2BP3 Knockdown Regulates p27, CDK2, Cyclin E1, and Phospho-RB

By comparing IGF2BP3 siRNA-transfected cells with NC siRNA-transfected cells, we comprehensively examined the differential expression of proteins related to cell cycle regulation by western blotting. IGF2BP3 siRNA transfection significantly increased the expression of p27 and decreased the expression of CDK2, cyclin E1, and phospho-RB in both mesothelial cell lines compared to those after NC siRNA transfection (**Figure 4**). IGF2BP3 knockdown in ACC-MESO1 cells increased p27 protein expression by 424.2% and

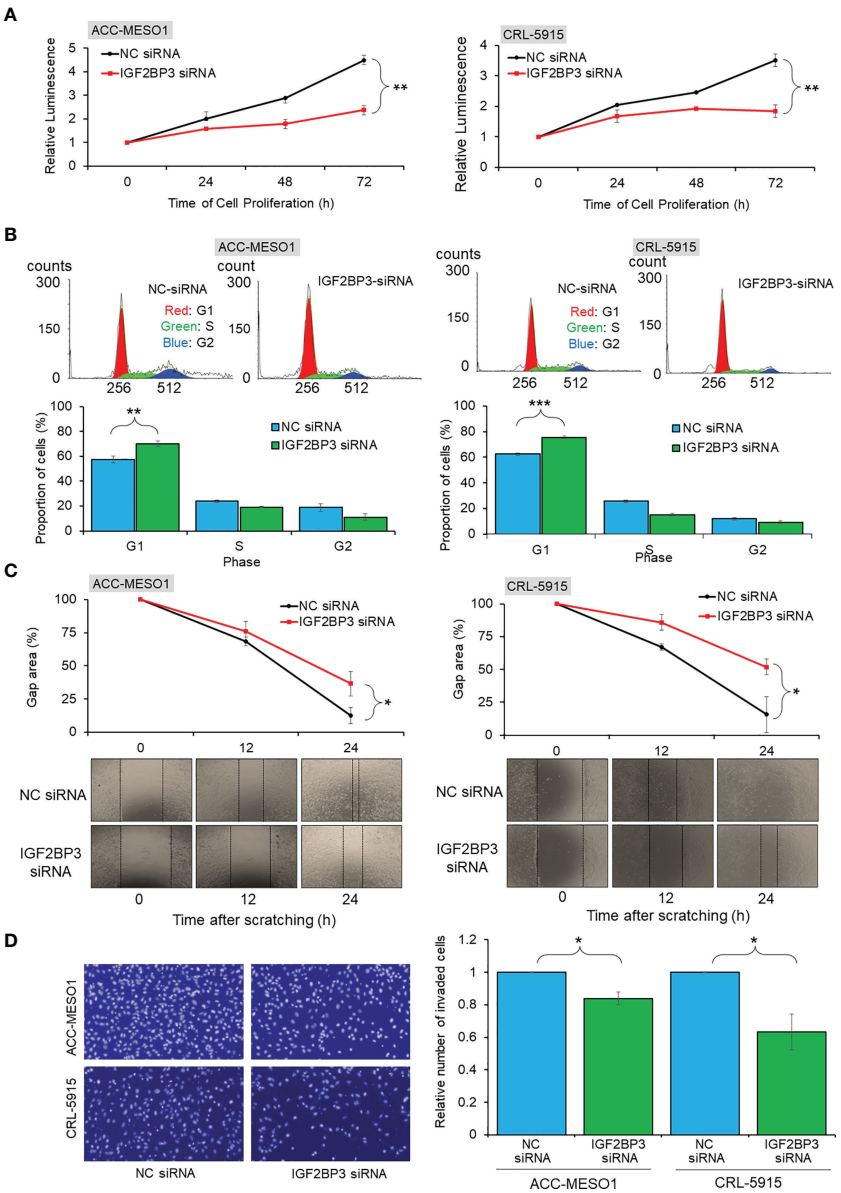

FIGURE 3 | Functional assays of IGF2BP3 expression. **(A)** Cell proliferation assay. Line chart showing reduced cell proliferation in ACC-MESO1 and CRL-5915 cells with IGF2BP3 siRNA transfection, compared with those cells transfected with NC siRNA. **(B)**Cell cycle assay. Cell cycle histogram and bar graph showing the G1 arrest of ACC-MESO1 and CRL-5915 by IGF2BP3 siRNA transfection. **(C)** Migration assay. Line chart and images showing reduced wound gap area of ACC-MESO1 and CRL-5915 following IGF2BP3 siRNA transfection. **(D)** Invasion assay. Bar graph and images showing reduced numbers of invading ACC-MESO1 and CRL-5915 cells, following transfection with IGF2BP3 siRNA. NC, negative control; NS, no significance; $^{*}p < 0.05$; $^{**}p < 0.01$; $^{***}p < 0.001$.

decreased the expression of CDK2 protein by 52.7%, cyclin E1 by 35.4%, and phospho-RB by 60.5%. The changes in protein expression of CRL-5915 were as follows: p27, 508.2%, CDK2, 65.4%; cyclin E1, 83.5%; and phospho-RB, 86.3%.

IGF2BP3 Increased Cell Proliferation by Suppressing p27

To investigate whether IGF2BP3 causes cell proliferation by suppressing p27, mesothelioma cells were transfected with either one or both IGF2BP3 siRNA and p27 siRNA. Western blotting showed the suppression of specific protein expression in IGF2BP3 or p27 siRNA-transfected cells (**Figure 5A**). Furthermore, when mesothelial cells were transfected with both IGF2BP3 and p27 siRNA, elevated p27 protein expression by IGF2BP3 knockdown was diminished, and repressed phospho-RB protein was recovered.

Mesothelioma cells simultaneously transfected with IGF2BP3 siRNA and p27 siRNA showed a significant recovery in cell proliferation, when compared with cells transfected with IGF2BP3

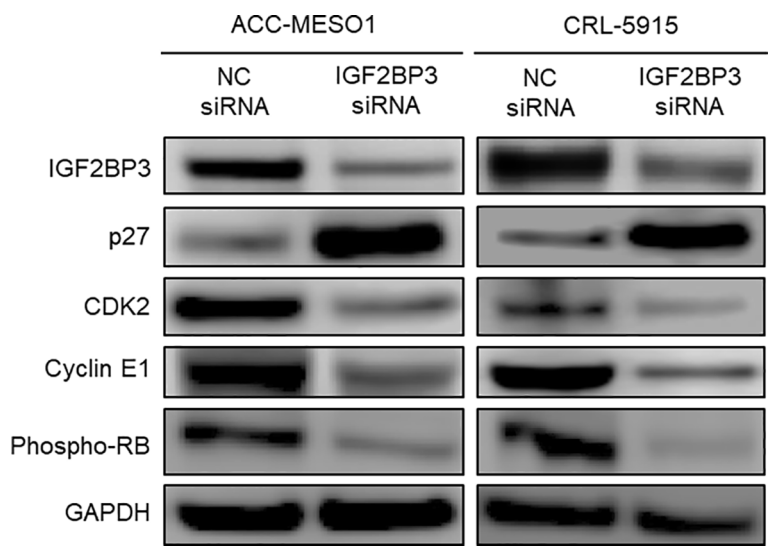

FIGURE 4 | Downstream regulation of IGF2BP3. Western blots of IGF2BP3, p27, CDK2, Cyclin E1, and phospho-RB proteins in ACC-MESO1 and CRL-5915 cells show increased expression of p27 and decreased expression of CDK2, Cyclin E1, and phospho-RB with IGF2BP3 siRNA transfection. NC: negative control.

siRNA alone. Specifically, in ACC-MESO1 cells, transfection with IGF2BP3 siRNA and p27 siRNA together increased cell proliferation; cells were initially transfected with IGF2BP3 siRNA alone, then transfected with the combination of IGF2BP3 and p27 siRNAs after 72 h and 96 h, resulting in increases in cell proliferation of 31.8% and 30.4%, respectively. Similarly, when IGF2BP3 siRNA and p27 siRNA were transfected together in CRL-5915 cells, there was a 43.8% increase in cell proliferation with addition 72 h after transfection of IGF2BP3 siRNA alone, and a 48.8% increase with addition after 96 h. In contrast, mesothelial cells transfected with p27 siRNA alone showed no significant change in cell proliferation compared with that of cells transfected with NC siRNA (**Figure 5B**). These results indicate that the repression of p27 expression is significant for IGF2BP3 to activate cell proliferation in mesothelioma cells.

Furthermore, we examined the effects of IGF2BP3 and p27 on cell cycle progression. When p27 siRNA and IGF2BP3 siRNA were simultaneously transfected into mesothelioma cells, there was an increase in the percentage of cells in the G1 phase of the cell cycle compared with the cell numbers after transfection with IGF2BP3 siRNA alone. Specifically, when IGF2BP3 siRNA and p27 siRNA were transfected together, the percentage of cells in the G1 phase was reduced by 18.0% in ACC-MESO1 cells and by 7.6% in CRL-5915 cells. However, when p27 siRNA alone was transfected into mesothelioma cells, there was no significant difference in the percentage of cells in the G1 phase compared with that after NC siRNA transfection (**Figure 5C**).

DISCUSSION

Malignant mesothelioma is a tumor with a poor prognosis that develops in mesothelial cells, primarily due to asbestos exposure. The current first-line treatment for malignant mesothelioma is a combination of cisplatin and pemetrexed (23), and very few patients undergo surgery (24). The survival rate for patients with malignant pleural mesothelioma is still low; a population-based study reported average survival times ranging from 5 months to 13.2 months (25). Although immunotherapeutic approaches to malignant mesothelioma have received much attention, further studies are needed to show a clear advantage over standard chemotherapy (26). A recent study of immunotherapeutic approach also showed significant and clinically meaningful improvements in overall survival versus standard chemotherapy (27). It is essential to develop novel treatments and to explore effective therapeutic targets against malignant mesothelioma.

In this study, we searched for genes that were significantly altered in malignant mesothelioma compared with those in reactive mesothelial hyperplasia to identify therapeutic targets. We analyzed 11 malignant mesothelioma cell samples and 2 reactive mesothelial hyperplasia samples from the microarray dataset GSE 29370. IGF2BP3 expression was significantly increased in mesothelioma cell samples compared with that in reactive mesothelial hyperplasia.

IGF2BP3 is an oncogenic protein that is overexpressed in many human cancers. IGF2BP3 functions as a biomarker of aggressiveness and metastasis in many tumors (28–31). IGF2BP3 expression correlates with poor prognosis in malignant mesothelioma (32). Structurally, IGF2BP3 has two N-terminal RNA recognition motifs (RRMs) and four C-terminal messenger ribonucleoprotein K homology (KH) domains (33). IGF2BP3 has been shown to target RNA as an RNA-binding protein and promote tumorigenesis primarily through regulation at the transcriptional level (34). IGF2BP3 was first identified for its ability to promote the translation of IGF2 mRNA (34). The currently-identified mRNA targets of IGF2BP3 include CD44

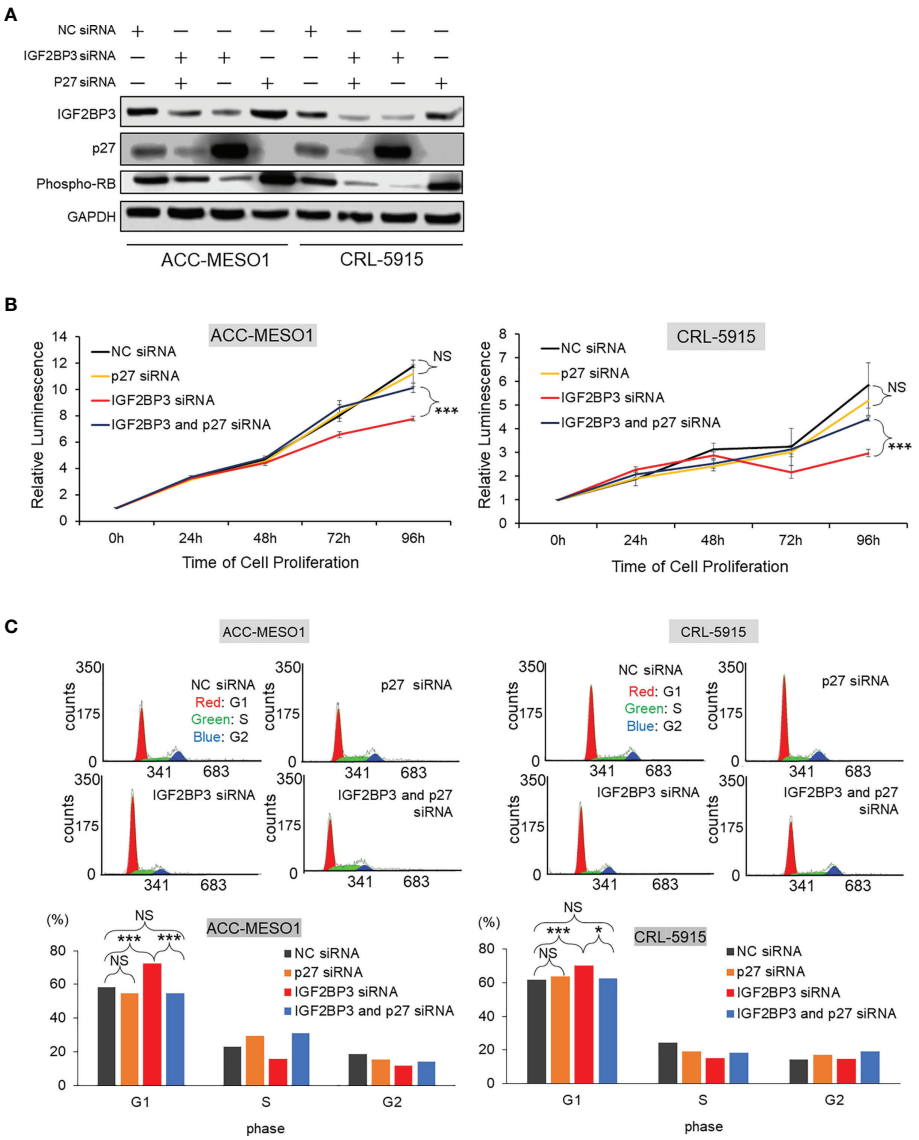

FIGURE 5 | Effect of IGF2BP3 and p27 on cell proliferation and G1 cell cycle phase arrest. **(A)** Western blot of IGF2BP3, p27, and phospho-RB proteins. IGF2BP3 or p27 siRNA- transfected cells show the suppression of specific protein expression in ACC-MESO1 and CRL-5915 cells. Cell lines transfected simultaneously with both IGF2BP3 and p27 siRNAs re-diminish p27 protein expression and recover phospho-RB protein expression. **(B)** Cell proliferation assay. In ACC-MESO1 and CRL-5915, transfection with IGF2BP3 siRNA and p27 siRNA together show a significant increase in cell proliferation at 72 h and 96 h from transfection of IGF2BP3 siRNA alone. Note the cells transfected with p27 siRNA alone show no significant change from those transfected with NC siRNA. **(C)** Cell cycle assay. ACC-MESO1 and CRL-5915 cells transfected with IGF2BP3 siRNA and p27 siRNA together, show significant reduction in the percentage of cells in G1 phase of the cell cycle. Note the cells transfected with p27 siRNA alone show no significant difference in the percentage of cells in G1 phase compared with those cells transfected with NC siRNA. NC, Negative control; NS, no significance; $^{*}p < 0.05$; $^{***}p < 0.001$.

(6), MMP9 (15), HMGA2 (35), and PDPN (36). This is the first study to investigate the biological functions of IGF2BP3 in mesothelioma cells.

First, we performed IGF2BP3 knockdown in mesothelioma cell lines (ACC-MESO1 and CRL-5915) using siRNA to analyze its biological functions, including cell proliferation, cell cycle, cell migration, and cell invasion. IGF2BP3 knockdown suppressed cell proliferation and induced G1 cell cycle arrest in both cell lines. Furthermore, IGF2BP3 knockdown suppressed cell migration and invasion. These results suggest that IGF2BP3 strongly contributes to tumorigenesis in malignant mesothelioma.

The regulation of cell cycle proteins has long been an important field of oncology research (37). Cells proliferate successfully by passing through the G1, S, G2, and M phases of the cell cycle. A central component of the cell cycle regulatory system is cyclin-dependent kinase (CDK), which is regulated by cyclin binding, phosphorylation, and CDK inhibitors (37). A cell cycle assay revealed that IGF2BP3 knockdown induced G1 phase arrest.

Therefore, we comprehensively examined the effect of IGF2BP3 knockdown on the expression of proteins related to cell cycle regulation. We found that IGF2BP3 knockdown significantly increased the expression of p27, followed by markedly decreasing CDK2 and cyclin E1 expression, and suppressing the phosphorylation of RB. Among the E2F family as transcriptional factors, E2F1, E2F2, and E2F3 were shown to be associated with RB in cell proliferation (38). In addition, E2F promotes transcription by targeting E2F itself and TYMS, POLA1, ORC1, FBXO5, and RRM2 as mentioned in G1/S- specific transcription pathway of Reactome website (https://reactome.org/PathwayBrowser/#/R-HSA-453279&SEL=R-HSA-69205&PATH=R-HSA-1640170,R-HSA-69278) as known targets of E2F, which are involved in DNA biosynthesis, regulation, and G1/S transition. Therefore, we investigated the expression of E2F1, E2F2, E2F3, and TYMS, POLA1, ORC1, FBXO5, and RRM2 as targets of E2F. The real time qPCR showed, in both ACC-MESO1 and CRL-5915 cell lines, the reduced expression of E2F family and E2F target genes by IGF2BP3 siRNA transfection compared to NC siRNA transfection (**Supplementary Figure**). The CDK inhibitor, p27, was first identified as a tumor suppressor protein able to induce G1 phase arrest (39); it binds to the CDK2/Cyclin E complex and inhibits its activity (40, 41). Overactivation of the cyclin CDK2/Cyclin E complex results in genomic instability and the development of tumors (42). Activation of the CDK2/Cyclin E complex induces RB protein phosphorylation and releases activated E2F, resulting in cell cycle progression from the G1 phase to S phase and cell proliferation (43–45). In summary, our results suggest that IGF2BP3 activates CDK2/Cyclin E1 and phosphorylates RB and activates E2F by suppressing the expression of p27, thereby facilitating the progression from the G1 phase of the cell cycle (**Figure 6A**).

We further verified that p27 suppression is a critical factor in IGF2BP3-induced cell proliferation. First, mesothelioma cells transfected with p27 siRNA alone did not show significant changes in cell proliferation compared with those transfected with NC siRNA. In mesothelioma cells without knockdown of IGF2BP3, the expression of p27 itself is usually a low level, suggesting that p27 knockdown alone did not cause significant changes in cell proliferation. Next, when IGF2BP3 siRNA and p27 siRNA were simultaneously transfected into the cells, cell proliferation was significantly restored toward to that of mesothelioma cells transfected with only NC siRNA. This is thought to result from the suppression of p27 expression (by transfection of cells with p27 siRNA), which would otherwise be increased by transfection with IGF2BP3 siRNA. Similarly, simultaneous transfection alleviated G1 cell cycle arrest (**Figure 6B**).

Numerous studies have investigated the molecular mechanisms underlying the oncogenic function of IGF2BP3; it is associated with several regulators of cell proliferation and the cell cycle, including cyclin D1, D3, G1, and CDK6 (46, 47). *In vitro* biological analysis has shown that IGF2BP3 promotes cell proliferation and cell cycle progression from the G1 phase to S phase (48). The identification of cell cycle regulatory proteins with particularly close associations is an important clue in elucidating the metabolic mechanism of IGF2BP3.

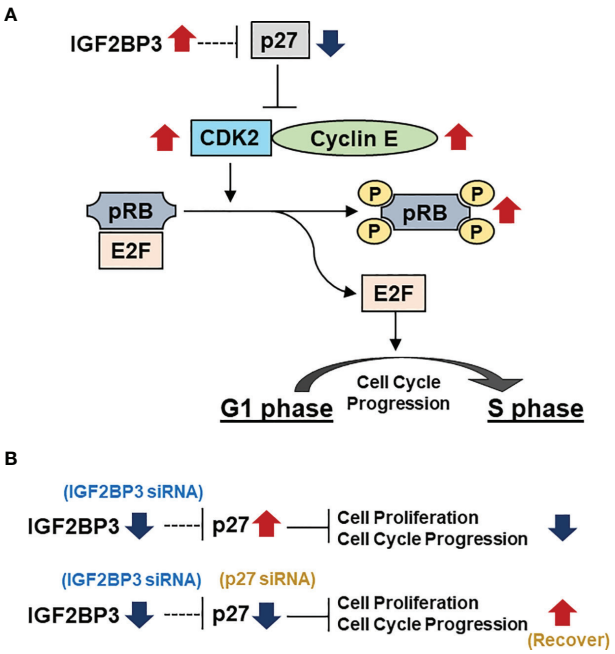

FIGURE 6 | IGF2BP3 represses p27, thereby affecting the downstream pathway and finally causing G1 arrest. **(A)** IGF2BP3 activates the CDK2/Cyclin E complex by repressing p27, which leads to the phosphorylation of RB and the release of the transcription factor E2F from RB, leading to the progression from G1 to S phase in the cell cycle. **(B)**Transfection with IGF2BP3 siRNA alone results in inhibition of cell proliferation with G1 phase arrest by increasing the expression of p27. Simultaneous transfection with IGF2BP3 and p27 siRNA prevents p27 upregulation by IGF2BP3 siRNA, leading to alleviation of G1 phase arrest and restoration of cell proliferation.

In this study, we focused on the association between IGF2BP3 and p27. However, it is essential to note that it is not clear whether the effect of IGF2BP3 on p27 expression is due to its function as an RNA-binding protein or otherwise and whether it acts directly or indirectly. Further investigation is necessary to determine the relationship between IGF2BP3 and p27.

In summary, IGF2BP3 is involved in the proliferation of mesothelioma cells by decreasing p27 expression, which regulates the progression from the G1 phase to S phase of the cell cycle. This study highlights the potential of IGF2BP3 as a therapeutic target for the treatment of malignant mesothelioma.

DATA AVAILABILITY STATEMENT

Publicly available datasets were analyzed in this study. This data can be found here: https://www.ncbi.nlm.nih.gov/geo/query/acc.cgi?acc=GSE29370.

AUTHOR CONTRIBUTIONS

IE, VA, and YT designed the study. VA and YT supervised and facilitated the study IE, TN, KK, TK, and YF performed the

experiments. IE analyzed the data. IE and VA interpreted the results, and IE prepared the manuscript. All authors contributed to the article and approved the submitted version.

ACKNOWLEDGMENTS

We thank Ms. Yukari Go and Mr. Tatsuya Nakagawa of the Technical Center, Hiroshima University for their excellent technical assistance, and Ms. Naomi Fukuhara for administrative support. We would like to thank Editage (www.editage.com) for English language editing.

SUPPLEMENTARY MATERIAL

The Supplementary Material for this article can be found online at: https://www.frontiersin.org/articles/10.3389/fonc.2021.795467/full#supplementary-material

REFERENCES

1. McDonald JC, McDonald AD. The Epidemiology of Mesothelioma in Historical Context. *Eur Respir J* (1996) 9:1932–42. doi: 10.1183/09031936.96.09091932
2. Myojin T, Azuma K, Okumura J, Uchiyama I. Future Trends of Mesothelioma Mortality in Japan Based on a Risk Function. *Ind Health* (2012) 50:197–204. doi: 10.2486/indhealth.MS1184
3. Zhang W, Wu X, Wu L, Zhang W, Zhao X. Advances in the Diagnosis, Treatment and Prognosis of Malignant Pleural Mesothelioma. *Ann Transl Med* (2015) 3:182. doi: 10.3978/j.issn.2305-5839.2015.07.03
4. Milano MT, Zhang H. Malignant Pleural Mesothelioma: A Population-Based Study of Survival. *J Thorac Oncol* (2010) 5:1841–8. doi: 10.1097/JTO.0b013e3181f1cf2b
5. Mancarella C, Pasello M, Manara MC, Toracchio L, Sciandra EF, Picci P, et al. Insulin-Like Growth Factor 2 mRNA-Binding Protein 3 Influences Sensitivity to Anti-IGF System Agents Through the Translational Regulation of IGF1R. *Front Endocrinol* (2018) 9:178. doi: 10.3389/fendo.2018.00178
6. Vikesaa J, Hansen TVO, Jønson L, Borup R, Wewer UM, Christiansen J, et al. RNA-Binding IMPs Promote Cell Adhesion and Invadopodia Formation. *EMBO J* (2006) 25:1456–68. doi: 10.1038/sj.emboj.7601039
7. Runge S, Nielsen FC, Nielsen J, Lykke-Andersen J, Wewer UM, Christiansen J. H19 RNA Binds Four Molecules of Insulin-Like Growth Factor II mRNA-Binding Protein. *J Biol Chem* (2000) 275:29562–9. doi: 10.1074/jbc.M001156200
8. Mancarella C, Scotlandi K. IGF2BP3 From Physiology to Cancer: Novel Discoveries, Unsolved Issues, and Future Perspectives. *Front Cell Dev Biol* (2019) 7:363. doi: 10.3389/fcell.2019.00363
9. Wang T, Fan L, Watanabe Y, McNeill PD, Moulton GG, Bangur C, et al. L523S, an RNA-Binding Protein as a Potential Therapeutic Target for Lung Cancer. *Br J Cancer* (2003) 88:887–94. doi: 10.1038/sj.bjc.6600806
10. Pryor JG, Bourne PA, Yang Q, Spaulding BO, Scott GA, Xu H. IMP-3 Is a Novel Progression Marker in Malignant Melanoma. *Mod Pathol* (2008) 21:431–7. doi: 10.1038/modpathol.3801016
11. Li D, Yan D, Tang H, Zhou C, Fan J, Li S, et al. IMP3 is a Novel Prognostic Marker That Correlates With Colon Cancer Progression and Pathogenesis. *Ann Surg Oncol* (2009) 16:3499–506. doi: 10.1245/s10434-009-0648-5
12. Jeng Y-M, Chang C-C, Hu F-C, Chou H-YE, Kao H-L, Wang T-H, et al. RNA-Binding Protein Insulin-Like Growth Factor II mRNA-Binding Protein 3 Expression Promotes Tumor Invasion and Predicts Early Recurrence and Poor Prognosis in Hepatocellular Carcinoma. *Hepatology* (2008) 48:1118–27. doi: 10.1002/hep.22459
13. Clauditz TS, Wang C-J, Gontarewicz A, Blessmann M, Tennstedt P, Borgmann K, et al. Expression of Insulin-Like Growth Factor II mRNA-Binding Protein 3 in Squamous Cell Carcinomas of the Head and Neck. *J Oral Pathol Med* (2013) 42:125–32. doi: 10.1111/j.1600-0714.2012.01178.x
14. Qian L-X, Cao X, Du M-Y, Ma C-X, Zhu H-M, Peng Y, et al. KIF18A Knockdown Reduces Proliferation, Migration, Invasion and Enhances Radiosensitivity of Esophageal Cancer. *Biochem Biophys Res Commun* (2021) 557:192–8. doi: 10.1016/j.bbrc.2021.04.020
15. Samanta S, Sharma VM, Khan A, Mercurio AM. Regulation of IMP3 by EGFR Signaling and Repression by Erβ: Implications for Triple-Negative Breast Cancer. *Oncogene* (2012) 31:4689–97. doi: 10.1038/onc.2011.620
16. Huang Y-Y, Zhang C-M, Dai Y-B, Lin J-G, Lin N, Huang Z-X, et al. USP11 Facilitates Colorectal Cancer Proliferation and Metastasis by Regulating IGF2BP3 Stability. *Am J Transl Res* (2021) 13:480–96.
17. Zhang X, Wang D, Liu B, Jin X, Wang X, Pan J, et al. IMP3 Accelerates the Progression of Prostate Cancer Through Inhibiting PTEN Expression in a SMURF1-Dependent Way. *J Exp Clin Cancer Res* (2020) 39:190. doi: 10.1186/s13046-020-01657-0
18. Hui S, Guo-Qi Z, Xiao-Zhong G, Chun-Rong L, Yu-Fei L, Dong-Liang Y. IMP3 as a Prognostic Biomarker in Patients With Malignant Peritoneal Mesothelioma. *Hum Pathol* (2018) 81:138–47. doi: 10.1016/j.humpath.2018.07.003
19. Shi M, Fraire AE, Chu P, Cornejo K, Woda BA, Dresser K, et al. Oncofetal Protein IMP3, a New Diagnostic Biomarker to Distinguish Malignant Mesothelioma From Reactive Mesothelial Proliferation. *Am J Surg Pathol* (2011) 35:878–82. doi: 10.1097/PAS.0b013e318218985b
20. Minato H, Kurose N, Fukushima M, Nojima T, Usuda K, Sagawa M, et al. Comparative Immunohistochemical Analysis of IMP3, GLUT1, EMA, CD146, and Desmin for Distinguishing Malignant Mesothelioma From Reactive Mesothelial Cells. *Am J Clin Pathol* (2014) 141:85–93. doi: 10.1309/AJCP5KNL7QTELLYI
21. Kushitani K, Amatya VJ, Mawas AS, Miyata Y, Okada M, Takeshima Y. Use of Anti-Noxa Antibody for Differential Diagnosis Between Epithelioid Mesothelioma and Reactive Mesothelial Hyperplasia. *Pathobiology* (2016) 83:33–40. doi: 10.1159/000442092
22. Yoshikawa Y, Sato A, Tsujimura T, Morinaga T, Fukuoka K, Yamada S, et al. Frequent Deletion of 3p21.1 Region Carrying Semaphorin 3G and Aberrant Expression of the Genes Participating in Semaphorin Signaling in the Epithelioid Type of Malignant Mesothelioma Cells. *Int J Oncol* (2011) 39:1365–74. doi: 10.3892/ijo.2011.1158
23. Nowak AK. Chemotherapy for Malignant Pleural Mesothelioma: A Review of Current Management and a Look to the Future. *Ann Cardiothorac Surg* (2012) 1:508–15. doi: 10.3978/j.issn.2225-319x.2012.10.05
24. Yap TA, Aerts JG, Popat S, Fennell DA. Novel Insights Into Mesothelioma Biology and Implications for Therapy. *Nat Rev Cancer* (2017) 17:475–88. doi: 10.1038/nrc.2017.42
25. Montanaro F, Rosato R, Gangemi M, Roberti S, Ricceri F, Merler E, et al. Survival of Pleural Malignant Mesothelioma in Italy: A Population-Based Study. *Int J Cancer* (2009) 124:201–7. doi: 10.1002/ijc.23874
26. Terenziani R, Zoppi S, Fumarola C, Alfieri R, Bonelli M. Immunotherapeutic Approaches in Malignant Pleural Mesothelioma. *Cancers* (2021) 13. doi: 10.3390/cancers13112793
27. Baas P, Scherpereel A, Nowak AK, Fujimoto N, Peters S, Tsao AS, et al. First-Line Nivolumab Plus Ipilimumab in Unresectable Malignant Pleural Mesothelioma (CheckMate 743): A Multicentre, Randomised, Open-Label, Phase 3 Trial. *Lancet* (2021) 397:375–86. doi: 10.1016/S0140-6736(20)32714-8
28. Zhang J, Ji Q, Jiao C, Ren L, Zhao Y, Chen Y, et al. IGF2BP3 as a Potential Tissue Marker for the Diagnosis of Esophageal High-Grade Intraepithelial Neoplasia. *Onco Targets Ther* (2017) 10:3861–6. doi: 10.2147/OTT.S141179
29. Sasaki M, Sato Y. Insulin-Like Growth Factor II mRNA-Binding Protein 3 (IMP3) Is a Marker That Predicts Presence of Invasion in Papillary Biliary Tumors. *Hum Pathol* (2017) 62:152–9. doi: 10.1016/j.humpath.2016.12.028
30. Kanzaki A, Kudo M, Ansai S-I, Peng W-X, Ishino K, Yamamoto T, et al. Insulin-Like Growth Factor 2 mRNA-Binding Protein-3 as a Marker for Distinguishing Between Cutaneous Squamous Cell Carcinoma and Keratoacanthoma. *Int J Oncol* (2016) 48:1007–15. doi: 10.3892/ijo.2016.3323
31. Lochhead P, Imamura Y, Morikawa T, Kuchiba A, Yamauchi M, Liao X, et al. Insulin-Like Growth Factor 2 Messenger RNA Binding Protein 3 (IGF2BP3) Is a Marker of Unfavourable Prognosis in Colorectal Cancer. *Eur J Cancer* (2012) 48:3405–13. doi: 10.1016/j.ejca.2012.06.021

32. Chang S, Oh M-H, Ji S-Y, Han J, Kim T-J, Eom M, et al. Practical Utility of Insulin-Like Growth Factor II mRNA-Binding Protein 3, Glucose Transporter 1, and Epithelial Membrane Antigen for Distinguishing Malignant Mesotheliomas From Benign Mesothelial Proliferations. *Pathol Int* (2014) 64:607–12. doi: 10.1111/pin.12216
33. Bell JL, Wächter K, Mühleck B, Pazaitis N, Köhn M, Lederer M, et al. Insulin-Like Growth Factor 2 mRNA-Binding Proteins (IGF2BPs): Post-Transcriptional Drivers of Cancer Progression? *Cell Mol Life Sci* (2013) 70:2657–75. doi: 10.1007/s00018-012-1186-z
34. Lederer M, Bley N, Schleifer C, Hüttelmaier S. The Role of the Oncofetal IGF2 mRNA-Binding Protein 3 (IGF2BP3) in Cancer. *Semin Cancer Biol* (2014) 29:3–12. doi: 10.1016/j.semcancer.2014.07.006
35. Sheen Y-S, Liao Y-H, Lin M-H, Chu C-Y, Ho B-Y, Hsieh M-C, et al. IMP-3 Promotes Migration and Invasion of Melanoma Cells by Modulating the Expression of HMGA2 and Predicts Poor Prognosis in Melanoma. *J Invest Dermatol* (2015) 135:1065–73. doi: 10.1038/jid.2014.480
36. Jia C, Tang H, Yang Y, Yuan S, Han T, Fang M, et al. Ubiquitination of IGF2BP3 by E3 Ligase MKRN2 Regulates the Proliferation and Migration of Human Neuroblastoma SHSY5Y Cells. *Biochem Biophys Res Commun* (2020) 529:43–50. doi: 10.1016/j.bbrc.2020.05.112
37. Otto T, Sicinski P. Cell Cycle Proteins as Promising Targets in Cancer Therapy. *Nat Rev Cancer* (2017) 17:93–115. doi: 10.1038/nrc.2016.138
38. Bracken AP, Ciro M, Cocito A, Helin K. E2F Target Genes: Unraveling the Biology. *Trends Biochem Sci* (2004) 29:409–17. doi: 10.1016/j.tibs.2004.06.006
39. Polyak K, Kato JY, Solomon MJ, Sherr CJ, Massague J, Roberts JM, et al. p27Kip1, a Cyclin-Cdk Inhibitor, Links Transforming Growth Factor-Beta and Contact Inhibition to Cell Cycle Arrest. *Genes Dev* (1994) 8:9–22. doi: 10.1101/gad.8.1.9
40. Sheaff RJ, Groudine M, Gordon M, Roberts JM, Clurman BE. Cyclin E-CDK2 Is a Regulator of p27Kip1. *Genes Dev* (1997) 11:1464–78. doi: 10.1101/gad.11.11.1464
41. Chu I, Sun J, Arnaout A, Kahn H, Hanna W, Narod S, et al. P27 Phosphorylation by Src Regulates Inhibition of Cyclin E-Cdk2. *Cell* (2007) 128:281–94. doi: 10.1016/j.cell.2006.11.049
42. Chu C, Geng Y, Zhou Y, Sicinski P. Cyclin E in Normal Physiology and Disease States. *Trends Cell Biol* (2021) 31:732–46. doi: 10.1016/j.tcb.2021.05.001
43. Inoshita S, Terada Y, Nakashima O, Kuwahara M, Sasaki S, Marumo F. Regulation of the G1/S Transition Phase in Mesangial Cells by E2F1. *Kidney Int* (1999) 56:1238–41. doi: 10.1046/j.1523-1755.1999.00705.x
44. Koff A, Giordano A, Desai D, Yamashita K, Harper JW, Elledge S, et al. Formation and Activation of a Cyclin E-Cdk2 Complex During the G1 Phase of the Human Cell Cycle. *Science* (1992) 257:1689–94. doi: 10.1126/science.1388288
45. Lee G-E, Lee C-J, An H-J, Kang HC, Lee HS, Lee JY, et al. Fargesin Inhibits EGF-Induced Cell Transformation and Colon Cancer Cell Growth by Suppression of CDK2/Cyclin E Signaling Pathway. *Int J Mol Sci* (2021) 22. doi: 10.3390/ijms22042073
46. Rivera Vargas T, Boudoukha S, Simon A, Souidi M, Cuvellier S, Pinna G, et al. Post-Transcriptional Regulation of Cyclins D1, D3 and G1 and Proliferation of Human Cancer Cells Depend on IMP-3 Nuclear Localization. *Oncogene* (2014) 33:2866–75. doi: 10.1038/onc.2013.252
47. Palanichamy JK, Tran TM, Howard JM, Contreras JR, Fernando TR, Sterne-Weiler T, et al. RNA-Binding Protein IGF2BP3 Targeting of Oncogenic Transcripts Promotes Hematopoietic Progenitor Proliferation. *J Clin Invest* (2016) 126:1495–511. doi: 10.1172/JCI80046
48. Huang W, Li Y, Zhang C, Zha H, Zhou X, Fu B, et al. IGF2BP3 Facilitates Cell Proliferation and Tumorigenesis *via* Modulation of JAK/STAT Signalling Pathway in Human Bladder Cancer. *J Cell Mol Med* (2020) 24:13949–60. doi: 10.1111/jcmm.16003

Conflict of Interest: The authors declare that the research was conducted in the absence of any commercial or financial relationships that could be construed as a potential conflict of interest.

frontiers | Frontiers in Oncology

BRIEF RESEARCH REPORT
published: 28 April 2022
doi: 10.3389/fonc.2022.836751

Complete Pathological Response After Neoadjuvant Chemo-Immunotherapy in Malignant Pleural Mesothelioma

Francinne T. Tostes, Miguel Zugman, Vitor R. Paes and Gustavo Schvartsman *

Centro de Oncologia e Hematologia Einstein Familia Dayan-Daycoval, Hospital Israelita Albert Einstein, São Paulo, Brazil

Keywords: mesothelioma malignant, chemo-immunotherapy combinations, checkpoint inhibition therapy, complete pathologic response (pCR), pleural mesothelioma, PD-L1 (22C3)

OPEN ACCESS

Edited by:
Luciano Mutti,
Temple University, United States

Reviewed by:
Paolo Andrea Zucali,
Humanitas University, Italy
Chao H. Huang,
University of Kansas Medical Center Research Institute, United States

***Correspondence:**
Gustavo Schvartsman
gustavoschv@gmail.com

Specialty section:
This article was submitted to Thoracic Oncology, a section of the journal Frontiers in Oncology

Received: *15 December 2021*
Accepted: *21 March 2022*
Published: *28 April 2022*

Citation:
Tostes FT, Zugman M, Paes VR and Schvartsman G (2022) Complete Pathological Response After Neoadjuvant Chemo-Immunotherapy in Malignant Pleural Mesothelioma. Front. Oncol. 12:836751. doi: 10.3389/fonc.2022.836751

INTRODUCTION

Malignant pleural mesothelioma (MPM) is a rare, aggressive disease that harbors a poor prognosis. Most patients are diagnosed with advanced disease, in which platinum-based combinations, with or without bevacizumab, yielded poor long-term outcomes. Recently, immune checkpoint inhibitors (ICI) have demonstrated promising activity for the treatment of MPM and have been incorporated as treatment options (1).

Around 20% of patients are eligible for attempted curative surgery at diagnosis. Treatment for such cases often involves multimodal therapy, including preoperative chemotherapy, followed by extrapleural pneumonectomy/pleural decortication and radiotherapy (2). Despite a comprehensive treatment, systematic reviews have demonstrated a median overall survival (OS) of only 13 to 23.9 months, likely due to the poor efficacy of systemic therapy, achieving 1.3% complete radiological responses and 5% pathological complete responses documented after neoadjuvant chemotherapy, warranting further improvement in the early-stage setting (3).

The combination of chemotherapy and immunotherapy showed promising results in several tumor types, with good tolerability. In advanced MPM, the combination of durvalumab with chemotherapy resulted in an objective tumor response rate of 48%, with a median overall survival of 18.4 months, higher than historical control with chemotherapy alone, irrespective of program death-ligand 1 (PD-L1) expression (4). Herein, we report a case of a borderline-resectable epithelioid pleural mesothelioma who underwent neoadjuvant therapy with cisplatin, pemetrexed and off-label pembrolizumab who was able to be operated, and obtained a complete pathological response (pCR) with sustained benefit, currently disease and treatment-free 14 months after surgery.

CASE REPORT

This is a 73-year-old female patient, non-smoker, with a prior history of occupational exposure to perchloroethylene during a 5-year period working at a dry-cleaning facility twenty years ago. She presented to the emergency department with a 4-week history of worsening dyspnea. She underwent pulmonary computed tomography (CT) that demonstrated a right-sided moderate pleural effusion,

several nodules on the parietal, mediastinal and diaphragmatic ipsilateral pleura (**Figure 1A**). CT-guided biopsy of the pleura was compatible with epithelioid MPM (**Figure 2**).

Positron emission tomography – computed tomography (PET-CT) and brain magnetic resonance imaging (MRI) were unremarkable for metastatic disease. The PET-CT did show, however, ipsilateral paratracheal and anterior mediastinal lymph nodes (**Figure 3A**). Clinical staging, according to the American Joint Committee on Cancer 8th edition, was defined as cT1cN2M0. The mediastinal lymph nodes were not biopsied prior to therapy initiation.

The patient was considered borderline resectable due to local extent of disease, high symptom burden and patient frailty. A PD-L1 immunohistochemistry with 22C3 antibody clone was performed, resulting in an expression in tumor cells of 80% (**Figure 4A**). After discussion of risks and benefits, she was treated with cisplatin (75 mg/m^2), pemetrexed (500 mg/m^2) and pembrolizumab (2 mg/kg) every three weeks for 4 cycles, with no significant adverse events, except for tinnitus. An initial restaging PET-CT after 2 cycles showed a mixed response, with improvement in pleural implants but increase in the mediastinal lymph nodes' FDG uptake and size (**Figure 3B**). Due to the patient's clinical improvement, therapy was continued and a repeat scan after the fourth cycle demonstrated a complete metabolic response in pleural implants and near-complete improvement in the lymph nodes (**Figures 1B**, **3C**). Her case was discussed at multidisciplinary tumor board and she was considered eligible for surgical resection, no additional pathological exam was performed at the time prior to the surgical procedure. A pleural decortication and mediastinal lymph node dissection was performed and after thorough pathological review of the 105 slides, pCR was achieved in all sites (ypT0ypN0, **Figures 4B–D**). Adjuvant radiotherapy was omitted due to the pathologic response, and the patient is currently on surveillance with no evidence of disease after 14 months of her surgery and 18 months from systemic therapy initiation.

DISCUSSION

Treatment of advanced MPM had not seen major improvement in the last 20 years since the combination of cisplatin and pemetrexed was established as standard of care in the first-line setting, with a median overall survival of less than 12 months and less than 5% of patients remaining alive after 5 years (2). ICI have been studied in phase I/II trials in the refractory setting with promising response rates, though a randomized phase 3 trial published after our patient's treatment decision failed to demonstrate improvement in progression-free and overall survival (5). Recently, CheckMate-743 evaluated the use of nivolumab plus ipilimumab in untreated patients, leading to a 26% reduction in the risk of death versus chemotherapy. At 2 years, 41% of patients were alive, compared with 27% who received chemotherapy (1).

PD-1 inhibitors are currently being investigated in several tumors as a neoadjuvant treatment, either as single agent, or combined with anti-CTLA-4 or chemotherapy. Pre-clinical and clinical data have postulated that early use of ICI may lead to improved efficacy, possibly due to a less immunosuppressive environment and enhanced priming of T-cells with the primary tumor's antigens still present (6). In melanoma, the use of combination immunotherapy provided a 61% rate of pCR/near-pCR, with 96% of them relapse-free after 2 years (7). In non-small cell lung cancer, the combination of chemotherapy and nivolumab increased the pCR rate from 2% to 24%, compared with chemotherapy alone (8).

Thus, due to the overall poor prognosis of the disease, off-label strategies were discussed with the patient. Chemotherapy was warranted due to the potential resectability and high symptom burden. The rationale for the combination of chemotherapy and immunotherapy was based on the phase 2 DREAM trial, which treated patients in the advanced setting with durvalumab and standard chemotherapy, achieving a 48% overall response rate

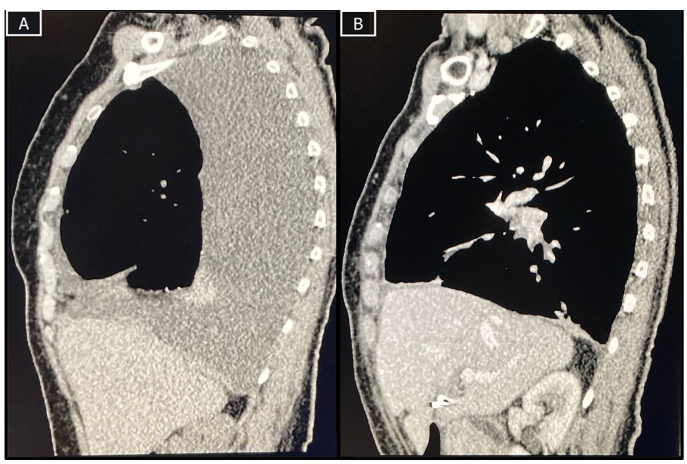

FIGURE 1 | CT-scans at baseline and after surgery. **(A)** Baseline CT-scan demonstrating pleural effusion, thickening and nodules and a rounded atelectasis; **(B)** Restaging CT-scan with improvement of pleural effusion and minimal focal pleural thickening.

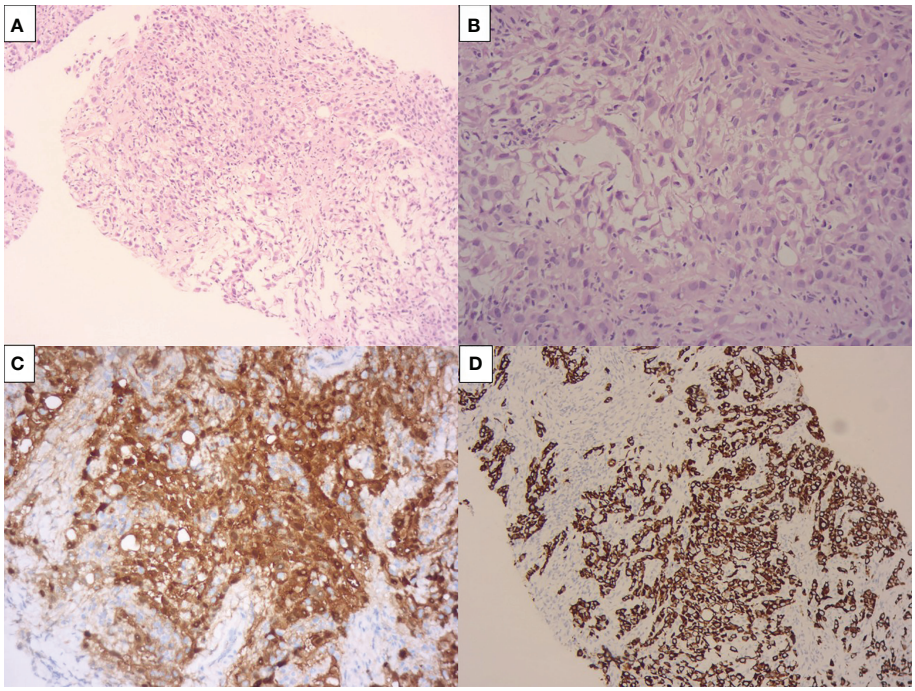

FIGURE 2 | Pre-treatment pleural biopsy compatible with epithelioid malignant pleural mesothelioma. The pictures show a pleomorphic, solid epithelioid neoplasia **(A)**, with pseudoglandular formations and scattered lymphocytes **(B)**. This neoplasia was positive por CK7 **(C)** and calretinin **(D)** and negative por MOC31/BerEP4.

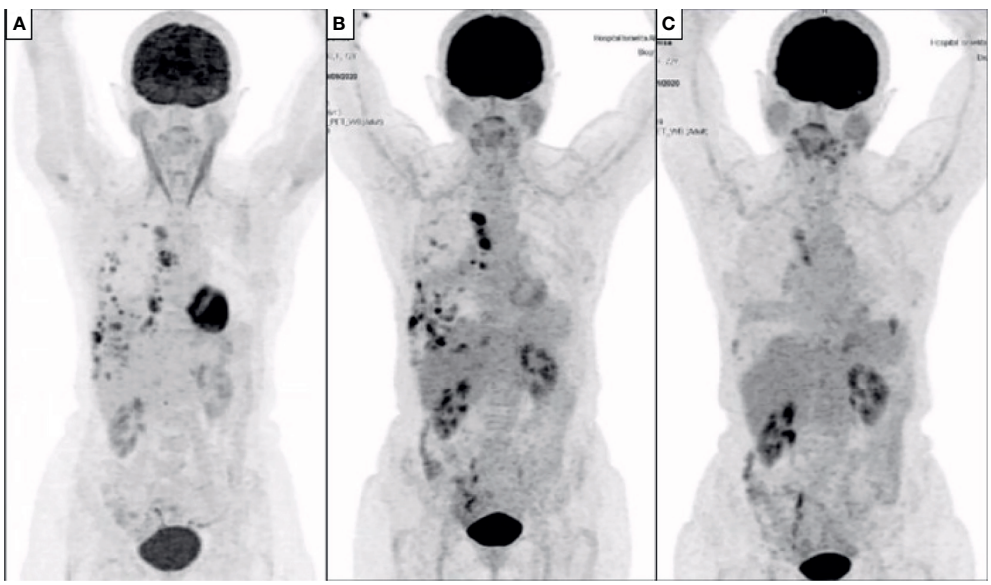

FIGURE 3 | PET-CT at baseline and during treatment. **(A)** Baseline PET-CT demonstrating right pleural implants and mediastinal lymph node involvement; **(B)** restaging PET-CT after 2 cycles of treatment showing improvement in pleural nodules, but enlargement of lymph nodes; **(C)** PET-CT after 4 cycles showing complete improvement in pleural implants, and near-complete improvement of lymph nodes.

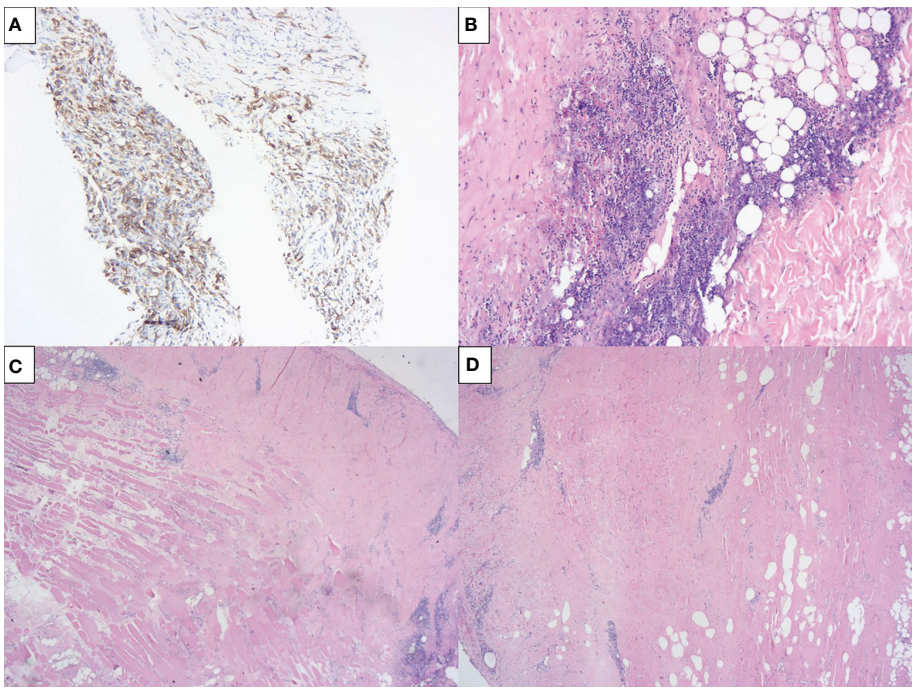

FIGURE 4 | PD-L1 immunohistochemistry and pleural decortication slides. **(A)** Membrane PD-L1 expression on 80% of tumor cells (22C3 antibody) without significant lymphocytic infiltrate in the pre-treatment biopsy; **(B–D)** Pleural decortication slides showing a complete pathological response, characterized by fibrosis, multifocal chronic lymphocytic infiltrate and focal necrosis; no viable neoplastic cells were seen after exhaustive sampling.

(4). Pembrolizumab was chosen due to reduced costs on a 2 mg/kg regimen, with comparable efficacy in other settings to a flat 200 mg dose. Our patient had an initial mixed response, with increased lymph nodes' size and FDG uptake, a finding commonly seen with ICI, but less often seen when chemotherapy is associated. Pseudoprogression was reported in two cases in the DREAM trial. In such cases, this may represent a proof of concept that the immunotherapeutic agent likely played an important role in the documented efficacy. PD-L1 expression generally correlates with response to PD-1 inhibitors in several tumor types. Despite no clear association seen in mesothelioma trials, our patient had a high PD-L1 expression and an excellent response. After a pCR was achieved, no further treatment was administered and the patient is disease-free and well, corroborating the hypothesis of a durable benefit attributable to the anti-PD-1.

To the best of our knowledge, this is the first case report that illustrates the use of ICI in the neoadjuvant setting for MPM and the attainment of a pathological complete response. Further research in prospective clinical trials incorporating this strategy is warranted to improve clinical outcomes in patients with resectable tumors.

DATA AVAILABILITY STATEMENT

The original contributions presented in the study are included in the article/supplementary material. Further inquiries can be directed to the corresponding author.

AUTHOR CONTRIBUTIONS

All authors listed have made a substantial, direct, and intellectual contribution to the work, and approved it for publication.

REFERENCES

1. Baas P, Scherpereel A, Nowak AK, Fujimoto N, Peters S, Tsao AS, et al. First-Line Nivolumab Plus Ipilimumab in Unresectable Malignant Pleural Mesothelioma (CheckMate 743): A Multicentre, Randomised, Open-Label, Phase 3 Trial. *Lancet* (2021) 397(10272):375–86. doi: 10.1016/S0140-6736(20)32714-8
2. Cao CQ, Yan TD, Bannon PG, McCaughan BC. A Systematic Review of Extrapleural Pneumonectomy for Malignant Pleural Mesothelioma. *J Thorac Oncol* (2010) 5 (10):1692–703. doi: 10.1097/JTO.0b013e3181ed0489
3. Krug LM, Pass HI, Rusch VW, Kindler HL, Sugarbaker DJ, Rosenzweig KE, et al. Multicenter Phase II Trial of Neoadjuvant Pemetrexed Plus Cisplatin Followed by Extrapleural Pneumonectomy and Radiation for Malignant Pleural Mesothelioma. *J Clin Oncol* (2009) 27(18):3007–13. doi: 10.1200/JCO.2008.20.3943
4. Nowak AK, Lesterhuis WJ, Kok PS, Brown C, Hughes BG, Karikios DJ, et al. Durvalumab With First-Line Chemotherapy in Previously Untreated Malignant Pleural Mesothelioma (DREAM): A Multicentre, Single-Arm, Phase 2 Trial With a Safety Run-in. *Lancet Oncol* (2020) 21(9):1213–23. doi: 10.1016/S1470-2045(20)30462-9

5. Popat S, Curioni-Fontecedro A, Dafni U, Shah R, O'Brien M, Pope A, et al. A Multicentre Randomised Phase III Trial Comparing Pembrolizumab Versus Single-Agent Chemotherapy for Advanced Pre-Treated Malignant Pleural Mesothelioma: The European Thoracic Oncology Platform (ETOP 9-15) PROMISE-Meso Trial. *Ann Oncol* (2020) 31(12):1734–45. doi: 10.1016/j.annonc.2020.09.009
6. Liu J, Blake SJ, Yong MC, Harjunpää H, Ngiow SF, Takeda K, et al. Improved Efficacy of Neoadjuvant Compared to Adjuvant Immunotherapy to Eradicate Metastatic Disease. *Cancer Discov* (2016) 6(12):1382–99. doi: 10.1158/2159-8290.CD-16-0577
7. Menzies AM, Amaria RN, Rozeman EA, Huang AC, Tetzlaff MT, van de Wiel BA, et al. Pathological Response and Survival With Neoadjuvant Therapy in Melanoma: A Pooled Analysis From the International Neoadjuvant Melanoma Consortium (INMC). *Nat Med* (2021) 27:301–9. doi: 10.1038/s41591-020-01188-3
8. Spicer J, Wang C, Tanaka F, Saylors GB, Chen K-N, Liberman M, et al. Surgical Outcomes From the Phase 3 CheckMate 816 Trial: Nivolumab (NIVO) + Platinum-Doublet Chemotherapy (Chemo) vs Chemo Alone as Neoadjuvant Treatment for Patients With Resectable Non-Small Cell Lung Cancer (NSCLC). *J Clin Oncol* (2021) 39(15_suppl):8503. doi: 10.1200/JCO.2021.39.15_suppl.8503

Conflict of Interest: GS reports consultation fees from AstraZeneca, Merck, Sharp & Dome, Bristol-Myers Squibb, Sanofi Genzime, Novartis, Amgen and Roche.

The remaining authors declare that the research was conducted in the absence of any commercial or financial relationships that could be construed as a potential conflict of interest.

Publisher's Note: All claims expressed in this article are solely those of the authors and do not necessarily represent those of their affiliated organizations, or those of the publisher, the editors and the reviewers. Any product that may be evaluated in this article, or claim that may be made by its manufacturer, is not guaranteed or endorsed by the publisher.

frontiers | Frontiers in Oncology

REVIEW
published: 02 May 2022
doi: 10.3389/fonc.2022.886430

Current State of Pleural-Directed Adjuncts Against Malignant Pleural Mesothelioma

*Agnes Y. Choi, Anand Singh, Danyi Wang, Karthik Pittala and Chuong D. Hoang**

Thoracic Surgery Branch, National Cancer Institute, National Institutes of Health, Bethesda, MD, United States

Multimodality therapy including surgical resection is the current paradigm in treating malignant pleural mesothelioma (MPM), a thoracic surface cancer without cure. The main limitation of all surgical approaches is the lack of long-term durability because macroscopic complete resection (R1 resection) commonly predisposes to locoregional relapse. Over the years, there have been many studies that describe various intrapleural strategies that aim to extend the effect of surgical resection. The majority of these approaches are intraoperative adjuvants. Broadly, there are three therapeutic classes that employ diverse agents. The most common, widely used group of adjuvants are comprised of direct therapeutics such as intracavitary chemotherapy (± hyperthermia). By comparison, the least commonly employed intrathoracic adjuvant is the class comprised of drug-device combinations like photodynamic therapy (PDT). But the most rapidly evolving (new) class with much potential for improved efficacy are therapeutics delivered by specialized drug vehicles such as a fibrin gel containing cisplatin. This review provides an updated perspective on pleural-directed adjuncts in the management of MPM as well as highlighting the most promising near-term technology breakthroughs.

Keywords: malignant pleural mesothelioma, multimodality treatment, intraoperative adjuncts, intrathoracic, polymer, hydrogel, nanoparticle, microRNA

OPEN ACCESS

Edited by:
Marcello Migliore,
University of Catania, Italy

Reviewed by:
Sabahattin Cömertpay,
Kahramanmaras Sütçü Imam University, Turkey
Molnar Tamas,
University of Pécs, Hungary

***Correspondence:**
Chuong D. Hoang
chuong.hoang@nih.gov

Specialty section:
This article was submitted to Thoracic Oncology, a section of the journal Frontiers in Oncology

Received: *28 February 2022*
Accepted: *04 April 2022*
Published: *02 May 2022*

Citation:
Choi AY, Singh A, Wang D, Pittala K and Hoang CD (2022) Current State of Pleural-Directed Adjuncts Against Malignant Pleural Mesothelioma. Front. Oncol. 12:886430. doi: 10.3389/fonc.2022.886430

INTRODUCTION

Malignant pleural mesothelioma (MPM) is a rare, highly aggressive, and recalcitrant tumor arising from the mesothelial lining of the pleura. To date, there is no clinical standard (1) that might yield satisfactory long-term outcomes. It remains incurable. Selected patients, however, enjoy improved overall survival (OS) and recurrence-free survival with multimodality approaches. These strategies involve surgical resection by either extra-pleural pneumonectomy (EPP) or pleurectomy-decortication (PD) plus chemotherapy and/or radiotherapy (2, 3). The most critical success-limiting factor in the treatment of patients afflicted with MPM is the high recurrence rates of local disease ranging from 30% to 75% (4). This failure has prompted further investigations into intraoperative adjuncts to improve locoregional control by curbing microscopic residual foci (R1 margin) more effectively. In this review, we identify three major therapeutic classes (i.e., strategies) for pleural-directed adjuncts that summate the entire emerging field. We discuss the pros and cons of specific examples to illustrate the concept underlying each class of adjuvant that spans the application of direct therapeutics, to delivery vehicles carrying therapeutic(s), and to drug-device combinations (**Figure 1**, **Table 1**).

DIRECT THERAPEUTIC

A focused review and update of intrapleural therapeutic modalities (i.e., agents) that can augment surgical resection and address microscopic residual tumor foci (R1 margin) is presented here. Particular attention is dedicated to verifying the molecular mechanisms of action for each type of agent used in this class of surgical adjuvants.

Intracavitary Chemotherapy ± Hyperthermia

Results from intracavitary chemotherapy in ovarian carcinoma in the 1980s (5) led to pharmacokinetic studies of intrapleural cisplatin and mitomycin as intraoperative adjuvants to PD in the 1990s (6), followed by the first phase II trial in MPM patients (60-minute perfusion time without heating) (7). The use of intracavitary chemotherapy was predicated on some perceived advantages like improved drug penetration at higher doses to residual tumor foci and less systemic toxicity. Later, adding hyperthermia was thought to improve the efficacy of intracavitary chemotherapy by increasing absorption into cancer cells and potentiating the tumoricidal activity of the chemotherapy agent. A small study of 10 MPM patients compared PD with normothermic intracavitary cisplatin (100 mg/m^2) versus PD or EPP with hyperthermic intraoperative chemotherapy (HIOC) at 41.5°C (8). A higher local tissue to perfusate ratio of cisplatin concentration after hyperthermic perfusion suggested a pharmacokinetic advantage imparted by heat. This observation, thus, paved the way for numerous HIOC studies in MPM patients.

Since 1994, there have been at least 20 studies using HIOC in MPM surgical studies (9). A recent phase I trial assessed safety and feasibility of combination drug HIOC in 59 patients undergoing EPP and 41 receiving PD (10). The observed morbidity rates in EPP and PD groups were 54% and 42%, respectively, while there were two perioperative deaths (2%). Dosing for cisplatin at 175 mg/m^2 and gemcitabine at 1000 mg/m^2 was established during 60 minutes of perfusion at 40 to 42°C. Median OS for patients with epithelioid histology was 26 and 59 months for the EPP versus PD cohorts, respectively, compared to 11 and 21 months for patients with non-epithelioid tumors. Similar outcomes were reported in a retrospective single institution study of 71 MPM patients who all underwent PD followed by 90 minutes of HIOC at 42°C using cisplatin (200 mg) and doxorubicin (100 mg) (11). For MPM HIOC studies to date (mostly observational, retrospective, underpowered phase I-II studies), cohorts ranged from four to 104 patients with survival between 11 and 36 months (9). Despite these encouraging outcomes with HIOC-based multimodality therapy, lack of improvement in locoregional control is still the major shortcoming. In a follow-up retrospective study of 132 patients undergoing EPP plus HIOC (cisplatin 175 – 225 mg/m^2 for 60 minutes at 42°C) followed by adjuvant chemoradiation (according to modern techniques and standards), there was a disappointing overall recurrence rate of 75% (4). The ipsilateral hemithorax was the most common site of recurrence and both hemithoraces recurred independent of stage. Other non-thoracic sites of recurrence were observed more frequently according to higher stages. This study emphasizes the unreliable therapeutic effect of HIOC in MPM surgery and the critical need for better locoregional therapies.

Currently, there are no available phase III studies to help guide current multi-modality approaches for MPM. Meaningful

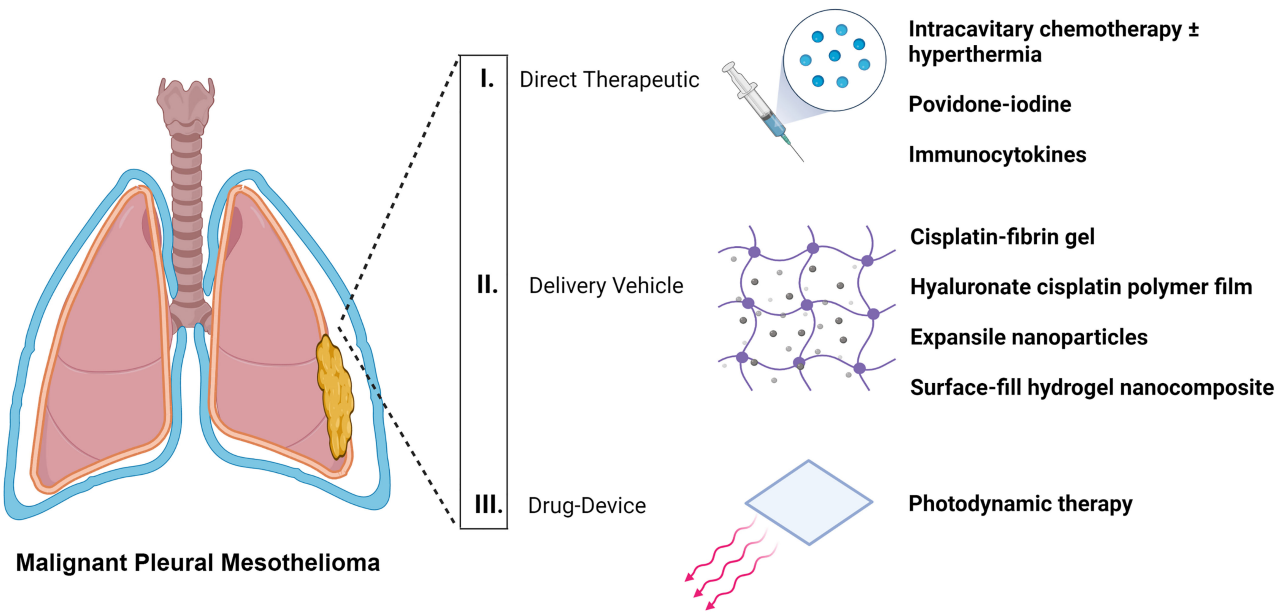

FIGURE 1 | Classification of locoregional pleural-directed adjuncts for surgical-based therapy of mesothelioma.

TABLE 1 | Locoregional pleural-directed adjuncts against mesothelioma: pros & cons.

Pleural Adjuncts	Form Factor	Administration	Therapeutic Cargo	Cancer Targeting Mechanism	Toxicity	Current Status
DIRECT THERAPEUTIC						
Intracavitary chemotherapy ± hyperthermia (HIOC)	Liquid	Intracavitary perfusion	Chemotherapy	Unknown	Systemic effects Grade III+ AE	• Phase I/II studies • No standardized protocol
Povidone-iodine (PVP-I) ± hyperthermia	Liquid	Intracavitary perfusion	Povidone-iodine	Unknown	Systemic effects Grade I-III AE	• Single institution Phase I/II studies • No standardized protocol
Immunocytokines	Liquid	Intracavitary infusion	Interleukin-2	Activation of immune cells (LAK cells)	Systemic effects Grade I-II AE	• Single Phase II study • No standardized protocol • No follow-up studies
DELIVERY VEHICLE						
Cisplatin-fibrin gel	Gel	VATS spray-on application (Vivostat)	Chemotherapy	Unknown	Systemic effects Grade I-IV AE	• Single Phase I study • Lack of dose-dependent drug levels in tumor tissue • Phase II study started
Hyaluronate cisplatin (HYALCIS) film	Thin-Film	Direct surface application	Chemotherapy	Unknown	Systemic drug concentration No major effects	• Preclinical studies orthotopic xenograft tumor models • Preclinical large animal pharmacokinetic study • EMA & FDA approval
Expansile nanoparticles (eNP)	Nanoparticle	Intrapleural injection	Chemotherapy	Unknown	Not studied	• Preclinical study with orthotopic xenograft tumor models
Surface-fill hydrogel (SFH) nanocomposite	Hydrogel nanocomposite	Intrapleural injection and spray-on application	microRNA	Local application & Positive-charged microRNA-peptide nanoparticles selectively target negative-charged cancer cells	microRNA undetectable in systemic circulation No major effects	• Preclinical study with orthotopic xenograft tumor models
DRUG-DEVICE						
Photodynamic therapy (PDT)	Laser Light	Intracavitary + Systemic	Photosensitizer	Volume of light irradiation & uptake of photosensitizer & oxygen	Systemic effects (photosensitizer) Grade I-V AE	• Phase I-III studies • No standardized protocol • Unclear efficacy

AE, Adverse Events categorized according to common toxicity criteria (CTC) or Clavian-Dindo grade, EMA, European Medicines Agencyp; FDA, Food and Drug Administration (USA); VATS, Video-assisted Thoracoscopic Surgery.

comparisons of short- and long-term outcomes between HIOC regimens is impossible owing to diverse implementation of parameters like temperature, duration, type, numbers and combinations of chemotherapy agents, drug concentrations, volume of perfusate fluid, nephroprotective agents, etc. Thus, there is not yet a clinical consensus on a standardized HIOC procedure, although there is a multi-institution, international effort to define some basic working parameters (9). Aligned with this effort to realize the clinical value of HIOC, is the current call for acknowledging HIOC as a feasible practice to augment MPM surgical resection and that it should be mentioned as a therapeutic option in society guidelines, which will continue to evolve as more data becomes available in future trials (12).

Critical review of the literature reveals only a few, if any, basic science studies that lend to the fundamentals of HIOC mechanism of action. In fact, the precise mechanism of preferential drug delivery to cancer cells in the specific context of HIOC remains unknown (13). The bulk of experimental evidence purporting a rationale for using HIOC as a drug delivery strategy is based on older pharmacokinetic studies which inferred successful delivery/unloading of agent from concentration differences across tissue (chest wall or lungs) to perfusate content to the measured plasma levels (6, 8, 14). The relative contribution of temperature versus local drug dose to selectively kill cancer cells remains obscure (13). In one of the very few MPM-specific studies (*in vitro*) (15), the ongoing rationale to employ HIOC in multimodality therapy of MPM was called into question. When MPM cell lines were compared to other types of cancer cell lines, the MPM cells were not particularly heat sensitive and cisplatin alone was less effective. Importantly, the temperature of the perfusate did not consistently match the actual internal temperature of tissues/cells. Clinically relevant cancer cytotoxicity in this study did not occur until temperature exceeded 45°C, which is higher than temperatures commonly used in HIOC human trials (namely 42°C) (9).

Povidone-Iodine

Povidone-iodine [PVP-I, poly-(1-vinyl-2-pyrrolidone)] is a time-honored antiseptic agent commonly used throughout clinical practices for handwashing, skin cleansing, and irrigation/lavage of body cavities for disinfection (16, 17). Since 2004, a single European group has been assessing the impact of adding hyperthermic PVP-I as an intraoperative adjuvant for MPM patients undergoing PD followed by prophylactic radiotherapy and later chemotherapy. The latest update on a cohort of 102 patients encompassing all MPM histologies and stages I-IV who received intraoperative PVP-I 10% (mixed with 5-6 L sterile water over 15 minutes total exposure time at 40 to 41°C) showed encouraging outcomes that continued to improve from their previous reports when the cohort size was 36 and 54 patients (18). The median OS was 32 months, and 5-year survival rate was 23.1%. Thirty-day mortality was nil and 30 patients (29.4%) sustained postoperative complications. Despite demonstrating feasibility and safety, further investigations of whether PVP-I use intrinsically impacts MPM outcomes and whether there is any necessity for hyperthermia are warranted.

The basic scientific support for this clinical practice is based on limited *in vitro* studies without any *in vivo* demonstration of PVP-I-specific effects in cancer cells. It is generally thought in human MPM cancer cell lines that PVP-I causes cellular necrosis *via* reactive oxygen intermediates which might contribute to stimulating anti-tumor inflammatory reactions (19, 20). One *in vitro* study showed that the necrotic phenotype (< 1% cell viability) was evident at 0.01 to 0.1% PVP-I concentration by 7.5 minutes post-exposure, without further improvement at longer exposures times up to 48 hours (20). Another *in vitro* study showed that sarcomatoid cells required a higher PVP-I concentration of 1% for cell killing while non-sarcomatoid histologies exhibited similar cell killing effect at the 0.1% concentration after a 10-minute incubation period (19). In both studies, no hyperthermia was needed in their experimental conditions. Moreover, cellular necrosis was a non-specific effect with similar cell killing observed in the MeT-5A "normal" pleural mesothelial cells (immortalized with SV40 large T antigen) (21). Importantly, no further experimental data were provided from animal studies or other *in vivo* results. Recently, there is conflicting data reported on the possible mechanism of cellular killing exerted by normothermic (37°C) PVP-I where thymic epithelial cells and MeT-5A were indiscriminately killed by cellular fixation after 30 minutes of exposure (22). Why different cells/tissues would die by distinctly different cellular mechanisms (cellular fixation is not necrosis or apoptotic cell death) using the identical PVP-I agent is perplexing.

Immunocytokines

The least explored intrapleural adjuvant strategy to date is the direct use of immunomodulatory agents that can induce anti-tumor effects. A phase II trial of 49 stage II-III MPM patients explored the feasibility and efficacy of a unique four-modality intervention, including immunotherapy (23). Patients underwent: 1) pre-operative intrapleural IL-2 infusion *via* pigtail 12Fr catheter, 2) PD procedure, 3) post-operative sequential intrapleural chemotherapy followed with IL-2 infusions, and 4) adjuvant chemoradiotherapy plus long-term subcutaneous IL-2. Median OS reached 26 months without any operative fatality. Since then, there have not been more similar-minded studies in MPM.

Overall, this was a complicated clinical regimen. There was not an abundance of convincing preliminary data to support all elements of trial design, much less in combining them all. Consequently, it has been difficult to discern why this trial was conceived as such since there was not an easily recognized logical step-building from previous trials. In fact, there was not a specific hypothesis stated. The total length of treatment for enrolled patients was never specified (at least 4 months from study entry to the start of maintenance immunotherapy). The final outcomes were difficult to discern, especially in being able to pinpoint whether surgery, immunotherapy, chemotherapy, or radiation (and in what order: pre-, intra-, post-operative) was most beneficial. The role of immunotherapy as an intrapleural

adjuvant remains undefined, yet should be revisited now in the context of approved frontline use of immune checkpoint inhibitors in certain scenarios of MPM (24).

Pre-clinical mechanistic studies directly warranting use of intrapleural IL-2 therapy in MPM treatment are sparse. An *in vitro* study demonstrated that IL-2 in combination with lymphokine-activated killer cells could effectively lyse the MPM cells whereas NK cells were ineffective (25, 26). Extrapolation of *in vitro* results and success of cytokine therapy in other solid tumors ultimately led to, for example, a phase II MPM trial of intrapleural IL-2 as frontline monotherapy (n = 22 patients) (27). Over one-half (55%) of the patients showed at least a partial response with median OS of 18 months, but this was complicated by significant systemic toxicities. Subsequently, widespread adoption of immunocytokines as part of a multimodal strategy never fully materialized. The pharmacokinetics of (28) and the detailed cellular mechanisms and all relevant cell effectors that are induced by intrapleural IL-2 remain incompletely characterized *in vivo* in the context of MPM.

DELIVERY VEHICLE CARRYING THERAPEUTIC

Newer strategies for the delivery of intracavitary local therapy are being developed and tested in pre-clinical models and human trials. The broad aim is to achieve durable and effective treatments against MPM by leveraging novel technologies to specifically enhance cancer cell-targeted strategies. These drug delivery depot systems (i.e., vehicle) encompass a variety of form-factors such as drug-releasing gels, thin films, or nanoparticles. It is anticipated that when these approaches mature, improved clinical efficacy over intrapleural application of direct therapeutics may be attained.

Cisplatin-Fibrin Gel

Building upon the clinical experience of pleural-directed drug adjuvants to improve the local effect of MPM surgical resection, therapeutic agents have been combined with delivery vehicles to maximize local drug concentrations while limiting systemic adverse events. Pre-clinical MPM studies demonstrated anti-tumor efficacy using cisplatin combined with fibrin (gel) delivered by an intracavitary injection technique (29, 30). The intracavitary cisplatin-fibrin treatment increased local cisplatin tissue concentrations while significantly reducing systemic cisplatin distribution as compared to the chemotherapeutic solution alone.

A phase I dose escalation trial followed, in which 12 non-sarcomatoid MPM patients with mostly stages III-IV underwent extended PD procedure (31). Cisplatin was mixed with patient autologous plasma-derived fibrin which was prepared using the Vivostat system (32) where the cisplatin-fibrin gel was sprayed on pleural surfaces intraoperatively. The mortality rate at 30 and 90 days was 0% and four patients (33%) experienced major morbidity. Median OS was 21 months with a median freedom from recurrence of 8 months, where 83% of patients recurred at 1-year post-operative. Based on tissues biopsies of the chest wall, cytotoxic cisplatin concentrations (12-133 μg/g) were achieved for all treatment dose levels. Moreover, drug levels remained detectable in chest wall musculature for extended timepoints (cytotoxic concentrations in one patient at day 74 and detectable non-cytotoxic levels in another patient beyond 6 months of therapy). Despite locoregional administration, cisplatin distributed systemically and 10% to 27% of the total cisplatin was excreted in the urine within the first 48 hours. Tissue cisplatin levels were highly variable, not dose dependent. Overall, this study demonstrated safety and feasibility of cisplatin-fibrin gel, leading to initiation of a phase II trial.

However, many questions remain for further investigation. How the fibrin interacts with cisplatin and specifically how it forms a conjugate with cisplatin remains unknown because no mechanistic data have been presented. Whether the fibrin has any impact on the efficacy of cisplatin is unknown. Most importantly, the mechanism of cisplatin release from fibrin still needs to be investigated. These unknowns contribute to the lack of dose-dependent cisplatin tissue levels and its high variability as measured in each patient (i.e., inconsistent dose delivery). Without this prerequisite knowledge, it remains uncertain whether this delivery strategy will be able to selectively target tumor cells/tissues and, thereby, be any more efficacious compared to direct instillation of cisplatin. The off-target effects of cisplatin-fibrin are concerning as reflected by the urine excretion of systemic-leak cisplatin and its persistence in deep tissues outside of the pleural surfaces where MPM originates.

Hyaluronate Cisplatin Polymer Film

Hyaluronate (hyaluronan or hyaluronic acid) is a polysaccharide of repeating units of D-glucuronic acid and (1-β-3) N-acetyl-D-glucosamine with physiochemical attributes useful in drug delivery strategies (33). Polymer flexible thin sheets of hyaluronate loaded with cisplatin (HYALCIS) have thus been applied in an orthotopic rat MPM recurrence model (after pneumonectomy) to investigate efficacy and toxicity as compared to direct cisplatin solution (34). Oddly, the cisplatin level in rat pleural tissue at autopsy was lower in the HYALCIS group compared to intrapleural cisplatin. Compared to direct intrapleural cisplatin, significant cisplatin levels (6- to 7-fold higher) were detected in plasma over an extended time (6 days). Histologic and biochemistry tests did not reveal major systemic toxicity in HYALCIS-treated mice. A follow-up pharmacokinetic study in an ovine (non-tumor) pneumonectomy model treated with 1% w/w HYALCIS films demonstrated the feasibility of inserting large polymer sheets into an animal cavity and delivery of relevant doses of cisplatin *in vivo* (35). Cisplatin concentrations in diaphragm, parietal pleura, and pericardium were markedly higher than those of intrapleural cisplatin solution and intravenous cisplatin for up to 24 days. However, cisplatin levels increased dramatically in plasma after treatments and continued to persist at clinically relevant levels for over 21 days despite there being no reported major systemic toxicities in treatment subjects.

These pre-clinical results support the next step of human trials that have yet to be conducted. Polymer films loaded with cisplatin for intrapleural therapy have been approved by regulatory agencies in Europe and the U.S. (e.g., Food and Drug Administration). Nevertheless, many facets of this technology remain obscure and could potentially predict suboptimal outcomes in future clinical settings. This methodology lacks a cancer-specific targeting mechanism. None of the *in vivo* studies in MPM have directly traced the fate of cisplatin once released from the hyaluronate film. Despite no major systemic side-effects in animals, there remains concern for treatment-related morbidity in humans considering the significant higher plasma levels seen with HYALCIS. More basic research is needed to understand the impact of the hyaluronate-cisplatin complex (36) to improve release kinetics and drug elimination rates. Furthermore, it remains unclear how efficiently a polymer sheet would perform in non-pneumonectomy situations which represent a more physically challenging anatomic landscape to effectively coat. Uneven application in areas where sufficient contact with certain surfaces is more difficult to achieve (e.g., curved lung lobes) may result in inconsistent drug delivery. Additionally, the possibility of even higher systemic drug absorption and secondary toxicity with the application of HYALCIS to the lung remains unknown.

Expansile Nanoparticles

An alternative strategy to locoregional drug delivery can be achieved with novel synthetic polymer nanoparticle carriers (100 nm diameter) which swell upon exposure to acidic pH and subsequently release their therapeutic cargo within 24 hours (i.e., expansile nanoparticles, eNP) (37). A study using murine MPM orthotopic xenograft models demonstrated that macroscopic complete resection of tumor vis-à-vis pneumonectomy followed by intrapleural multidose (3x) treatment with paclitaxel-loaded eNP more than doubled median OS (55 vs. 22 days) as compared to controls (38). Ultraviolet light showed that intrapleural injection of fluorescent-labeled paclitaxel-loaded eNP co-localized to unresected tumor deposits (4 days post-treatment) and immunohistology showed that the nanoparticle construct further found its way into cancer cells. Thus, locoregional nanoparticle drug delivery was feasible post-resection and represents another potential strategy in multimodality MPM treatment.

This study did not explain, however, why the paclitaxel-loaded eNP remained intact once inside cancer cells in the co-localization studies (both *in vitro* and *in vivo*). There were no direct data to indicate the drug was properly unloaded intracellularly, nor were there supporting results measuring tissue levels of drug after injection of eNP. It will be interesting to see this technology mature with the flexibility to load other drugs that are known to have better intrinsic efficacy against MPM. More research is needed to elucidate the mechanism of eNP drug binding and the mechanism/kinetics of drug release as it remains unknown at this time. Future studies will need to distinguish the cytotoxic effect of eNPs from the effects of physical cell swelling, in addition to how eNPs preferentially target cancer cells *in vivo*. Furthermore, the fate of how eNPs are metabolized *in vivo* will have to be traced to assess for any off-target systemic toxic side-effects.

Surface-Fill Hydrogel Nanocomposite

Recently, a new materials platform harnessing the compelling therapeutic traits of microRNA (39) (miRNA or miR) that can resolve some of the limitations of MPM intracavitary therapies has been described. A novel biodegradable thin-film depot and delivery material consisting of nanoparticles, prepared by complexing amphiphilic cationic peptides (first polymer) with negatively charged miRNA, which are then embedded into a shear-thinning, self-assembling peptide (second polymer) hydrogel, exerted preferential anti-cancer effects in several murine MPM xenografts (40). This peptide-based surface-fill hydrogel (SFH) nanocomposite can be applied directly to a body cavity *via* percutaneous or surgical access by syringe injection or sprayed to coat anatomic surfaces. After application, positively charged peptide-miRNA spherical nanoparticles (~150 nm diameter) are released over time from the net-positive charged hydrogel matrix to adjacent tissues and taken up more selectively by cancer cells [net-negative surface charge (41)]. The particle surface charge state, its size, miRNA encapsulation efficiency, and the peptide's conformation are important for clathrin-mediated cell entry and endosomal trafficking. Once internalized, miRNA is released from the peptide nanoparticle and capable of affecting cellular function.

Biodistribution analysis of different anatomic sites after intrapleural treatment with miRNA-loaded SFH revealed that the miRNA preferentially reached MPM cells without observable delivery to other vital organs. The ability of SFH to deliver its payload locally was further confirmed by the lack of detectable miRNA in circulating plasma over a series of timed experiments. A systematic histopathologic and biochemical analysis in the murine models revealed no significant toxicities. Furthermore, the efficacy of SFH with encapsulated miR-215 (42) or miR-206 (43) nanoparticles in a single administration were evaluated in pre-clinical models of MPM. Tumor resection sites receiving adjuvant SFH miR-215 or miR-206 therapy showed minimal tumor recurrence compared to resection controls without miRNA treatment (40).

Unlike the other modalities, this SFH delivery depot has a precisely described mechanism for selective cancer cell killing which is dependent on the local delivery route, biophysical properties of the hydrogel, the deranged miRNA profile of the tumor, and relative resilience of normal tissues to miRNA perturbation (42). As this technology continues to mature, it will be interesting to see if efficacy and/or durability can be improved with augmentation such as using a cocktail of anti-MPM miRNA or novel drug and miRNA combinations. Potential drawbacks could be the relative high cost of such biomaterials or the lack of pre-existing infrastructure for large-scale manufacturing. Nevertheless, novel biomaterials with cancer-selective effects represent a promising MPM treatment strategy.

DRUG-DEVICE COMBINATION

In contrast to single modality approaches, drug-device combinations are inherently more complex owing to requirements of drug/agent design in tandem with technology and manufacturing innovations of the accompanying device hardware.

Photodynamic Therapy

Photodynamic therapy (PDT) is a unique approach to treat MPM that relies on wavelength-specific visible light generated by a laser device focused on target tissues which have accumulated light-absorbing photosensitizing agent (i.e., drug) in the presence of oxygen. The localized interaction of these three components induces a tumoricidal photochemical reaction to produce reactive singlet oxygen leading to damage of the tumor cell wall and neovasculature (44). After MPM resection, light detectors are placed intracavitary to monitor light dose, light is delivered by a hand-held laser fiber device that illuminates surfaces where it is pointed towards while the chest cavity is filled with light-dispersing intralipid solution (45). Multiple factors can be adjusted to produce a desired cell killing effect customizable to the clinical situation and anatomy of specific patients including photosensitizer agent and dose, target tissue geometry, mode of light application, light source, irradiation parameters (e.g., wavelength), interval between drug and light illumination, etc. PDT can be administered repeatedly without cumulative toxicity and does not hinder other therapies or could be synergistic with certain specialized modalities. Depth of penetration is limited by wavelength and typically 5 to 10 mm of therapeutic effect can be achieved in clinical scenarios (46).

Since 1991, there have been 11 feasibility and safety trials, three retrospective survival studies and two prospective trials totaling 337 MPM patients who received intrapleural PDT during multimodality therapy of MPM including macroscopic complete resection (47). Since the trials were so heterogeneous any firm conclusions about PDT and its specific effect on OS are unrealistic. The lone phase III trial assessing PDT in MPM patients with maximal debulking surgery found no difference in median OS in PDT (14.4 months, n = 25 patients) versus no-PDT (14.1 months, n = 23 patients), nor in disease-free survival (8.5 months versus 7.7 months, respectively) (48). In contrast, a non-randomized prospective study comparing 14 PD plus PDT with hyperbaric oxygen patients versus 11 PD no-PDT patients, demonstrated significantly improved median OS (15 versus 10 months, respectively) and recurrence incidence of 4/14 versus 8/11, respectively (49). Neither study included enough patients to reach statistical power. Use of a hyperbaric oxygenation chamber

TABLE 2 | Diverse mesothelioma treatment studies with a component of Intrapleural therapy.

Author	Cohort Size (N)	Study Design	Surgery	Epithelioid Histology	Neoadjuvant Drug Therapy	Pleural Therapy	Timing	Adjuvant Therapy
DIRECT THERAPEUTIC								
Rusch et al. (7)	27	Phase II	PD	70% (19/27)	None	Cisplatin + mitomycin	Intraoperative	Cisplatin + mitomycin
Ratto et al. (8)	10	Phase I	PD (6/10) EPP (4/10)	Not specified	None	PD - Cisplatin (3/10) - Heated cisplatin (3/10) EPP - Heated cisplatin (4/10)	Intraoperative	Radiotherapy
Burt et al. (10)	104	Phase I	PD (41/104) EPP (59/104) Debulk (4/104)	PD: 71% (29/41) EPP: 53% (31/59) Debulk: 50% (2/4)	None	Heated cisplatin + gemcitabine	Intraoperative	Discretionary chemotherapy radiotherapy
Klotz et al. (11)	71	Retrospective cohort	Extended PD	77% (55/71)	Cisplatin + navelbine or pemetrexed	Heated cisplatin + doxorubicin	Intraoperative	None
Lang-Lazdunski et al. (17)	102	Phase I/II	PD	72% (73/102)	Cisplatin + pemetrexed	Heated Povidone Iodine	Intraoperative	Radiotherapy Cisplatin ± pemetrexed
Lucchi et al. (22)	49	Phase II	PD	80% (39/49)	Intrapleural Interleukin-2	Epidoxorubicin + Interleukin-2	Postoperative	†Cisplatin + gemcitabine + Interleukin-2
DELIVERY VEHICLE								
Opitz et al. (30)	12	Phase I	Extended PD	67% (8/12)	Cisplatin + pemetrexed	Cisplatin-fibrin gel	Intraoperative	None
DRUG-DEVICE								
Pass et al. (47)	48	Phase III	PD (23/48) EPP (25/48)	69% (33/48)	None	Photodynamic therapy	Intraoperative	Cisplatin + interferon-α 2b + tamoxifen
Matzi et al. (48)	34	Phase II	PD	62% (21/34)	None	Photodynamic therapy Hyperbaric oxygen	Intraoperative	None

PD, Pleurectomy-decortication; EPP, extra-pleural pneumonectomy, †Postoperative radiation was administered prior to adjuvant chemo-immunotherapy.

is logistically self-limiting and unlikely to be widely adopted in hospitals. There is, nevertheless, good demonstration of PDT safety and feasibility by different institutions as well as tolerability with overall low toxicity in modern regimens. More clinical insight on the role for PDT is awaited as there is an ongoing randomized phase II trial of radical PD with or without intraoperative PDT (NCT02153229).

With apparent lack of superior efficacy over other local ablation strategies, more basic investigations are necessary to improve upon inherent shortcomings of this technology in the context of cancer surgery. The chest cavity geometry is a very challenging location to ensure even and consistent irradiation of light, especially when the intralipid solution cannot entirely fill up the chest during surgical procedures. More innovation is needed in devices to deliver PDT. Anticancer effects are dependent on oxygen levels in close proximity to tumor tissue, but the MPM microenvironment is characteristically hypoxic (50). Even more challenging is how to ensure co-localization of the photosensitizer agent along with molecular oxygen in critical subcellular organelles (e.g., mitochondria) to take full advantage of the cytotoxic effects of singlet oxygen. Most importantly, there is need for preferential cancer cell-specific targeting of systemically administered photosensitizer. The photosensitizers currently in use assume there is an enhanced permeability and retention effect that occurs in tumors, but this phenomenon has been called into question (51).

CONCLUSIONS

MPM remains a fatal disease in need of highly effective therapeutic agents and strategies. Macroscopic complete resection as part of multimodality care certainly can contribute to positive outcomes. However, verifying a direct effect and quantifying the relative merit of surgical resection when used in a multimodality treatment scheme has been elusive. The lack of good clinical outcomes in MPM therapy is impacted by numerous heterogeneous factors including, for example: extent of surgical resection (EPP vs. PD), tumor histology (e.g., epithelioid vs. sarcomatoid), systemic therapy (neoadjuvant vs. adjuvant, etc.), and how the interventions are employed in a sequence. Such clinical parameters add complexity to the process of study designs best equipped to demonstrate direct benefits of pleural-directed adjuncts in MPM therapy (**Table 2**). Yet, an emerging trend is that pleural-directed adjuncts for control of microscopic residual disease (R1 margin) are a promising group of approaches that merit further investigation and development. Despite direct instillation of chemotherapy drugs being the most widely used, data from large, randomized trials are not available to guide clinical practices according to any standardized technique. It is likely that other novel drug-device combinations may be described in the near future that can address some of the major limitations of PDT, which has been largely underutilized. The most promising class of adjuncts dependent on a vehicle carrier to deliver local therapeutics is likely to receive more attention as biomedical technologies improve.

AUTHOR CONTRIBUTIONS

AC, AS, DW, and KP - writing of text and table, drawing figure, and editing. CH - writing, revision and editing, concept and design. All authors contributed to the article and approved the submitted version.

FUNDING

This work was supported by NIH Intramural Research Program with funding from National Cancer Institute - Center for Cancer Research Grant ZIA BC 011657 (to CH).

ACKNOWLEDGMENTS

We would like to thank Yolanda L. Jones, senior writer-editor in the NIH Library Editing Service, for reviewing the manuscript.

REFERENCES

1. Network NCC. *Malignant Pleural Mesothelioma* (2022). Available at: https://www.nccn.org/professionals/physician_gls/pdf/mpm.pdf.
2. Bueno R, Opitz ITaskforce IM. Surgery in Malignant Pleural Mesothelioma. *J Thorac Oncol* (2018) 13(11):1638–54. doi: 10.1016/j.jtho.2018.08.001
3. Cao C, Tian D, Park J, Allan J, Pataky KA, Yan TD. A Systematic Review and Meta-Analysis of Surgical Treatments for Malignant Pleural Mesothelioma. *Lung Cancer* (2014) 83(2):240–5. doi: 10.1016/j.lungcan.2013.11.026
4. Baldini EH, Richards WG, Gill RR, Goodman BM, Winfrey OK, Eisen HM, et al. Updated Patterns of Failure After Multimodality Therapy for Malignant Pleural Mesothelioma. *J Thorac Cardiovasc Surg* (2015) 149(5):1374–81. doi: 10.1016/j.jtcvs.2014.10.128
5. Lopez JA, Krikorian JG, Reich SD, Smyth RD, Lee FH, Issell BF. Clinical Pharmacology of Intraperitoneal Cisplatin. *Gynecol Oncol* (1985) 20(1):1–9. doi: 10.1016/0090-8258(85)90118-0
6. Rusch VW, Niedzwiecki D, Tao Y, Menendez-Botet C, Dnistrian A, Kelsen D, et al. Intrapleural Cisplatin and Mitomycin for Malignant Mesothelioma Following Pleurectomy: Pharmacokinetic Studies. *J Clin Oncol* (1992) 10 (6):1001–6. doi: 10.1200/JCO.1992.10.6.1001
7. Rusch V, Saltz L, Venkatraman E, Ginsberg R, McCormack P, Burt M, et al. A Phase II Trial of Pleurectomy/Decortication Followed by Intrapleural and Systemic Chemotherapy for Malignant Pleural Mesothelioma. *J Clin Oncol* (1994) 12(6):1156–63. doi: 10.1200/JCO.1994.12.6.1156
8. Ratto GB, Civalleri D, Esposito M, Spessa E, Alloisio A, De Cian F, et al. Pleural Space Perfusion With Cisplatin in the Multimodality Treatment of Malignant Mesothelioma: A Feasibility and Pharmacokinetic Study. *J Thorac Cardiovasc Surg* (1999) 117(4):759–65. doi: 10.1016/S0022-5223(99)70297-7
9. Markowiak T, Larisch C, Hofmann HS, Ried M. Hyperthermic Intrathoracic Chemotherapy (Hithoc): Narrative Review of the Current Literature, Recommendations and Future Studies. *Ann Transl Med* (2021) 9(11):955. doi: 10.21037/atm-20-5444
10. Burt BM, Richards WG, Lee HS, Bartel S, Dasilva MC, Gill RR, et al. A Phase I Trial of Surgical Resection and Intraoperative Hyperthermic Cisplatin and Gemcitabine for Pleural Mesothelioma. *J Thorac Oncol* (2018) 13(9):1400–9. doi: 10.1016/j.jtho.2018.04.032

11. Klotz LV, Lindner M, Eichhorn ME, Grutzner U, Koch I, Winter H, et al. Pleurectomy/Decortication and Hyperthermic Intrathoracic Chemoperfusion Using Cisplatin and Doxorubicin for Malignant Pleural Mesothelioma. *J Thorac Dis* (2019) 11(5):1963–72. doi: 10.21037/jtd.2019.04.93
12. Migliore M, Ried M, Molins L, Lucchi M, Ambrogi M, Molnar TF, et al. Hyperthermic Intrathoracic Chemotherapy (Hithoc) Should Be Included in the Guidelines for Malignant Pleural Mesothelioma. *Ann Transl Med* (2021) 9 (11):960. doi: 10.21037/atm-20-7247
13. Sticca RP, Dach BW. Rationale for Hyperthermia With Intraoperative Intraperitoneal Chemotherapy Agents. *Surg Oncol Clin North Am* (2003) 12 (3):689–701. doi: 10.1016/s1055-3207(03)00029-2
14. Ausmus PL, Wilke AV, Frazier DL. Effects of Hyperthermia on Blood Flow and Cis-Diamminedichloroplatinum(Ii) Pharmacokinetics in Murine Mammary Adenocarcinomas. *Cancer Res* (1992) 52(18):4965–8.
15. Cameron RB, Hou D. Intraoperative Hyperthermic Chemotherapy Perfusion for Malignant Pleural Mesothelioma: An In Vitro Evaluation. *J Thorac Cardiovasc Surg* (2013) 145(2):496–504. doi: 10.1016/j.jtcvs.2012.10.042
16. Bigliardi PL, Alsagoff SAL, El-Kafrawi HY, Pyon JK, Wa CTC, Villa MA. Povidone Iodine in Wound Healing: A Review of Current Concepts and Practices. *Int J Surg* (2017) 44:260–8. doi: 10.1016/j.ijsu.2017.06.073
17. Schneiter D, Cassina P, Korom S, Inci I, Al-Abdullatief M, Dutly A, et al. Accelerated Treatment for Early and Late Postpneumonectomy Empyema. *Ann Thorac Surg* (2001) 72(5):1668–72. doi: 10.1016/s0003-4975(01) 03083-1
18. Lang-Lazdunski L, Bille A, Papa S, Marshall S, Lal R, Galeone C, et al. Pleurectomy/Decortication, Hyperthermic Pleural Lavage With Povidone-Iodine, Prophylactic Radiotherapy, and Systemic Chemotherapy in Patients With Malignant Pleural Mesothelioma: A 10-Year Experience. *J Thorac Cardiovasc Surg* (2015) 149(2):558–65. doi: 10.1016/j.jtcvs.2014.10.041
19. Fiorelli A, Pentimalli F, D'Urso V, Di Marzo D, Forte IM, Giordano A, et al. Antineoplastic Activity of Povidone-Iodine on Different Mesothelioma Cell Lines: Results of in Vitro Study. *Eur J Cardiothorac Surg* (2014) 45(6):993–1000. doi: 10.1093/ejcts/ezt534
20. Opitz I, Sigrist B, Hillinger S, Lardinois D, Stahel R, Weder W, et al. Taurolidine and Povidone-Iodine Induce Different Types of Cell Death in Malignant Pleural Mesothelioma. *Lung Cancer* (2007) 56(3):327–36. doi: 10.1016/j.lungcan.2007.01.024
21. Connell ND, Rheinwald JG. Regulation of the Cytoskeleton in Mesothelial Cells: Reversible Loss of Keratin and Increase in Vimentin During Rapid Growth in Culture. *Cell* (1983) 34(1):245–53. doi: 10.1016/0092-8674(83) 90155-1
22. Lee HS, Jang HJ, Lo EM, Truong CY, Groth SS, Friedberg JS, et al. Povidone-Iodine Results in Rapid Killing of Thymic Epithelial Tumour Cells Through Cellular Fixationdagger. *Interact Cardiovasc Thorac Surg* (2019) 28(3):353–9. doi: 10.1093/icvts/ivy248
23. Lucchi M, Chella A, Melfi F, Dini P, Ambrogi M, Fino L, et al. A Phase Ii Study of Intrapleural Immuno-Chemotherapy, Pleurectomy/Decortication, Radiotherapy, Systemic Chemotherapy and Long-Term Sub-Cutaneous Il-2 in Stage Ii-Iii Malignant Pleural Mesothelioma. *Eur J Cardiothorac Surg* (2007) 31(3):529–33. doi: 10.1016/j.ejcts.2006.11.046
24. Baas P, Scherpereel A, Nowak AK, Fujimoto N, Peters S, Tsao AS, et al. First-Line Nivolumab Plus Ipilimumab in Unresectable Malignant Pleural Mesothelioma (Checkmate 743): A Multicentre, Randomised, Open-Label, Phase 3 Trial. *Lancet* (2021) 397(10272):375–86. doi: 10.1016/S0140-6736(20) 32714-8
25. Fitzpatrick DR, Manning LS, Musk AW, Robinson BW, Bielefeldt-Ohmann H. Potential for Cytokine Therapy of Malignant Mesothelioma. *Cancer Treat Rev* (1995) 21(3):273–88. doi: 10.1016/0305-7372(95)90004-7
26. Manning LS, Bowman RV, Darby SB, Robinson BW. Lysis of Human Malignant Mesothelioma Cells by Natural Killer (Nk) and Lymphokine-Activated Killer (Lak) Cells. *Am Rev Respir Dis* (1989) 139(6):1369–74. doi: 10.1164/ajrccm/139.6.1369
27. Astoul P, Picat-Joossen D, Viallat JR, Boutin C. Intrapleural Administration of Interleukin-2 for the Treatment of Patients With Malignant Pleural Mesothelioma: A Phase II Study. *Cancer* (1998) 83(10):2099–104. doi: 10.1002/(sici)1097-0142(19981115)83:10<2099::aid-cncr8>3.0.co;2-3
28. Astoul P, Bertault-Peres P, Durand A, Catalin J, Vignal F, Boutin C. Pharmacokinetics of Intrapleural Recombinant Interleukin-2 in Immunotherapy for Malignant Pleural Effusion. *Cancer* (1994) 73(2):308–13. doi: 10.1002/1097-0142(19940115)73:2<308::aid-cncr2820730213>3.0.co;2-4
29. Lardinois D, Jung FJ, Opitz I, Rentsch K, Latkoczy C, Vuong V, et al. Intrapleural Topical Application of Cisplatin With the Surgical Carrier Vivostat Increases the Local Drug Concentration in an Immune-Competent Rat Model With Malignant Pleuromesothelioma. *J Thorac Cardiovasc Surg* (2006) 131(3):697–703. doi: 10.1016/j.jtcvs.2005.08.012
30. Opitz I, Erne BV, Demirbas S, Jetter A, Seifert B, Stahel R, et al. Optimized Intrapleural Cisplatin Chemotherapy With a Fibrin Carrier After Extrapleural Pneumonectomy: A Preclinical Study. *J Thorac Cardiovasc Surg* (2011) 141 (1):65–71. doi: 10.1016/j.jtcvs.2010.09.032
31. Opitz I, Lauk O, Meerang M, Jetter A, Aeschlimann B, Seifert B, et al. Intracavitary Cisplatin-Fibrin Chemotherapy After Surgery for Malignant Pleural Mesothelioma: A Phase I Trial. *J Thorac Cardiovasc Surg* (2019) 159 (1):330–40.e4. doi: 10.1016/j.jtcvs.2019.07.073
32. Kjaergard HK, Trumbull HR. Vivostat System Autologous Fibrin Sealant: Preliminary Study in Elective Coronary Bypass Grafting. *Ann Thorac Surg* (1998) 66(2):482–6. doi: 10.1016/s0003-4975(98)00470-6
33. Yadav AK, Mishra P, Agrawal GP. An Insight on Hyaluronic Acid in Drug Targeting and Drug Delivery. *J Drug Target* (2008) 16(2):91–107. doi: 10.1080/10611860802095494
34. Ampollini L, Sonvico F, Barocelli E, Cavazzoni A, Bilancia R, Mucchino C, et al. Intrapleural Polymeric Films Containing Cisplatin for Malignant Pleural Mesothelioma in a Rat Tumour Model: A Preliminary Study. *Eur J Cardiothorac Surg* (2010) 37(3):557–65. doi: 10.1016/j.ejcts.2009.08.012
35. Ampollini L, Barocelli E, Cavazzoni A, Petronini P, Mucchino C, Cantoni AM, et al. Polymeric Films Loaded With Cisplatin for Malignant Pleural Mesothelioma: A Pharmacokinetic Study in an Ovine Model. *J Thorac Dis* (2018) 10(Suppl 2):S207–S20. doi: 10.21037/jtd.2017.10.74
36. Cai S, Xie Y, Davies NM, Cohen MS, Forrest ML. Pharmacokinetics and Disposition of a Localized Lymphatic Polymeric Hyaluronan Conjugate of Cisplatin in Rodents. *J Pharm Sci* (2010) 99(6):2664–71. doi: 10.1002/jps.22016
37. Griset AP, Walpole J, Liu R, Gaffey A, Colson YL, Grinstaff MW. Expansile Nanoparticles: Synthesis, Characterization, and in Vivo Efficacy of an Acid-Responsive Polymeric Drug Delivery System. *J Am Chem Soc* (2009) 131 (7):2469–71. doi: 10.1021/ja807416t
38. Chu NQ, Liu R, Colby A, de Forcrand C, Padera RF, Grinstaff MW, et al. Paclitaxel-Loaded Expansile Nanoparticles Improve Survival Following Cytoreductive Surgery in Pleural Mesothelioma Xenografts. *J Thorac Cardiovasc Surg* (2020) 160(3):e159–e68. doi: 10.1016/j.jtcvs.2019.12.076
39. Rupaimoole R, Slack FJ. Microrna Therapeutics: Towards a New Era for the Management of Cancer and Other Diseases. *Nat Rev Drug Discov* (2017) 16 (3):203–22. doi: 10.1038/nrd.2016.246
40. Majumder P, Singh A, Wang Z, Dutta K, Pahwa R, Liang C, et al. Surface-Fill Hydrogel Attenuates the Oncogenic Signature of Complex Anatomical Surface Cancer in a Single Application. *Nat Nanotechnol* (2021) 16 (11):1251–9. doi: 10.1038/s41565-021-00961-w
41. Chen B, Le W, Wang Y, Li Z, Wang D, Ren L, et al. Targeting Negative Surface Charges of Cancer Cells by Multifunctional Nanoprobes. *Theranostics* (2016) 6(11):1887–98. doi: 10.7150/thno.16358
42. Singh A, Bhattacharyya N, Srivastava A, Pruett N, Ripley RT, Schrump DS, et al. Microrna-215-5p Treatment Suppresses Mesothelioma Progression *Via* the Mdm2-P53-Signaling Axis. *Mol Ther* (2019) 27(9):1665–80. doi: 10.1016/j.ymthe.2019.05.020
43. Singh A, Pruett N, Pahwa R, Mahajan AP, Schrump DS, Hoang CD. Microrna-206 Suppresses Mesothelioma Progression *Via* the Ras Signaling Axis. *Mol Ther Nucleic Acids* (2021) 24:669–81. doi: 10.1016/j.omtn.2021.04.001
44. Li X, Lovell JF, Yoon J, Chen X. Clinical Development and Potential of Photothermal and Photodynamic Therapies for Cancer. *Nat Rev Clin Oncol* (2020) 17(11):657–74. doi: 10.1038/s41571-020-0410-2
45. Friedberg JS, Culligan MJ, Mick R, Stevenson J, Hahn SM, Sterman D, et al. Radical Pleurectomy and Intraoperative Photodynamic Therapy for Malignant Pleural Mesothelioma. *Ann Thorac Surg* (2012) 93(5):1658–65. doi: 10.1016/j.athoracsur.2012.02.009
46. Simone CB2nd, Cengel KA. Photodynamic Therapy for Lung Cancer and Malignant Pleural Mesothelioma. *Semin Oncol* (2014) 41(6):820–30. doi: 10.1053/j.seminoncol.2014.09.017

47. Munck C, Mordon SR, Scherpereel A, Porte H, Dhalluin X, Betrouni N. Intrapleural Photodynamic Therapy for Mesothelioma: What Place and Which Future? *Ann Thorac Surg* (2015) 99(6):2237–45. doi: 10.1016/j.athoracsur.2014.12.077
48. Pass HI, Temeck BK, Kranda K, Thomas G, Russo A, Smith P, et al. Phase Iii Randomized Trial of Surgery With or Without Intraoperative Photodynamic Therapy and Postoperative Immunochemotherapy for Malignant Pleural Mesothelioma. *Ann Surg Oncol* (1997) 4(8):628–33. doi: 10.1007/BF02303746
49. Matzi V, Maier A, Sankin O, Lindenmann J, Woltsche M, Smolle J, et al. Photodynamic Therapy Enhanced by Hyperbaric Oxygenation in Palliation of Malignant Pleural Mesothelioma: Clinical Experience. *Photodiagnosis Photodyn Ther* (2004) 1(1):57–64. doi: 10.1016/S1572-1000(04)00009-2
50. Brown JM, Wilson WR. Exploiting Tumour Hypoxia in Cancer Treatment. *Nat Rev Cancer* (2004) 4(6):437–47. doi: 10.1038/nrc1367
51. Danhier F. To Exploit the Tumor Microenvironment: Since the Epr Effect Fails in the Clinic, What Is the Future of Nanomedicine? *J Control Release* (2016) 244(Pt A):108–21. doi: 10.1016/j.jconrel.2016.11.015

Conflict of Interest: The authors declare that the research was conducted in the absence of any commercial or financial relationships that could be construed as a potential conflict of interest.

frontiers | Frontiers in Oncology

ORIGINAL RESEARCH
published: 06 May 2022
doi: 10.3389/fonc.2022.851785

Headspace Volatile Organic Compound Profiling of Pleural Mesothelioma and Lung Cancer Cell Lines as Translational Bridge for Breath Research

Eline Janssens[1,2], Zoë Mol[3], Lore Vandermeersch[3], Sabrina Lagniau[4,5,6], Karim Y. Vermaelen[4,5,6], Jan P. van Meerbeeck[1,2,4,7], Christophe Walgraeve[3], Elly Marcq[8†] and Kevin Lamote[1,2,4†]*

[1] Laboratory of Experimental Medicine and Pediatrics, University of Antwerp, Antwerp, Belgium, [2] Infla-Med Center of Excellence, University of Antwerp, Antwerp, Belgium, [3] Department of Green Chemistry and Technology, Environmental Organic Chemistry and Technology (EnVOC) Research Group, Ghent University, Ghent, Belgium, [4] Department of Internal Medicine and Pediatrics, Ghent University, Ghent, Belgium, [5] Department of Respiratory Medicine, Ghent University Hospital, Ghent, Belgium, [6] Tumor Immunology Lab, Ghent University, Ghent, Belgium, [7] Department of Pulmonology and Thoracic Oncology, Antwerp University Hospital, Edegem, Belgium, [8] Center for Oncological Research (CORE), Integrated Personalized and Precision Oncology Network (IPPON), University of Antwerp, Antwerp, Belgium

Introduction: Malignant pleural mesothelioma (MPM) is a lethal cancer for which early-stage diagnosis remains a major challenge. Volatile organic compounds (VOCs) in breath proved to be potential biomarkers for MPM diagnosis, but translational studies are needed to elucidate which VOCs originate from the tumor itself and thus are specifically related to MPM cell metabolism.

Methods: An *in vitro* model was set-up to characterize the headspace VOC profiles of six MPM and two lung cancer cell lines using thermal desorption-gas chromatography-mass spectrometry. A comparative analysis was carried out to identify VOCs that could discriminate between MPM and lung cancer, as well as between the histological subtypes within MPM (epithelioid, sarcomatoid and biphasic).

Results: VOC profiles were identified capable of distinguishing MPM (subtypes) and lung cancer cells with high accuracy. Alkanes, aldehydes, ketones and alcohols represented many of the discriminating VOCs. Discrepancies with clinical findings were observed, supporting the need for studies examining breath and tumor cells of the same patients and studying metabolization and kinetics of *in vitro* discovered VOCs in a clinical setting.

Conclusion: While the relationship between *in vitro* and *in vivo* VOCs is yet to be established, both could complement each other in generating a clinically useful breath model for MPM.

Keywords: mesothelioma, lung cancer, biomarkers, volatile organic compounds, headspace analysis

OPEN ACCESS

Edited by:
Jessica Desiree Menis, Integrated University Hospital Verona, Italy

Reviewed by:
Sabahattin Cömertpay, Kahramanmaras Sütçü Imam University, Turkey
Francesca Maffei, University of Bologna, Italy

***Correspondence:**
Kevin Lamote
kevin.lamote@uantwerpen.be

†These authors have contributed equally to this work and share senior authorship

Specialty section:
This article was submitted to Thoracic Oncology, a section of the journal Frontiers in Oncology

Received: *10 January 2022*
Accepted: *29 March 2022*
Published: *06 May 2022*

Citation:
Janssens E, Mol Z, Vandermeersch L, Lagniau S, Vermaelen KY, van Meerbeeck JP, Walgraeve C, Marcq E and Lamote K (2022) Headspace Volatile Organic Compound Profiling of Pleural Mesothelioma and Lung Cancer Cell Lines as Translational Bridge for Breath Research. Front. Oncol. 12:851785. doi: 10.3389/fonc.2022.851785

1 INTRODUCTION

Malignant pleural mesothelioma (MPM) is a rare and lethal thoracic cancer, arising from the mesothelial cells lining the lungs and chest wall. A clear causal relationship has been established between asbestos exposure and MPM development (1). Although the use of asbestos was banned in most Western countries many years ago, the incidence of MPM is expected to increase during the next years in numerous countries due to the long latency period (of up to 50 years) between first exposure and the onset of symptoms (1, 2). Moreover, people who have been exposed to asbestos are also at higher risk of developing lung cancer, which even increases synergistically when combined with tobacco smoke exposure (3).

With a five-year survival rate of less than 5%, prognosis for MPM remains very poor (4). MPM is classified into three major histological subtypes (epithelioid, sarcomatoid and biphasic) with a non-epithelioid histology being an unfavorable prognostic factor (5). One of the major challenges concerning this type of cancer is its early-stage diagnosis. The delayed onset of (non-specific) symptoms causes MPM to be mainly diagnosed in an advanced stage, which limits curative treatment options. The diagnostic process can be complex, as radiological findings represent a wide range of manifestations and may mimic lung cancer, for example, requiring histopathological confirmation to reach a definite diagnosis (5, 6). With standard-of-care combination chemotherapy, median survival in selected patients is around 13 months, which can be modestly improved up to 18 months with either the addition of the anti-angiogenic agent bevacizumab or dual immunotherapy with ipilimumab and nivolumab (7). Diagnosing MPM in an earlier stage is hypothesized to improve patient survival (8). It is therefore important to develop reliable early diagnostic tools, which are currently lacking, that would allow screening and surveillance of individuals who have been exposed to asbestos (9). Although much effort has been put into finding suitable blood biomarkers such as mesothelin, high-mobility group box protein 1 and fibulin-3, this has not yet led to a clinically useful one (10).

The analysis of exhaled breath on the other hand, is an emerging research field in this quest for reliable, early-stage biomarkers. Several clinical studies have proven that volatile organic compounds (VOCs), present in breath, could adequately distinguish MPM patients from asbestos-exposed control groups, which was also demonstrated in our previous work (11–15). However, the clinical implementation of these VOC-based diagnostic models is hampered due to the lack of validation and biological translation studies. To gain knowledge about the biochemical origin and metabolization of these VOC biomarkers, it is crucial to investigate VOC production at the cellular level (16). By studying pure populations of tumor cells, the contribution of tumor-associated stromal cells (e.g. immune infiltrates, fibroblasts) or the microbiome (bacterial, fungal or others) to VOC profiles can be eliminated, making it easier to identify which VOCs are truly tumor cell-derived. Additionally, *in vitro* VOC research allows investigation of potential biomarkers while bypassing confounding factors that could influence (breath) VOC profiles in clinical settings (age, diet, medication use, smoking status etc.) (16). Hence, an *in vitro* approach makes it possible to pinpoint specific tumor cell-derived VOCs, which can improve the current discriminative models. Presently there are many of this type of *in vitro* studies for lung cancer (17), but for MPM these are sparse as only two studies reported data on *in vitro* headspace analysis of MPM cells (18, 19).

To learn more about the cellular origin of breath VOCs, the goal of this study was to analyze and characterize the VOC profiles in the headspace of six different MPM cell lines, representing the three major histological subtypes of MPM (epithelioid, sarcomatoid and biphasic), and two lung cancer cell lines, using thermal desorption-gas chromatography-mass spectrometry (TD-GC-MS). A comparative analysis was carried out to identify VOCs that could discriminate between MPM and lung cancer, as well as between the histological subtypes within MPM. This approach could discover compounds that arise from MPM cells and have the potential to be diagnostic or, in extension, even prognostic MPM biomarkers.

2 MATERIALS AND METHODS

2.1 Cell Culture

Six different human MPM cell lines were used, representing the major histological subtypes of MPM: two sarcomatoid (NCI-H2731 and H-MESO-1), two epithelioid (NCI-H2795 and NCI-H2818) and two biphasic (NKI04 and MSTO-211H) (**Supplementary Figure S1A**). To assess the specificity of the VOCs, two non-small cell lung cancer (NSCLC) cell lines (NCI-H2228 and NCI-H1975), representing the most common type of lung cancer, were also included. The NCI-H2731, NCI-H2795, NCI-H2818 and NKI04 cell lines were kindly provided by Prof. Dr. Paul Baas from the Netherlands Cancer Institute (NKI, Amsterdam, The Netherlands). The MSTO-211H, NCI-H2228 and NCI-H1975 cell lines were purchased from ATCC (Manassas, Virginia, USA). The H-MESO-1 cell line was purchased from CLS Cell Lines Service GmbH (Eppelheim, Germany). All cell lines tested negative for mycoplasma contamination through routine testing.

All cell lines were cultivated under standard conditions at 37°C and 5% CO_2. NCI-H2818, NCI-H2795, NCI-H2731 and NKI04 cells were grown in DMEM/F-12 Glutamax™ supplemented with 10% fetal bovine serum (FBS), penicillin (100 000 units/L) and streptomycin (100 mg/L). H-MESO-1, MSTO-211H, NCI-H2228 and NCI-H1975 cells were grown in RPMI 1640 supplemented with 10% FBS, penicillin (100 000 units/L), streptomycin (100 mg/L) and L-glutamine (2 mM). Upon reaching 70-90% confluence, the cells were harvested with 0,05% trypsin and seeded in new culture flasks to increase the number of cells.

Before sampling, the cells were seeded in 175 cm^2 culture flasks and incubated for exactly 48 hours. The seeding ratio was determined from the growth rate of the different cell lines, so confluence would be reached after the 48-hour incubation period. Culture flasks with blank medium (complete DMEM/

F-12 Glutamax™ or RPMI 1640), incubated under the same experimental conditions, were used as controls. At least five replicates of each histological subtype and control type were used.

2.2 Headspace Sampling

Sampling was performed in a laminar flow cabinet to minimize environmental contamination. Headspace VOCs were collected on Tenax®GR sorbent tubes (Markes, Llantrisant, UK), after the 48-hour incubation period, by drawing the headspace air through the sorbent tube at a flow rate of 100 ml/min for 16 min (**Supplementary Figure S1B**). After sampling, the tubes were immediately sealed with brass storage caps fitted with PTFE ferrules and stored in a glass container, protected from air and light. Prior to sampling, these sorbent tubes were conditioned for one hour at 300°C while being flushed with helium (50 ml/min) and loaded with 10.8 ng toluene-d8 as internal standard (20). Immediately after sampling, both cell number and viability in each culture flask were assessed using the trypan blue exclusion method (TC20™ automated cell counter, Bio-Rad).

2.3 VOC Analysis by TD-GC-MS

After sampling, headspace VOCs were desorbed from the Tenax®GR sorbent tubes using a Unity series 2 Thermal Desorption system (Markes, Llantrisant, UK). First, the sorbent tubes were dry purged for 4 min at 20 ml/min to remove any water and pre-purged with helium for 2 min at 20 ml/min to remove any air which could cause oxidation. Next, the VOCs were desorbed from the tubes by heating them to 260°C for 10 min under a helium flow of 20 ml/min. The analytes were then refocused on a cooled microtrap (-10°C) filled with 29 mg Tenax®TA 35/60 and 28.3 mg Carbograph 1TD 40/60 sorbent. The microtrap was desorbed by flash-heating at 280°C for 3 min. The analytes were then carried to the capillary GC column by a helium-flow, after splitting the flow at 10 ml/min (**Supplementary Figure S1C**). The flow path was heated to 130°C. The GC (Focus GC, Thermo Scientific, Milan, Italy) contains a 30 m FactorFour VF-1ms low bleed bounded phase capillary GC column (Varian, Sint-Katelijne-Waver, Belgium; 100% polydimethylsiloxane, internal diameter 0.25 mm, film thickness 1 µm). The temperature of this column was adjusted in four steps: initially, the temperature was set at 35°C during the first 10 min after injection. Next, the temperature started to increase with 2°C/min until a temperature of 60°C was reached. Subsequently, the temperature was increased to 170°C at 8°C/min and finally to 240°C at 15°C/min which was maintained for 10 min. The transfer line to the mass spectrometer was heated to 240°C. The DSQII Single Quadrupole mass spectrometer (Thermo Scientific, Austin, TX, USA) uses electron ionization (70 eV). Ions with a mass-to-charge (m/z) ratio from 29 to 300 were recorded in full scan mode (200 ms/scan).

2.4 Data Processing and Statistical Analysis

Chromatograms and mass spectra were processed using Thermo XCalibur 2.2 software. Compounds were tentatively identified based on their retention time, fragmentation patterns and spectral match with the National Institute of Standards and Technology (NIST) Mass Spectral (MS) search V2.0 database. The internal standard toluene-d8 was used to correct for variability in TD-GC-MS performance. Hence, the peak area relative to the internal standard (RPA) was determined for every compound and used for further processing. The quality of the dataset was examined by checking the reproducibility of the replicates. Compounds with a relative standard deviation exceeding 30% in ≥60% of the sample types were discarded (21). Internal standard-based normalization and scaling to unit variance were applied to the data prior to statistical analysis.

Statistical analysis was performed using R software with the R Studio interface. Before comparing the VOC profiles of the different cell lines, a background correction was applied to correct for the background signals originating from the two cell culture media (full DMEM/F-12 Glutamax™ and RPMI 1640 medium) and cell culture flasks used (22). This was done by subtracting the average RPA of each VOC of the corresponding media samples (control samples) from the RPA of each cell culture sample. Next, unsupervised methods were applied including principal component analysis (PCA) and hierarchical clustering analysis (HCA) to explore the data. Differences in VOC profiles between sample types were investigated using the supervised method least absolute shrinkage and selection operator (lasso) regression. Different lasso classification models were created: (1) MPM versus lung cancer (one model), (2) MPM histological subtypes versus lung cancer (three models) and (3) MPM histological subtype versus MPM histological subtype (three models). The *glmnet* R-package (v2.0-2) was used for fitting binominal lasso logistic models. The constructed discrimination models were validated by leave-one-out cross-validation. For visualization, receiver operating characteristic (ROC) curves were created followed by estimation of the model characteristics [sensitivity, specificity, accuracy and area under the curve (AUC_{ROC})] with their 95% confidence intervals. Furthermore, the number of times (folds) a VOC was selected by the lasso regressions was also determined. Variables were considered as important in the discrimination when selected in a large proportion of folds (>80%).

3 RESULTS

3.1 Cell Viability

The average viability (%) and number of viable cells (± standard deviation) of the six MPM and two NSCLC cell lines are shown in **Table 1**. The average cell viability ranged from 87.2 ± 13.3% to 100 ± 0.0%, showing that cell culture conditions did not substantially affect the viability of the cells. The released VOCs thus mainly come from living cells, reflecting the normal metabolism of the analyzed cell lines.

3.2 Headspace VOC Profiling

3.2.1 Data Exploration: PCA and HCA

In total, 277 VOC peaks were selected in the obtained chromatograms of which 77 could be identified. These 77

TABLE 1 | Average cell viability (%) and number of viable cells (x10^6) of the replicates of the different cell lines after 48 hours of incubation [n=5, except for NKI04 (n=3), NCI-H2228 (n=3) and NCI-H1975 (n=2)].

Cell line	Cell type	Average viability (%)	Average number of viable cells (x10^6)
H-MESO-1	Sarcomatoid MPM	98.4 ± 0.5	21.3 ± 3.4
NCI-H2731	Sarcomatoid MPM	98.0 ± 2.9	6.8 ± 2.0
NCI-H2795	Epithelioid MPM	98.8 ± 0.8	6.1 ± 1.3
NCI-H2818	Epithelioid MPM	87.2 ± 13.3	7.6 ± 0.7
MSTO-211H	Biphasic MPM	99.0 ± 1.0	5.8 ± 1.9
NKI04	Biphasic MPM	99.3 ± 1.2	3.0 ± 0.5
NCI-H2228	NSCLC	100 ± 0.0	9.8 ± 1.7
NCI-H1975	NSCLC	99.0 ± 0.0	6.0 ± 0.6

MPM, malignant pleural mesothelioma; NSCLC, non-small cell lung cancer.
Average values are presented with their standard deviation.

identified compounds could be assigned to eleven different chemical classes: alcohols, aldehydes, aliphatic hydrocarbons, aromatic hydrocarbons, esters, halogenated compounds, ketones, nitrogen compounds, siloxanes, sulphides and terpenes (**Supplementary Table S1**). The unidentified compounds were named according to their retention time (e.g. RT_17.65). For thirteen of the 277 VOCs, the relative standard deviation of their RPA exceeded 30% in ≥60% of the sample types, indicating low stability over the replicates. Therefore, they were disregarded in further analysis.

After pre-processing and background correction, unsupervised data exploration was performed by PCA and HCA to visualize the differences between the VOCs present in the headspace of the various cell lines. The largest variation in the samples is explained by PC1 (44.8%), with PC2 and PC3 explaining an additional 12.9% and 9.8% of the total variation in the data respectively (**Figure 1**). Although some overlap is seen between a few individual cell lines, indicating partial similarity between the VOC profiles, some separation could still be observed, meaning there are also differences in VOCs (**Figure 1A**). When the cell lines of the same histology are pooled, the groups are closer together and more overlap can be observed, but the separation is still noticeable (**Figure 1B**).

In the hierarchically clustered heatmap, the VOC profiles tend to naturally cluster together per cell line, demonstrating that each cell line generated a distinct VOC profile (**Figure 2**). Only the cell lines NCI-H2818 and MSTO-211H are more dispersed and show a larger spread around their centroid in the PCA plot, which indicates more variation between the replicates. Remarkably, no clustering could be observed between the two cell lines of the same histological subtype of MPM or lung cancer.

3.2.2 Classification Modeling: Lasso Regression

To identify differentially profiled VOCs between the different cell types, supervised statistical methods can be applied. We used lasso regression to create seven different classification models. The characteristics of the models as well as the selected discriminating VOCs are listed in **Table 2**. The associated ROC curves are shown in **Figure 3**.

MPM and lung cancer cells could be clearly differentiated, resulting in 97.0% accuracy, 80.0% sensitivity and 100% specificity. The area under the constructed ROC curve (AUC_{ROC}) was 0.964. Twenty-four VOCs were found to be important in this discrimination, of which propylbenzene and trichloromethane could be identified.

New lasso models were constructed for the pairwise comparisons between the three major histological subtypes of MPM and lung cancer. Epithelioid and biphasic MPM cells could be discriminated perfectly from the lung cancer cells with 100% sensitivity, specificity, accuracy and an AUC_{ROC} of 1.000. The sarcomatoid subtype of MPM was less distinguishable from lung cancer, with 70.0% sensitivity, 60.0% specificity, 66.7% accuracy and an AUC_{ROC} of 0.740. The identified VOCs, selected as discriminatory in at least one of the three pairwise comparisons, are; 1-propanol, 1,2,4-trimethylcyclopentane, 1,3-bis (1,1-dimethylethyl)benzene, 2-butanol, 2-methylbutanal, 2-otanone, 3,3-dimethyl-2-butanone, 3-hexanone, 3-undecanone, 5-methyl-3-heptanone, benzaldehyde, cyclohexane, dichloromethane, dodecane, ethylcyclohexane, methylcyclopentane, n-decane, nonanal, n-undecane, pentanal and tetradecane.

To find out whether a differentiation between the different histological subtypes of MPM was also possible, the VOC profiles of the three subtypes were compared to each other. All three subtypes could be differentiated from each other with high sensitivity, specificity and accuracy values (ranging from 90 to 100%) with epithelioid MPM being most distinguishable from biphasic MPM. The identified VOCs that contributed most to at least one of these differentiations are; 2,2,4,4-tetramethyloctane, 3-methylpentane, 2,3-dimethylpentane, 2-propanol, 5-methyl-3-heptanone, benzene, butanal, dichloromethane, dodecane, ethyl acetate, ethylcyclohexane, hexanal, n-decane, n-undecane, pentanal, isopropyl nitrate, propylbenzene, propyl nitrate, styrene and tetradecane.

4 DISCUSSION

Clinical studies focusing on VOC biomarkers for MPM have demonstrated the great potential of VOC analysis as a non-invasive, simple and easy-to-use diagnostic tool (11). However, the pathophysiological mechanisms behind alterations in VOC levels are still largely unknown, hampering implementation in clinical practice. In this regard, analysis of MPM cell lines could provide valuable insights into the origin of VOCs and their link to the pathogenesis of MPM, filling in the gaps that still exist today. To our knowledge, we present the first study to report *in*

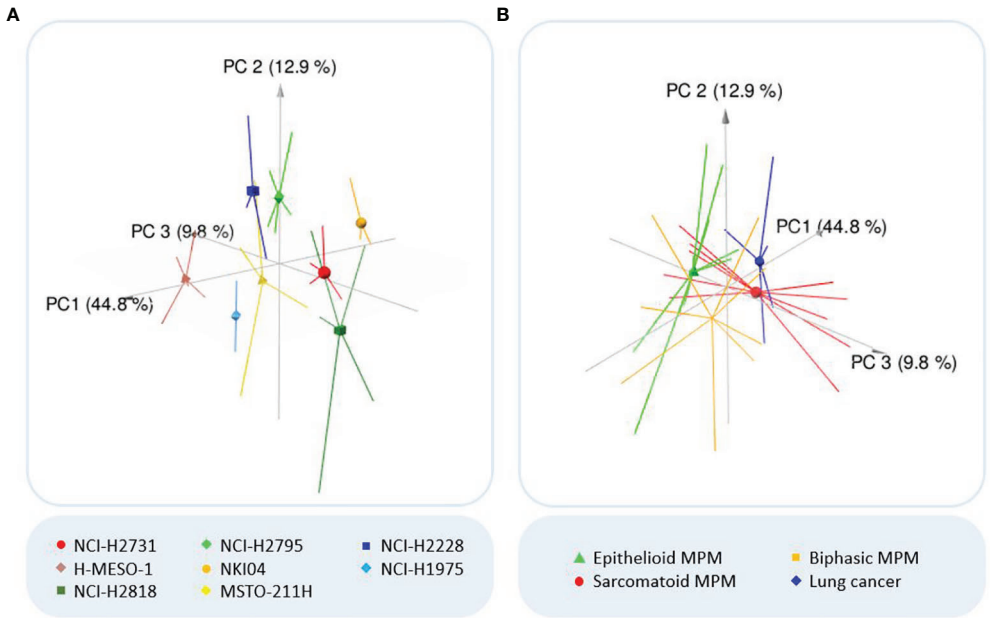

FIGURE 1 | Outcome principal component analysis (PCA). **(A)** Three-dimensional PCA plot of all analyzed cell lines. Colors of the cell lines: light/dark green = epithelioid MPM; red/brown = sarcomatoid MPM; yellow/orange = biphasic MPM; dark/light blue = lung cancer. **(B)** Three-dimensional PCA plot of the MPM subhistologies and lung cancer. PCA reduces the large number of variables to a few principal components (PCs), which account for the most variation in the data. As the first three PCs account for most of the variation, the three-dimensional PCA plot shows clusters of samples based on their similarity. Consequently, the more distant the samples are, the more they differ (according to the variation explained by the axes). The symbols indicate the centroids of the sample replicates.

vitro VOC analysis data of all three histological subtypes of MPM. Moreover, this is the first study to identify differential VOCs between MPM and lung cancer cells.

Unsupervised analysis of the TD-GC-MS data showed a clear visual separation between the different cell lines, revealing differences in the VOC profiles generated by the MPM and lung cancer cells (**Figure 1**). Furthermore, the hierarchically clustered heatmap did not show any cell culture media-based clustering, indicating the effectiveness of the applied background correction (**Figure 2**). Surprisingly, neither both cell lines of the same histological subtype of MPM nor both lung cancer cell lines did seem to cluster very closely together, implying that each individual cell line generates a unique VOC profile. These observations are in line with the findings of Peled et al. (23), who observed differences in VOC profile between individual lung cancer cell lines from the same histological subtype, but with different genetic mutations, including both lung adenocarcinoma cell lines used in our study. It is therefore possible that our observed differences are also caused by genetic variation.

Many of the discriminative VOCs that are identified in studies concerning a specific type of cancer are also described in studies involving other cancer types (24–26). Therefore, comparison between different types of cancer is of utmost importance to pinpoint VOC profiles that are specific for the tumor of interest and are not just related to cancer in general (24). This was addressed in our study by discriminating MPM and lung cancer cells with 97% accuracy (**Table 2**). Only Gendron et al. (18) previously described the distinction between an MPM cell line and lung cancer cell lines, using eNose. However, no individual VOCs were identified and no performance characteristics were reported in their study, allowing no direct comparison. With 97% accuracy, our *in vitro* model even outperformed the *in vivo* situation where MPM patients could be discriminated from lung cancer patients with only 72% accuracy (13). Such an accurate distinction between two types of thoracic malignancies emphasizes the difference in metabolic profile which is important for the clinical utility of VOCs as biomarkers for differential diagnosis. Twenty-four VOCs were found to be important in this *in vitro* discrimination, of which only propylbenzene and trichloromethane could be identified. Propylbenzene has been previously described as a possible biomarker for lung cancer both *in vitro* and *in vivo* (27, 28). This is the first time a significant difference in propylbenzene abundance between MPM and lung cancer cells is reported, demonstrating the potential of this compound as discriminator. The second compound, trichloromethane, has already been identified as possible breath biomarker to discriminate MPM patients from asbestos-exposed individuals in a clinical study (14). This *in vitro* observation confirms a possible relationship between this compound and MPM. However, since trichloromethane could also be a solvent contamination, its interpretation should be done carefully and requires further investigation.

Regarding the subtypes of MPM, both epithelioid and biphasic MPM cells could be discriminated from the lung

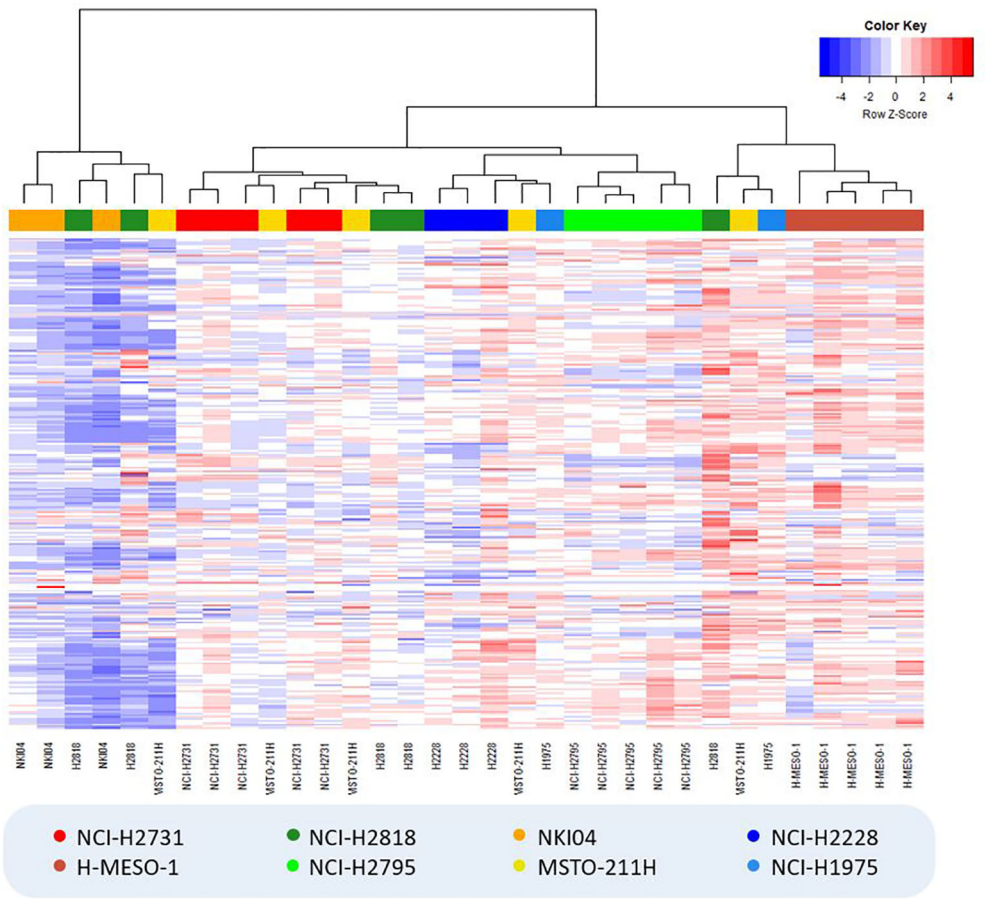

FIGURE 2 | Hierarchically clustered heatmap showing the result of hierarchical clustering analysis (Manhattan distance, Ward's linkage) for all cell culture samples. VOC relative peak areas are shown in a color gradient, with blue colors indicating less produced VOCs (or more consumed VOCs in the case of negative background-corrected values) compared to the average of all samples (i.e. columns), while red colors indicate the exact opposite. Colors of the cell lines: light/dark green = epithelioid MPM; red/brown = sarcomatoid MPM; yellow/orange = biphasic MPM; dark/light blue = lung cancer.

cancer cells with 100% accuracy (**Table 2**). The distinction between the sarcomatoid subtype and lung cancer appeared to be less clear with an accuracy value of 66.7%, suggesting that these cell types have a more similar volatile fingerprint which may result from the activity of similar pathways. However, as the epithelioid and biphasic subtype account for approximately 90% of all MPM cases, a correct distinction between lung cancer and the two most prevalent subtypes is a promising outcome (5).

Alkanes and aldehydes represent many of the discriminatory VOCs when comparing MPM histological subtypes with lung cancer. These compounds can result from cell membrane phospholipid peroxidation, caused by the large amount of radicals produced in the tumor cells (oxidative stress) (29). It has been stated that the phospholipid composition of lung cancer cells is different compared to non-malignant cells, implying that lipid peroxidation may cause production of cancer-specific VOC profiles (30). Some of the selected compounds like n-undecane, pentanal, n-decane and methylcyclopentane have already been identified in other studies as lung cancer biomarkers, confirming their possible discriminatory properties (28, 31). In one of our previous studies, methylcyclopentane was even selected as potential biomarker for MPM when comparing exhaled breath from patients with that of asbestos-exposed persons, suggesting that the concentration of this compound might differentiate between at-risk controls, MPM patients and lung cancer patients (14). Additionally, different ketones are among the selected discriminators, which is not unexpected as they are known to be related to the increased oxidation rate of fatty acids during carcinogenesis. Furthermore, in many cancer types a significantly higher activity of alcohol dehydrogenase is observed, which oxidizes alcohols to ketones (24).

Differentiation between the three MPM subtypes could also be achieved with high accuracy (ranging from 90 to 100%), (**Table 2**). Since the epithelioid and sarcomatoid subtype are associated with the best and worst prognosis respectively, determining VOCs in exhaled breath could potentially have a prognostic value (5). To date, no clinical studies have been carried out comparing the breath VOC profile of MPM patients with different histological subtypes, since MPM is a rare disease and the epithelioid subtype is the most prevalent. Little et al. (19) are the only other group, besides Gendron

TABLE 2 | Characteristics of the discrimination models created with least absolute shrinkage and selection operator (lasso) regression and their 95% confidence interval.

	MPM *versus* NSCLC	MPM histological subtype *versus* NSCLC			MPM histological subtype *versus* subtype		
		Epithelioid MPM *versus* NSCLC	Sarcomatoid MPM *versus* NSCLC	Biphasic MPM *versus* NSCLC	Epithelioid *versus* sarcomatoid MPM	Sarcomatoid *versus* biphasic MPM	Biphasic *versus* epithelioid MPM
N	**28 *versus* 5**	**10 *versus* 5**	**10 *versus* 5**	**8 *versus* 5**	**10 *versus* 10**	**10 *versus* 8**	**8 *versus* 10**
Sensitivity %	80.0 (33.5-99.0)	100 (74.1-100)	70.0 (38.0-91.7)	100 (68.8-100)	90.0 (59.7-99.5)	100 (68.8-100)	100 (68.8-100)
Specificity %	100 (89.9-100)	100 (54.9-100)	60.0 (18.3-92.6)	100 (54.9-100)	90.0 (59.7-99.5)	90.0(59.7-99.5)	100 (74.1-100)
Accuracy %	97.0 (86.0-99.9)	100 (81.9-100)	66.7 (40.1-86.6)	100 (79.4-100)	90.0 (70.8-98.3)	94.4 (75.6-99.7)	100 (84.7-100)
AUC_{ROC}	0.964 (0.871-1.000)	1.000 (1.000-1.000)	0.740 (0.460-0.960)	1.000 (1.000-1.000)	0.940 (0.820-1.000)	0.962 (0.850-1.000)	1.000 (1.000-1.000)
VOCs	propylbenzene, trichloromethane, RT_5.71, RT_9.92, RT_13.77, RT_17.14_C6H12O6, RT_18.94, RT_23.01, RT_24.13, RT_26.28, RT_28.81, RT_30.05, RT_32.39, RT_33.42, RT_33.99, RT_35.44, RT_36.31, RT_36.93, RT_38.35, RT_39.07, RT_39.72, RT_41.03, RT_42.00, RT_46.22_C16H16	methylcyclopentane, n-decane, n-undecane, pentanal, tetradecane, RT_5.34, RT_17.65, RT_21.62, RT_24.01, RT_27.14, RT_29.63, RT_31.45, RT_33.99, RT_36.70, RT_37.92, RT_39.21, RT_41.81	methylcyclopentane, n-decane, n-undecane, pentanal, tetradecane, RT_5.34, RT_17.65, RT_21.62, RT_24.01, RT_27.14, RT_29.63, RT_31.45, RT_33.99, RT_36.70, RT_37.92, RT_39.21, RT_41.81	1-propanol, 1,2,4-trimethylcyclopentane, 1,3-bis (1,1-dimethylethyl)benzene, 2-butanol, 2-methylbutanal, 2-otanone, 3,3-dimethyl-2-butanone, 3-hexanone, 3-undecanone, 5-methyl-3-heptanone, benzaldehyde, cyclohexane, dichloromethane, dodecane, ethylcyclohexane, nonanal, RT_7.73, RT_13.51, RT_17.82, RT_22.30_CH16, RT_23.43, RT_24.13, RT_26.88, RT_28.30, RT_29.15, RT_31.79, RT_33.04, RT_33.35, RT_33.99, RT_34.29, RT_35.57, RT_36.39, RT_36.70, RT_37.76, RT_39.65, RT_39.91, RT_40.77, RT_41.03, RT_42.00, RT_42.49	3-methylpentane, ethylcyclohexane, hexanal, n-undecane, isopropyl nitrate, tetradecane, RT_17.65, RT_29.63, RT_31.84, RT_33.59, RT_37.09, RT_38.71, RT_42.49	2,2,4,4-tetramethyloctane, 5-methyl-3-heptanone, benzene, butanal, dichloromethane, n-undecane, pentanal, propyl nitrate, RT_7.94, RT_18.03, RT_20.70, RT_22.91, RT_24.01, RT_26.28, RT_27.61, RT_29.15, RT_31.45, RT_32.00, RT_33.16, RT_34.36, RT_36.24, RT_36.93, RT_37.66, RT_38.47, RT_39.21, RT_39.91, RT_40.77, RT_41.48, RT_42.53	2,2,4,4-tetramethyloctane, 2,3-dimethylpentane, 2-propanol, 5-methyl-3-heptanone, benzene, butanal, dichloromethane, dodecane, ethyl acetate, n-decane, n-undecane, pentanal, propylbenzene, propyl nitrate, styrene, tetradecane, RT_7.94, RT_17.65, RT_18.03, RT_20.70, RT_22.30_C8H16, RT_22.91, RT_24.01, RT_25.66, RT_26.28, RT_27.61, RT_29.15, RT_31.45, RT_32.00, RT_33.16, RT_34.23, RT_34.36, RT_36.09, RT_36.24, RT_36.93, RT_37.66, RT_38.47, RT_38.93, RT_39.21, RT_39.91, RT_40.77, RT_41.48, RT_42.30, RT_42.53

AUC_{ROC}, area under the receiver operating characteristic curve; MPM, malignant pleural mesothelioma; NSCLC, non-small cell lung cancer; RT, retention time; VOC, volatile organic compound.
The shown VOCs were selected in at least 80% of folds.

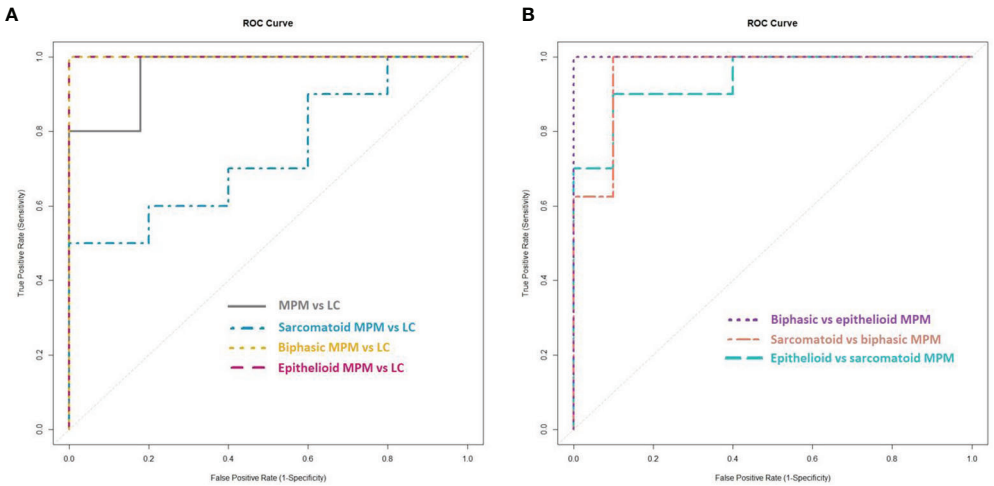

FIGURE 3 | Receiver operating characteristic (ROC) curves of the created lasso models. **(A)** ROC curves of the lasso models for the discrimination between the cell lines of (the histological subtypes of) malignant pleural mesothelioma (MPM) and lung cancer (LC). **(B)** ROC curves of the lasso models for the discrimination between the cell lines of the histological subtypes of MPM.

et al., that analyzed the headspace of MPM cells. They compared one biphasic MPM (MSTO-211H), one epithelioid MPM (NCI-H28) and one non-malignant mesothelial (MET-5A) cell line using solid-phase microextraction GC-MS (19). They identified 2-ethyl-1-hexanol to be significantly increased in both MPM cell lines compared to the non-malignant cell line. In addition, ethyl propionate and cyclohexanol were seen to be specifically increased in the biphasic MPM cell line, while dodecane was only increased in the epithelioid MPM cell line. In line with these findings, dodecane was also selected in our study as an important discriminator between biphasic and epithelioid MPM, suggesting a potential role as subtype-specific marker. However, dodecane was also found to be related to lung cancer and breast cancer in other studies, implying it could also be a more general cancer marker (27).

Our study has several strengths compared to the previous studies analyzing the headspace of MPM cells. Firstly, to cover the natural heterogeneity of the disease, we included six different MPM cell lines of different histological subtypes, rather than replicates of only one or two cell lines. Differences in number of cells were to be expected due to differences in cell size and growth rate, which is why we opted for obtaining equal metabolic surface areas after the incubation period, rather than an equal number of cells. Secondly, unlike many other VOC studies, we have chosen not to rule out unidentified compounds since these could also be important discriminators. This is demonstrated by the considerable number of unidentified VOCs selected by the regression models. This number indicates that there is still room for improvement of analytical techniques to achieve maximum VOC identification, which should certainly be addressed in future research. Lastly, given the high number of VOCs that are present in human matrices and the fact that numerous VOCs seem to be of importance in different diseases, a VOC panel rather than a single biomarker should be used for MPM diagnosis (11). By performing multivariate statistics, the optimal combination of VOCs (VOC patterns) is selected to distinguish the indicated groups. This is a more suitable approach than applying univariate statistics, as applied by the group of Little (19), which focusses on individual VOCs that may lack specificity when it comes to other diseases (32). It is important to further validate these identified VOC profiles by involving a wider range of diseases.

Several clinical studies proposed different VOCs as breath biomarkers for MPM, however, only limited overlap is seen with our *in vitro* results (13–15, 33, 34). These discrepancies between *in vitro* and *in vivo* findings can be the result of changes in cell metabolism due to differences in oxygen levels or standard 2D culturing conditions (35, 36). Furthermore, the transmission of VOCs from cells to breath is poorly understood, involving possible conversion of compounds by the liver or kidney metabolism (36, 37). These factors make *in vitro* and *in vivo* results difficult to compare, stressing the need for studies investigating simultaneously breath and tumor cells of the same patients and investigating metabolization and kinetics of *in vitro* discovered VOCs in the *in vivo* setting.

Despite the added value of our study, these discrepancies lead us to some study limitations that should be recognized. The experiments were performed under standard 2D culturing conditions, disregarding the 3D structure and oxygen deficient tumor microenvironment *in vivo*. More advanced, specialized set-ups, better mimicking *in vivo* conditions, should be used in further studies when available. Secondly, we have chosen not to make a comparison between malignant and non-malignant mesothelial cells, since our focus was on the specificity of the VOC biomarkers. Therefore, we used lung cancer cells as control group. Little et al. (19) alternatively used normal mesothelial cells in their experimental set-up. However, the sparsely commercially available normal mesothelial cell lines are not considered well representative of *in vivo* mesothelial cells (38). Hence, such cells might not be an accurate normal cell control for MPM. As an alternative, primary

mesothelial cells could be isolated from human pleura, but they have the disadvantage of being difficult to cultivate *in vitro*, limiting their use for *in vitro* headspace analysis. A final potential limitation relates to the possible exogenous origin of VOCs. Although a background correction was made to correct for exogenous VOCs originating from the used culture media, materials and sampling environment, this does not guarantee that all measured VOCs are of endogenous origin. This should always be kept in mind when interpreting the results. However, despite these possible limitations, the presented study shows new and valuable results as one of the first studies to investigate VOC production at the cellular level for MPM.

5 CONCLUSIONS

Breath analysis has proven to be a promising tool for the non-invasive diagnosis of MPM. To gain insight into the biological processes underlying VOC production, *in vitro* VOC analysis can provide valuable additional information. This study identified MPM-specific VOC profiles capable of differentiating MPM subtypes and lung cancer cells with high accuracy. However, discrepancies between these identified *in vitro* VOC profiles and clinically reported breath profiles were observed, which could be explained by differences in oxygen levels, 3D structure, metabolization, etc. This supports the need for further investigation of these *in vitro* discovered VOCs and their metabolic pathways as well as their kinetics *in vivo*. While the relationship between *in vitro* and *in vivo* VOCs is still largely unknown, both could complement each other in generating a clinically useful breath model for MPM.

DATA AVAILABILITY STATEMENT

The raw data supporting the conclusions of this article will be made available by the authors, without undue reservation.

AUTHOR CONTRIBUTIONS

Conceptualization, KV, JvM, and KL; data curation, EJ and ZM; formal analysis, EJ and ZM; investigation, EJ, ZM, LV, and SL; methodology, EJ, ZM, LV, SL, KV, CW, EM, and KL; supervision, JvM, EM, and KL; visualization, EJ; writing – original draft preparation, EJ; writing – review and editing, EJ, ZM, LV, KV, JvM, CW, EM, and KL. All authors have read and agreed to the published version of the manuscript.

FUNDING

This research was funded by Kom op tegen Kanker (Stand up to Cancer), the Flemish cancer society (grants KOTK UA/2016/10710/1 and 'Emmanuel van der Schueren') and by the Antwerp University Research Fund (BOF-KP 36051).

SUPPLEMENTARY MATERIAL

The Supplementary Material for this article can be found online at: https://www.frontiersin.org/articles/10.3389/fonc.2022.851785/full#supplementary-material

REFERENCES

1. Neumann V, Löseke S, Nowak D, Herth FJF, Tannapfel A. Malignant Pleural Mesothelioma: Incidence, Etiology, Diagnosis, Treatment, and Occupational Health. *Dtsch Arztebl Int* (2013) 110:319–26. doi: 10.3238/arztebl.2013.0319
2. Nicolini F, Bocchini M, Bronte G, Delmonte A, Guidoboni M, Crinò L, et al. Malignant Pleural Mesothelioma: State-Of-the-Art on Current Therapies and Promises for the Future. *Front Oncol* (2020) 9:1519. doi: 10.3389/fonc.2019.01519
3. Brims FJH, Kong K, Harris EJA, Sodhi-Berry N, Reid A, Murray CP, et al. Pleural Plaques and the Risk of Lung Cancer in Asbestos-Exposed Subjects. *Am J Respir Crit Care Med* (2019) 201:57–62. doi: 10.1164/RCCM.201901-0096OC
4. Mutti L, Peikert T, Robinson BWS, Scherpereel A, Tsao AS, de Perrot M, et al. Scientific Advances and New Frontiers in Mesothelioma Therapeutics. *J Thorac Oncol* (2018) 13:1269–83. doi: 10.1016/j.jtho.2018.06.011
5. van Zandwijk N, Clarke C, Henderson D, Musk AW, Fong K, Nowak A, et al. Guidelines for the Diagnosis and Treatment of Malignant Pleural Mesothelioma. *J Thorac Dis* (2013) 5:E254–307. doi: 10.3978/j.issn.2072-1439.2013.11.28
6. Rossi G, Davoli F, Poletti V, Cavazza A, Lococo F. When the Diagnosis of Mesothelioma Challenges Textbooks and Guidelines. *J Clin Med* (2021) 10:2434. doi: 10.3390/JCM10112434
7. Janes SM, Alrifai D, Fennell DA. Perspectives on the Treatment of Malignant Pleural Mesothelioma. *N Engl J Med* (2021) 385:1207–18. doi: 10.1056/NEJMra1912719
8. Chen Z, Gaudino G, Pass HI, Carbone M, Yang H. Diagnostic and Prognostic Biomarkers for Malignant Mesothelioma: An Update. *Transl Lung Cancer Res* (2017) 6:259–69. doi: 10.21037/tlcr.2017.05.06
9. Bianco A, Valente T, de Rimini ML, Sica G, Fiorelli A. Clinical Diagnosis of Malignant Pleural Mesothelioma. *J Thorac Dis* (2018) 10:S253–61. doi: 10.21037/jtd.2017.10.09
10. Schillebeeckx E, van Meerbeeck J, Lamote K. Clinical Utility of Diagnostic Biomarkers in Malignant Pleural Mesothelioma: A Systematic Review and Meta-Analysis. *Eur Respir Rev* (2021) 30:210057. doi: 10.1183/16000617.0057-2021
11. Brusselmans L, Arnouts L, Millevert C, Vandersnickt J, van Meerbeeck JP, Lamote K. Breath Analysis as a Diagnostic and Screening Tool for Malignant Pleural Mesothelioma: A Systematic Review. *Transl Lung Cancer Res* (2018) 7:520–36. doi: 10.21037/tlcr.2018.04.09
12. Catino A, de Gennaro G, di Gilio A, Facchini L, Galetta D, Palmisani J, et al. Breath Analysis: A Systematic Review of Volatile Organic Compounds (VOCs) in Diagnostic and Therapeutic Management of Pleural Mesothelioma. *Cancers (Basel)* (2019) 11:831. doi: 10.3390/cancers11060831
13. Lamote K, Vynck M, Thas O, Van Cleemput J, Nackaerts K, van Meerbeeck JP. Exhaled Breath to Screen for Malignant Pleural Mesothelioma: A Validation Study. *Eur Respir J* (2017) 50:1700919. doi: 10.1183/13993003.00919-2017
14. Lamote K, Brinkman P, Vandermeersch L, Vynck M, Sterk PJ, van Langenhove H, et al. Breath Analysis by Gas Chromatography-Mass Spectrometry and Electronic Nose to Screen for Pleural Mesothelioma: A Cross-Sectional Case-Control Study. *Oncotarget* (2017) 8:91593–602. doi: 10.18632/oncotarget.21335
15. Lamote K, Vynck M, Van Cleemput J, Thas O, Nackaerts K, van Meerbeeck JP. Detection of Malignant Pleural Mesothelioma in Exhaled Breath by Multicapillary Column/Ion Mobility Spectrometry (MCC/IMS). *J Breath Res* (2016) 10:46001. doi: 10.1088/1752-7155/10/4/046001

16. Filipiak W, Mochalski P, Filipiak A, Ager C, Cumeras R, E. Davis C, et al. Troppmair JCompendium of Volatile Organic Compounds (VOCs) Released By Human Cell Lines. *A Curr Med Chem* (2016) 23:2112–31. doi: 10.2174/0929867323666160510122913
17. Janssens E, van Meerbeeck JP, Lamote K. Volatile Organic Compounds in Human Matrices as Lung Cancer Biomarkers: A Systematic Review. *Crit Rev Oncol Hematol* (2020) 153:103037. doi: 10.1016/j.critrevonc.2020.103037
18. Gendron KB, Hockstein NG, Thaler ER, Vachani A, Hanson CW. *In Vitro* Discrimination of Tumor Cell Lines With an Electronic Nose. *Otolaryngol Head Neck Surg* (2007) 137:269–73. doi: 10.1016/j.otohns.2007.02.005
19. Little LD, Carolan VA, Allen KE, Cole LM, Haywood-Small SL. Headspace Analysis of Mesothelioma Cell Lines Differentiates Biphasic and Epithelioid Sub-Types. *J Breath Res* (2020) 14:046011. doi: 10.1088/1752-7163/abaaff
20. Walgraeve C, Demeestere K, Dewulf J, Van Huffel K, Van Langenhove H. Diffusive Sampling of 25 Volatile Organic Compounds in Indoor Air: Uptake Rate Determination and Application in Flemish Homes for the Elderly. *Atmos Environ* (2011) 45:5828–36. doi: 10.1016/j.atmosenv.2011.07.007
21. Jia Z, Zhang H, Nam Ong C, Patra A, Lu Y, Teck Lim C, et al. Detection of Lung Cancer: Concomitant Volatile Organic Compounds and Metabolomic Profiling of Six Cancer Cell Lines of Different Histological Origins. *ACS Omega* (2018) 3:5131–40. doi: 10.1021/acsomega.7b02035
22. Jia Z, Patra A, Kutty VK, Venkatesan T. Critical Review of Volatile Organic Compound Analysis in Breath and *In Vitro* Cell Culture for Detection of Lung Cancer. *Metabolites* (2019) 9:52. doi: 10.3390/metabo9030052
23. Peled N, Barash O, Tisch U, Ionescu R, Broza YY, Ilouze M, et al. Volatile Fingerprints of Cancer Specific Genetic Mutations. *Nanomedicine* (2013) 9:758–66. doi: 10.1016/j.nano.2013.01.008
24. Janfaza S, Khorsand B, Nikkhah M, Zahiri J. Digging Deeper Into Volatile Organic Compounds Associated With Cancer. *Biol Methods Protoc* (2019) 4: bpz014. doi: 10.1093/biomethods/bpz014
25. Krilaviciute A, Heiss JA, Leja M, Kupcinskas J, Haick H, Brenner H. Detection of Cancer Through Exhaled Breath: A Systematic Review. *Oncotarget* (2015) 6:38643–57. doi: 10.18632/oncotarget.5938
26. Amor RE, Nakhleh MK, Barash O, Haick H. Breath Analysis of Cancer in the Present and the Future. *Eur Respir Rev* (2019) 28:190002. doi: 10.1183/16000617.0002-2019
27. Thriumani R, Zakaria A, Hashim YZH-Y, Jeffree AI, Helmy KM, Kamarudin LM, et al. A Study on Volatile Organic Compounds Emitted by *In-Vitro* Lung Cancer Cultured Cells Using Gas Sensor Array and SPME-GCMS. *BMC Cancer* (2018) 18:362. doi: 10.1186/s12885-018-4235-7
28. Phillips M, Gleeson K, Hughes JMB, Greenberg J, Cataneo RN, Baker L, et al. Volatile Organic Compounds in Breath as Markers of Lung Cancer: A Cross-Sectional Study. *Lancet* (1999) 353:1930–3. doi: 10.1016/S0140-6736(98)07552-7
29. Hakim M, Broza YY, Barash O, Peled N, Phillips M, Amann A, et al. Volatile Organic Compounds of Lung Cancer and Possible Biochemical Pathways. *Chem Rev* (2012) 112:5949–66. doi: 10.1021/cr300174a
30. Töreyin ZN, Ghosh M, Göksel Ö, Göksel T, Godderis L. Exhaled Breath Analysis in Diagnosis of Malignant Pleural Mesothelioma: Systematic Review. *Int J Environ Res Public Health* (2020) 17:1110. doi: 10.3390/ijerph17031110
31. Li M, Yang D, Brock G, Knipp RJ, Bousamra M, Nantz MH, et al. Breath Carbonyl Compounds as Biomarkers of Lung Cancer. *Lung Cancer* (2015) 90:92–7. doi: 10.1016/j.lungcan.2015.07.005
32. Kasbohm E, Fischer S, Küntzel A, Oertel P, Bergmann A, Trefz P, et al. Strategies for the Identification of Disease-Related Patterns of Volatile Organic Compounds: Prediction of Paratuberculosis in an Animal Model Using Random Forests. *J Breath Res* (2017) 11:047105. doi: 10.1088/1752-7163/aa83bb
33. de Gennaro G, Dragonieri S, Longobardi F, Musti M, Stallone G, Trizio L, et al. Chemical Characterization of Exhaled Breath to Differentiate Between Patients With Malignant Pleural Mesothelioma From Subjects With Similar Professional Asbestos Exposure. *Anal Bioanal Chem* (2010) 398:3043–50. doi: 10.1007/s00216-010-4238-y
34. Di Gilio A, Catino A, Lombardi A, Palmisani J, Facchini L, Mongelli T, et al. Breath Analysis for Early Detection of Malignant Pleural Mesothelioma: Volatile Organic Compounds (VOCs) Determination and Possible Biochemical Pathways. *Cancers (Basel)* (2020) 12:1262. doi: 10.3390/cancers12051262
35. Kalluri U, Naiker M, Myers MA. Cell Culture Metabolomics in the Diagnosis of Lung Cancer—the Influence of Cell Culture Conditions. *J Breath Res* (2014) 8:27109. doi: 10.1088/1752-7155/8/2/027109
36. Schmidt K, Podmore I. Current Challenges in Volatile Organic Compounds Analysis as Potential Biomarkers of Cancer. *J Biomarkers* (2015) 2015:1–16. doi: 10.1155/2015/981458
37. De Lacy Costello B, Amann A, Al-Kateb H, Flynn C, Filipiak W, Khalid T, et al. A Review of the Volatiles From the Healthy Human Body. *J Breath Res* (2014) 8:14001. doi: 10.1088/1752-7155/8/1/014001
38. Pruett N, Singh A, Shankar A, Schrump DS, Hoang CD. Translational Physiology: Normal Mesothelial Cell Lines Newly Derived From Human Pleural Biopsy Explants. *Am J Physiol Lung Cell Mol Physiol* (2020) 319:L652–60. doi: 10.1152/ajplung.00141.2020

Conflict of Interest: The authors declare that the research was conducted in the absence of any commercial or financial relationships that could be construed as a potential conflict of interest.

Publisher's Note: All claims expressed in this article are solely those of the authors and do not necessarily represent those of their affiliated organizations, or those of the publisher, the editors and the reviewers. Any product that may be evaluated in this article, or claim that may be made by its manufacturer, is not guaranteed or endorsed by the publisher.

frontiers | Frontiers in Oncology

ORIGINAL RESEARCH
published: 20 June 2022
doi: 10.3389/fonc.2022.870352

Prognostic Role of Tumor Immune Microenvironment in Pleural Epithelioid Mesothelioma

Hely Ollila[1,2,3], Mikko I. Mäyränpää[4], Lassi Paavolainen[1], Juuso Paajanen[2,3], Katja Välimäki[1], Eva Sutinen[2,3], Henrik Wolff[4,5], Jari Räsänen[6], Olli Kallioniemi[1], Marjukka Myllärniemi[2,3], Ilkka Ilonen[2,6†] and Teijo Pellinen[1†]*

[1] Institute for Molecular Medicine Finland (FIMM), Helsinki Institute of Life Science (HiLIFE), University of Helsinki, Helsinki, Finland, [2] Individualized Drug Therapy Research Program, Faculty of Medicine, University of Helsinki, Helsinki, Finland, [3] Department of Pulmonary Medicine, Heart and Lung Center, University of Helsinki and Helsinki University Hospital, Helsinki, Finland, [4] Department of Pathology, University of Helsinki and Helsinki University Hospital, Helsinki, Finland, [5] Laboratory of Pathology, Finnish Institute of Occupational Health, Helsinki, Finland, [6] Department of General Thoracic and Esophageal Surgery, Heart and Lung Center, University of Helsinki and Helsinki University Hospital, Helsinki, Finland

Background: Pleural mesothelioma (MPM) is an aggressive malignancy with an average patient survival of only 10 months. Interestingly, about 5%–10% of the patients survive remarkably longer. Prior studies have suggested that the tumor immune microenvironment (TIME) has potential prognostic value in MPM. We hypothesized that high-resolution single-cell spatial profiling of the TIME would make it possible to identify subpopulations of patients with long survival and identify immunophenotypes for the development of novel treatment strategies.

Methods: We used multiplexed fluorescence immunohistochemistry (mfIHC) and cell-based image analysis to define spatial TIME immunophenotypes in 69 patients with epithelioid MPM (20 patients surviving ≥ 36 months). Five mfIHC panels (altogether 21 antibodies) were used to classify tumor-associated stromal cells and different immune cell populations. Prognostic associations were evaluated using univariate and multivariable Cox regression, as well as combination risk models with area under receiver operating characteristic curve (AUROC) analyses.

Results: We observed that type M2 pro-tumorigenic macrophages ($CD163^+pSTAT1^-$ HLA-$DRA1^-$) were independently associated with shorter survival, whereas granzyme B^+ cells and $CD11c^+$ cells were independently associated with longer survival. $CD11c^+$ cells were the only immunophenotype increasing the AUROC (from 0.67 to 0.84) when added to clinical factors (age, gender, clinical stage, and grade).

Conclusion: High-resolution, deep profiling of TIME in MPM defined subgroups associated with both poor (M2 macrophages) and favorable (granzyme B/CD11c positivity) patient survival. CD11c positivity stood out as the most potential prognostic cell subtype adding prediction power to the clinical factors. These findings help to understand the critical determinants of TIME for risk and therapeutic stratification purposes in MPM.

Keywords: pleural mesothelioma, tumor immune microenvironment, multiplexed fluorescence immunohistochemistry, prognosis, dendritic cells

OPEN ACCESS

Edited by:
Marco Lucchi,
University of Pisa, Italy

Reviewed by:
Luka Brcic,
Medical University of Graz, Austria
Cristiana Bellan,
University of Siena, Italy

****Correspondence:***
Hely Ollila
hely.ollila@helsinki.fi

†These authors share last authorship

Specialty section:
This article was submitted to Thoracic Oncology, a section of the journal Frontiers in Oncology

Received: *06 February 2022*
Accepted: *08 March 2022*
Published: *20 June 2022*

Citation:
Ollila H, Mäyränpää MI, Paavolainen L, Paajanen J, Välimäki K, Sutinen E, Wolff H, Räsänen J, Kallioniemi O, Myllärniemi M, Ilonen I and Pellinen T (2022) Prognostic Role of Tumor Immune Microenvironment in Pleural Epithelioid Mesothelioma. Front. Oncol. 12:870352. doi: 10.3389/fonc.2022.870352

1 INTRODUCTION

Pleural mesothelioma (MPM) is an aggressive malignancy arising from mesothelial cells lining the chest cavity and lungs. MPM prognosis is poor with a median survival of 10 months (1). Despite the dismal general prognosis, a small portion of patients with MPM (5%–10%) survive remarkably longer following diagnosis (2, 3). The underlying biology explaining the differential patient survival is yet to be explored. Prior studies have highlighted the potential prognostic role of the tumor immune microenvironment (TIME) in MPM (4, 5). Although immunotherapies have shown beneficial outcomes in MPM in clinical trials (6, 7), biomarkers are needed to guide patient selection for conventional chemotherapy versus novel immunotherapies (8).

The TIME of MPM consists of several immune cell populations including subtypes of macrophages, T and B lymphocytes, natural killer (NK) cells, myeloid-derived suppressor cells (MDSCs), and dendritic cells (DCs). Several of these immune cell populations present in MPM tumor tissue have been shown to associate with overall survival. For example, higher numbers of $CD20^+$ B lymphocytes and $CD4^+$ or $CD8^+$ T lymphocytes have been associated with improved prognosis (9–15), although the data regarding CD8 association with survival are controversial (12, 16). Higher numbers of intratumoral regulatory T lymphocytes and programmed cell death protein 1 (PD-1–), lymphocyte-activation gene 3 (LAG3–), and T cell immunoglobulin and mucin domain-containing protein 3 (TIM3)–expressing tumor-infiltrating ($CD4^+$) T lymphocytes have been associated with poor prognosis (17), although TIM3 expression alone has been reported to be an independent prognostic factor for longer survival (11). In macrophages, higher expression of CD163 (M2-like) has been identified to associate with shorter survival, especially in relation to CD68 macrophage marker (M1-like) or in relation to either CD8 or CD20 (9, 18). Further, higher densities of tumor infiltrating $CD68^+$ macrophages have been identified to associate with poor prognosis in patients with MPM with non-epithelioid histology (19). Finally, it has been shown that intratumor-infiltrating MDSCs are associated with poorer progression-free survival and overall survival (17).

Given the many controversial findings regarding immunophenotypes and survival in MPM, we aimed to systematically profile and classify immune cell populations in MPM TIME with 21 immune cell–specific antibodies using formalin-fixed paraffin-embedded tissue microarrays including samples from 69 patients with epithelioid MPM. We utilized multiplexed fluorescence immunohistochemistry (mfIHC) and digital cell–based image analysis for analyzing the immune cell populations present in tumor-associated stroma and correlated the expressions with patient survival.

Abbreviations: MPM, pleural mesothelioma; TIME, tumor immune microenvironment; NK, natural killer; MDSCs, myeloid-derived suppressor cells; DCs, dendritic cells; mfIHC, multiplexed fluorescence immunohistochemistry; CK5, cytokeratin 5; CK5/6, cytokeratin 5/6; c-MAF, transcription factor of musculoaponeurotic fibrosarcoma gene; pSTAT1, phospho-STAT1; TNM, tumor, nodes, metastases; TAM, tumor-associated macrophage; IO, immuno-oncological; AUROC, area under receiver operating characteristic curve.

2 MATERIALS AND METHODS

2.1 Patients, Clinical Data, and Tissue Microarrays

The clinical characteristics of the study population and specific details regarding the tissue microarrays have been described (20). We excluded patients with biphasic histology (n = 5). The study population consisted of 69 Finnish patients with epithelioid MPM diagnosed between 2000 and 2012. The median survival of the patients was 19 months, and the median age at the time of diagnosis was 66 years. Overall survival of 20 patients (29%) was longer than 36 months, and 57 (83%) of the patients were male. The tissue samples were taken at the time of diagnosis, so the patients had not received any treatment by then. The ethics committee of Helsinki University Hospital approved the study (HUS/1057/2019).

2.2 Multiplexed Fluorescence Immunohistochemistry and Digital Cell–Based Image Analysis

The mfIHC staining, scanning, and digital cell–based image analysis methods have been previously described (20, 21) and were utilized in the current study as described previously. Briefly, we designed and optimized five mfIHC panels (shown in **Supplementary Table S1**) including 21 antibodies targeting immune cell–specific antigens and analyzed the immune cell populations of interest (**Table 1**) from the multichannel images using cell-based image analysis method. We detected all cells in tissue samples using nuclei 4′,6-diamidino-2-phenylindole (DAPI) staining and classified them either as tumoral or stromal cells based on mesothelial staining [cytokeratin 5 (CK5) or a combination of CK5, cytokeratin 5/6 (CK5/6), and calretinin) so that the cells positive for mesothelial markers were defined as tumor cells and remaining cells as stromal cells. Further, we classified the cells either as positive or negative for each specific immune cell marker and marker combinations by using a cutoff for each channel individually based on mean intensity and standard deviation. Finally, we measured the number of immune cells in tumor-associated stroma and calculated the relative amount (%) of cells in the stroma by dividing the number of cells with the total number of stromal cells.

2.3 Immune Cell Populations

We investigated the following immune cell populations in MPM tumor tissue: T lymphocytes (including subpopulations expressing checkpoint and exhaustion molecules), B lymphocytes, NK cells, macrophages (including type M1 and type M2 macrophages), DCs, and MDSCs. We identified T lymphocytes using CD3 and CD8 antibodies and detected exhausted T lymphocytes using indoleamine 2,3-dioxygenase (IDO), LAG3, and TIM3 antibodies. For detecting T

TABLE 1 | Immune cell markers and the main marker combinations analyzed in this study.

Main cell population	Marker/marker combination	Specific subpopulation
T lymphocytes	$CD3^+$	T lymphocytes
	$CD3^+PD\text{-}1^+$	PD-1 expressing T lymphocytes
	$CD3^+PD\text{-}L1^+$	PD-L1 expressing T lymphocytes
	$CD3^+PD\text{-}1^+PD\text{-}L1^+$	PD-1 and PD-L1 expressing T lymphocytes
	$CD3^+CD8^+$	Cytotoxic T lymphocytes
	$CD3^+CD8^+PD\text{-}L1^+$	PD-L1 expressing cytotoxic T lymphocytes
	$CD3^+CD8^+PD\text{-}1^+$	PD-1 expressing cytotoxic T lymphocytes
	$CD8^+CD11b^+$	CD11b-positive cytotoxic T lymphocytes
	$CD8^+$granzyme B^+	Granzyme B–positive cytotoxic T lymphocytes
	$CD8^+CD11b^+$granzyme B^+	CD11b and granzyme B–positive cytotoxic T lymphocytes
	$CD3^+IDO^+$	IDO expressing T lymphocytes
	$CD3^+LAG3^+$	LAG3 expressing T lymphocytes
	$CD3^+TIM3^+$	TIM3 expressing T lymphocytes
B lymphocytes	$CD20^+$	B lymphocytes
Macrophages	$CD11c^+CD16^+$	
	$CD68^+$	M1 macrophages
	$CD68^+pSTAT1^+$	
	$CD68^+HLA\text{-}DRA1^+$	
	$CD68^+pSTAT1^+HLA\text{-}DRA1^+$	
	$CD163^+pSTAT1^-HLA\text{-}DRA1^-$	M2 macrophages
	$CD163^+IDO^+$	Exhausted M2 macrophages
	$CD163^+LAG3^+$	
	$CD163^+TIM3^+$	
NK cells	granzyme B^+	NK cells or cytotoxic T lymphocytes
	granzyme B^+CD11b^-	CD11b-negative NK cells or cytotoxic T lymphocytes
	granzyme B^+CD11b^+	Granzyme B–positive NK cells
	$CD8^+CD3^-$	
	$PD\text{-}1^+CD3^-$	
	$PD\text{-}1^+CD3^-CD8^-$	
DCs	$CD11c^+$	Dendritic cells
	$CD11c^+CD16^-$	
Tumor cells	$CleavedCaspase3^+Meso^+$	Cleaved caspase 3–positive tumor cells

NK, natural killer; DCs, dendritic cells; MDSCs, myeloid-derived suppressor cells.

lymphocytes expressing checkpoint molecules, we used PD-1 and PD-L1 antibodies, respectively. Proliferating T lymphocytes (and other stromal cells and mesothelial tumor cells) were detected using Ki67 antibody. However, because of the high number of $Ki67^+$ cells present in many tumor samples, it was difficult to accurately classify as being positive in tumor cells or immune cells. For this reason, we did not include the Ki67 antibody in the analyses. Tumor mitotic count was defined as number of mitoses per 10 high-power field (HPF), and it was calculated using whole tissue sections before constructing the tissue microarrays. CD20 was used for detecting B lymphocytes.

Macrophages and their subpopulations (pro-tumorigenic M2 macrophages and anti-tumorigenic M1 macrophages) were identified using CD68, the transcription factor of musculoaponeurotic fibrosarcoma gene (c-MAF), phosphorylated signal transducer and activator of transcription 1 (pSTAT1), human leukocyte antigen DR alpha 1 (HLA-DRA1) and CD163 antibodies, and NK cells using CD11b, granzyme B, CD56, and CD16 antibodies. In addition, CD11c and CD33 antibodies were utilized for detecting myeloid DCs and cleaved caspase 3 for identifying cleaved caspase 3^+ tumor cells. The main characterized immune cell populations using specific markers and marker combinations are presented in **Table 1**, and detailed information regarding used antibodies is presented in **Supplementary Table S2**. All characterized immune cell populations are presented in **Supplementary Table S3**. Regarding macrophage markers, it is important to note that CD68 staining was significantly weaker than CD163 staining, and therefore, they were not used in combination.

2.4 Statistical Analyses

Statistical analyses were performed using R [R Core Team (2017); R: A language and environment for statistical computing; R Foundation for Statistical Computing, Vienna, Austria] and SPSS (version 25.0, IBM, Armonk, NY, USA). All-cause mortality was used as an outcome measurement. We used univariate Cox regression analysis and continuous values for studying the immune cell populations associated with patient survival. The relative number of specific immune cell types was compared between long- and average-term survivors (cutoff, 36 months) using Mann–Whitney U-test.

Multivariable Cox regression analysis was adjusted for variables associated with survival (p-value of <0.05) in univariate Cox regression and previously known prognostic clinical factors: age, gender, grade, and stage of the disease [defined on the basis of the eight edition of the TNM and further dichotomized into low (IA, IB, and II) and high (IIIA, IIIB, and IV) groups] (3). Nuclear grading (low- and high-grade groups), were defined on the basis of the 2021 WHO classification of epithelioid mesothelioma by two expert pathologist (MIM and HW) (22–24). The proportional hazards

assumption was tested by assessing the relationship between Schoenfeld residuals and time. Continuous data were evaluated for skewness by using histograms. The Spearman's rank correlation coefficient was used to assess correlation between continuous nonparametric variables.

AUROC [area under receiver operating characteristic (ROC) curve comparison using the DeLong's test for two correlated ROC curves] analysis was used for studying whether the prognostic immune cell subtypes as single variables may add prognostic value to the clinical variables and further increase confidence in a prediction model. For AUROC analyses, all continuous variables (including immune cell variables and age) were dichotomized using median cutoffs, and the follow-up time was cut to 3 years, as longer time did not increase the confidence when significant (not shown). Novel combination risk scores were also transformed to Kaplan–Meier log rank statistics with full follow-up time.

Survival time was calculated as the time from pathological diagnosis (the date the diagnostic tissue sample was taken) to date of death. Three patients were still alive at the end of follow-up (July 2, 2019).

3 RESULTS

3.1 Univariate Cox Regression Analysis of Immune Cell Populations

The prognostic role of each measured immune cell type (n = 179) present in tumor-associated stroma was studied using univariate Cox regression and continuous values (**Supplementary Table S3**). We found that type M2 macrophages, classified as $CD163^+pSTAT1^-HLA\text{-}DRA1^-$ cells, were associated with shorter survival [hazard ratio (HR) = 1.07; p = 0.002], whereas type M1 macrophages, classified as $CD68^+pSTAT1^+HLA\text{-}DRA1^+$ cells, were associated with longer survival (HR= 0.95; p = 0.033). Granzyme B^+ cells and $CD11c^+$ cells were associated with longer survival (HR = 0.32; p = 0.005, and HR = 0.94; p < 0.001) (**Table 2**). As CD11c is expressed both by DCs and monocytes (25), we analyzed the number of $CD11c^+$ cells either positive or negative for a monocyte marker, CD16. In addition, 97.1% of $CD11c^+$ cells were negative for CD16 ($CD11c^+CD16^-$), and, respectively, 2.9% of $CD11c^+$ cells were positive for CD16 ($CD11c^+CD16^+$), suggesting that the CD11c-associated prognostic effect is largely contributed by DCs. Indeed, $CD11c^+CD16^-$ cells were associated with favorable prognosis, whereas $CD11c^+CD16^+$ did not (**Table 2**). Example images of immune cell phenotypes associated with survival are presented in **Figure 1**. Regarding checkpoint inhibitors (PD-1 and PD-L1) and exhaustion markers (TIM3, LAG3, and IDO), which are targets of immunotherapies and thus are also currently of great interest also in mesothelioma research (26), we did not observe any associations with patient survival (**Supplementary Table S4**) (6, 7).

3.2 The Relative Numbers of Prognostic Immune Cell Types Between Average-Term and Long-Term Survivors

The relative number (percentage of all stromal cells) of each immune cell type was measured, and their distributions in long- and average-term survivors (cutoff, 36 months) were compared. The immune cell phenotypes associating with survival in univariate Cox regression (from **Table 2**) are presented in **Figure 2**. Granzyme B^+ cells and $CD11c^+$ cells were more abundant in long-term survivors, whereas M2-like macrophages were less frequent in long-term survivors (**Figure 2**).

3.3 Multivariable Cox Regression and Combination Risk Models

In multivariable Cox regression adjusting for age, gender, grade, clinical stage, and each prognostic immune cell type separately, type M2 macrophages, granzyme B^+ cells, and $CD11c^+$ cells remained associated with survival. When combining clinical factors and prognostic immune cell types (type M2 macrophages, granzyme B, and CD11c) in one model, all three immune cell populations remained independently associated with survival. All multivariable Cox regression results are presented in **Table 3**. To assess whether type M2 macrophages, granzyme B, or CD11c as single variables would add power in a

TABLE 2 | Selected immune cell classes and their survival effects (continuous cell classes).

Marker/marker combination	HR	p-value	Prognosis
Granzyme B^+	0.32	<0.01	Favorable
Granzyme B^+CD8^+	1.76	0.55	
Granzyme B^+CD11b^+	0.08	0.31	
Granzyme B^+CD11b^-	0.32	<0.01	
$CD11c^+$	0.94	<0.01	
$CD11c^+CD16^-$	0.93	<0.01	
$CD11c^+CD16^+$	0.88	0.47	
$CD68^+$	0.99	0.12	
$CD68^+pSTAT1^+HLA\text{-}DRA1^+$	0.95	0.03	
$CD163^+$	1.00	0.97	Unfavorable
$CD163^+pSTAT1^-HLA\text{-}DRA1^-$	1.07	<0.01	

A HR of >1 indicates an increased risk of death, and HR of <1 indicates a decreased risk of death. The relative number of each immune cell type was measured in tumor-associated stroma. All univariate Cox regression results are presented in ***Supplementary Table S3****.*
HR, hazard ratio.

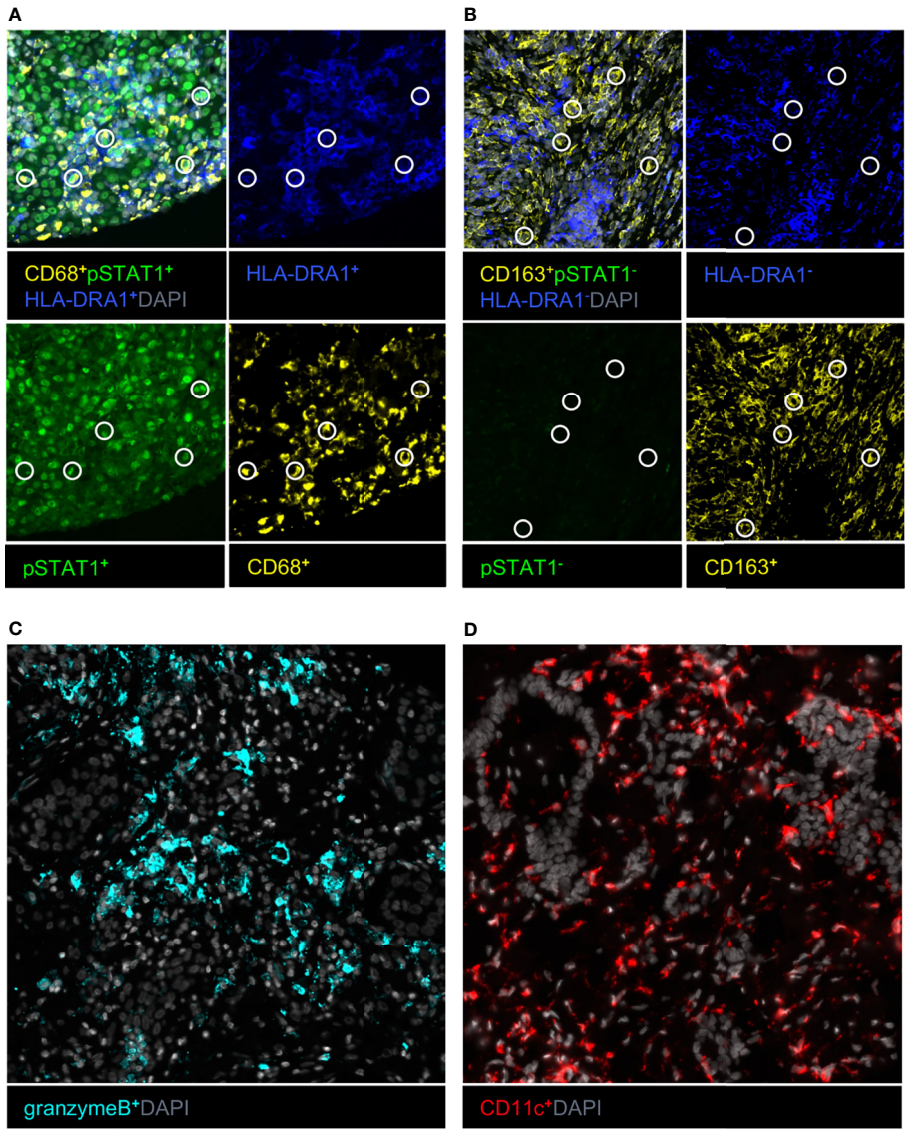

FIGURE 1 | Example images of immune cell phenotypes associated with survival in univariate Cox regression. **(A)** Type M1 macrophage marker combination with circles indicating a specific marker combination. **(B)** Type M2 macrophage marker combination with circles indicating a specific marker combination. **(C)** Granzyme B–positive cells. **(D)** CD11c-positive cells.

prediction model together in combination with the following clinical variables: age, gender, clinical stage, and grade, we performed AUROC comparisons between the models. CD11c was the only immune cell subtype increasing confidence in a prediction model, and therefore, CD11c stood out as the most significant prognostic factor of the immune cell subtypes studied (**Figure 3**).

3.4 Correlations Between Prognostic Immune Cell Types

Both type M1 and type M2 macrophages correlated positively with Ki67$^+$-proliferating cells (Spearman's rho 0.27, p = 0.03 and 0.34, p = 0.01, respectively), and CD11c$^+$ cells correlated negatively with type M2 macrophages (Spearman's rho −0.32, p = 0.01). Ki67$^+$-proliferating cells correlated positively with mitoses (Spearman's rho 0.30, p = 0.02), whereas there was no correlation between type M2 macrophages and mitoses (Spearman's rho 0.08, p = 0.54).

4 DISCUSSION

In this study, we investigated the prognostic immune cell phenotypes present in tumor-associated stroma of epithelioid mesothelioma. In univariate analysis, we found that type M2 macrophages were associated with shorter survival. Further, type

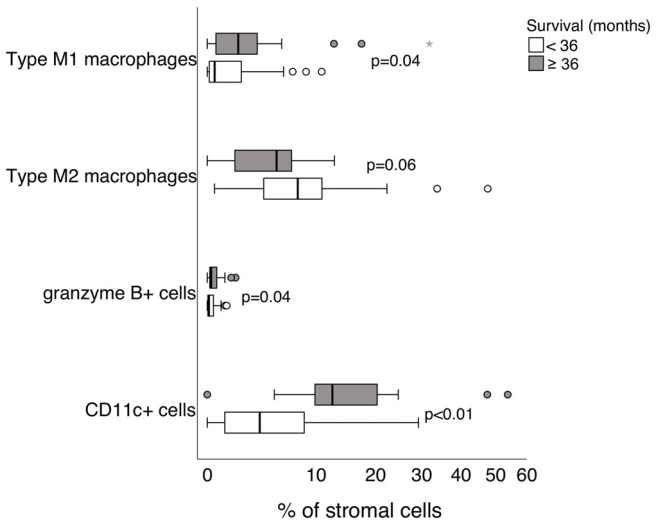

FIGURE 2 | The relative number (%) of each immune cell type of all stromal cells in long-term and average-term survivors (cutoff, 36 months). The cell classes that are significantly associated with survival in univariate Cox regression are shown. Differences between groups were tested by using the Mann–Whitney U-test.

TABLE 3 | Multivariable Cox regression analysis.

Variable	HR (95% CI)	p-value
Individual markers (n = 66*)		
$CD68^+pSTAT1^+HLA\text{-}DRA1^+$	0.94 (0.87–1.01)	0.11
$CD163^+pSTAT1^-HLA\text{-}DRA1^-$	1.06 (1.02–1.10)	<0.01
granzyme B^+	0.32 (0.12–0.87)	0.03
$CD11c^+$	0.93 (0.89–0.98)	<0.01
All markers combined (n = 66*)		
Age	1.00 (0.97–1.03)	0.88
Gender		
Male	1.0	
Female	0.96 (0.48–1.95)	0.92
Clinical stage		
Low	1.0	
High	1.77 (1.00–3.12)	0.05
Grade		
Low	1.0	
High	1.13 (0.50–2.55)	0.76
$CD163^+pSTAT1^-HLA\text{-}DRA1^-$	1.05 (1.01–1.10)	0.02
granzyme B^+	0.29 (0.11–0.76)	0.01
$CD11c^+$	0.94 (0.90–0.99)	0.01

Multivariable Cox regression adjusted for age, gender, grade, and clinical stage. A HR of >1 indicates an increased risk of death, and a HR of <1 indicates a decreased risk of death.
**TNM staging missing for one patient, univariate Cox regression results missing for 2 patients.*
All models fulfilled the proportional hazard assumption.
HR, hazard ratio; CI, confidence interval.

M1 macrophages and CD11c or granzyme B expressing cells were associated with longer survival. When comparing the relative numbers of these cell types between average and long-term survivors (cutoff, 36 months), especially higher numbers of CD11c expressing cells were associated with long-term survival. In multivariable Cox regression adjusting separately for prognostic immune cell phenotypes (from univariate analysis), age, gender, grade, and stage of the disease, all phenotypes excluding type M1 macrophages remained independently associated with survival. When taking into account all prognostic phenotypes, type M2 macrophages, granzyme B, and CD11c remained independently associated with survival. Overall, the most important findings of this study were that M2-like macrophages are independently associated with shorter survival, and granzyme B and CD11c with longer survival in MPM. Finally, CD11c was the only immune cell subtype increasing confidence in a prediction model.

We observed that type M2 macrophages were associated negatively with survival, also when it was adjusted for other

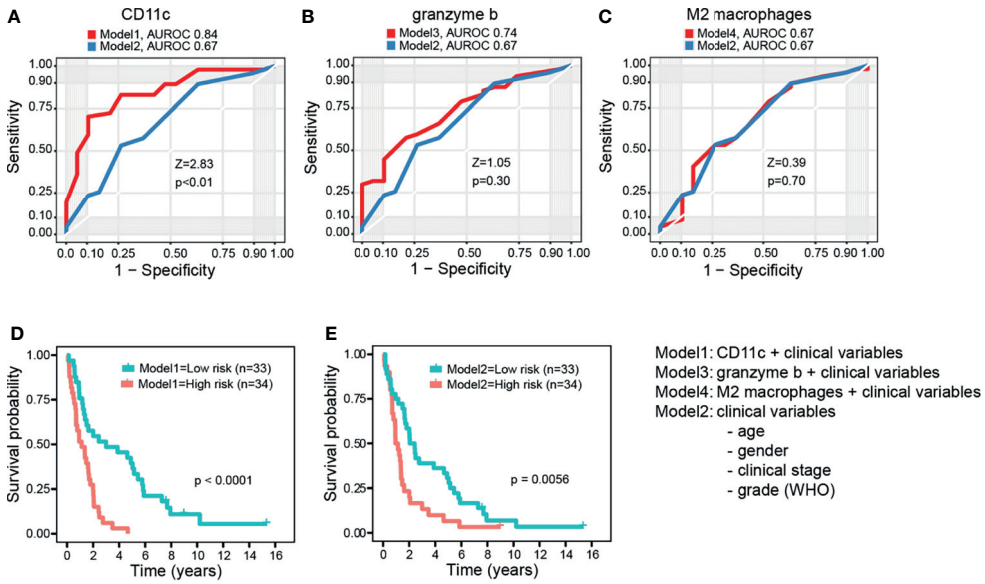

FIGURE 3 | Survival prediction power of combination models. **(A)** Area under the receiver operating characteristic curves (AUROC) for combined clinical factors (age, gender, clinical stage, and grade) (Model2) and for clinical factors plus CD11c (median dichotomized) (Model1). **(B, C)** Same as in **(A)**, but now granzyme B and M2 macrophages in Models 3 and 4, respectively. The DeLong's test for two correlated ROC curves. **(D, E)** Kaplan–Meier curves for low- and high-risk dichotomized patient groups with and without CD11c in the model, respectively. Log rank test.

immunophenotypes together with clinical factors in a multivariable model. Prior studies have shown that type M2 macrophages increase the proliferation of MPM cells and their resistance to chemotherapy (27). We also observed a positive correlation between type M2 macrophages and Ki67 but not between type M2 macrophages and mitosis. Further, higher CD163/CD8 and CD163/CD20 ratios have been shown to be independent prognostic factors of shorter survival in MPM (9), and patients with MPM with higher M2/total tumor-associated macrophage (TAM) ratio have been shown to be more prone to develop local tumor outgrowth compared with those with low M2/TAM ratio (28). However, a previous study indicated no prognostic value for M2 macrophages, possibly due to median-based cutoff values for the percentage of macrophages, whereas we assessed the survival effect by using continuous values (17). Our findings also demonstrated that $CD68^+$ M1 macrophages associate with longer survival, although they were not independent of other factors in a multivariable model. These findings where M2 and M1 macrophages associate with poor and favorable survival, respectively, are logical, as many studies in other cancers, in addition to the aforementioned studies in MPM (9, 27), indicate the same (29). We classified M2 macrophages as $CD163^+pSTAT1^-HLA\text{-}DRA1^-$ cells and M1 macrophages as $CD68^+pSTAT1^+HLA\text{-}DRA1^+$ cells.

Our finding regarding type M2 macrophages supports the previous observations that higher number of them in MPM TIME predicts shorter survival in patients with MPM. Therefore, the number of M2 macrophages in MPM TIME may be used as prognostic tool when prognosticating the survival of patients with MPM. Further, it is known that type M2 macrophages are typically present in Th2-type processes (30, 31), and in tumor immunology, this is usually considered immunologically cold. Such tumors typically do not respond well to immuno-oncological (IO) treatments (32). On the basis of our findings, immunologically hot MPM tumors seem to have better prognosis even without treatment, but they are also likely to respond better when treated. This may be a potential future prospect when targeting IO treatments to patients with MPM.

Granzyme B is known to be expressed by cytotoxic T cells, NK cells, mast cells, plasma cells, and myeloid cells (33–35). Marcq et al. investigated the prognostic value of granzyme B in patients with pretreated and unpretreated MPM but reported no association between granzyme B expression and patient survival (11). Further, Mankor et al. reported that patients with MPM who were responding to aPD-1/aCTLA-4 combination treatment (nivolumab combined with ipilimumab) had a higher amount of granzyme B expressing $CD8^+$ cytotoxic T cells (36). We investigated the prognostic value of granzyme B alone as well as in combination with CD8 (marker for cytotoxic T cells) or with CD11b (marker for myeloid cells). Marker combinations were not of prognostic value, but we showed that granzyme B alone is an independent positive prognostic factor in MPM. Therefore, granzyme B could be used for prognostication of survival, and it remains to be explored if it could potentially also be a marker for targeting IO treatments (as aPD-1/aCTLA-4 combination treatment) to a more specific subgroup of patients.

CD11c is expressed by the cells of myeloid origin and is typically used as a marker of differentiated DCs but may also be expressed by $CD16^+$ monocytes and macrophages. DCs are key antigen-

presenting cells, important in mediating immune activation in the tumor microenvironment of several types of malignancies (25). Expression of DCs is also proposed to result in a loss of function of CD4 and CD8 T cells (37). Here, we observed that higher numbers of $CD11c^+$ cells predicted longer survival, also when adjusting for other prognostic factors including other immune cell types. We postulate that the prognostic $CD11c^+$ cells are DCs, as the double-positive phenotype with the monocyte/macrophage marker, CD16, represented only a small fraction of $CD11c^+$ cells (2.9%) and was not of prognostic value. $CD11c^+$ DCs stood out as the most significant prognostic immune cell subtype, as demonstrated by combination survival prediction models using AUROC analyses. Therefore, we suggest that CD11c alone or with clinical factors could be used as a prognostic marker for predicting the survival of patients with MPM.

4.1 Strengths and Limitations

Although the prognostic values of different immune cell markers in MPM TIME have been investigated before, we utilized methodology enabling deep simultaneous quantitative examination of many immune cell types in a unique cohort of patients with MPM including rare long-term survivors. This allowed us to characterize the specific prognostic immune cell populations in a systematic manner and compare the TIME landscape between average and long-term survivors. Because MPM is a rare malignancy, it will be necessary to confirm the data in larger independent cohorts of patients. Our study population included only patients with MPM with epithelioid histology, so the results may not apply to other histological subtypes of MPM.

5 CONCLUSIONS

After univariate and multivariable analyses, we found that higher number of M2 macrophages in MPM stroma is an independent prognostic factor for shorter survival. In contrast, higher numbers of $CD11c^+$ stromal cells and granzyme B^+ stromal cells in MPM are independent prognostic factors for longer survival. These specific cell types (especially CD11c expressing DCs) may potentially be used as prognostic factors when estimating the risk of disease progression in patients with MPM. Further, these findings warrant for further studies to ask if they could be used to guide targeting of IO treatments to specific subgroups of patients with MPM.

DATA AVAILABILITY STATEMENT

The raw data supporting the conclusions of this article will be made available by the authors, without undue reservation.

ETHICS STATEMENT

The studies involving human participants were reviewed and approved by the Ethics Committee of Helsinki University Hospital (HUS/1057/2019). Written informed consent for participation was not required for this study in accordance with the national legislation and the institutional requirements.

AUTHOR CONTRIBUTIONS

HO analyzed the data, performed the statistical analyses, and wrote the paper. LP developed the scripts for conducting the cell-based image analysis. JP collected the clinical data. HW and ES gathered the study cohort and were responsible for constructing the tissue microarrays (TMAs). KV coordinated and carried out the mfIHC experiments. TP designed the mfIHC panels. OK, MM, and JR provided their special expertise for designing and conducting the study. II, MIM, and TP were responsible for the study design and supervised the project. All authors contributed to the article and approved the submitted version.

FUNDING

This study was supported by a special governmental subsidy for health and science research from the Helsinki University Hospital, The Finnish Work Environment Fund, Svenska kulturfonden, K. Albin Johansson stiftelse, Finska Läkaresällskapet, Mjölbolsta stiftelse för medicinsk forskning, Medicinska Understödsföreningen Liv och Hälsa, The Finnish Medical Foundation, Sigrid Jusélius Foundation, Tampereen tuberkuloosisäätiö, Väinö ja Laina Kiven Säätiö, and Hengityssairauksien tutkimussäätiö.

ACKNOWLEDGMENTS

The authors would like to thank Annabrita Schoonenberg and the FIMM Digital Microscopy and Molecular Pathology Unit supported by HiLIFE and Biocenter Finland for scanning services and Eeva Kettunen for contributing to the sample annotations for constructing the tissue microarrays, and Oscar Brück for helping with the statistical analyses.

SUPPLEMENTARY MATERIAL

The Supplementary Material for this article can be found online at: https://www.frontiersin.org/articles/10.3389/fonc.2022.870352/full#supplementary-material

REFERENCES

1. Laaksonen S, Ilonen I, Kuosma E, Sutinen E, Wolff H, Vehmas T, et al. Malignant Pleural Mesothelioma in Finland: Regional and Gender Variation. *Acta Oncol (Madr)* (2019) 58:38–44. doi: 10.1080/0284186X.2018.1532599
2. Milano MT, Zhang H. Malignant Pleural Mesothelioma: A Population-Based Study of Survival. *J Thorac Oncol* (2010) 5:1841–8. doi: 10.1097/JTO.0b013e3181f1cf2b
3. Van Gerwen M, Alpert N, Wolf A, Ohri N, Lewis E, Rosenzweig KE, et al. Prognostic Factors of Survival in Patients With Malignant Pleural Mesothelioma: An Analysis of the National Cancer Database. *Carcinogenesis* (2019) 40:529–36. doi: 10.1093/CARCIN/BGZ004
4. Hiltbrunner S, Mannarino L, Kirschner MB, Opitz I, Rigutto A, Laure A, et al. Tumor Immune Microenvironment and Genetic Alterations in Mesothelioma. *Front Oncol* (2021) 11:660039/BIBTEX. doi: 10.3389/FONC.2021.660039/BIBTEX

5. Harber J, Kamata T, Pritchard C, Fennell D. Matter of TIME: The Tumor-Immune Microenvironment of Mesothelioma and Implications for Checkpoint Blockade Efficacy. *J Immunother Cancer* (2021) 9:e003032. doi: 10.1136/JITC-2021-003032
6. Fennell DA, Ewings S, Ottensmeier C, Califano R, Hanna GG, Hill K, et al. Nivolumab Versus Placebo in Patients With Relapsed Malignant Mesothelioma (CONFIRM): A Multicentre, Double-Blind, Randomised, Phase 3 Trial. *Lancet Oncol* (2021) 0:1530–40. doi: 10.1016/S1470-2045(21)00471-X
7. Baas P, Scherpereel A, Nowak AK, Fujimoto N, Peters S, Tsao AS, et al. First-Line Nivolumab Plus Ipilimumab in Unresectable Malignant Pleural Mesothelioma (CheckMate 743): A Multicentre, Randomised, Open-Label, Phase 3 Trial. *Lancet* (2021) 397:375–86. doi: 10.1016/S0140-6736(20)32714-8
8. Nicolini F, Bocchini M, Bronte G, Delmonte A, Guidoboni M, Crinò L, et al. Malignant Pleural Mesothelioma: State-Of-the-Art on Current Therapies and Promises for the Future. *Front Oncol* (2020) 9:1519. doi: 10.3389/fonc.2019.01519
9. Ujiie H, Kadota K, Nitadori J, Aerts JG, Woo KM, Sima CS, et al. The Tumoral and Stromal Immune Microenvironment in Malignant Pleural Mesothelioma: A Comprehensive Analysis Reveals Prognostic Immune Markers. *Oncoimmunology* (2015) 4:e1009285-1–9. doi: 10.1080/2162402X.2015.1009285
10. Anraku M, Cunningham KS, Yun Z, Tsao M-S, Zhang L, Keshavjee S, et al. Impact of Tumor-Infiltrating T Cells on Survival in Patients With Malignant Pleural Mesothelioma Anraku Et Al General Thoracic Surgery. *J Thorac Cardiovasc Surg* (2008) 135:823. doi: 10.1016/j.jtcvs.2007.10.026
11. Marcq E, Siozopoulou V, de Waele J, Van Audenaerde J, Zwaenepoel K, Santermans E, et al. Prognostic and Predictive Aspects of the Tumor Immune Microenvironment and Immune Checkpoints in Malignant Pleural Mesothelioma. *Oncoimmunology* (2016) 6:e1261241-3–10. doi: 10.1080/2162402X.2016.1261241
12. Pasello G, Zago G, Lunardi F, Urso L, Kern I, Vlacic G, et al. Malignant Pleural Mesothelioma Immune Microenvironment and Checkpoint Expression: Correlation With Clinical-Pathological Features and Intratumor Heterogeneity Over Time. *Ann Oncol Off J Eur Soc Med Oncol* (2018) 29:1258–65. doi: 10.1093/ANNONC/MDY086
13. Fusco N, Vaira V, Righi I, Sajjadi E, Venetis K, Lopez G, et al. Characterization of the Immune Microenvironment in Malignant Pleural Mesothelioma Reveals Prognostic Subgroups of Patients. *Lung Cancer* (2020) 150:53–61. doi: 10.1016/J.LUNGCAN.2020.09.026
14. Chee SJ, Lopez M, Mellows T, Gankande S, Moutasim KA, Harris S, et al. Evaluating the Effect of Immune Cells on the Outcome of Patients With Mesothelioma. *Br J Cancer* (2017) 117:1341–8. doi: 10.1038/BJC.2017.269
15. Yamada N, Oizumi S, Kikuchi E, Shinagawa N, Konishi-Sakakibara J, Ishimine A, et al. CD8+ Tumor-Infiltrating Lymphocytes Predict Favorable Prognosis in Malignant Pleural Mesothelioma After Resection. *Cancer Immunol Immunother* (2010) 59:1543–9. doi: 10.1007/s00262-010-0881-6
16. Losi L, Bertolini F, Guaitoli G, Fabbiani L, Banchelli F, Ambrosini-Spaltro A, et al. Role of Evaluating Tumor–Infiltrating Lymphocytes, Programmed Death–1 Ligand 1 and Mismatch Repair Proteins Expression in Malignant Mesothelioma. *Int J Oncol* (2019) 55:1157–64. doi: 10.3892/IJO.2019.4883
17. Salaroglio IC, Kopecka J, Napoli F, Pradotto M, Maletta F, Costardi L, et al. Potential Diagnostic and Prognostic Role of Microenvironment in Malignant Pleural Mesothelioma. *J Thorac Oncol* (2019) 14:1458–71. doi: 10.1016/J.JTHO.2019.03.029
18. Cornelissen R, Lievense LA, Maat AP, Hendriks RW, Hoogsteden HC, Bogers AJ, et al. Ratio of Intratumoral Macrophage Phenotypes Is a Prognostic Factor in Epithelioid Malignant Pleural Mesothelioma. *PloS One* (2014) 9:e106742-1–9. doi: 10.1371/journal.pone.0106742
19. Burt BM, Rodig SJ, Tilleman TR, Elbardissi AW, Bueno R, Sugarbaker DJ. Circulating and Tumor-Infiltrating Myeloid Cells Predict Survival in Human Pleural Mesothelioma. *Cancer* (2011) 117:5234–44. doi: 10.1002/cncr.26143
20. Ollila H, Paajanen J, Wolff H, Ilonen I, Sutinen E, Välimäki K, et al. High Tumor Cell Platelet-Derived Growth Factor Receptor Beta Expression Is Associated With Shorter Survival in Malignant Pleural Epithelioid Mesothelioma. *J Pathol Clin Res* (2021) 7:482–94. doi: 10.1002/cjp2.218
21. Hollandi R, Szkalisity A, Toth T, Tasnadi E, Molnar C, Mathe B, et al. Nucleaizer: A Parameter-Free Deep Learning Framework for Nucleus Segmentation Using Image Style Transfer. *Cell Syst* (2020) 10:453–458.e6. doi: 10.1016/J.CELS.2020.04.003
22. Schulte JJ, Chapel DB, Attanoos R, Brcic L, Burn J, Butnor KJ, et al. Comparison of Nuclear Grade, Necrosis, and Histologic Subtype Between Biopsy and Resection in Pleural Malignant Mesothelioma: An International Multi-Institutional Analysis. *Am J Clin Pathol* (2021) 156:989–99. doi: 10.1093/AJCP/AQAB054
23. Nicholson AG, Sauter JL, Nowak AK, Kindler HL, Gill RR, Remy-Jardin M, et al. EURACAN/IASLC Proposals for Updating the Histologic Classification of Pleural Mesothelioma: Towards a More Multidisciplinary Approach. *J Thorac Oncol* (2020) 15:29–49. doi: 10.1016/J.JTHO.2019.08.2506
24. Dacic S. Pleural Mesothelioma Classification – Update and Challenges. *Mod Pathol* (2022) 35:51–6. doi: 10.1038/s41379-021-00895-7
25. Cabeza-Cabrerizo M, Cardoso A, Minutti CM, Pereira Da Costa M, Reis E Sousa C. Dendritic Cells Revisited. *Annu Rev Immunol* (2021) 39:131–66. doi: 10.1146/ANNUREV-IMMUNOL-061020-053707
26. Janes SM, Alrifai D, Fennell DA. Perspectives on the Treatment of Malignant Pleural Mesothelioma. *N Engl J Med* (2021) 385:1207–18. doi: 10.1056/NEJMRA1912719
27. Chéné AL, D'Almeida S, Blondy T, Tabiasco J, Deshayes S, Fonteneau JF, et al. Pleural Effusions From Patients With Mesothelioma Induce Recruitment of Monocytes and Their Differentiation Into M2 Macrophages. *J Thorac Oncol* (2016) 11:1765–73. doi: 10.1016/J.JTHO.2016.06.022
28. Cornelissen R, Lievense LA, Robertus JL, Hendriks RW, Hoogsteden HC, Hegmans JPJJ, et al. Intratumoral Macrophage Phenotype and CD8+ T Lymphocytes as Potential Tools to Predict Local Tumor Outgrowth at the Intervention Site in Malignant Pleural Mesothelioma. *Lung Cancer* (2015) 88:332–7. doi: 10.1016/J.LUNGCAN.2015.03.013
29. Qian BZ, Pollard JW. Macrophage Diversity Enhances Tumor Progression and Metastasis. *Cell* (2010) 141:39–51. doi: 10.1016/J.CELL.2010.03.014
30. Muraille E, Leo O, Moser M. Th1/Th2 Paradigm Extended: Macrophage Polarization as an Unappreciated Pathogen-Driven Escape Mechanism? *Front Immunol* (2014) 5:603. doi: 10.3389/FIMMU.2014.00603
31. Ellyard JI, Simson L, Parish CR. Th2-Mediated Anti-Tumour Immunity: Friend or Foe? *Tissue Antigens* (2007) 70:1–11. doi: 10.1111/J.1399-0039.2007.00869.X
32. Bonaventura P, Shekarian T, Alcazer V, Valladeau-Guilemond J, Valsesia-Wittmann S, Amigorena S, et al. Cold Tumors: A Therapeutic Challenge for Immunotherapy. *Front Immunol* (2019) 10:168/BIBTEX. doi: 10.3389/FIMMU.2019.00168/BIBTEX
33. Strik MCM, de Koning PJA, Kleijmeer MJ, Bladergroen BA, Wolbink AM, Griffith JM, et al. Human Mast Cells Produce and Release the Cytotoxic Lymphocyte Associated Protease Granzyme B Upon Activation. *Mol Immunol* (2007) 44:3462–72. doi: 10.1016/J.MOLIMM.2007.03.024
34. Xu W, Narayanan P, Kang N, Clayton S, Ohne Y, Shi P, et al. Human Plasma Cells Express Granzyme B. *Eur J Immunol* (2014) 44:275–84. doi: 10.1002/EJI.201343711
35. Wagner C, Stegmaier S, Hänsch GM. Expression of Granzyme B in Peripheral Blood Polymorphonuclear Neutrophils (PMN), Myeloid Cell Lines and in PMN Derived From Haemotopoietic Stem Cells *In Vitro*. *Mol Immunol* (2008) 45:1761–6. doi: 10.1016/J.MOLIMM.2007.09.033
36. Mankor JM, Disselhorst MJ, Poncin M, Baas P, Aerts JGJV, Vroman H. Efficacy of Nivolumab and Ipilimumab in Patients With Malignant Pleural Mesothelioma is Related to a Subtype of Effector Memory Cytotoxic T Cells: Translational Evidence From Two Clinical Trials. *EBioMedicine* (2020) 62:103040. doi: 10.1016/J.EBIOM.2020.103040
37. Tran Janco JM, Lamichhane P, Karyampudi L, Knutson KL. Tumor-Infiltrating Dendritic Cells in Cancer Pathogenesis. *J Immunol* (2015) 194:2985–91. doi: 10.4049/JIMMUNOL.1403134

Conflict of Interest: The authors declare that the research was conducted in the absence of any commercial or financial relationships that could be construed as a potential conflict of interest.

this article, or claim that may be made by its manufacturer, is not guaranteed or endorsed by the publisher.

Frontiers in Oncology

Advances knowledge of carcinogenesis and tumor progression for better treatment and management

The third most-cited oncology journal, which highlights research in carcinogenesis and tumor progression, bridging the gap between basic research and applications to imrpove diagnosis, therapeutics and management strategies.

Discover the latest Research Topics

See more →

Frontiers

Avenue du Tribunal-Fédéral 34
1005 Lausanne, Switzerland
frontiersin.org

Contact us

+41 (0)21 510 17 00
frontiersin.org/about/contact